Year : 2020

Development of novel methods for high-throughput analyses of human tumor antigen-specific CD4 T cell responses

Rockinger Georg Alexander

Rockinger Georg Alexander, 2020, Development of novel methods for high-throughput analyses of human tumor antigen-specific CD4 T cell responses

Originally published at : Thesis, University of Lausanne

Posted at the University of Lausanne Open Archive http://serval.unil.ch
Document URN : urn:nbn:ch:serval-BIB_7417869DA8E81

UNIL | Université de Lausanne
Faculté de biologie et de médecine

Department of oncology

Development of novel methods for high-throughput analyses of human tumor antigen-specific CD4 T cell responses

Doctoral thesis ès sciences de la vie (PhD)

presented to

the Faculty of Biology and Medicine of the University of Lausanne

By

Georg Alexander ROCKINGER

Master of Science in Molecular Life Sciences of the University of Lausanne

Jury

Prof. Thierry Roger, President

Prof. Pedro Romero, thesis director

Prof. Camilla Jandus, Thesis co-director

Prof. Matthieu Perreau, expert

Prof. Lionel Apetoh, expert

Lausanne 2020

UNIL | Université de Lausanne
Faculté de biologie et de médecine

Ecole Doctorale
Doctorat ès sciences de la vie

Imprimatur

Vu le rapport présenté par le jury d'examen, composé de

Président·e	Monsieur	Prof.	Thierry	**Roger**
Directeur·trice de thèse	Monsieur	Prof.	Pedro	**Romero**
Co-directeur·trice	Madame	Prof.	Camilla	**Jandus**
Expert·e·s	Monsieur	Prof.	Matthieu	**Perreau**
	Monsieur	Prof.	Lionel	**Apetoh**

le Conseil de Faculté autorise l'impression de la thèse de

Monsieur Georg Alexander Rockinger

Maîtrise universitaire ès Sciences en sciences moléculaires du vivant, Université de Lausanne

intitulée

Development of novel methods for high-throughput analyses of human tumor antigen-specific CD4 T cell responses

Lausanne, le 28 février 2020

pour le Doyen
de la Faculté de biologie et de médecine

Prof. Niko GELDNER
Directeur de l'Ecole Doctorale

Département d'oncologie

Développement de nouvelles méthodes pour l'analyses à haut débit des réponses des lymphocytes T CD4 spécifiques aux antigènes tumoraux humains

Thèse de doctorat ès sciences de la vie (PhD)

Présenté a

La Faculté de Biologie et de médicine de l'Université de Lausanne

par

Georg Alexander ROCKINGER

Master en Science Molecular Life Sciences de l'Université de Lausanne

Jury

Prof. Thierry Roger, Président

Prof. Pedro Romero, Directeur de thèse

Prof. Camilla Jandus, Co-directrice de thèse

Prof. Matthieu Perreau, expert

Prof. Lionel Apetoh, expert

Lausanne 2020

UNIL | Université de Lausanne
Faculté de biologie et de médecine

Ecole Doctorale
Doctorat ès sciences de la vie

Imprimatur

Vu le rapport présenté par le jury d'examen, composé de

Président·e	Monsieur	Prof.	Thierry	**Roger**
Directeur·trice de thèse	Monsieur	Prof.	Pedro	**Romero**
Co-directeur·trice	Madame	Prof.	Camilla	**Jandus**
Expert·e·s	Monsieur	Prof.	Matthieu	**Perreau**
	Monsieur	Prof.	Lionel	**Apetoh**

le Conseil de Faculté autorise l'impression de la thèse de

Monsieur Georg Alexander Rockinger

Maîtrise universitaire ès Sciences en sciences moléculaires du vivant, Université de Lausanne

intitulée

Development of novel methods for high-throughput analyses of human tumor antigen-specific CD4 T cell responses

Lausanne, le 28 février 2020

pour le Doyen
de la Faculté de biologie et de médecine

Prof. Niko GELDNER
Directeur de l'Ecole Doctorale

A Résumé (français)

Le rôle anti-tumoral des lymphocytes T CD4 et leur capacité à reconnaître les néo-antigènes tumoraux n'a été établi que récemment, alors que le rôle des lymphocytes T CD8 dans les mêmes processus est bien connu. Le faible nombre de cellules T CD4 spécifiques des tumeurs dans la circulation limite en effet leur étude. Notre but est d'élargir les connaissances actuelles sur les lymphocytes T CD4 spécifiques des tumeurs et d'étudier leur capacité à éliminer les cellules tumorales. Pour ce faire nous avons mis au point une procédure optimisée pour la détection des lymphocytes T spécifiques des tumeurs directement à partir d'échantillons ex vivo. La fonctionnalité de ces cellules détectées pourra ainsi être évaluée au niveau de la cellule seule. De plus une des clefs à l'utilisation des cellules T CD4 dans l'immunothérapie dépendra de notre capacité de mieux comprendre comment réguler la différentiation de ces cellules de manière à promouvoir la formation de cellules « stem cell memory » ou bien « central memory ».

Au cours de ma thèse, j'ai développé une nouvelle approche pour une meilleure détection des lymphocytes T CD4 reconnaissant des déterminants viraux, bactériens et tumoraux. En utilisant une combinaison de molécules améliorant l'interaction TCR-pCMH de classe II ainsi que l'utilisation d'un panel de multimères pCMH de classe I et II marqués par de multiples fluorochromes, nous avons pu améliorer la détection de cellules spécifiques à partir d'échantillons in vitro et ex vivo de patients grâce à une MFI augmentée ainsi qu'une augmentation du pourcentage de cellules détectées. Malgré ces avancées, l'évaluation de l'affinité du TCR des lymphocytes T CD4 reste compliquée en raison de leur faible affinité. Pour résoudre ce problème, nous explorons des méthodes innovantes telles que la SPR, basée sur l'analyse de cellules entières pour déterminer la capacité fonctionnelle des lymphocytes T CD4 spécifiques à la tumeur. Nous développons un biocapteur nanoplasmonique sophistiqué capable d'évaluer avec un grand débit, en temps réel et sans marquage, le sécrétome de cellules individuelles. La combinaison de ces outils aura un impact sur les connaissances futures liées aux lymphocytes T CD4 et notre capacité à étudier ces cellules dans les essais cliniques liés au cancer.

Au cours de ma thèse, j'ai également contribué à valider un prédicteur bio-informatique pour la liaison de peptide aux molécules du CMH de classe II. Ce nouveau prédicteur est capable de prédire avec une plus grande précision les peptides qui se lieraient au complexe MHC classe II en comparaison aux prédicteurs actuels. Nous avons effectué des tests d'immunogénicité pour valider les peptides prédits par le logiciel et identifier de nouvelles cibles qui pourraient être étudiées dans le domaine des lymphocytes T CD4 anti-tumoraux.

Enfin, nous avons cherché à mieux comprendre comment réguler la différenciation des lymphocytes T CD4 par la modulation de l'expression des miARN. Notre objectif est de promouvoir la formation de phénotypes TSCM et TCM en raison de leur grande capacité à proliférer et à générer des cellules effectrices. Nous avons

cherché à identifier des candidats miARN (miR) qui pourraient être thérapeutiquement ciblés pour influencer la différenciation des cellules T CD4 naïves en cellules TSCM et TCM CD4 spécifiques des cellules tumorales. Plus de recherche est nécessaire pour valider l'impact sur la différenciation lymphocytes T CD4 des miARN identifiés dans ce projet en modulant leur expression avec des analogues ou des inhibiteurs de miARN dans des cellules primaires humaines ainsi que dans des modèles murins.

B Summary (english)

In contrast to the well-known role of CD8 T cells in tumor cell recognition and elimination, CD4 T have only recently gained increasing importance in tumor immunity, including the recognition of neo-antigens. However, due to the low numbers of circulating tumor-specific CD4 T cells, their characterization at antigen level is still very limited. Our goal is to expand the knowledge on tumor-specific CD4 T cells and their ability to eliminate tumor cells by optimizing tools for their direct *ex-vivo* visualization and functional profiling at the single cell level. Moreover, a key to CD4 T cell usage in immunotherapy will also depend on a better understanding of the regulation of their differentiation, to promote stem cell memory and central memory phenotypes.

During my thesis I developed a novel approach for the improved detection of viral-, bacterial- and tumor-specific CD4 T cells. by using a combination of compounds improving TCR-pMHC class II interaction as well as the use of multicolor coded panel of pMHC class I and II multimers. We were able to improve on specific cell detection as a higher MFI of staining and an increase in percentage of cell detected was achieved on both *in vitro* and *ex vivo* patient samples. Despite these advances the evaluation of CD4 T cells TCR affinity remains complicated due to their low affinity. We have started exploring methods for such evaluation using innovative methods such as whole cell based SPR as well performing functional analysis of tumor-specific CD4 T cells at increased throughput we are developing an advanced nanoplasmonic biosensor which evaluates in real time and label-free manner the secretome of individual cells. the combination of these tools will impact the future knowledge we possess on CD4 T and our capacity to monitor these cells within cancer related clinical trials.

During my thesis I also contributed to validating a bioinformatic predictor for peptide binding to MHC class II molecules. This new predictor could predict with greater accuracy peptides that would bind to the MHC class II complex compared to the predictors that are already available. We performed immunogenicity assays to validate the peptides predicted by the software and identified novel targets which could be investigated in the anti-tumor CD4 T cell field.

Finally, we aimed to better understand how to regulate CD4 T cell differentiation through the modulation of miRNA expression. Our goal was to promote T_{SCM} and T_{CM} phenotype formation due to their great capacity to proliferated and generate effector cells. We aimed at identifying optimal miRNA (miR) candidates that could be therapeutically targeted to influence the differentiation of Naïve CD4 T cells into T_{SCM} and T_{CM} CD4 T cells capable of targeting tumor cells. more work is needed to validate the impact on CD4 T differentiation of miRNA identified in this project by modulating their expression with miRNA mimics or inhibitors in primary cells and latter in murine models.

C Résumé large public (français)

Le cancer en Suisse représente 30% des décès chez les hommes et 23% de décès chez les femmes selon l'office fédérale de la santé publique. Cette proportion n'est pas négligeable et s'étend à travers le monde. De nouvelles et nombreuses études pour guérir le cancer sont en cours d'investigation mais les plus prometteuses sont celles ayant pour but de moduler le système immunitaire du patient de manière à éliminer les tumeurs. Nombre de ces études se basent sur l'utilisation de cellules lymphocytaires qui portent à leur surface la protéine CD8 et donc nommés CD8. Ces cellules ont la capacité de tuer directement les cellules tumorales mais cela n'est pas suffisant pour complétement éradiquer les cellules cancéreuses. Il y a de plus en plus de preuves qui démontrent que l'utilisation d'autres cellules lymphocytaires, qui cette fois-ci expriment la protéine CD4 et donc nommés CD4, ont un effet bénéfique pour l'éradication de cellules cancéreuses. Toutefois dû au faible nombre de ces cellules spécifiques en circulation et un manque d'outils pour la détection de ces cellules il est difficile de les étudier.

Ce projet de thèse a donc pour but d'améliorer la détection et la surveillance de ces cellules CD4 capables de reconnaitre les tumeurs. La problématique a été divisée en trois axes. Le premier consistent à améliorer l'identification de ces lymphocytes CD4 reconnaissant les tumeurs. L'utilisation de molécules appelées peptide-CMH class II (pCHM class II) couplées avec une molécule fluorescente ont été utilisées pour marquer les molécules TCR retrouver à la surface des cellules CD4. En plus des complexes pCHM, l'utilisation d'autres molécules optimisatrices ont été cruciales pour une meilleure détection de cellules reconnaissant les tumeurs dans les échantillons de patient. Le deuxième axe a été le fruit de notre collaboration avec le groupe du Professeur Gfeller qui a développé un algorithme capable de prédire des peptides qui pourraient être présentés à la surface des complexe CMH class II. Son utilisation permettrait de découvrir de nouveaux peptides qui pourraient être utilisé pour cibler, dans le cadre de thérapies contre le cancer, des cellules tumorales sans risque d'endommager les cellules saines. Nous avons démontré aux cours de ce projet que ce nouvel algorithme était plus performant que les algorithmes déjà existants. Finalement dans le dernier projet je me suis intéressé à la modulation du phénotype de cellules CD4 de manière à avoir des cellules capables de proliférer considérablement et capables de donner naissance à des cellules effectrice tueuses des cellules cancéreuses. Les micro-ARN sont capables d'inhiber ou d'activer de nombreuses fonctions cellulaires. Nous nous sommes donc intéressés à identifier des micro-ARN différemment exprimés parmi plusieurs sous-types de cellules CD4 et à comprendre si la modulation de l'expression de ces micro-ARN résultait en un changement du phénotype des cellules.

Nous espérons que ce travail permettra un meilleur suivi ainsi que l'utilisation des lymphocytes CD4 dans les futures thérapies visant les patients cancéreux.

D Acknowledgments

First, I would like to thank the Prof. Pedro Romero for giving me the opportunity to perform my PhD work in his lab. I would like to acknowledge all the conversations we have had during these years as part of the PhD meetings. These discussions have greatly helped with giving me direction regarding my projects and has allowed me to advance swiftly through my research. I would like to thank my co-director Prof. Camilla Jandus for all her support and day to day advices and discussions that she has provided me with during the entirety of my PhD thesis. The knowledge imparted to me by Prof. Camilla Jandus has been instrumental to my success and I wish her the best in her new position as professor at the university of Geneva. Moreover, both professors have given me the possibility to expand my knowledge by attending numerous conferences as well as to present my work. I would like to thank the members of my PhD evaluating committee: prof. Lionel Apetoh, prof. Thierry Roger and prof. Matthieu Perreau who have followed me throughout my entire PhD thesis and have been there in moments of need, for which I am extremely grateful.

I would like to acknowledge our collaborators without whom several of my projects would not have been possible. Firstly, the group of Profs. George Coukos and Prof. Daniel Speiser with whom we are publishing my main manuscript. From the group of the prof. Coukos, Dr. Alexandre Harari, Dr. Philippe Guillaume provided me with help and support throughout my project. I would like to particularly thank Dr. Julien Schmidt for his unwavering trust in me and his much-needed support and who's company I always appreciate. I would also like to show my appreciation for the group of the Prof. David Gfeller and his post-doc Dr. Julien Racle who's work and our collaborative efforts resulted in the publication in a high impact factor journal.

I was lucky to find a group with a team spirit thus I would like to thank Sara Trabanelli, Alejandra Gomez, Giuseppe Ercolano, Tania Wyss, Giulia Vanoni and our great technician whom we forgive for being from Geneva: Anthony Cornu. throughout the years I have seen valued colleague leaving such as Romain Loyon-Bonato, Carla Marisa Costa Nunes and Bérengère Salomé but I also have seen new arrivals to the team, people I very much appreciate such as Maryline Falquet, Margaux Saillard and our present master student Brenda Gaillard. I would like to thank them all for the good atmosphere in the lab.

Amongst my colleagues I have made invaluable friendships which greatly extend beyond the boundaries of the work place and for that I am extremely grateful to Amandine Bovay, Claire Imbratta, Nina Dumauthioz as well as Christophe Martignier with whom I have spent many hours playing video games and with whom we share a great many interests. A particular thank you goes to Amélie Cachot, who has been a colleague, a confident, a support during hard times and foremost someone I am proud to call a friend.

Another pillar without whom it would have had difficulties to go through my PhD are my friends from Lausanne and all around the world: Garance Vögeli, Mathieu Droux, Alex Unnervik, Marie-Laure Arn, Sevan Spiess, Stephanie Junod, Frank Hugi, Camille Berger Laura Mordasini and Marjola Bruci. I was always able to

count on my lifetime friends Edouard de Casteja and Victor Lesieur as well as the support from my brother Florian Tosello. They all have contributed to my successes and I hope to share many more fun moments with them.

Overall, I would like to thank everyone who has accompanied me on this journey. Including my parents who have always been there for me in the good and the worst moments of my life and have always pushed me to excellence. Their love and support were invaluable. Last but not least I would like to thank my partner Kaat de Jonge, she has always been by my side in the good and bad moments of this long journey ever since we first meet at the beginning of our respective thesis. I would like to thank the trust she places in me on a day to day basis as well as her belief in me even in moments where I have none for myself.

E Abbreviations

Ab	Antibody
ACT	Adoptive cell transfer therapy
ADCC	Antibody dependent cell cytotoxicity
AICD	Activation induced cell death
ALR	AIM2-like receptor
APC	Professional antigen presenting cells
BCR	B cell receptor
Breg	Regulatory B cell
C	Complement system
CARs	Chimeric antigen receptor
CBM	CARMA1/Bcl10/MALT1 complex
cDC	Common DC
CDC	Complement-dependent cytotoxicity
CLIP	Class II-associated invariant chain peptide
CLR	C-type lectin receptor
CP	Connecting peptide
CTLA-4	Cytotoxic T-lymphocyte-associated antigen 4
CXCR3	Chemokine receptor-3
DAG	Diacylglycerol
DAMP	Danger associated molecular pattern
DC	Dendritic cell
ECD	Extracellular domain

ELISA	Enzyme-linked immunosorbent assay
ELISpot	Enzyme-linked immunosorbent spot
EOT	Extraordinary optical transmission
ER	Endoplasmic reticulum
FcR	Fc receptor
ICD	Immunologic cell death
IFN-γ	Interferon-gamma
IL	Interleukin
ILC	Innate lymphoid cell
IP3	Inositol 1,4,5-trisphosphate
IRF	IFN regulatory factor
ITAM	Immunoreceptor-tyrosine-based activation motifs
LacNAc	N-Acetyl-D-lactosamine
MAIT	Mucosal-associated invariant T
MAPK	Mitogen-activated protein kinase
MHC	Major histocompatibility complex
MP-SPR	Multiparametric Surface Plasmon Resonance
NEMO	NF-κB essential modifier
NK	Natural killer cell
NLR	NOD-like receptor
NOD	Nucleotide-binding oligomerization domain
NTAmers	Reversible multimer
nTreg	Natural regulatory T cell

PAMP	Pathogen associated molecular pattern
PBMCs	Peripheral blood mononuclear cells
PD-1	Programmed cell death protein 1
pDC	Plasmacytoid DC
PGE2	Prostaglandin E2
PH	Pleckstrin homology domain
PIP3	Phosphatidylinositol 3,4,5-trisphosphate
PKI	Protein kinase inhibitor
pMHC	Peptide MHC
RAG	Recombination-activating gene
RIG-I	Retinoid acid-inducible gene I
RISC	RNA-induced silencing complex
RLR	RIG-I-like receptor
RT	Reverse transcribed
SCA-1	Stem cell antigen-1
scFv	Antibody single chain
SLP	Synthetic long peptide
SPR	Surface Plasmon Resonance
TCR	T cell receptor
TEM	Effector memory T cells
Tfh	T follicular helper cell
ThCTL	T cytolytic cell
TLR	Toll-like receptor

TN	Naïve T cell
TNFα	Tumor necrosis factor alpha
TRAF6	Necrosis factor receptor-associated factor 6
TReg	Regulatory T cell
TRIF	TIR domain-containing adaptor inducing IFN-β
TRM	Tissue-resident memory T cell
TSCM	Stem cell memory T cell
TTE or TEMRA	Terminal effector T cell
TTM	T “transitional” memory T cell

F Table of contents

G Introduction

G.1 The immune system

On a day to day basis our body is subjected to numerous viruses, bacteria and other foreign agents. To protect itself, it has devised three lines of defence. The first line of defence consists of a physical barrier composed of tissues such as the epithelia surfaces, the mucosa in the gastrointestinal tract and the respiratory tract. These first lines of defence are lined with enzymes and mucus which inhibit the attachment of microbes or have direct antimicrobial properties. Once these barriers are breached and pathogens can access the inner layers of tissues they will encounter the innate immune system which is the fast and non-specific acting branch of our immune system. Where this initial response is not enough to control or to clear the foreign pathogen, the adaptive immune system becomes activated and will help clearing the infection site by a specific targeting of the invading bodies. Both the innate and adaptive systems are tightly interrelated (1).

G.1.1 Innate immunity

The innate immune system is a fast acting and non-pathogen-specific system which is composed of cells such as neutrophils, basophils, monocytes, macrophages, mast cells, dendritic cells, natural killer cells (NK) and innate lymphoid cells (ILCs) and soluble molecules, such as the complement system and anti-microbial peptides. Since innate immune cells are not able to specifically detect the pathogens, they must rely on other mechanisms to discriminate between self and non-self. Pathogens express constitutively molecules such as lipoproteins, lipopolysaccharide, peptidoglycan, lipoteichoic acids and nucleic acids of viral or bacterial origin, that make up a panel of signals known as pathogen associated molecular patterns (PAMPs). Innate immune cells can also respond to signals derived from stressed or dying cells, known as danger associated molecular patterns (DAMPs) (2). These conserved structures are recognized through a limited number of germ line-encoded pattern recognition receptors (PRR) found on immune cells. These receptors can be divided in five different classes: the more extensively studied Toll-like receptor (TLR) (3), nucleotide-binding oligomerization domain (NOD)-like receptors (NLRs) (3), retinoid acid-inducible gene I (RIG-I)-like receptors (RLRs) (3), C-type lectin receptors (CLRs) (4) and two AIM2-like receptors (ALRs) (5). Upon PAMP recognition by PRRs, proinflammatory and antimicrobial responses will be triggered. Adaptor molecules (MyD88, TIR domain-containing adaptor inducing IFN-β (TRIF)) will be triggered and will determine the quality of the response (6,7). To ensure a downstream activation via phosphorylation, ubiquitination, or protein-protein interactions TLR will recruit several adaptor molecules which will induce the activation of transcription factors such as NF-κB, mitogen-activated protein kinases (MAPKs) or IFN regulatory factors (IRFs) (6,8,9), resulting in the synthesis of a broad range of molecules, including cytokines, chemokines, cell adhesion molecules, and immunoreceptors (8). This mechanism is crucial for the early response to infections, but it also plays an important role in the activation and maturation of the adaptive immune response (10).

As mentioned above, the innate immune system is comprised of multiple cell types. which develop in the bone marrow before migrating to the periphery (11). Granulocytes play an important role in early inflammatory reactions as they have the capacity to migrate from the blood into the tissues in response to chemoattractants such as interleukin (IL)-8 and eotaxin (12). Once in the site of infection, granulocytes detect via a multitude of PRR at their cell surface or within the cell the foreign bodies and become fully active. At this point they will start to release granules containing antimicrobial agents, enzymes and toxic reactive oxygen derived products (13). Granulocytes are short lived cells, yet their lifespan can be modulated depending on the length and intensity of the infection (14). Mast cells are part of the granulocyte lineage, and when mature, they are tissue resident. Mast cells main activation mechanism relies on IgE-mediated reaction via the FcεRI and mediate functions such as vasodilation, angiogenesis, bacterial and parasite elimination. As these cells secrete multi-potent molecules they are involved in regulating organ and tissue functions as well as regulating other cells of the immune system (15). NK appeared early during evolution compared to adaptive immune cells, and still outnumber B cells in the circulation by a 3-to-1 ratio (16). NK cells are cytotoxic in nature and have the capacity to lyse any target that lacks self-major histocompatibility complex (MHC) class I molecules (missing self-theory). Human NK cells can be divided into two main subsets based on the expression levels of CD56 (neural adhesion molecule NCAM) and CD16 (low affinity Fc receptor) (16). The CD56bright NK cells are around 5% of total circulating NK cells, they express high levels of CD56 and no CD16. Functionally they have little cytolytic capacity but are capable of strong cytokine secretion. On the contrary NK CD56dim constitute 95% of circulating NK cells and have high expression of CD16 and dim expression of CD56. They can efficiently lyse target cells (16). ILCs have been recently described and considered as the innate counterparts of CD4 T lymphocytes, as they lack rearranged antigen receptors but mirror CD4 T helper (Th)1, Th2, Th17 in function (17). T-bet expressing, interferon-gamma (IFN-γ) secreting ILC1s react to intracellular pathogens like viruses and to tumors, ILC2s express the transcription factor GATA3 and respond to helminths and allergens by secreting type 2 cytokines. Finally, ILC3s depend on the expression of the transcription factor RORγT and can produce IL-17 and/or IL-22. ILC3 main function is to protect the body against extracellular microbes such as fungi and bacteria (17). ILCs intervene early in the immune response by reacting swiftly to signals and can provide pro and anti-inflammatory effector functions. Macrophages are non-migratory, strategically positioned, myeloid cells characterized by their avid phagocytosis (18). They can be classified into two categories: the classically activated M1 macrophages which are associated with viral and bacterial inflammation and IFNγ signaling and the alternatively activated M2 macrophages who respond to allergies, helminths and asthma and secrete type two cytokines like IL-4 and IL-13 (19). Macrophages are equipped with a large array of sensing molecules which help them to ingest dead cells, debris and foreign material from their immediate surroundings. Macrophages are capable of orchestrating the inflammatory reaction by providing chemokines and cytokines that will recruit and activate other players of the innate immune system as well as by secreting growth factors (18). Contrary to

macrophages, dendritic cells (DCs) are highly mobile sentries capable of triggering T cell responses by presenting antigen through their numerous surface peptide MHC class I and II complexes, upon migration to the tissue-draining lymph nodes. DCs are considered as professional antigen presenting cells (APC) and are a bridge between the innate and adaptive immune system. DCs have many different subsets of which the two major common DC (cDC) are cDC1 and cDC2. cDC1 are present in blood and in lymphoid and non-lymphoid tissues, they are characterized by the expression of CD141, the chemokine receptor XCR1, C-type lectin CLEC9A, the cell adhesion molecule CADM1 (20). This subpopulation is capable to perform cross-presentation and prime CD8 T cells efficiently. cDC2 can be found in blood, lymphoid and non-lymphoid tissues. This subpopulation is heterogeneous and is characterized by different markers depending on their localization, for example CD1a in the dermis and CD103 in the gut (21,22). cDC2s have been described to be potent stimulators of naïve T cell proliferation and to be able to cross-present antigens. Another important subpopulation is known as plasmacytoid DCs (pDCs) which are specialized in inducing anti-viral immune responses and secreting type I interferons (23).

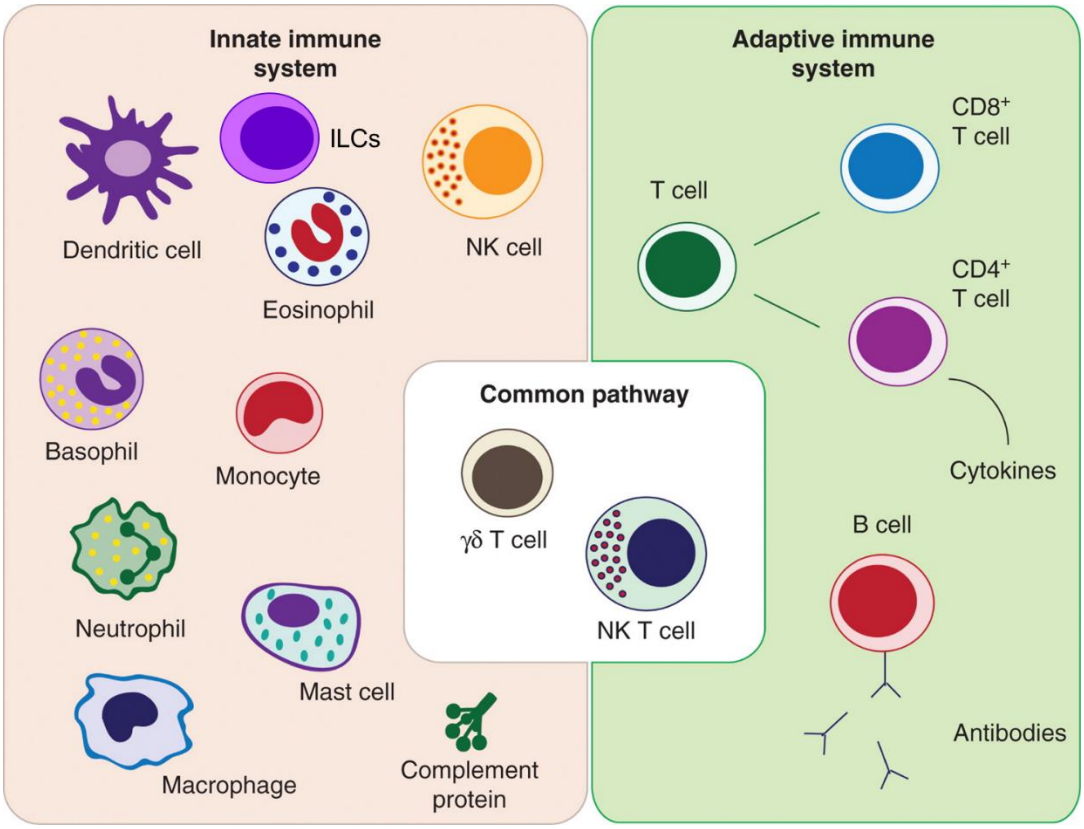

Figure 1: representation of cells from the innate and of the adaptive immune systems. The cells of the innate immune system are fast acting but do not act in a specific manner. The adaptive immune system is slow acting but acts in a specific manner and it induces a memory in case of future encounters with the same pathogen. Adapted from (24).

The complement (C) system is part of the innate immune system and regroups many distinct plasma proteins that work with one another to opsonize pathogens and prompt inflammatory responses necessary to fight infections. Several of the complement proteins are proteases which act through a triggered-enzyme cascade (25). They can mediate protection against infection through three ways: by covalently binding pathogens

(opsonization) to engulfing them by phagocytes via complement receptors. By acting as chemoattractants and activators of phagocytes at the site of the complement activation. By creating pores in the bacterial membrane resulting in damage and bacterial death (26).

Furthermore, there are cell types such as NKT, γδT cells and Mucosal-associated invariant T (MAIT) with particular phenotypic traits which set them in between the two main innate and adaptive immune systems. NKT cells were first discovered in mice as cells with intermediate expression of αβ-TCR and robust expression of key cytokines such as IL-4, IFN-γ and TNF-α, thus increasing the interest of these cells (27). NKT cells were reported in other species such as humans and other primates and can be divided in two subsets: Type I NKT with an invariant TCRα-chain Vα14-Jα18 and Type II NKT which have more TCR diversity (27). These cells did not require MHC class II expression for their development but were reactive to the CD1d molecules (28). Both capacities to recognize MHCI molecules and their capacity to secrete cytokines suggest a distinct immunoregulatory function. γδT cells also are hybrid cells that are, for the most part CD8 and CD4 negative and their γδ TCR length and conformation resemble less to conventional TCRs but more to immunoglobulins (29). This observation seemed to imply that γδT cells recognize antigens as would an antibody instead of a conventional MHC/peptide/TCR complex recognized by αβT cells. Furthermore, the expression by γδT cells of the NKG2D activating receptor is similar to the one of NK cells. Stress antigen recognizing γδT cells functions include wound healing, removing of distressed and transformed cells and modulating excessive inflammation. Finally, these cells are of remarkable plasticity as they can undertake the role and appearance of professional antigen presenting cells (29). Part of this set of unconventional cells are the MAIT cells which are involved in multiple infection and non-infectious diseases. MAIT cell activation is innate-like rapid and is TCR-dependent but can also be independent. their TCR has a particular affinity for the microbial riboflavin-derivative antigens which is presented by MHC class II–like protein MR1 molecules (30). MAIT cell role in immunity is still to this date unclear.

G.1.2 Adaptive immunity or acquired immunity

The previously described innate immune system is fast acting but has the restriction of not being pathogen specific. In contrast, the adaptive immune system is slower in responding to an infection but will then involve cells that are highly specialized and are able to specifically recognize pathogens. A fraction of these cells will then be capable of forming a memory to a specific pathogen in order to reduce the response time to the same pathogen and to generate a stronger response upon a second encounter (31). The capacity of B and T cells to recognize specific antigens is ensured via the high frequency of gene rearrangement during the development of the B and T cell receptors (BCR and TCR) in these cell populations. This high diversity allows for a staggering number of possibilities: 10^{18} BCR and 10^{15} α:β TCRs are theoretically estimated (32,33).
B-lymphocytes are bone marrow maturing lymphocytes, involved in the humoral responses which are characterized by the production of antibodies by B cells and their progeny, plasma cells (34). The binding of

the BCR to a specific antigen will induce a first activation signal that along with the associated TLR signals and the cytokine costimulatory helper signal will cause the B cell to activate and to differentiate into plasma cells and secrete antibodies (35). Antibodies are 150KDa molecules composed of four structures: two “heavy” and two “light” chains which are linked to one another by disulphide bonds. The region which determines an antibody specificity is found at the N-terminus, called the antigen-binding site. Antibodies can be classified in five isotype classes: IgM, IgD, IgG, IgA, and IgE. They are distinguishable according to the C-terminus regions of the heavy chains which does not participate in antigen binding and is constant (34). Antibodies can work in three main ways to hinder pathogens: they are capable of binding to the target surface and neutralizing it. They can activate macrophages and other immune cells by binding to Fc receptors (FcRs) or finally by activating the complement system pathway by binding to C1q. Complementing their humoral role, B cells are considered as professional APC enhancing T lymphocyte-mediated immunity (36). Furthermore, they have the capacity to secrete pro-inflammatory cytokines which will impact T cell activation. Finally a population of B cells known as regulatory B cells (Bregs) is able to modulate the immune responses via IL-10 or IL-35 secretion (37,38).

The second major player of the adaptive immune system is comprised of T lymphocytes which can be subdivided into two major subgroups: CD8 and CD4 T cells. T cells first originate from thymocytes which are hematopoietic progenitor cells found in the thymus. These precursor cells will differentiate into T cells through the process of thymopoiesis. The cells will undergo a process of beta-selection, positive selection, and negative selection that will shape the cells into a set of T cells able to respond to foreign pathogens, while being immunologically tolerant towards self-antigens (39). The TCR is the key component that allows a T cell to recognize a foreign antigen presented to them by professional APC in the lymph nodes which will trigger T -cell activation (40). To be able to recognize a wide variety of peptides, each T cell has its own unique TCR, generated by the action of the recombination-activating genes (RAG) (41). RAG genes encodes for the RAG-1 and RAG-2 recombinase enzymes capable to generate DNA double breaks which initiate V(D)J recombination (42). CD8 T cell TCRs and co-receptor CD8 protein will bind to the MHC Class I molecules. CD4 T cell TCRs and co-receptors CD4 on the other hand can bind to Class II MHC molecules (43). Once activated T cells will undergo clonal expansion and will migrate to the site of infection where they will carry out their primary function which for CD8 T cells it will consist in cytotoxic functions (44). Helper CD4 T cells will contribute to cytotoxic T cell activation and growth, as well as B cell antibody class switching. Their helper capacity extends to the innate immune system were they can for example maximize bactericidal activity by macrophages (45–47). Beyond the helper function of CD4 T cells, direct cytolytic function by CD4 T cells is being presently investigated, with preliminary evidence already published (48,49). Furthermore, CD4 T cells can also assume a regulatory phenotype (T_{Reg}) whose purpose is to maintain peripheral tolerance, prevent autoimmunity and limit chronic inflammatory diseases. Their presence can be detrimental in some circumstances such as cancer as they suppress immunity and limit anti-tumor immunity (50).

G.2 CD4 T cell-mediated immunity

CD4 T cells were first discovered in 1960s (51) and named as such in 1970s (52). These cells have been the focus of extensive research as they are an essential part of the human adaptive immune response. Depending on the threat encountered these cells will be able to initiate an adapted response to the pathogen by helping CD8 cytotoxic T cells and B lymphocytes, as well as the innate immune system (53).

G.2.1 The development of CD4 T cells

T cell progenitors consist of hematopoietic stem cells that migrate from the bone marrow to the thymus. At this point these precursor cells lack the expression of CD4 or CD8 surface proteins and are called double negative (DN). Once they have reached the subcapsular zone in the thymus the lymphocytes will be rearranging their TCR γ, δ, α and β in order to form two linages of T cells: α/β or γ/δ. A cell with a correctly assembled receptor will be allowed to survive and transition to the next stage where it will become double positive (DP) as it will concomitantly express CD4 and CD8 surface proteins (54). At this stage cells express the master transcription factors RORγ, TCF-1 and LEF-1 without which the cell would dye (55–57). The functional cells will undergo positive and negative selections which consist of evaluating the capacity of the lymphocyte TCR to bind to the peptide-MHC (58).

Positive selection will consist of verifying the capacity of lymphocytes to bind to MHC complexes. MHC class I and class II will be loaded with peptides and in the case the T cell does not bind the MHC it will undergo apoptosis. On the contrary when the TCR binds to the MHC complex a survival signal is initiated and thus the cell will be positively selected. At this stage depending on whether the TCR bound strongly or not to an MHC class II complex the cell will commit to be a single positive (SP) CD4 T cell or a SP CD8 T cell, respectively. In fact, by binding to the MHC class II complex, intracellular signals will be sent inducing the upregulation or downregulation of master transcription factor such as ThPOK or Runx3. ThPOK will reduce the expression of Runx3 driving downregulation of CD8 expression; on the contrary if there is a poor TCR-MHC class II binding ThPOK levels will be low resulting in Runx3 levels to be high and drive upregulation of CD8. These genes will drive SP CD4 or CD8 T cell differentiation (59).

Lymphocytes should have the capacity to recognize a pathogenic antigen presented by the MHC but also tolerate our own cells thus the need for a negative selection process. As TCR's bind to a moderate degree to MHC and thus pass positive selection, cell whose TCR will bind too strongly to the MHC complex will be destined to be eliminated (60). It is believed that the cell death stems from a strong activation of the cells resulting in an activation induced cell death (AICD) (61). This system will eradicate immature lymphocytes that will most likely be self-reactive and attacking our own cells. Cell passing both selection stages will be allowed to leave the thymus and to circulate as mature T cells (54).

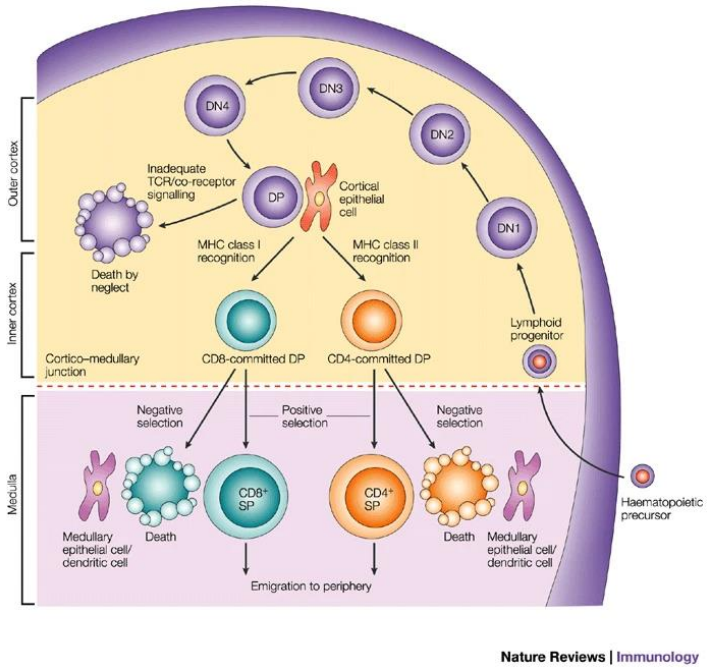

Figure 2: T cell development in the thymus. Lymphoid progenitors migrating from the bonne marrow to the thymus, will undergo a complex maturation process after which, if they pass amongst other a positive and a negative selection step, they will be ready for export to peripheral lymphoid sites as single positive cells. Adapted from (62).

G.2.2 Peptide-MHC molecules and antigen presentation

The TCR, a cell surface heterodimer, is the key component that allows a T cell to recognize a foreign antigen by recognizing sequences of peptides (called epitopes) that are presented by the MHC. The MHC is a cell surface protein found on all cells. The MHC complex holds in its peptide-binding groove the antigen epitope bound by T cells' TCR and subsequently trigger T-cell activation (40). The MHC gene family is divided into three subgroups: class I, class II, and class III (63). Class I MHC molecules have a α3 domain not present in MHC class II molecules, therefore they can only be recognized by CD8 co-receptors which binding domain is a conserved loop in the α3 domain. CD4 co-receptors can recognize class II MHC molecules as they can bind the MHC complex at the β2 and α2 domains (43). Class III molecules are Bf, C2, and C4 components of the complement system genetically located between class I and class II genes (64).

To be able to recognize a wide variety of peptides, each T cell has its own unique T cell receptor obtained through TCR rearrangement. Unlike most genes, which have a stable sequence in each cell which expresses them, the T cell receptor is made up of a series of alternative gene fragments. With the help of DNA-interacting enzymes, the DNA is cut and gene segments are put together which signifies that each T cell will have its unique TCR coded from a unique genomic sequence. Furthermore, the uniqueness of each TCR is reinforced by errors introduced during the cutting and joining process (41). This phenomenon will impact the type of peptide the TCR will recognize as well as which MHC it will recognize it from. The TCR will be able to discriminate between the MHC class I: HLA-A, -B, -C, which structure can accommodate peptides between 8–10 residues. The peptide is accommodated in the peptide binding groove of the MHC molecule and will be bound through conserved hydrogen bonds. These peptides are anchored to the MHC as well through the

peptide side chains at the P2 or P5/6 and PΩ residue sites (65). The assembly of the peptide-MHC class I complex happens within the endoplasmic reticulum (ER) where the high affinity peptide is loaded with the help of catalysing proteins such as Tapasin and the help of other chaperons before traveling to the cell surface (66). MHC class II molecules are encoded by the gene regions HLA-DR, -DP, -DQ, which in turn can accommodate longer peptides: from 13 to 25 residues. They are also bound within the MHC binding groove but the side chains are docked at the P1, P4, P6, and P9 MHC pockets (65). The loading of the peptide onto MHC class II will happen in late endosomal compartments. The loading process follows the following steps: firstly, the invariant chain, a protein folded with the MHC in the ER, is cleaved by cathepsin proteases. Secondly a short fragment called class II-associated invariant chain peptide (CLIP) will remain bound to the peptide-binding groove of the MHC class II (65). Lastly the CLIP peptide is replaced by a higher affinity peptide, this exchange will be accelerated by the HLA-DM complex or inhibited by the HLA-DO complex (67,68). The peptide-MHC class II complex will then migrate to the cell membrane.

The binding of the peptide within the MHC class II groove can assume different “registers”. The change of register refers to the possibility of one peptide assuming different binding modes by sliding through the MHC class II binding groove (69). Specific TCR may selectively recognise specific registers. One clear illustration is the one observed for the OVA (325-336) peptide that was found to bind to the I-A^d MHC class II with four different registers of which two resulted in a failed stimulation of T-cell hybridoma OVA (325-336) specific (70). The observation that T cells could not cross-recognise between different registers highlighted the possibility that TCR binding is affected by the position of the peptide within the MHC binding groove which results in distinct T cell responses. This type of shift might as well present an opportunity in exploiting cells that have the capacity to defeated central tolerance (69).

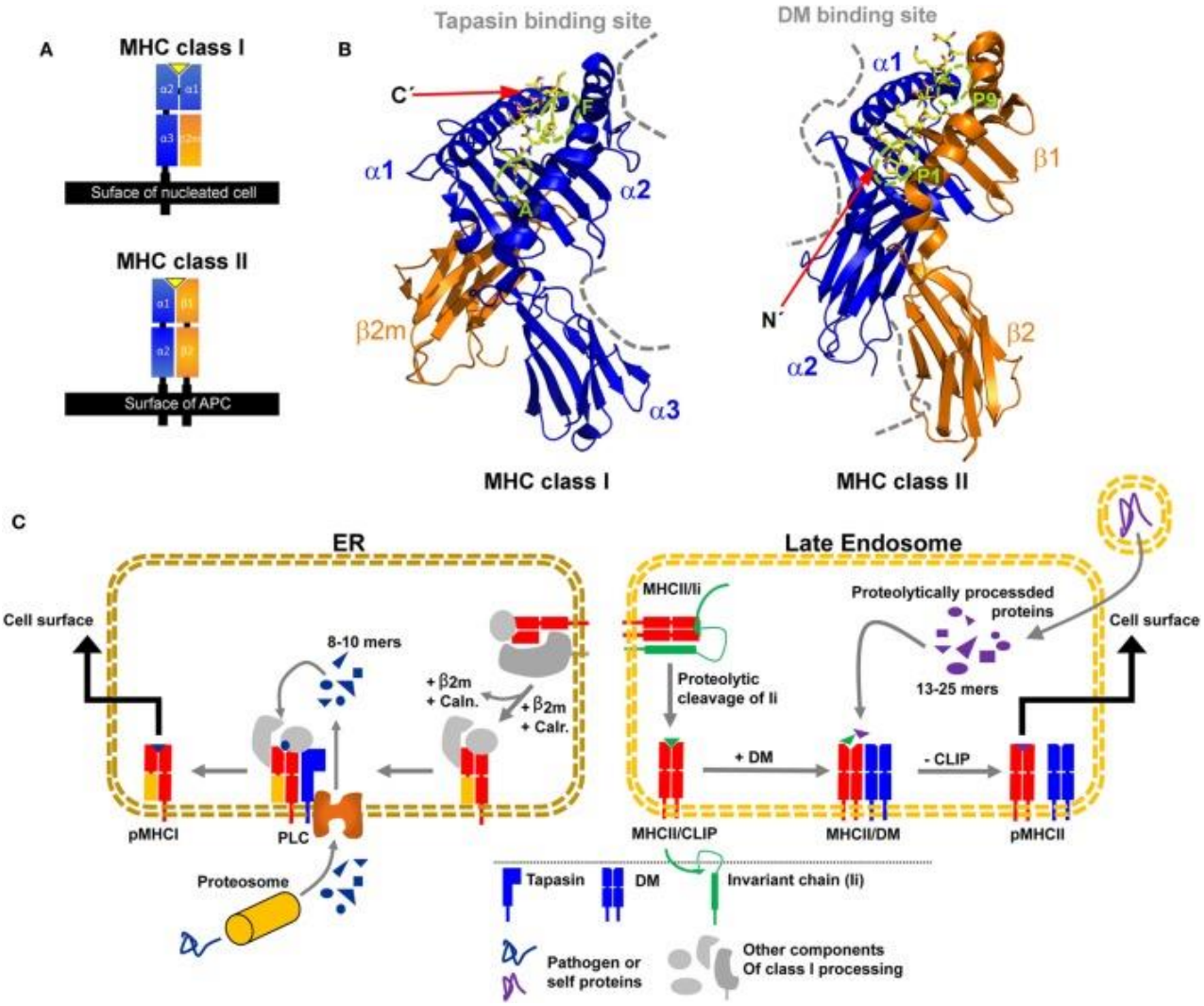

Figure 3: structural differences between MHC class I and class II molecules and peptide loading mechanisms. A) Structure representation of both MHC class I and class II molecules. **B)** Structures of MHC class I and class II molecules, respectively bound to a HIV- derived peptide and a hemagglutinin-derived peptide (in yellow). The binding pockets for these peptides are marked in green. Finally Indicated in grey are the binding sites for the catalyzing proteins either Tapasin or MHC-DM. **C)** a simplified representation of the processing steps required for the loading of high affinity peptides to the MHC class I or II complexes. Adapted from (65).

G.2.3 TCR structure and signaling

T cell receptors are composed of two polypeptide chains, each consisting of a constant (C) region and a variable (V) terminal region which contributes to the antigen binding domain. The exons encoding for the antigen binding domain are assembled from the V (variable), D (diversity), and J (joining) gene segments which by DNA rearrangement make up the complex process of V(D)J recombination (71). The V(D)J DNA region undergoes heavy editing where double strand breaks are introduced to delete or invert fragments and ligate segments together (72).The process is regulated as the genome rearrangement will start by the D and J joining followed by the V segment joining to the DJ segment. This recombination is what brings the great diversity among TCR structures enabling them to recognize theoretically up to 10^{15} different antigens (73).

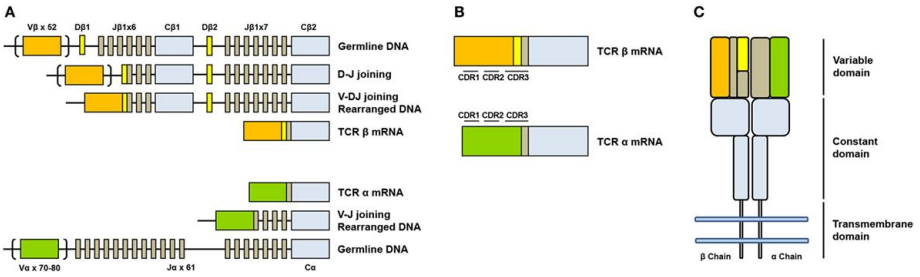

Figure 4: somatic V(D)J recombination of alpha and beta chains of the TCR complex. (A) Progressive and organized rearrangements of the V, D and J segments for TCR beta chains and V and J segments for the TCR alpha chains is guaranteed by recombination steps. **(B)** Subdivision of TCR variable region domains in CDR1, CDR2 and CDR3 regions. **(C)** Final TCR organization of the two subunits: constant region and variable region. Adapted from (74).

Structurally the TCR heterodimer is composed of TCRα and TCRβ chains, both of which have an extracellular domain (ECD) with variable (Vα and Vβ) and constant (Cα and Cβ) domains, a membrane proximal connecting peptide (CP) (75), a transmembrane segment and a cytoplasmic tail (76). The variable region of the TCR that will bind to the antigen presented by MHC complexes is made of hypervariable CDR3α and CDR3β loops (77). Despite their capacity in antigen recognition the two TCR subunits do not possess an intracellular signaling domain. It is thus associated in a noncovalent way to three dimeric signaling modules: CD3δε, CD3γε, and CD3ζζ in a 1:1:1:1 stoichiometry (78). The CD3γ, δ or ε subunits are composed of an extracellular immunoglobulin domain, a short CP, a transmembrane segment and intracellular immunoreceptor-tyrosine-based activation motifs (ITAMs). The CD3ζ subunit differs from the other 3 as it is composed of a short extracellular sequence and three ITAMs, as well as a transmembrane segment (79).

Upon peptide MHC (pMHC) binding to the TCR, the CD4 co-receptor molecule will bind to the pMHC and thus recruiting the LcK kinase to the TCR complex where it will phosphorylate ITAM signaling motifs. The phosphorylation of two tyrosines in the ITAM motifs will create binding sites for the tandem SH2 domains of the ZAP70 kinase (80). Once ZAP70 has been recruited and activated it will phosphorylate the linker for activation of T cells (LAT), which acts as a signaling hub as it has four major phosphorylation sites Y132, Y171, Y191, and Y226 which are implicated in downstream signaling (81,82). The Y132 site is implicated in recruiting PLCγ1 which will activate the Ras-MAPK pathway and provide calcium. The other 3 sites phospho-Y171, -Y191, and -Y226 will recruit Grb2 and Gads, adaptors to whom will bind the SOS and SLP-76 proteins which in turn will result in the activation of Ras, Raf and Rho GTPase effector responses (81,83–85). The combination of the activation of the Ras-GTPase and SOS protein leads to a rapid and bistable amplification of the Ras activation. Raf is activated by Ras leading to the MEK activation and ultimately the activation of the MAP kinase ERK (86). MAP kinase activates transcriptional regulators such as Elk which culminate in T cell activation (87). In addition to the LAT signalosome assembly and downstream activation, the TCR and the CD28 costimulatory molecule activate PI3K. By a chain of phosphorylation's starting from PI3K on phosphatidylinositol 4,5-Bisphosphate (PIP_2) followed by phosphatidylinositol (3,4,5)-trisphosphate (PIP_3) the ITK kinase can be recruited to the plasma membrane (88). The pleckstrin homology (PH) domain of PIP_3 is used by ITK to bind to. So, SPL-76 will bind to ITK through its SH3 domain. These interactions will localize

ITK at the plasma membrane and cause its activation. Activated ITK can phosphorylate PLC-1 resulting in its activation. PLC-1 activation will result in the hydrolysis of PIP_2 to generate secondary messengers' inositol 1,4,5-trisphosphate (IP_3) and diacylglycerol (DAG). At this point IP_3 is no longer bound to the membrane but is free to diffuse in the cytoplasm where it will bind to its receptor IP_3R found in the ER. The binding to its cognate receptor will result in the release of Ca^{2+} stored in the ER. Ca^{2+} will cause an influx of extracellular calcium through plasma membrane channels. High levels of Ca^{2+} in the cytoplasm have per effect to activate many proteins such as the transcription factor NFAT (80) leading to T cell activation. Two further mechanisms are able to regulate gene expression after TCR engagement and they are the PKCθ-IKK-NF-κB pathway and the TSC1/2-mTOR signaling pathway. DAG is the trigger for PKCθ signaling through the C1 lipid binding domain (89). PKCθ will cause the formation of a tri-molecular complex called the CARMA1/Bcl10/MALT1 (CBM) complex by phosphorylating each of the adaptor molecules forming the complex (90,91). The complex will recruit tumor necrosis factor receptor-associated factor 6 (TRAF6) to degrade the regulatory protein of the IKK complex the IKKγ, or NF-κB essential modifier (NEMO) (92,93). This release of inhibition will results in the phosphorylation of IκB inducing it's ubiquitination and degradation, as a result NF-κB is released and translocated into the nucleus to regulate gene expression (94,95). Finally upon TCR engagement PI3K-Akt and DAG-RasGRP1-Ras-Mek1/2- Erk1/2 pathways will activate both mTORC1 and mTORC2 (96). This activation pathway has been linked with the regulation of effector CD4 T helper cell generation (97).

To ensure that the TCR responds to appropriate ligands and for the proper duration a negative regulation of the TCR signaling exists, which is regulated by either TCR-generated signals or stemming from other surface receptors. As a few examples, the SHP-1 phosphatase dephosphorylates Lck and thus blocks further phosphorylation within the complex. This will allow phosphatases such as SHIP-1 and CD45 to dephosphorylate unprotected sites leaving only a partial ζ domain phosphorylation (98). The well-known Cytotoxic T-lymphocyte-associated antigen 4 (CTLA-4) inhibitory receptor binds to CD80 and CD86 which results in the recruitment of the phosphatase SHP1 and PPA2 to inhibit TCR signaling (99). The equally known programmed cell death protein 1 (PD-1) inhibitory receptor binds to the PD-L1 and PD-L2 ligands and results in the recruitment of SHP1 inhibiting as well TCR signaling (100).

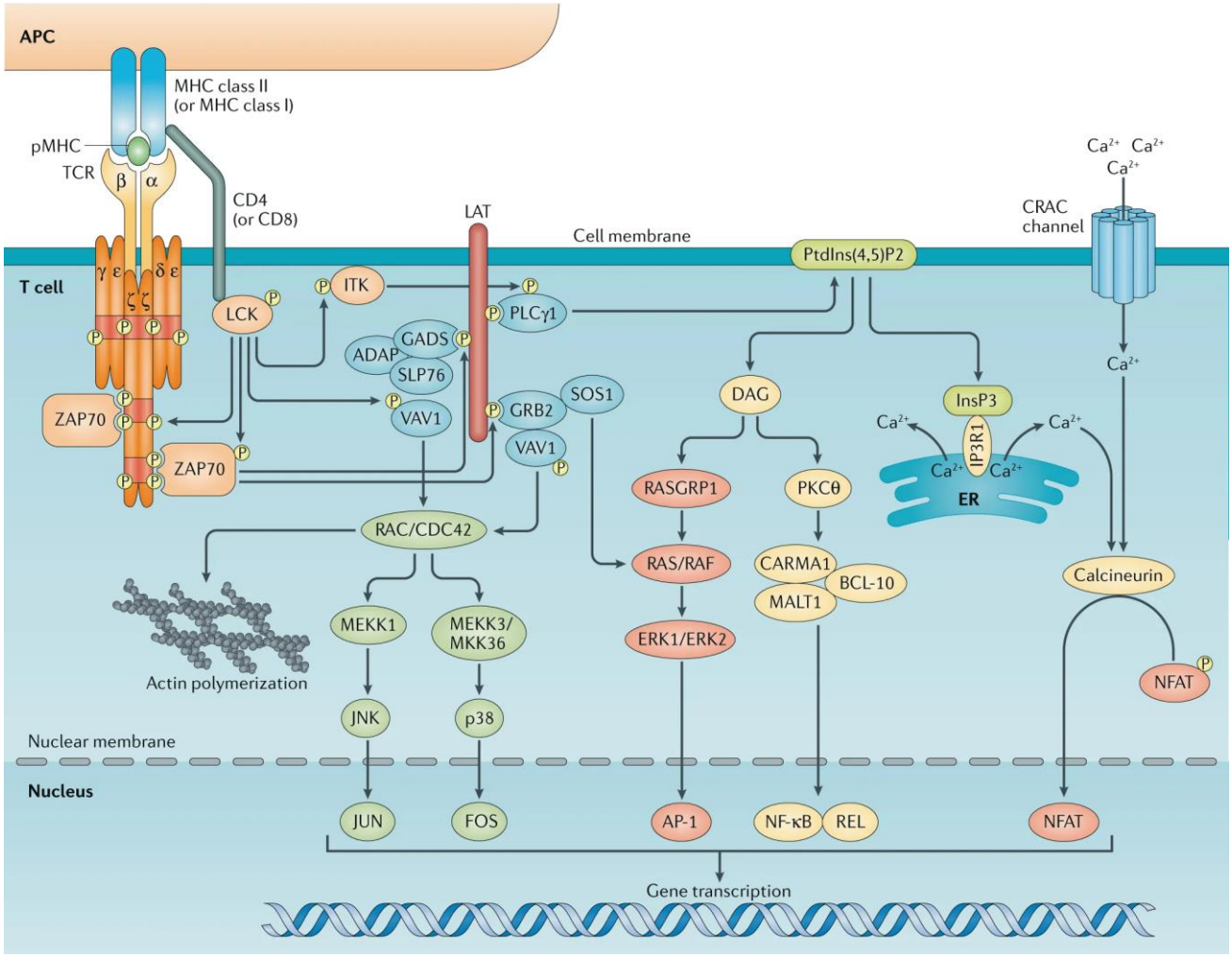

Figure 5: representation of the major TCR signalling pathways. Upon binding of the peptide MHC complex to the TCR a signalling cascade will ensue resulting in the activation of DNA transcription factors such as NF-κB, NFAT, FOS, JUN and AP-1. Adapted from (101).

G.2.4 TCR-pMHC interaction

The interaction between TCR and the pMHC complex is key to T cell activation and therefore for a robust protective response against pathogenic occurrences. The TCR is highly specialized in recognizing multiple pMHC yet can discriminate between pMHC even if there is only one amino acid that is different. Once the recognition of a pMHC occurs there is the formation of a immunological synapse: a contact point between the T cell and the APC involving the TCR and pMHC complexes as well as associated co-receptors, integrins and varied signaling proteins (102). The result is a complex signaling cascade resulting in T cell activation as explained in the previous chapter. The current advances in the field of TCR and pMHC interaction stem from a large number of crystallographic studies. The point of interaction between the TCR and the pMHC resides in the variable loops CDR1 and CDR2 coded by 42 Vα and 46 Vβ genes, respectively (103,104). The randomly joining of V and J in the TCRα chain or by V, D and J in the TCRβ make up the third variable loops CDR3. Crystallographic study suggested the presence of the CDR3 region to be in the centre of the binding site where it comes into contact with the peptide. The CDR1 and CDR2 loops on the contrary are located on the side regions of the TCR which make contact with the MHC complex in specific and conserved way (105). On

the TCR the CDR2 loops of the α and β subunits only gets in contact with the MHC structure, on the contrary the CDR1 and CDR3 loops get into contact with both peptide and MHC atoms (106).

The portion of the TCR coming into contact with the pMHC is relatively flat, sometimes with a central cavity. On the other hand the MHC surface contains two high peaks which allows it to achieve a large interface to which the TCR can bind best (107). At the opposite, one could imagine that not all amino acids bound to the MHC are in contact with the TCR. In fact, only one-third of the peptide surface is not occluded and available to be recognized by contact to a TCR. TCRs contact from 5 to 7 of a span of 8 residues of MHC class I bound peptides (8-mers and 9-mers) and from 6 to 7 of a span of 9 residues of MHC class II bound peptides (13-mers and 16-mers) (106). It is understood in the field that the affinity of a CD4 T cell TCR for a pMHC class II is weak in comparison to CD8 T cell TCRs, respectively K_D =13 µM and K_D=52 µM (108). Despite this weak protein to protein binding affinity it has been raised that in regards to CD4 T cells the low-affinity cells are major responders in the primary immune response (109).

Upon formation of the immune synapse the co-receptors are recruited, in the case of T helper cells it is the CD4 co-receptor that will interact with class II pMHC. CD4 proteins are transmembrane glycoproteins consisting of four Ig-like extracellular domains, a short stalk linking them to the transmembrane domain and a cytoplasmic tail that interacts with Lck (110). The CD4 binds MHC class II through its membrane-distal D1 domain which binds the α2 and β2 domains of the MHC class II molecule. Although there is a great polymorphism among MHC class II molecules (HLA- DR, -DP, and -DQ alleles) the region to which CD4 binds the MHC is relatively conserved. For the β-chains, 11 of 12 residues are absolutely conserved and for the α-chains, all three CD4-contacting residues are conserved among all human MHC class II alleles resulting in a cross-reactivity of CD4 to MHC class II proteins (110). On the contrary to pMHC class I complex which are stabilized by the CD8 complex to the TCR, the pMHC class II complex cannot rely on such help as the dissociation constant (K_D) between the CD4 protein and the pMHC complex has been evaluated to be between K_D 150 and 200 µM compared to CD8 co-receptor having a K_D of 10 to 200 µM for the pMHC class I (111). Despite this low affinity for the pMHC class II by the CD4 co-receptor its involvement remains highly important for the efficient phosphorylation of adjacent TCRs thanks to its protein kinase $p56^{lck}$, therefore contributing to CD4 T cell activation.

G.2.5 Tools for the evaluation of TCR specificity

Ever since their first usage more than 20 years ago (112), fluorescent multimerized pMHC molecules have been used and evolved to detect antigen-responsive T cells, from the first tetramer staining (112), to the first use of a pMHC microarray allowing cell-capture based on specificity (113,114), to the use of heavy metal ions as tags in mass cytometry which increased the number of specificities up to 109 (115), to the new approach utilizing a combination of fluorochromes to label either in a dual color code (116), or with a multivalent code (115) pMHC class I multimers, or using panels of more than 100 pMHC class I DNA-barcoded multimers (117).

Novel tools also include NTAmers, which are pMHC class I multimers built on NTA-Ni^{2+}-His-tag interactions that upon addition of imidazole instantly decay in their constituents. By using Cy5 labelled pMHC molecules, NTAmers allow measurements of pMHC monomer dissociation kinetics on CD8 T cells (118).

Despite all the advances made in epitope-specific detection with pMHC class I multimers, little progress has been made with pMHC class II molecules. This is linked with the CD4 molecule not greatly increasing pMHC binding avidity, the overall lower affinity between TCR and MHC class II complexes, the conformational diversity of pMHC complexes, the high polymorphism of HLA-DP, -DQ, -DR molecules and the poor quality of class II multimers linked to technical difficulties in the generation of these reagents (119). Recent advances have improved pMHC class II multimers: the addition of a leucine zipper instead of the transmembrane and cytoplasmic domains to prevent dissociation of the alpha and beta chains (120), the addition of a C-terminal His-tag, which allows gentle affinity purification of the complexes (121), the use of conditional peptide tags to improve the degree of peptide loading (122), or the linking of the peptide to the beta chain via a long and flexible linker (123). These advances have led to improved staining of antigen-specific CD4 T cells as demonstrated in a recent publication which used a combinatorial pMHC class II tetramer staining to successfully visualize up to 6 different CD4 T cell specificities after vaccination with the seasonal flu shot in rheumatoid arthritis patients (124). To ameliorate detection of low affinity cells, new structures are being developed using large backbones such as dextran to increase the number of single pMHC class II monomers that can interact with TCR structures, thus increasing avidity (125).

G.2.6 CD4 T cell priming and differentiation

Once a CD4 T cell leaves the thymus, it will circulate in the body until it will recognize via their TCR, in the secondary lymphoid organs, an antigen presented by the MHC complex at the surface of an APC cell. Upon formation of the immune synapse a first signal of activation will be transmitted to the cell core of the CD4 T cell (126). The secondary signal necessary for T cell activation is provided by co-stimulatory molecules such as CD28 on T helper cells which will bind to the B7.1 (CD80) or the B7.2 (CD86) APC surface proteins, that will launch CD4 T cell proliferation. This vital signal for T cell activation can be inhibited by the expression of CTLA-4 (CD152) at the surface of T cells and will compete for B7 binding thus reducing T cell activation (127). T cells will also rely on survival signals which are transmitted to the cell upon recognition of foreign antigens. These signals are given by T cell surface proteins such as ICOS, 4-1BB and OX40 binding to their respective ligands ICOSL, 4-1BBL and OX40L presented by APC cells following pathogen recognition (127). The third signal resides in the cytokines found in the microenvironment surrounding the CD4 T cell (128). These will determine the polarization of CD4 T cells and the function they will have (see next sub-chapter). The result of these 3 signals will lead to CD4 T proliferation and activation.

Upon antigen recognition naïve T cells will become activated and will change their expression of various homing molecules resulting in a cell with effector functions, migrating to the infection site (129). Once the

pathogen has been eradicated, the majority of effector cells (90 to 95%) will die by apoptosis. Only a few of a heterogeneous pool of T cells will be left behind, which will compose the "memory" reservoir of T cells. The memory cells are divided into two distinct groups based on their effector function, proliferative capacity, and migration potential. These subsets are named: central memory T cells (T_{CM}) and effector memory T cells (T_{EM}). On the one hand, T_{CM} are characterized by their ability to extensively proliferate, they express CCR7 and CD62L (L-selectin) and produce interleukin (IL)-2. On the other hand T_{EM} are less proliferative, they do not express CCR7 and CD62L but are capable of producing effector cytokines such as IFNγ (130). Neither of these subsets express CD45RA on the contrary to Naïve cells. Their localization differs as T_{CM} are predominantly found in secondary lymphoid organs and T_{EM} in peripheral compartments and have immediate effector functions (130,131). Memory T cells can persist for a lifetime in the absence of antigen and even MHC molecules. In addition to these two main memory subsets there are others which have been described such as the T_{SCM} population with retains a stem cell-like property and a naïve phenotype as they express CCR7, CD45RA, CD62L, CD27, CD28 and IL-7Rα. They can be distinguished from naïve cells as they express the two additional markers CD95 and CD58 (132). These cells have been shown to have a strong self-renewal capacity and multipotent ability to generate all memory subsets including T_{CM}, T_{EM} and effector cells. T_{SCM} are viral and self-tumor antigen specific which has been used to efficiently reconstitute immunodeficient hosts and mediate superior antitumor responses in mouse models (133). The T "transitional" memory (T_{TM}) cells are found in the peripheral blood of healthy individuals. T_{TM} do not express CCR7 or CD62L but do express CD28. As the phenotype of T_{TM} and the magnitude of proliferation in response to IL-15 , T_{TM} cells have been characterized as more differentiated than T_{CM} but not more than T_{EM} cells (134). The administration of IL-15 will result in the expansion of a subset of T_{EM} cell that will re-express the CD45RA marker, these cells are called terminal effector (T_{TE} or T_{EMRA}) (135). T_{TE} cells will therefore express CD45RA but none of the other markers such as CCR7, CD27, CD28 or CD62L. They are often considered as terminally differentiated cells as they express markers of senescence such as KLRG-1, CD57 and phosphorylation of histone H2AX as well as by having low proliferative and functional capacity (134). Finally, an additional population of memory T cells has been identified within barrier tissues such as mucosal surfaces and epithelia. As they are non-circulating cells, they have been called tissue-resident memory (T_{RM}). Due to their strategic localization T_{RM} cells are capable to rapidly respond to antigens and execute immediate effector functions. The expression of adhesion molecules like CD44 and CD69 will help the cell to remain in the peripheral tissues as will the downregulation of CD62L and CCR7 proteins (136). These multiple subsets of differentiated CD4 T cells might be formed following one of the multiple suggested differentiation mechanisms. One of these is the "*one cell one fate",* were one naïve T cell gives rise to either memory or effector cells (137). Or the "*one cell multiple fates",* were one Naïve T cell gives rise to both memory or effector cells. This second differentiation model regroups three proposed models which try to explain T cell differentiation into memory and effector cells. The *asymmetric division model,* where upon formation of an immunological synapse between APC and T cells, asymmetric

division will give birth to two daughter cells with different fates. The *signal strength model,* where the strength of the three activatory signals necessary for T cell activation will determine the amplitude of expansion and the fate of the primed T cell. Finally, the *decreasing-potential model* where upon the repeated encounter of antigens, T cells will differentiate towards more differentiated cells culminating with terminal effector cells (137). This model is thought to follow a linear progression along the major subsets T_N, T_{SCM}, T_{CM}, T_{TM}, T_{EM}, and T_{TE} depending on cell proliferative capacity and loss of function (134).

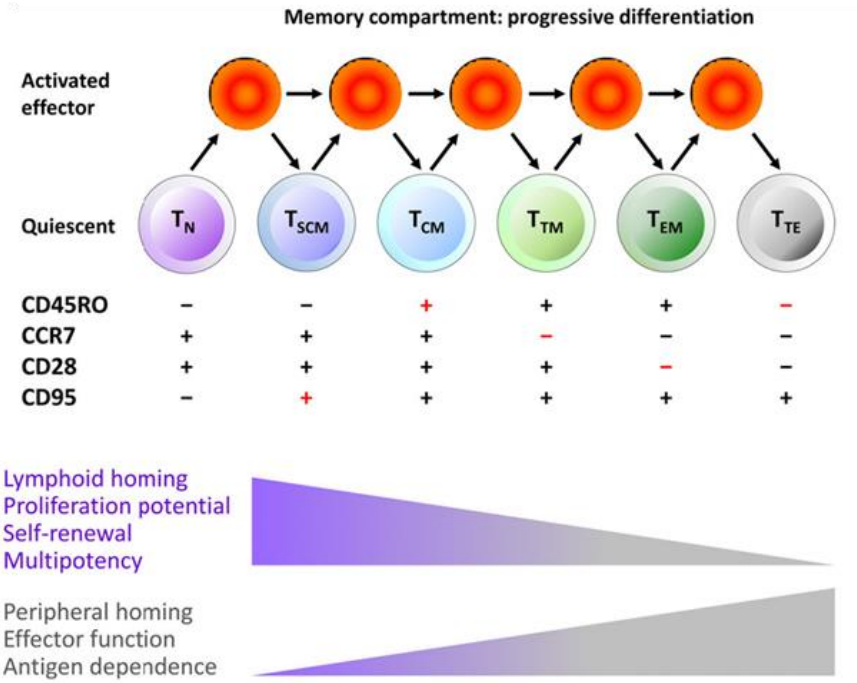

Figure 6: faith of the Naïve T cell upon priming. Representation of the linear progression of major T cell subsets with their loss of proliferation potential and the increase of their effector function. Adapted from (134).

G.2.7 CD4 T cell polarization and plasticity

After antigen stimulation of CD4 T cells not only will they go through the differentiation process described above, but they will acquire a defined functional, highly plastic cell fate influenced by the microenvironment (138). CD4 T cell subsets can be characterized by the expression of lineage defining master transcription factors, distinct cell surface markers and by the secretion of unique sets of cytokines. Distinguishable CD4 T cell subsets include Th1, Th2, Th17, Th17-Th1, Th22, Th9, T follicular helper cells (Tfh), T regulatory (Treg) and T cytolytic (ThCTL) (139–142). **Table 1** depicts a picture of the multiple facets of CD4 T cell polarization: the sets of activating cytokines present in the microenvironment around the T cells will send distinct signals resulting in the expression of master transcription factors. The T cells will then acquire a phenotype characterized by sets of cell surface markers and the secretion of sets of cytokines with a precise end goal. Effector cytokines produced by polarized CD4 T cells will contribute by positive feedback to increase the differentiation of further naïve T cells while inhibiting the polarization of opposing subsets (143). As an example, Th1 cells producing IFNγ will inhibit Th2 cytokine production and therefore Th2 commitment. In the same manner IL-4 production will inhibit IFNγ and IL-12 production thus inhibiting Th1 commitment (144).

The fate of one CD4 T cell is not unchangeable, in fact it is now well known that these different CD4 T cell subsets own substantial heterogeneity and plasticity which means that a Th cell can share characteristics of other Th cells and potentially lose its original feature and transition to another Th subset (145). As an example Th17 cells have been extensively studied as they have the capacity to acquire Th1 phenotype under chronic inflammation, but also can regulate the resolution of the immune response by converting to Tregs (146). This flexibility of T cells stems from a flexible expression of multiple master regulators. It is now believed that master regulators such as T-bet and GATA3, transcription factors for respectively Th1 and Th2 commitment, can be co-expressed as in post-viral infection in Th2 cells resulting in Th2+1 cells which feature both Th1 and Th2 cell characteristics (147). The expression of the multiple master transcription factors is controlled positively and negatively by factors such as the STAT DNA binding protein family. On the contrary to cytokine receptors which can be downmodulated, STATs are not differentially expressed among different subsets and their action can be redundant. For example, T-bet expression is driven by IL-12 acting via the STAT4 pathway. Th2 cells are resistant to the effect of IL-12 as they downregulate the IL-12 receptor. However, T-bet expression can still be induced via type I IFNs acting via the STAT1 signaling pathway resulting in the repolarization of Th2 cells in the setting of viral infection (148). Stemming from these few examples it would be naïve to believe that a simple transcription factor is all that regulates a T helper cell subset. It is more likely that complex cellular decisions are regulated by multiple transcription factors working in concert.

CD4 T CELL POLARISATION	ACTIVATING CYTOKINES	MASTER TRANSCRIPTION FACTORS	PHENOTYPE	CYTOKINE EXPRESSION	PRIMARY FUNCTION
TH1 T HELPER TYPE 1	IL-12 IFN-γ	Tbet, STAT4	CXCR3+	IFN-γ TNF-α and β	Production of pro-inflammatory cytokines; cell-mediated immunity
TH2 T HELPER TYPE 2	IL-4 IL-2	GATA3, STAT6	CRTH2+ CCR4+	IL-4, IL-5 IL-13	Production of anti-inflammatory cytokines; promote allergic response; evoke strong antibody response
TH17 T HELPER TYPE 17	TGF-β, IL-6, IL-21, IL-23	RORγt, STAT3	CCR6+ CD161+	IL-17, IL-21 IL-22, IL-26	Respond to bacteria, fungi, and viruses; Auto-immune diseases
TH17-TH1 T HELPER TYPE 17/1	IL-12	RORγt, T-bet	CXCR3+, CCR6+, CD161+	IFN-γ, IL-17	Contributions to inflammation and autoimmunity
TH22 T HELPER TYPE 22	IL-6	BNC2, FOXO4, AhR	CCR4+ CCR10+	IL-22	Mucosal immune response; inflammatory diseases; barrier defence
TH9 T HELPER TYPE 9	TGF-β IL-4	PU.1, IRF4	CCR6+	IL-9	Humoral immunity through B cell interactions; functions on many cell types including mast cells and other CD4 T cells
TFH FOLLICULAR HELPER T CELLS	IL-6 IL-21	BCL6, IRF4	CXCR5+ ICOS+	IL-4 IL-21	Antigen specific B cell immunity
NTREG NATURAL REGULATORY T CELLS	TGF-β IL-2	FoxP3, STAT5	CD25+ FOXP3+	TGF-β IL-10	Maintenance of self-tolerance
THCTL T CYTOLYTIC	IL-2	EOMES	?	Granzyme B, Perforin, FASL	Killing of infected cells

Table 1: Summary of CD4 T cell polarization. Each CD4 T cell polarization can be defined by the presence of cell surface molecules, a master transcription factor and an array of produced cytokines. The polarization of the CD4 T cells is influenced by the set of cytokines and other molecules present in the environment. Table compiled from (139–142)

G.2.8 microRNA involvement in CD4 T cell differentiation and polarization

As each CD4 T cell secretes sets of defined cytokines they also are unique by their microRNAs (miRNAs) profiles, that undergo specific changes when a naïve T cell respond to specific TCR-mediated activation and commit to a defined cell fate (149). miRNAs are small non-coding RNAs found in many organisms including humans and mice whose function is to regulate the expression of protein-encoding genes at the post-transcriptional level. The production of miRNA starts with the polymerase II which transcribes what is called a primary transcript (pri-miRNA), which is composed of two paired sequences linked by a stem-loop structure and can be the size of several hundred nucleotides to several kilobases. The stem-loop is cleaved in the nucleus by RNAse III family nucleases Drosha and Pasha and releases a 60- to 110- nucleotide pre-miRNA hairpin precursor (150). The newly formed pre-miRNAs are exported to the cytoplasm via a RanGTP/exportin 5 dependent mechanism (151). In the cytoplasm the Dicer enzyme will further process the miRNA by cleaving the loop holding the two sequences together thus releasing the duplex in single 19- to 22- nucleotide mature miRNA. The miRNA will be incorporated into the RNA-induced silencing complex (RISC) which can direct the cleavage and/or translational repression of messenger RNAs (152,153). The belief that repression of messenger RNAs is the only function of miRNA is far from the truth. It is becoming evident that miRNAs have also nuclear functions as they might be positively activating genes or inhibiting their transcription, block maturation of non-coding RNAs, affect alternative splicing (154–158). Other functions of miRNAs within the nucleolus such as affecting ribosomal RNA maturation are controversial (158).

Previous studies have shown the central role of miRNAs in regulating the development and homeostasis of the immune system. By using mice deficient for genes involved in the maturation of miRNAs a deregulation of differentiation was reported, as Dicer-deficient CD4 Th2 cells switched into Th1 (159). Similarly, the induction of Treg cell differentiation is influenced by a miR network including miR-99a and miR-150 which cooperates to repress the expression of the Th17-promoting factor mTOR (160). The critical impact on CD4 T cell differentiation that miRNAs have was further demonstrated when the involvement on Th17 differentiation of miRNA-18a was identified (161). The presence of miRNA-18a limited Th17 differentiation and upon the use of inhibitors for this miRNA the expression levels of CCR6 and the master transcription factor RORγt increased in mouse and human CD4 T cell resulting in increased numbers of Th17 cells. The expression levels of one miRNA was shown to influence the outcome of Th cell differentiation. By modulating the expression of miRNA, it was possible to modulate not only the formation of one cell subset but multiple processes such as the T cell cycle, survival and memory T cell differentiation. In fact the elimination of miRNA -15/16 family showed such an impact (162). Yet, a clear view on targetable miR candidates influencing human CD4 T cell differentiation is still lacking. Since T_{SCM} have gained increased interest in cancer immunology due

to their stem cell like nature (163), the targeting of miRs to influence the differentiation of CD4 T cell could be very beneficial to cancer immunotherapy (164). In fact the transfer of T_{SCM} in a humanized mouse model mediated superior antitumor responses as they had a long-term persistence in the host and high proliferative capacity (133). A key to using these cells is to understand the epigenetic modification, including miR expression, that could mediate T_{SCM} induction or maintenance.

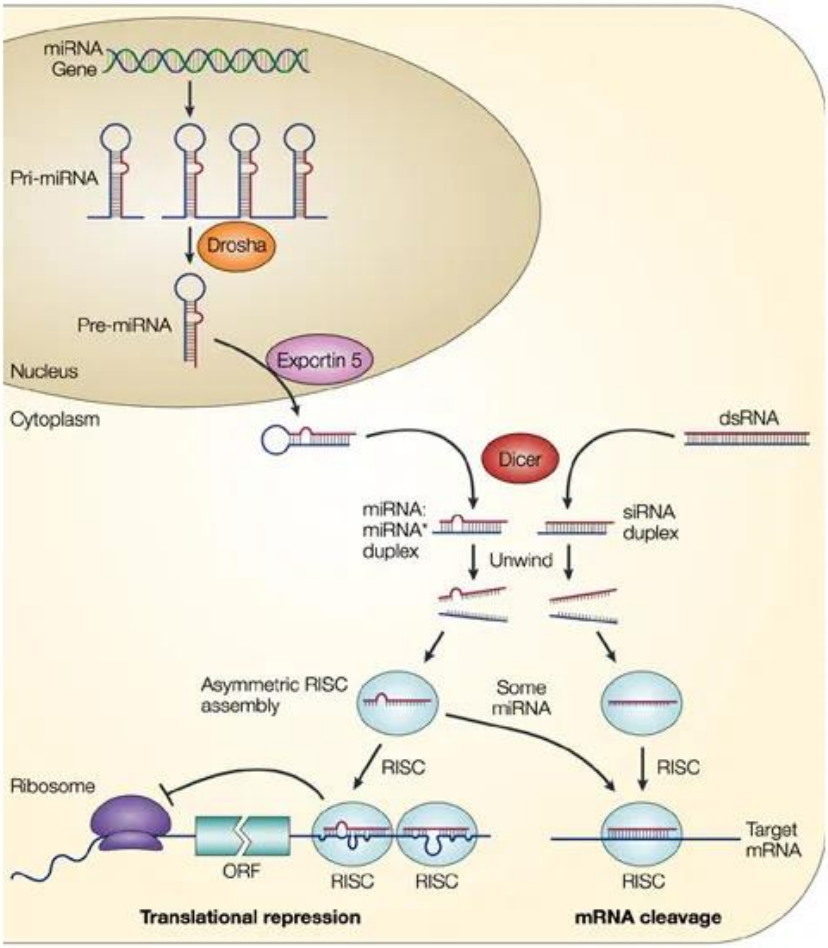

Figure 7: Current model on the microRNA biogenesis and post-transcriptional suppression of mRNA. Initially starting as Pri-mRNA transcripts they are processed into pre-mRNA which are in turn transported to the cytoplasm by Exportin 5. In the cytoplasm double strands from Pre-miRNA as well as dsRNA are released through the action of Dicer complexes. This process will give rise to miRNA or siRNA. One of the strands of either miRNA and siRNA will be assembled in RISC complex and will target mRNA through translational repression or mRNA cleavage. Adapted from (165).

G.3 Cancer immunity

The immune system was primarily shaped to discriminate between self and non-self. This ability confers the immune system the capacity to protect the host against invading pathogens such as viruses, bacteria and fungi with at the same time the capacity to tolerate host cells. Tumor cells being self-derived and T lymphocytes undergoing negative selection there is a limited set of antigens to which lymphocytes can respond to in case of tumor formation. Despite this limitation there is a recognition and an attack by lymphocytes on tumor cells (166). However, the antitumoral immunity is often insufficient to reject established neoplastic lesions. This goes in line with the three Es theory of cancer immunoediting: elimination, equilibrium and escape (167), where the elimination phase is indeed when cancer cells are

eliminated by cells of the innate and adaptive immune system. “Equilibrium” when the cancer cells that have not been eliminated are constantly subjected to selection pressure which contains them but does not eradicate them completely. And the last E is the Escape phase resulting from the selective pressure when mutant cells with resistance to immune detection and/or elimination will be able to expand. To avoid both the innate and adaptive immune system, tumor cells can make use of several immune evasion strategies.

G.3.1 Cancer recognition by the innate immunity

The last two decades have provided a large number of studies supporting the role of the innate immune system in controlling cancer. For early control of viral infection NK cells are important due to their capacity in killing target cells without prior encounter. Their role has also been observed in regards to the surveillance of malignant transformation induced by carcinogen or transplanted tumors (168,169). Clinical evidence in cancer patients has suggested that tumor biopsies which have NK cell infiltrates are associated with a favorable prognosis (170). Direct tumor lysis by NK cells is believed to be principally perforin mediated but can also be mediated through death receptor-mediated pathways such as TRAIL and FasL (171,172). Amongst other ways NK cells can kill their target, they can bind via the CD16 membrane protein to Fc regions of antibodies bound to tumor cells and provoke an antibody dependent cell cytotoxicity (ADCC) event (173). Upon activation NK cells are powerful cytokine producers and secrete TNFα and IFNγ amongst other cytokines. IFNγ is thought to have anti-tumor activity as it induces MHC class I expression sensitizing tumor cells to CD8 T-cell killing (174). The further combination of IFNγ and TNFα cytokines can drive senescence of tumor cells (175). By secreting multiple cytokines NK cells will not only act directly on tumor cells but also indirectly by modulating the activity of other leukocytes.

Besides NK cells, cells such as macrophages are highly present in the tumor stroma. Myeloid cells are highly plastic resulting in different effector functions depending on the signals they receive from the environment. As described in chapter G.1.1, macrophages can be divided into two subtypes M1 and M2. The M1 macrophages are considered to be pro-inflammatory, inhibiting angiogenesis and supporting the adoptive immune response. Inversely M2 macrophages support angiogenesis and are immunosuppressive (176). Macrophages found in the tumor bed are known as Tumor-associated macrophages (TAMs). They have been associated with a poor prognosis for patients as they facilitate angiogenesis, immunosuppression, and inflammation thus promoting tumor growth (177).

DCs with their two main populations pDCs and conventional DCs have a part to play in tumor immunity. The environment in the tumor site will influence DC functions like it does for macrophages. A lack of T cell costimulatory signals is observed in DCs in a immunosuppressive microenvironment as well as an expression of inhibitory PD-L1 molecules and IDO (178). PAMP molecules are needed in order to achieve a pro-inflammatory phenotype by DCs and induce an protective T cell response. Yet PAMPs are lacking in the tumor environment. However, DAMPs can be released upon immunologic cell death (ICD) of tumor cells resulting

in the activation of DCs. To boost the immune response against tumor cells ICD can be induced by treatment of tumor cells with cytotoxic anti-tumor therapy. This process is a double edged sword as the release of DAMPs may promote the development or progression of tumors as a result of triggered chronic inflammation (179).

G.3.2 Cancer recognition by the adaptive immunity

Similarly to the innate immunity several components of the adaptive immunity can either eradicate cancer cells or promote their proliferation (180). The adaptive immunity will aim to target antigens specific of tumor cells by the usage antibodies, B cells, T cells. Despite tumors being part of self, cancer derived peptides such as cancer-testis antigens (i.e. NY-ESO-1), differentiation antigens (i.e. Melan A) do exist (180). Furthermore frequent mutations within tumor cells will result in the formation of neoantigens which will be phagocytosed by APC cells or pinocytosed by DCs (180). After processing, exogenous peptides will be presented by MHC class II molecules and endogenous peptides will be presented by MHC class I molecules (181). Peptides bound to MHC class II will be presented to CD4 T cells resulting in their subsequent activation and proliferation. Activated CD4 T cells can mediate the activation of naïve B cells within the lymph nodes which subsequently will secrete antibodies which can bind to tumor-derived antigens (182). The binding of antibodies will initiate ADCC or Complement-dependent cytotoxicity (CDC) dependent lysis of tumor cells (182). Similar to CD4 T cell activation, CD8 T cells will also become activated upon interaction with tumor-derived peptides presented by MHC class I molecules. CD8 T cell will traffic to the tumor bed where they will exert cytotoxicity, release inflammatory signals and tumor antigens to feed the cycle of antigen presentation (180). Despite the action of both the innate and the adaptive immune system, it is often not enough to control and eradicate tumors.

CD4 T cell subsets can be characterized by the expression of lineage defining master transcription factors, distinct cell surface markers and the secretion of unique sets of cytokines as described in chapter G.2.6. All subsets of CD4 T cells can be found in the tumor core and at its margins; however, the presence of certain CD4 T cell subpopulations have been associated with distinct clinical outcome in cancer patients. In the meta-analysis performed by Fridman et al., the presence of Th1 polarized CD4 T cells was linked with a good prognosis in most cancer types such as melanoma, head and neck, breast, bladder, urothelial, ovarian, colorectal, renal, prostatic and lung cancer (183). Th1 cells have been linked with the generation and maintenance of effector cytotoxic CD8 T cells tumor specific and memory T cells through the licensing of dendritic cells through CD40-CD40L interactions (184,185). Th1 also have been described as capable of recognizing neoepitopes and were successful in recent vaccination trials (186–188). The recent discovery of the Th9 subset was also linked with favoring anti-cancer immunity and tumor elimination as these cells activate both innate and adaptive immune responses (189). Tfh cells seem to possess anti-tumoral activity since their presence was associated with the augmented CD8 T cell responses and an impairment of tumor

growth in mice (190). On the contrary in the presence of CD4 Th2, Th17 or Treg polarized cells, a poor prognosis was observed in the majority of tumors probably because of inhibition of cytotoxic responses and tumor control (191,192), with some exceptions. Indeed, Th2 cells have been associated with a favorable prognosis in Hodgkin's lymphoma and breast cancer, Th17 cell presence in esophageal and gastric cancer is associated with better survival and Treg presence associates with favorable overall survival in head and neck cancer, Hodgkin's lymphoma, colorectal, breast and bladder tumors (183). By considering the frequent negative effect of Treg on tumor immunity, a trial using a humanized anti-CCR4 monoclonal antibody to deplete the Treg population was performed on 10 patients with solid cancers and 4 out of 10 patients had a prolonged survival (193). These observations argue for a critical role of CD4 T cells in dictating either a pro- or anti-tumoral milieu within the tumor bed. Yet, characterization of these cells in patients at antigen-specific level is still very limited. Furthermore, effective immunomonitoring techniques will become valuable if CD4 T cells are to be used in clinical settings.

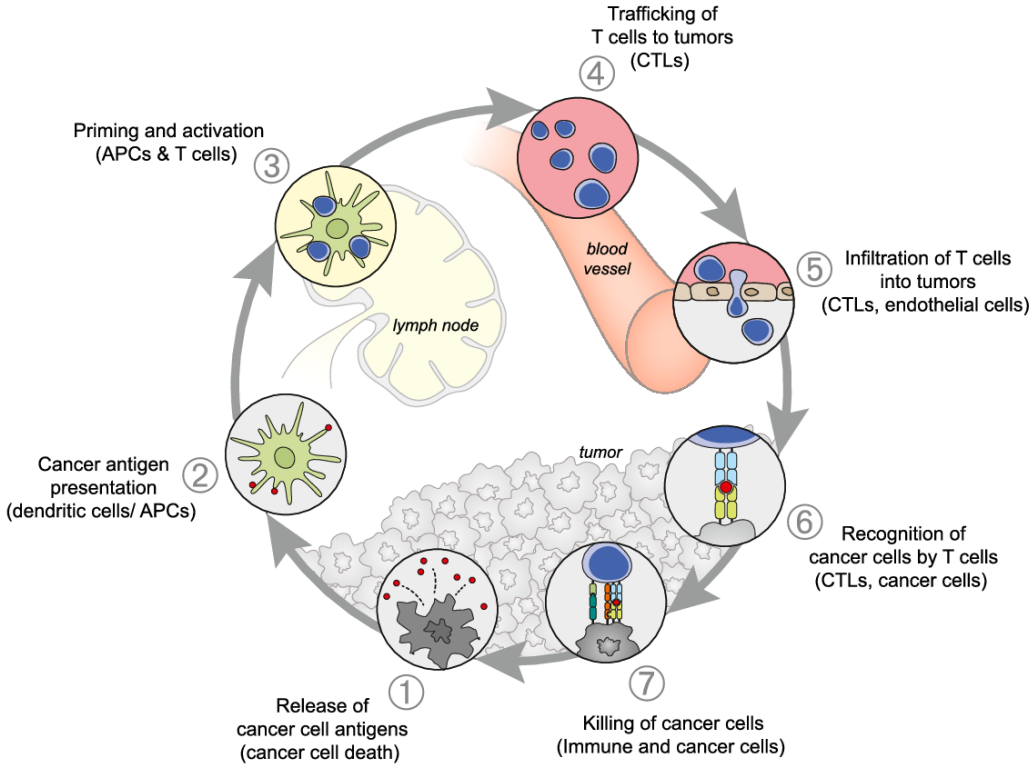

Figure 8: The cancer-immunity cycle. Illustration of each single step which is required for an effective antitumoral T cell response. Adapted from (180).

G.3.3 Cancer immune escape mechanisms

One of the reasons why it is so difficult to eliminate tumor cells is due to the mechanisms that they have to sabotage the cancer immunity cycle and counteract T cell-mediated rejection. Tumor cells are further aided by their supporting stroma as seen previously where the environment within and around tumors will have detrimental effects on DC maturation or will cause T cell tolerance or anergy in the absence of appropriate

co-stimulatory signals from APCs (194). Immature myeloid precursor are recruited by tumor which then become Myeloid-derived suppressor cells (MDSC) as they secrete immunosuppressive cytokines such as TGF-β and IL-10. TGF-β will inhibit T, B, and NK cell functions, while promoting the function of Tregs (195). IL-10 is known to inhibit macrophage and DC functions, promotes M2 polarization and indirectly prevents antigen-specific CD4 T cell activation (196). The presence of TAM contributes to immune escape as they directly or indirectly recruit natural regulatory T (nTreg) which natural function is to prevent excessive inflammation and autoimmunity (197). Tregs are "hijacked" by the tumors to induce a tolerogenic environment. In addition to the immunosuppressive cytokines secreted by Treg cells they are capable of depleting IL-2, inducing tolerogenic DC cells and causing cytolysis of effector CD8 T cells via Granzyme B and Perforin (50). TAM can also contribute to T cell suppression by depleting L-arginine in the tumor microenvironment. L-arginine is necessary for T cell function as its depletion results in the inhibition of the CD3 ζ chain re-expression after internalization of the TCR (197,198).

The second mechanism of tumor immunosuppression involves the expression of immunosuppressive molecules or their receptors. These molecules include PD-1, IDO, CTLA4 and LAG-3 among others, known as the immune checkpoints which can inhibit the activation of T lymphocytes leading to tumor escape (199). PD-L1 can be expressed constitutively by both tumor and stromal cells and can be induced by IFNγ (200). Upon binding between PD-1 and PD-L1 or PD-L2 there is an inhibition of immune cells such as activated T cells, B cells, monocytes, NK cells, and certain DCs (199). CTLA-4 similarly to PD-1 belongs to the CD28 family and upon interaction with its ligands (B7-1, B7-2) it delivers a negative signal (200). Tumor cells as well as Myeloid cells express another immunosuppressive key factor, the enzyme Indoleamine 2,3-dioxygenase (IDO). IDO reduces local tryptophan essential for effector T cell survival and the generation of cytotoxic metabolites (201). Finally, a last example of immunosuppressive mechanism within tumors resides in the expression of FasL. FasL expression was associated with poor CD8 infiltration and a high presence of Treg cells. FasL is upregulated in endothelial cells after tumor-derived vascular endothelial growth factor A (VEGF-A), IL-10 and prostaglandin E2 (PGE2) expression. FasL will confer to endothelial cells the capacity to kill effector CD8 T cells but not Treg cells (202).

G.4 Malignant Melanoma

Malignant melanoma is a type of cancer originating from melanocytes which are pigmented cells mostly found in the skin. The role of melanocytes is to protect the skin from the damaging effect of UV radiation by secreting melanin pigments. Melanoma is most frequently found in the skin but can also originate in the eye and inner ear (203–205).

G.4.1 Epidemiology

Despite the numerous advances made in the field of cancer treatment cutaneous melanoma is responsible for 75% of skin cancer mortality due to its invasive and metastatic nature. In fact during the 2011-2015 period

2% of all cancer deaths were attributed to melanoma (206). According to the world cancer research fund melanoma is the 19th most common cancer worldwide resulting in 300,000 new cases in 2018, with Switzerland ranking 8th on the overall highest rate of melanoma in the world (Australia being the country with the highest rate). This resulted in 3147 new cases of skin melanoma in Switzerland and 391 deaths in 2018 according to the international agency for research on Cancer from the world health organization (WHO) (source: Globocan 2018).

G.4.2 Risk factors

The risk factors linked to melanoma can be divided into two categories: environmental and genetic factors. The most known and important environmental risk factor for melanoma formation is the sun and the UV radiation it emits which leads to DNA damage. If this damage is not repaired by the nucleotide excision DNA repair machinery it will lead to the formation of aberrant cells (207,208). In human malignancies p53 is a tumor suppressor gene and one of the most frequently mutated genes (209). Unique to UV radiation mutations are found in the p53 genes which dysregulate many fundamental cell processes such as cell cycle arrest, DNA repair, apoptosis, genomic integrity maintenance, cellular senescence (210,211).

There is evidence where the ethnic origin of individuals is linked with the incidence of melanoma in populations. Individuals with increased amounts of melanin presence such as within the black population, will be 10 times less frequently affected by melanoma compared to the white population as they are better protected from the damaging effect of UV radiation emitted by the sun (209). Around 8 to 12% of patients have a family history of melanoma (212). Finally the number of naevi both common and atypical represents a good predictor for cutaneous malignant melanoma (205).

G.4.3 Diagnosis

The key to managing melanoma disease remains the early detection of skin abnormalities such as pigmentation alterations. A set of criteria can be used by clinicians and by the public to recognize melanoma in the early stages: Asymmetry, Border irregularity, Color variegation, Diameter > 6mm and Evolving which initials have been abbreviated into ABCDE criteria (213). Upon suspicion of a melanoma event a histological analysis is performed on a tissue biopsy to confirm the initial suspicion. The analysis of the tissues will give important information on the maximum thickness (mm) (Breslow thickness), the presence of ulcerations and clearance of the surgical margins. It is no longer included in the American Joint Committee on Cancer (AJCC) 8th edition (published in 2019) the need for the mitotic rate and the presence and extent of regression (214). The report will also include information on the anatomical location (including extra-cutaneous sites, such as mucosa, conjunctiva). A degree of sun damage of the surrounding skin is necessary. Finally the pathologist should also include the melanoma type (superficial spreading melanoma, lentigo maligna melanoma (LMM), acral lentiginous melanoma, nodular melanoma, and others) (214). Melanomas are then staged from I to IV,

IV being the most advanced stage in disease progression. The stages are based on the tumor characteristics, presence of metastatic lymph nodes and the presence and location of distant metastases (214).

Clark scale (level of invasion)		Breslow scale (vertical thickness)	Risk for metastasis
I	Epidermis (in situ)	in situ	None
II	Invades papillary dermis	<0.75 mm	Minimal (excellent prognosis)
III	Fills the papillary dermis to papillary-reticular junction	0.75–1.5 mm	Significant/medium
IV	Invades reticular dermis	1.51–4.0 mm	High
V	Invades subcutaneous fat/tissue	>4.0 mm	Extremely high

Table 2: Clark and Breslow staging of melanoma and the risks associated to the progression level. Adapted from (215)

G.4.4 mutations

Valuable information has been learned in recent years about the molecular basis of melanoma genesis, progression and response to therapy. The frequently (40% to 60% of cases) found mutation of BRAF V600 in melanoma is a predictor of efficacy of RAF inhibitors (216). Mutational aberrations activating KIT may predict response to tyrosine kinase inhibitors. Sensitivity to MEK inhibition might be found on NRAS-mutant tumors (217). The understanding of these gene mutations among others gives an understanding of melanoma malignancy which remains incomplete. Melanoma is a cancer with a high mutational load which is due to UV mutagenesis (218). UV-light mutations are linked with a high cytidine to thymidine (C>T) transitions. This results in either “passenger” mutations which do not confer a fitness advantage to tumor cells or will be “driver” mutations which do confer a fitness advantage. The drawback from these randomized mutational events results in very unique melanoma tumors from one patient to another which results in very different treatment responses (219).

G.4.5 Treatment of melanoma

There is an extensive guideline on the management of local and locoregional disease which has been published by the European Society for Medical Oncology (ESMO) (220). For localized melanoma it is recommended to excise the primary tumor within the safety margins. When surgery is not possible radiotherapy can be used. In the case of locoregional lymph node metastases or in-transit disease, therapeutic dissection is indicated. Non-resectable satellites may be treated using perfusion of melphalan a chemotherapeutical agent and/or tumor necrosis factor alpha (TNFα). In the case of systemic metastatic disease, good results have been obtained with α-CTLA-4 or α-PD-1 immunotherapy strategies as well as with kinase inhibitors (220). Chemotherapy can be used as a second line treatment. In the 2019 report it was emphasized the move in the field towards a personalized medicine for precision treatment of patient (220). Personalized medicine still present challenges as patients require to be screened for mutations of specific markers resulting in each individual patient requiring tailored drug therapies (221).

G.5 Cancer immunotherapy and immunomonitoring

The role of the immune system in the fight against cancer is now well established. Yet it is not sufficient on its own to clear out tumors. But the immune system can be manipulated to attack tumors which is the principle of cancer immunotherapy. This course of treatment in patients and it's high success rate in clinical trials, resulted in its classification as "breakthrough of the year" by Science in 2013 (222). This line of research saw the Nobel prize in Physiology or Medicine awarded to the immunologists James Allison and Tasuku Honjo for their research on targeting CTLA-4 or PD-1 for the improved elimination of tumors in patients (223). Unfortunately, the success rate varies with such course of treatment as it is still complicated to overcome mechanisms that cancer cells employ to evade immune surveillance. There are several strategies that have been tackled to modulate the immune system such as: vaccination, adoptive cell transfer and the use of immunomodulatory agents. During immunotherapy it is important to follow up on changes brought upon the immune system to provide insight on therapy efficacy and to evaluate the response at the cellular and molecular level, this is called immunomonitoring.

G.5.1 Tumor antigens and Neoantigens

As described before it is essential for cells of the adaptive immune system to recognize target antigens to elicit a specific anti-tumor T cell response. As to not elicit autoimmunity tumor antigens need to be specifically expressed on tumor cells, but ideally be absent on host cells. Tumor antigens can be split into antigens with high tumor specificity or low specificity. Within the category of antigens with high tumor specificity there are three classes of antigens: cancer-germline antigens, antigens derived from viral proteins and antigens resulting from point mutations (224). Several types of cancers originate from viruses, as such viral proteins are produced inside cancerous cells and peptides derived by these antigens can be detected by T cells (225). Another source of tumor-specific antigens are cancer-germline genes. This family of proteins is expressed in a wide variety of cancer types and little to no expression is observed in most normal tissues except on germline and trophoblastic cells. These antigens include melanoma-antigen encoding (MAGE) genes, *LAGE*/*NY-ESO1*, *SSX,…* (226–228). Finally, we find antigens which are encoded by mutated genes resulting in new antigenic peptides which are no more recognized as self, called neoantigens. Some tumors such as the previously described melanoma has a high mutational rate resulting in more mutated antigens and therefore are more immunogenic. The drawback of neoantigens is that they are patient-specific resulting in complications when it comes to immunotherapy protocols as no one treatment will fit all. Thanks to progresses made in sequencing technologies and in predictive tools, the field of cancer medicine is rapidly moving towards personalized treatment as mutated antigens from individual patients are screened for their immunogenic potential and used in vaccine trials (229–231). The second category of low affinity antigens comprises differentiated antigens and overexpressed antigens. Differentiation antigens are defined as proteins expressed by tumors of a particular histological type and the corresponding healthy tissue. Proteins such as tyrosinase, gp100/pmel and Melan-A/MART-1 are found for the most part in melanoma cells (232–

234). Overexpressed antigens as the name indicates, are proteins overexpressed by multiple tumor types as compared to their healthy counterpart, which makes them as attractive candidates for immunotherapy. However their targeting is associated with the risk of developing an autoimmune reaction as they are expressed on healthy tissues (224).

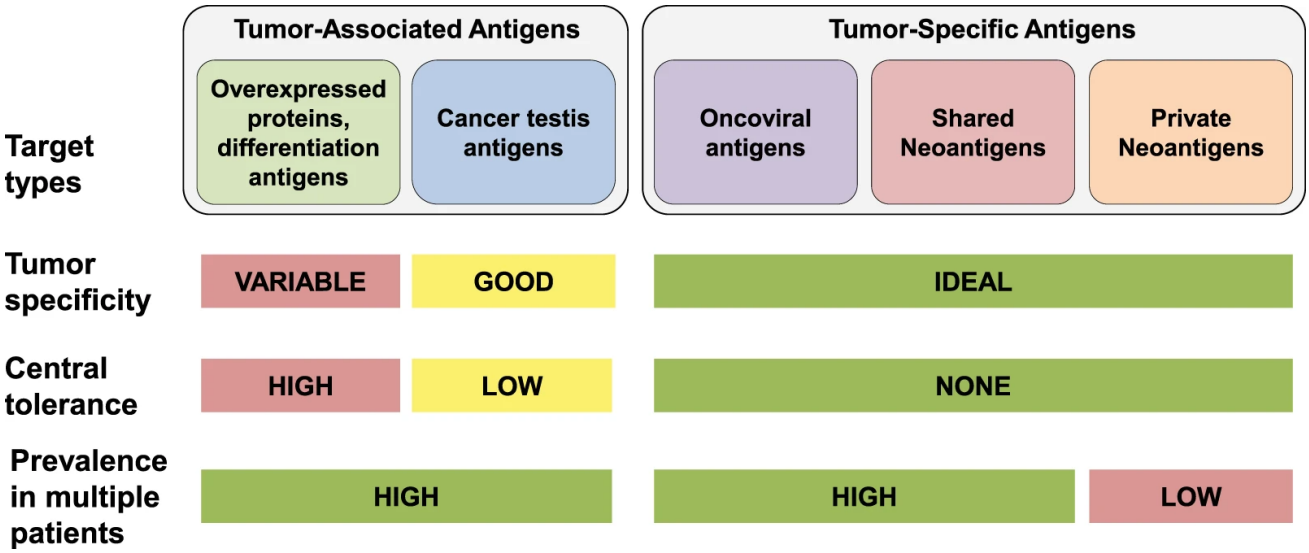

Figure 9: target antigen types for cancer immunotherapy. Classification of target antigens with their prevalence for tumor tissues as well as their capacity to break tolerance and finally their shared presence amongst multiple patients. Adapted from (235).

G.5.2 Anti-tumor vaccination

Prophylactic vaccine aims to protect against viral and bacterial infections by inducing a strong neutralizing antibody response, therapeutic vaccines for cancer therapies aims to establish an active effector T cell response as well as to generate a memory pool of T cells against a specific tumor target. Peptide based vaccines are composed of an emulsion containing target peptides such as the ones described in the previous sub-chapter, and one or more immune stimulatory adjuvants. Since several tumor-associated antigens belong to the self and are present on healthy tissues, there is only a limited number of circulating T cells, mostly of low TCR affinity, capable of reacting to such peptides. To break tolerance strong adjuvants, co-stimulators and repeated vaccinations have to be used (235). Furthermore, these cells have to overcome the immunosuppressive environment found in and around tumors. Vaccination has initially been focused on targeting CD8 T cells. As a first example, between 2003 and 2011 a clinical trial (LUD 00-018 study, ClinicalTrials.gov Identifier NCT00112229) was performed by the Research groups at the Ludwig Institute of Cancer Research, the CHUV and UNIL. In this study 29 patients diagnosed with stage III or IV melanoma were vaccinated with Melan-A analogue (ELA) or native (EAA)peptide ± Tyrosinase (YMD) peptide, CpG-B-7909 and Montanide ISA-51 adjuvants in order to stimulate tumor antigenic specific CD8 T lymphocytes. In this study, a high frequency of functionally competent CD8 T cells response was indeed observed (236). A second example is vaccination based on the use of synthetic long peptides (SLP). SLP are a sequence of amino acids identical to the viral or tumor-associated antigens. The use of these SLP are crucial to activate dendritic cells, in fact they cannot directly bind MHC class I (237). Through the uptake and presentation on dendritic cells of

the peptide, CD4 and CD8 T cell anti-tumor responses will be induced. This type of vaccination process resulted in promising results as in phase I/II clinical trial 1 patient out of 35 resulted in complete disease regression and 5 patients achieved stable disease (237). Lastly vaccination trials were also based on recombinant tumor antigen proteins. In particular a study using the NY-ESO-1 protein, Montanide ISA-51, and CpG ODN 7909 was administered to patients (238). This formulation aimed to stimulate B cells and T helper cells in particular the anti-tumor Th1 CD4 cells. Most vaccinated patients generated antibody and Th1 responses post-vaccination and in a few of them it was followed by the generation of CD8 T cells specific for the NY-ESO-1 peptide. The presence of specific CD8 T cells resulted from the antibody induced cross-priming of the peptide by the dendritic cells (238). This study showed the importance of not only inducing T helper responses but also inducing antibody response as they helped to generate tumor-specific CD8 T cells. The combination of multiple cell responses can determine the efficiency of a vaccination treatment. The role of CD4 T cells is becoming more evident in anti-tumor vaccinations as Th1 cells have been described to support the generation and maintenance of effector tumor-specific CD8 cytotoxic and memory T cells, by licensing dendritic cells through CD40-CD40L interactions (184,185) and to recognize peptides encoded by mutated genes within the tumor, the so called neoantigens (186,187). A recent vaccination trial targeted up to 20 personal tumor neoantigens by using long-synthetic peptides and showed strong T cell response. Class II stimulation was achieved with 60% of the predicted neoantigens whereas for class I only 20% of neoantigens induced a response. In this trial, 4 out of 6 patients had no recurrence at 25 month post-vaccination (188).
Neoepitopes offer new and interesting targets for personalized cancer immunotherapy due to their selective expression on cancerous tissues as a consequence of somatic mutations (239). The identification of these mutations in patients is possible through the analysis of the immunopeptidome by mass spectrometry which is labor-intensive but yields invaluable information on the antigenic repertoire of tumors. The understanding of the immunopeptidome will improve on the development of T cell-based therapies and vaccines (240).

G.5.3 Adoptive T cell transfer

Adoptive cell transfer therapy (ACT) consists of the isolation of autologous tumor infiltrating lymphocytes from patients, the amplification *ex vivo* after the selection of tumor-reactive cells the re-infusion into patients as such or after the selection of tumor-reactive cells. Prior to ACT lymphodepletion is necessary to eliminate Treg cells and eliminate lymphocytes which would compete with transferred cells for the homeostatic cytokines such as IL-7 and IL-15. This course of treatment has resulted in good responses in metastatic melanoma patients and clinical tumor regressions (50% of patients) (241). ACT most currently uses CD8 T cells as the main effector cells due to their innate capacity to kill target cells. More and more CD4 T cells are coming under the spotlight as new evidence of their crucial role in anti-tumor immunity was revealed (242). The infusion of CD4 T cells specific for the NY-ESO-1 antigen in patients with refractory metastatic melanoma resulted in a durable clinical remission (243). Similarly the use of CD4 Th1 cells recognizing the erbb2 mutation isolated from a patient and reinfused in the same metastatic cholangiocarcinoma patient, resulted

in tumor regression and a stabilization of disease (186). Finally in a recent paper, the group of Rosenberg highlighted the feasibility of using autologous CD4 T cells transduced with a HLA-DP4 restricted TCR specific for the MAGE-A3$_{243-258}$ cancer testis antigen, as it resulted to be safe and efficient in controlling the tumor in a proportion of treated metastatic patients (244,245).

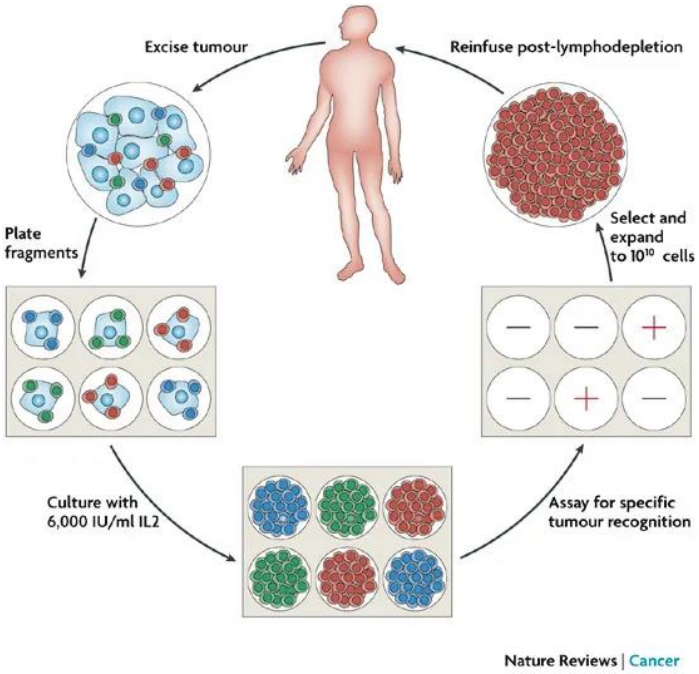

Figure 10: anti-tumor T cell generation for ACT. Cells are collected from patients followed by the establishment of various *in vitro* culture to generate cells for reinfusion into cancer patients. Adapted from (241).

G.5.4 CAR T cells

Limitations of ACT include the necessity to culture TIL. Furthermore, the limited availability of cancer specific antigens not expressed by healthy tissues can result in complications to identify proper cancer-specific T cells. ACT can circumvent such problems by using cells from patients which are genetically engineered to express tumor-specific TCRs or chimeric antigen receptors (CARs). The use of cells which have been modified to produce CARs has been explored with great success (246). The CAR is made of an antibody single chain (scFv), a hinge region and a transmembrane domain. The intracellular domain must be capable of intracellular signalling therefore it is most often composed of their CD3ζ, CD28 or 41BB depending on the CAR generation: 1st generation had CD3ζ only, 2nd generation had one costimulatory domain and CD3ζ and the 3rd generation had CD3ζ and two additional costimulatory domains (246,247). CAR T cells had so much success that the FDA rapidly approved the use of anti CD19 CAR T cells for the treatment of patients with B cell acute lymphoblastic leukaemia or large B cell lymphoma. Unfortunately, there is a high relapse rate within patients as there are still issues with acquired resistance (248). Despite the successes in the field of B cell malignancies CAR T cells results have been disappointing for solid tumors. Once more the identification of a proper tumor associated antigen is one of the hurdles for the generation of proper CAR T cell. Complications have also been encountered for the trafficking of the CAR T-cells to the solid tumor sites. Once at the tumor site the cells will

be met by a tumor microenvironment with an immunosuppressive effect (249). These issues, especially the immunosuppressive microenvironment will decrease the penetration capacity of the modified T cells. Finally resistance and toxicities are detrimental to CAR T cell therapy (250). Strategies to remediate such shortcomings are under investigation.

G.5.5 Checkpoint blockade

For the successful activation and function of an immune response a number of checkpoints have to be passed. These checkpoints are constituted of a large number of inhibitory pathways set in place to maintain self-tolerance as well as to modulate the duration and amplitude of physiological immune responses in peripheral tissues to avoid surrounding tissue damage. It is now clear that tumors use these mechanisms to evade the immune system resulting in immune resistance especially against T cells (251). Immune checkpoints are often made of a ligand and its receptor. The two most known inhibitory receptors are PD-1 and CTLA-4 whose TCR inhibitory function was covered in chapter G.2.3. By blocking the interaction between PD-1 and its ligand PD-L1 with nivolumab or pembrolizumab it is possible to restore T cell responses which were previously attenuated (252). Similarly, by injecting an anti-CTLA-4 (ipilimumab) antibody it was possible to unleash T cell functions (253). The great success these antibodies have had in clinical trials prompted the approval of these compounds by the regulatory agencies in many different countries. Their approval came despite the toxicities they displayed as to their ability to overcome immune tolerance, resulting in frequent autoimmune adverse events (254,255). The combination of both treatments anti PD-1 and anti-CTLA-4 resulted in increased rates of objective clinical responses (around 60%) thus showing their importance within cancer therapy strategies (256,257). Despite these remarkable results, patients showed a *de novo* or adaptive resistance to these treatments prompting the identification of additional molecules with similar effects such as TIGIT, VISTA, LAG-3, B7-H3, CD73 and others (258). As an example, TIGIT was initially identified in 2009 as it suppressed the activation of T cells. TIGIT binds to CD155 and CD112 on APC cells and competes for their binding with the CD266 or CD96. By competing with CD266 which delivers a positive co-stimulatory signal TIGIT can deliver an inhibitory signal to the cell (259). Promising results in preclinical trials resulted in the attention of many pharmaceutical companies (258). Similarly, LAG-3 was shown to limit the magnitude of CD4 T cell responses, thus including LAG-3 in the family of negative regulators of T cells. Anti-LAG-3 antibodies have been developed and amongst others, LAG525 antibody is undergoing phase I or II testing (260). The search for a new checkpoint inhibitor is a hot topic and the focus of numerous pharmaceutical companies.

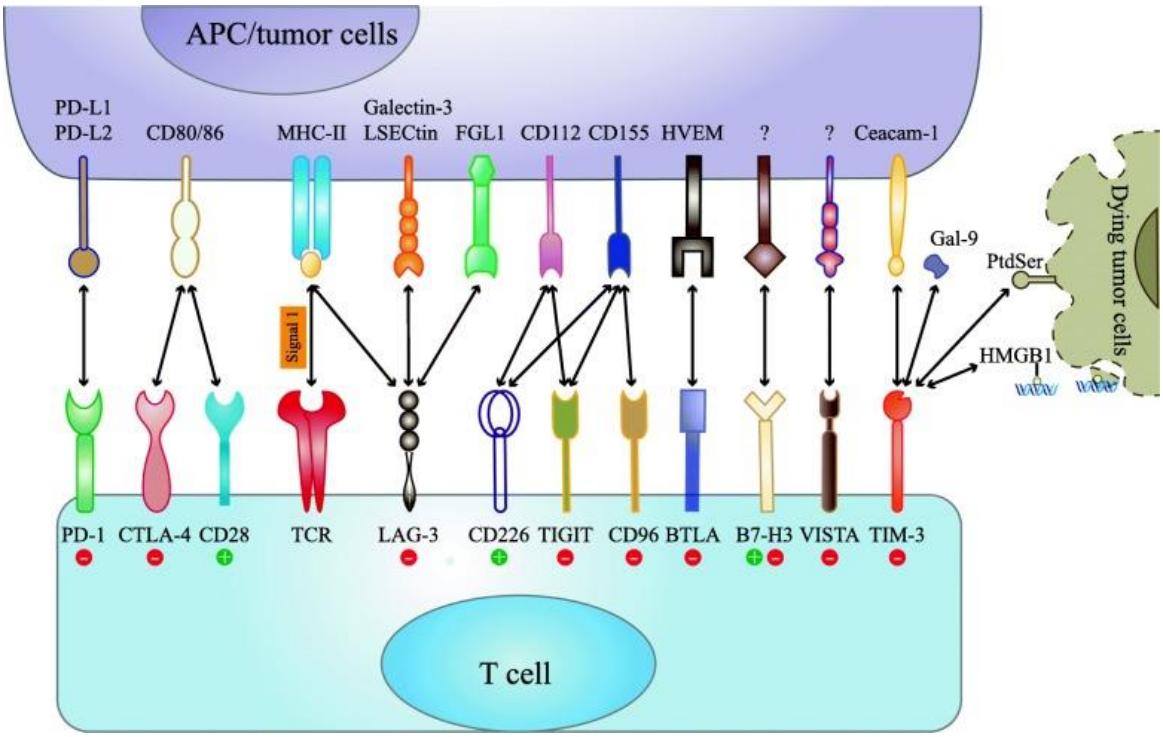

Figure 11: immune checkpoint receptors and ligands currently in use or as emerging candidates. Non-exhaustive representation of the various receptors and the ligands with whom they interact. Upon interaction the positive of negative signal generated are represented. Adapted from (258).

G.5.6 Immunomonitoring

The overall goal of immunotherapy is to tailor therapies depending on patient's needs. Great efforts are invested to customize the therapeutic agents such as peptides, vaccination protocols, ACT, CAR T cells and other checkpoint blockade inhibitors that will be given to patients in order to get the best immune response against tumor cells. One major hurdle in the field is the lack of effective immunomonitoring. It consists in monitoring the changes that occur in the immune system during immunotherapy bringing valuable insight into the efficacy of treatments and the identification possible biomarkers for patients' stratification. Up to date immunomonitoring techniques included classical techniques such as immunofluorescence, flow cytometry and mass cytometry but also of new techniques are emerging such as next-generation sequencing, immune profiling at the single cell level and metabolic studies (261). There is a need for more ways of monitoring the immune response generated from cells such as T lymphocytes. The use of pMHC class I multimers allowed to monitor antigen-specific CD8 T cell responses with great accuracy (262). Not much has been attempted in the field of CD4 T cells due to the difficult staining of CD4 T cells with pMHC class II multimers. Initial attempts have been made in the field with reasonable success but there is still a great margin for improvement (263).

H My PhD projects

Nowadays multiple roads are being extensively investigated for the cure of cancer patients. Yet, despite the numerous advances made in the field, there are still patients who are partially or not cured by current therapies. Current cell-based methods are often making use of CD8 T cells as main effectors due to their ability to recognize and eliminate tumors. CD4 T cells have only recently gained increasing importance in tumor immunity, including their capacity to recognize and respond to neo-antigens. However, due to the low numbers of circulating tumor-specific CD4 T cells, their characterization at antigen level is still very limited. Moreover, a key to CD4 T cell usage in immunotherapy will also depend on a better understanding of the regulation of their differentiation, to promote stem cell memory (T_{SCM}) and central memory (T_{CM}) phenotypes. These are some of the questions that I addressed during my PhD thesis.

My PhD work was divided into two main aims:

1. Develop and optimize new high-throughput tools for the direct ex-vivo functional evaluation of multiple tumor antigen-specific CD4 T cells.
2. Identify miRNA candidates influencing the differentiation of CD4 T cells for improved cancer immunotherapy.

The first aim was further subdivided in two projects. Firstly, the development of an optimized multimer staining procedure to detect larger percentages of tumor-specific cells and to better discriminate them from negative cells. The optimized procedure was used in a combinatorial staining setting to increase the number of specificities investigated within one precious patient sample.

The second sub-aim was a collaborative project with the group of Prof. David Gfeller and consisted in the cellular validation of a bioinformatic predictor for peptide binding to MHC class II molecules. By testing the immunogenicity of predicted peptides, we could confirm the potency of the predictor and identify novel targets to be investigated in the anti-tumor CD4 T cell field.

The second aim consisted in better understanding the regulation of CD4 T cell differentiation, to promote T_{SCM} and T_{CM} phenotypes. We aimed at identifying optimal miRNA (miR) candidates that could be therapeutically targeted to influence the differentiation of Naïve CD4 T cells into SCM or CM CD4 T cells capable of targeting tumor cells.

The overall goal of my work was to expand the knowledge on tumor antigen-specific CD4 T cells and to identify ways to better track them and exploit these cells in cancer immunotherapy.

I Optimized combinatorial pMHC class II multimer labelling for precision immune monitoring of tumor-specific CD4 T cells in patients

I.1 Introduction

In the CD8 T cell field great advances have been made via the development of peptide MHC class I tetramers, that allow the detection of antigen-specific T cells (112). From the initially generated molecules, several improvements have been made to increase the binding avidity of such complexes to CD8 T cell TCR's (121) and to concomitantly label cells of different specificities in the same sample, utilizing a combination of fluorochromes either in a dual color code (116), or with a multivalent code (115) or using panels of more than 100 pMHC class I DNA-barcoded multimers (117). Further, novel tools also include reversible multimers (NTAmers), that allow measurements of pMHC class I monomer dissociation kinetics on CD8 T cells (118). Improvements in multimer staining have not only come from improvements in the technology of multimer generation, but also by the usage of molecules such as Dasatinib, a protein kinase inhibitor (PKI) which has been shown to prevent TCR downregulation and to improve specific CD8 T cell detection (264–266). The further usage of an anti-fluorochrome antibody (Ab) to stabilize pMHC class I multimers at the T cell surface via Ab cross-linking also resulted in an improvement in tetramer staining (265,266).

Despite the advances in epitope-specific detection of CD8 T cells using pMHC class I multimers, little progress has been made with pMHC class II molecules. The reasons why the pMHC class II field has been lagging behind as well as the improvements made to remedy to production shortcomings were addressed in the chapter G.2.2. These advances have led to improved staining of antigen-specific CD4 T cells, mainly in the context of viral infections or autoimmunity (124). Instead, only scant results are available on the detection of human tumor-specific CD4 T cells in patients.

In the same line as the usage of Dasatinib to ameliorate detection of CD8 T cells, we reasoned that this reagent and other molecules which mediate a direct or indirect effect on TCR-pMHC class II interactions could improve the detection of antigen-specific CD4 T cells. We thus generated in house different pMHC class II multimers and reversible pMHC class II NTAmers and used them in combination with several molecules known to impact on TCR-pMHC interactions. For instance, previous studies have shown that galectin-3, a sugar-binding lectin, is capable to form a lattice on the cell surface and to bind to various glycosylated T-cell surface receptors such as TCR's (22), thus inhibiting the co-localization of TCR's with CD8 molecules (267,268) and impairing TCR-pMHC class I interaction. This effect is reversed by the addition of N-Acetyl-D-lactosamine (LacNAc), a competitive binder to galectin (267,268). Furthermore, it has been suggested that the presence of sialic acid may increase the affinity for galectins to the LacNAc motif of galectin-binding proteins (269). Neuraminidase, an enzyme specifically promoting desialylation, influences TCR clustering and the engagement of peptide/MHC ligands resulting in an enhancement in tetramer staining (269). Furthermore,

the usage of neuraminidase disrupts cell surface charges, allowing for a TCR and CD8 co-capping with pMHC (270).

I.2 Aim

The aim of this project is to bring innovation within the field of CD4 T cell immunomonitoring with improved monitor tools for the detection of tumor-specific CD4 T cells.

I.3 Co-author contribution

This work is presented in an article in second revision (add date and year) in the Journal for ImmunoTherapy of Cancer (JITC).

For this study I designed the experiments with my supervisors, I performed and analysed the majority of the experiments and I participated to the writing of the manuscript. The multimers used in this study were generated by Philippe Guillaume from the *Ludwig Institute for Cancer Research, Lausanne Branch, University of Lausanne, Switzerland*. Daniel Speiser, George Coukos and Alexandre Harari provided patient samples and reagents.

I.4 Manuscript

Optimized combinatorial pMHC class II multimer labelling for precision immune monitoring of tumor-specific CD4 T cells in patients

G.A. Rockinger[1,2], P. Guillaume[1,2], A. Cachot[1,2], M. Saillard[1,2], D.E. Speiser[1], G. Coukos[1,2], A. Harari[1,2], P. Romero[1], J. Schmidt[1,2] and C. Jandus[1,2]

[1] *Department of Oncology UNIL CHUV, University of Lausanne, Switzerland*

[2] *Ludwig Institute for Cancer Research, Lausanne Branch, University of Lausanne, Switzerland*

Corresponding author: Camilla Jandus: Department of Oncology UNIL CHUV and Ludwig Institute for Cancer Research, University of Lausanne, Lausanne, Chemin des Boveresses 155, CH-1066 Epalinges, Switzerland, Camilla.jandus@chuv.ch

Keywords: tumor-specific CD4 T cells, peptide MHC class II, multimers, immune monitoring, adoptive cell transfer

Conflicts of interest: the authors declare no conflicts of interest.

Words: 4226 **Figures**: 1 Table, 6 Figures

Abstract

Background: With immunotherapy gaining increasing approval for treatment of different tumor types, scientists rely on cutting edge methods for the monitoring of immune responses and biomarker development in patients. Due to the lack of tools to efficiently detect rare circulating human tumor-specific CD4 T cells, their characterization in patients still remains very limited.

Methods: We have used combinatorial staining strategies with peptide MHC class II (pMHCII) multimer constructs of different alleles to establish an optimized staining procedure for *in vitro* and direct *ex-vivo* visualization of tumor-specific CD4 T cells, in patient samples. Furthermore, we have generated reversible multimers to achieve optimal cell staining and yet disassemble prior to *in vitro* cell expansion, thus preventing activation induced cell death.

Results: We observed a vastly improved detection of tumor-, viral- and bacterial-specific cells with our optimization methods compared to the non-optimized staining procedure. By increasing the variety of fluorochromes used to label the pMHCII multimers we were also able to increase the parallel detection of different specificities within one sample, including antigen-specific CD8 T cells. A decrease in cell viability was observed when using the full optimization method, but this was mitigated by the removal of neuraminidase and the use of reversible multimers.

Conclusion: This new optimized staining procedure represents an advance towards better detection and analysis of antigen-specific CD4 T cells. It should facilitate state-of-the art precision monitoring of tumor-specific CD4 T cells and contribute to accelerate the use and the targeting of these cells in cancer immunotherapy.

Introduction

The identification of numerous tumor associated antigens and neo-antigens recognized by tumor reactive T cells in recent years has fueled the rapid progress in the field of cancer immunotherapy. Their exquisite specificity has been exploited in the exploration of several immunotherapeutic strategies including cancer vaccines, adoptive T cell transfer (ACT) and the use of immunomodulatory agents. To

46 date, cytotoxic CD8 T cells have been the major focus of cancer immunotherapy due to their capacity
47 to directly recognize and eliminate cancer cells (1). However, CD4 T cells are becoming more
48 appreciated due to new evidence emerging on their crucial role in cell-based therapies, peptide-based
49 vaccination and in the recognition of neo-antigens (2–4). Nonetheless, the low frequencies of circulating
50 tumor-specific CD4 T cells, their low affinity T cell receptors (TCRs) and the lack of tools to adequately
51 detect and isolate them have all hindered their characterization at the antigen specific level and their
52 clinical exploitation remain limited.

53 The direct measurement of antigen-specific T cell responses is done through the use of recombinant
54 MHC multimers assembled with antigenic peptides (pMHC) used in multiparameter flow cytometry or
55 mass cytometry. Major advances have been made in quantitative specific T cell frequency assays with
56 MHC class I peptide multimers (pMHCI), including high multiplex panels of more than 1000 pMHCI
57 DNA-barcoded multimers (5). However, little progress has been made with pMHC class II (pMHCII)
58 molecules. Several hurdles might explain this gap, such as low affinity TCR specific for MHC class II
59 complexes (6), modest coreceptor contribution to pMHCII binding avidity (7–9), the conformational
60 diversity of pMHCII complexes (10), the high polymorphism of HLA-DP, -DQ, -DR molecules and the
61 poor quality of pMHC class II multimers related to technical difficulties in their generation (6). In regard
62 to the latter, recent advances have improved the yields and stability of pMHCII multimers. These
63 include the addition of a leucine zipper instead of the transmembrane and cytoplasmic domains
64 preventing dissociation of the alpha and beta chains (11), the addition of a C-terminal His-tag, allowing
65 gentle affinity purification of the complexes (10), the use of conditional peptide tags improving the
66 degree of peptide loading (12), and the linking of the peptide to the β chain via a long and flexible linker
67 (13). In turn, these advances have led to improved identification of antigen-specific CD4 T cells, mainly
68 in the context of viral infections or autoimmunity (14), whereas very little data is available to date on
69 the detection of human tumor-specific CD4 T cells in patients.

70 Here we generated pMHCII multimers and reversible pMHCII NTAmers (15) and used them in
71 combination with several molecules known to impact on TCR-pMHC interactions to optimize antigen-
72 specific CD4 T cell detection and enumeration. These included galectin-3, a sugar-binding lectin that

is capable of forming a lattice on the cell surface and binding to various glycosylated cell surface receptors such as TCRs (16) and impairing TCR-pMHCI interaction. This effect is reversed by the addition of N-Acetyl-D-lactosamine (LacNAc), a competitive galectin-binder (17,18). Furthermore, the removal of sialic acid may increase (17,19,20) multimer staining with pMHCI multimers.

We show that the combined use of neuraminidase, dasatinib, LacNAc as well as an anti-fluorochrome antibodies (Ab) (13,21) improve the specific labeling of rare human tumor-specific CD4 T cells. This optimized multimer labeling assay enables the concomitant immunomonitoring of tumor-antigen specific CD4 and CD8 T cells from a single tube, thereby reducing the sample size needed. Furthermore, we report on the successful direct *ex-vivo* detection of tumor-specific CD4 T cells as well as the isolation and clonal expansion of these cells, for TCR-engineering and adoptive cell therapy approaches.

Methods

Patients, blood samples and ethical approval statement

Peripheral blood from stage III/IV melanoma patients was obtained from the Department of Oncology, University Hospital (CHUV), Lausanne, Switzerland, upon written informed consent based on the study protocol (NCT00112242) approved by the IRB and Swissmedic (3). The patients had been subjected to a vaccination protocol with the 30 amino acid peptide LSP NY-ESO-1_{79-108}, administered subcutaneously in combination with CpG-B (CpG-7909/ PF-3512676) and Montanide ISA-51, with or without low dose interleukin-2. Blood was diluted with PBS or RPMI 1640 (Invitrogen Corp., Paisley, UK), mononuclear cells were purified by centrifugation over Ficoll-Plaque TM Plus (Amersham Bioscience, Uppsala, Sweden) and washed three times with RPMI 1640. Lymphocytes were directly cryopreserved in 50% RPMI (Gibco/Thermo Fisher scientific, MA, USA), 40% FCS (PAA laboratories/GE healthcare, IL, USA), and 10% DMSO freezing medium (sigma-Aldrich, MO, USA). Vials of $10x10^6$ PBMC from melanoma patients were stored in liquid nitrogen.

Peptide epitopes

Peptides were synthesized by the Peptide and Tetramer Core Facility, UNIL-CHUV, Epalinges, Switzerland, by standard solid phase peptide synthesis on a multiple peptide synthesizer (Intavis,

Germany). All peptides were > 90% pure as indicated by UPLC-MS analysis. Lyophilized peptides were diluted in pure DMSO at 10 mg/ml or aliquots of 1 mg/ml in 10% DMSO were prepared and stored at -80°C. The peptide epitopes and their restricting HLA elements are listed in ***Table 1***.

Generation of pMHC II multimers

Peptide-MHC II multimers were produced by the Peptide and Tetramer Core Facility, UNIL-CHUV, Epalinges, Switzerland. The extracellular region of the HLA-DR/DPα and HLA-DR/DPβ chains were separately cloned into pMT\BiP\V5-His A (ThermoFisher scientific). The alpha chain construct harbors the acidic leucine zipper and terminates by a tandem His-tag (HHHHHHGGGSGGGSGSHHHHHH). The beta chain construct contains the basic leucine zipper and terminates with AviTag sequence. To generate cell lines expressing HLA-DR or HLA-DP the two plasmids with a third plasmid conferring puromycin resistance, were co-transfected into Drosophila S2 cells using Cellfectin (ThermoFisher scientific) according to the manufacturer protocol. Protein expression was induced by addition of 1 mM CuSO4. MHC class II molecules were purified from supernatants with Chelating Sepharose FF (Merck). Peptide loading was performed in 100 mM sodium citrate, pH 6.0 with 100 µM peptide at 37 °C for 24 h, buffer-exchanged on a HiPrep 26/10 desalting column (Merck) into AviTag buffer and subsequently biotinylated with the BirA enzyme according to the manufacturer instructions (Avidity, Denver, CO). Biotinylated MHC class II-peptide complexes were purified on a HisTrap HP column (Merck).

Peptide-MHC II monomers were multimerized using streptavidin-conjugated dyes and then aliquoted and kept at -80°C. Reversible pMHC II multimers (NTAmers) were prepared similarly other than the use of a proprietary streptavidin-NTA conjugate.

Generation of T cell clones

PBMC from patients with HLAs of interest were thawed and CD4 T cells enriched using anti-CD4 microbeads and MiniMACS magnetic separation columns (Miltenyi biotec, Bergisch Gladbach, Germany). These were then stimulated with autologous irradiated $CD4^-$ T cells in the presence of a pool of peptides (5 µM each), as indicated. After 2 days of culture 100 µl of RPMI 1640 containing 8%

125 of human serum, 2 mM glutamine, 1% (vol/vol) nonessential amino acids, 50μM 2β-mercaptoethanol,
126 penicillin (50 U/ml) and streptomycin (50 μg/ml) (R8 media), was replaced with fresh media containing
127 a final concentration of 100 IU/ml of human recombinant (hr) IL-2. After 10 days of in vitro expansion,
128 cultures were tested for the presence of antigen-specific CD4 T cells with pMHCII multimers loaded
129 with the same peptide used in the stimulation process. The detection of these cells was performed with
130 the standard multimer staining process: the PE or APC-conjugated multimers were added to the cells at
131 a final concentration of 10 μg/ml in a volume of 25 μl of R8 media and incubated for 45 min at room
132 temperature (RT). Twenty minutes before the end of the multimer incubation period, 25 μl of the
133 following antibody cocktail was added directly to each sample without washing: anti-CD3 AF700
134 (clone HIT3a, Biolegend, London, UK), anti-CD4 FITC (clone RPA-T4, Biolegend, London, UK) and
135 LIVE/DEAD fixable dead cell stain (Vivid, Invitrogen, CA, united states) diluted 1:800 in R8 media.
136 Where indicated, anti-CD45RA ECD (clone 2H4LDH11LDB9, Beckman Coulter, CA, USA) and anti-
137 CCR7 BV421 (clone G043H7, Biolegend, London, UK) were used. Samples were analysed with the
138 BD LSR II Flow Cytometry Analyzer (Becton Dickinson, NJ, USA). The data was analysed using
139 FlowJo software (FlowJo). The positive cultures were then sorted using FACS cytometers either Aria
140 IIU or the Aria III (Becton Dickinson, NJ, USA) using the same staining protocol.

141 Individual, sorted, epitope-specific T cells were stimulated with 1 μg/ml phytohemagglutinin (PHA)
142 (Thermo Fisher scientific, MA, USA) in the presence of irradiated (30Gy) allogeneic PBMC feeder
143 cells ($10x10^4$ per well) and hrIL-2 (100 IU/ml) and plated in Terasaki plates for clone generation. The
144 remaining sorted cells were stimulated and cultured in a 96-well plate as a bulk of epitope specific cells.
145 T cells were cultured for a minimum of 2 weeks post-restimulation before being used for experiments
146 or frozen.

147 **Optimized and reversible multimer staining**

148 For optimized CD4 T cell multimer staining, the cells were plated in 96-well V bottom plates and
149 centrifuged at 1500rpm (453g on Eppendorf 5810R). After removing the supernatant, the cells were
150 resuspended in 100μl of R8 media containing LacNAc (sigma-Aldrich, MO, USA) at a final
151 concentration of 5mM and incubated at 37°C for a period of 2 hours. Cells were washed with PBS,

centrifuged and resuspended in 100 µl of PBS containing dasatinib (Axon Medchem, VA, USA) and neuraminidase from Clostridium perfringens (C. welchii) (Sigma-Aldrich, MO, USA) at respective final concentrations of 50 nM and 0.7U/ml and then incubated for 30 minutes at 37°C. After a further PBS cell wash, standard multimer staining was performed (see above) after which 0.5 µg (10 µg/ml) of either mouse anti-PE unconjugated Ab (clone PE001, Biolegend, London, UK) or mouse anti-APC unconjugated Ab (clone APC003, Biolegend, London, UK) was added depending on the labelling fluorochrome bound to the multimer, and incubated for 20 minutes on ice in the dark. Cells were washed and resuspended in PBS and analysed with either the BD LSR II Flow Cytometry Analyzer (Becton Dickinson, NJ, USA) or with the CytoFLEX S Flow Cytometry Analyzer (Becton Dickinson, NJ, USA). When reversible multimers were used in this protocol, cells were treated with Imidazole at 100 mM in a volume of 100 µl of PBS for 2 min at 4°C, either at the end of the staining procedure, or immediately after single cell sorting.

Imaging flow cytometry

Following sample thawing, clonal cells were split in two wells of a 96 well V bottom plate. Half of the wells were subjected to the standard multimer staining procedure whereas the other half were treated with the optimized staining procedure. The cells were stained with multimers and cell surface markers. To avoid spill over between fluorochromes, the panel was modified to contain: the PE labelled specific multimer, anti-CD3 APC (clone UCHT1, Beckman Coulter, CA, USA), anti-CD4 BV605 (clone OXT4, Biolegend, London, UK) and LIVE/DEAD fixable dead cell stain (Vivid, Invitrogen, CA, united states). The remaining two wells were stained with the Mouse Anti-Human TCR αβ PE (clone T10B9.1A-31, Becton Dickinson, NJ, USA) for 45 minutes in 25 µl of R8 media at RT. Twenty minutes before the end of the incubation period 25 µl of R8 media containing the previously mentioned CD3 APC, CD4 BV605 and LIVE/DEAD fixable dead cell stain was added and incubated at RT. All samples were analysed with the Amnis Imaging flow cytometry (Luminex, TX, USA) and data processed with the IDEAS Software (Luminex, TX, USA).

177 **Evaluation of cell viability**

178 CD4 T cell clones were seeded in a 96 V bottom well plate and subjected to standard or optimized
179 multimer staining procedures and put in culture in a round bottom 96 well plate in R8 media containing
180 100 IU/ml of hrIL-2. At time points 6 h, 24 h and 48 h, the cells were collected and stained for viability
181 markers. Cells were washed with PBS and resuspended in 25 µl of PBS containing anti-CD3 AF700
182 (clone HIT3a, Biolegend, London, UK), anti-CD4 FITC (clone RPA-T4, Biolegend, London, UK) and
183 LIVE/DEAD fixable dead cell stain (Vivid, Invitrogen, CA, USA) diluted 1:800 in PBS. The cells were
184 incubated at RT for 30 minutes and washed with PBS. They were resuspended in 25 µl of AnnexinV
185 buffer 1X with AnnexinV-PE (Becton Dickinson, NJ, USA) and incubated for 20 minutes at 4°C. Cells
186 were then washed and resuspended in AnnexinV buffer 1X and analysed with the CytoFLEX S Flow
187 Cytometry Analyzer (Becton Dickinson, NJ, USA).

188 **Functional evaluation**

189 For the evaluation of the secreted cytokines upon specific stimulation, CD4 T cell clones were plated
190 in a 96 well U-shaped plate, left unstimulated, stimulated with 5 µM of specific $HA_{307-319}$ or NY-ESO-
191 1_{87-99} peptides or with 5 µM of an irrelevant peptide. The cells were incubated O/N with the addition of
192 2.5 µg/ml of Brefeldin A. The cells were then collected and transferred to a 96 well V-shaped plate for
193 flow cytometry staining. The cells were first incubated for 30 min at RT with anti-CD3 BV421 (clone
194 UCHT1, Biolegend, London, UK), anti-CD4 FITC (clone RPA-T4, Biolegend, London, UK) and
195 LIVE/DEAD fixable dead cell stain (Vivid, Invitrogen, CA, USA) diluted 1:800 in PBS. Cells were
196 then fixed and permeabilized following the recommendations provided with the eBioscience™ Foxp3
197 / Transcription Factor Staining Buffer Set. Cells were washed twice with the permeabilization buffer
198 1X provided with the kit and then incubated for a period of 30 min at RT with the anti-IFNγ PE (clone
199 B27, Biolegend, London, UK) and the anti-TNFα AF700 (Clone Mab11, Becton Dickinson, NJ, USA)
200 diluted in permeabilization buffer 1X. The cells were washed and analysed with the CytoFLEX S Flow
201 Cytometry Analyzer (Becton Dickinson, NJ, USA).

Statistical analysis

Statistical tests used were the Wilcoxon matched-pairs signed-ranks test for the results shown in ***Figure 3***, and two-way ANOVA followed by Tukey's multiple comparison test were used for the results shown in ***Figures 5*** *and* ***6***.

Results

Optimal staining of antigen-specific CD4 T cells by pMHC class II multimers is achieved at room temperature

To systematically optimize pMHCII multimer labeling of specific CD4 T cells, we first evaluated the effect of temperature on the labelling of a collection of human CD4 T cell clones of tumor-antigen and viral specificities by design multimers, as illustrated in ***Figure 1A***. We compared the staining efficiency at 4°C, 15°C, RT and 37°C. Although distinct labeling with HLA-DR7/NY-ESO-$1_{87\text{-}99}$ of specific CD4 T cell clones with the HLA-DR7/NY-ESO-$1_{87\text{-}99}$ multimer was obtained at all temperatures, maximal mean fluorescence intensity (MFI) was apparent at RT compared to other temperatures (***Figure 1B-D***). The increase in MFI was not accompanied by an increase in background staining, as assessed in criss-cross experiments with irrelevant clones (***Figure 1E***). Similar results were obtained using viral specific clones ($HA_{307\text{-}319}$ specific clones, restricted by HLA-DR7) (***Figure 1F***). These results suggest that optimal pMHCII multimer staining requires exposure of CD4 T cells to multimers at RT.

The use of optimizing molecules improves pMHCII multimer staining of human antigen-specific CD4 T cells

To determine whether the multimer staining quality could be further improved, a set of candidate molecules individually and in combination was included in the staining procedure. CD4 T cell clones specific for NY-ESO-$1_{87\text{-}99}$ or $HA_{307\text{-}319}$ were pretreated with neuraminidase, dasatinib or both, before multimer staining. In addition to the various cell treatments, a secondary antibody recognizing the phycoerythrin fluorochrome incorporated into the multimers was added prior to analysis. Addition of either neuraminidase or dasatinib significantly increased the fluorescent signal. Moreover, the addition of both had an additive effect (***Figure 2A and B***). The addition of the secondary antibody further

increased the detected MFI, with no impact on background staining of an irrelevant clone (***Figure 2C and D***).

Next, knowing that LacNAc, a competitive binder of galectin, affects TCR mobility on the cell membrane, we tested its effect on multimer staining. Clones were incubated with multimers after treatment with LacNAc alone, with the combination of optimizing molecules (dasatinib, neuraminidase and secondary Ab) or with the optimizing molecules plus LacNAc. The use of LacNAc alone did not improve the multimer staining. However, when used in combination with the other optimizing molecules it resulted in the highest specific MFI signals (***Figure 2E***). We used the Amnis Imaging flow cytometry technology to directly visualize the multimer distribution on the cell surface of clones labelled with either the standard or optimized staining procedure (OSP). This confirmed the increased MFI with the OSP compared to the standard procedure and revealed clustering of fluorescently labelled multimers only with the OSP protocol (***Figure 2F***). Together, these results indicate that the pre-treatment of T cells with the optimizing molecules LacNAc, neuraminidase and dasatinib followed by incubation with a secondary cross-linking Ab, leads to optimal multimer labeling as assessed by flow cytometry.

Optimizing molecules allow improved staining across multiple antigen specificities and HLA restrictions

In order to validate the OSP across multiple antigen-specificities, clones specific for HLA-DR7/$HA_{307-319}$, HLA-DR7/NY-ESO-1_{87-99}, HLA-DR4/$HA_{307-319}$, HLA-DP4/MAGE-$A3_{111-125}$, HLA-DP4/MAGE-$A3_{243-258}$, or HLA-DP4/tetanus toxoid $(TT)_{947-960}$, were labeled with either the standard procedure or the OSP (***Figure 3A***). An increase in MFI signals using the OSP was consistently observed compared to the standard procedure. No specific signal was observed when an irrelevant multimer was used (***Figure 3A***).

For immune monitoring purposes, improved identification of tumor-specific CD4 T cells is necessary directly *ex-vivo*, in patient-derived PBMC samples. *Ex-vivo* samples from HLA-$DR7^+$ and HLA-$DP4^+$ stage III-IV melanoma patients were labeled with either the standard procedure or the OSP. Increased frequencies of tumor antigen-specific CD4 T cells could be measured when using the OSP compared

255 to the standard procedure (***Figure 3B-C***) with no background staining difference between the two
256 ***(Figure 3B-D)***.

257 Samples from stage III-IV melanoma patients pre- and post-vaccination with the long synthetic peptide
258 (LSP) NY-ESO-$1_{79–108}$ were stained with the HLA-DR7/NY-ESO-1_{87-99} or HLA-DR4/$HA_{307-319}$
259 multimers. $HA_{307-319}$ specific cells were detected at a higher frequency when using the OSP compared
260 to the standard staining procedure, but their frequency did not vary during vaccination ***(Figure 3E)***. An
261 increase in NY-ESO-1_{87-99} specific CD4 T cell frequencies was observed following vaccination and
262 accentuated when using the OSP ***(Figure 3E)***. Furthermore, with the OSP a small population of NY-
263 ESO-1_{87-99} specific CD4 T cells was readily detectable in samples pre-vaccination. The detection of
264 larger proportions of viral- and tumor-specific cells using the OSP was further demonstrated after *in-*
265 *vitro* expansion of CD4 T cells from patients' post-vaccination ***(Figure 3G)***.

266 The use of the OSP in HD samples resulted in the detection of higher frequencies of NY-ESO-1_{87-99}
267 specific CD4 T cell compared to standard staining ***(Figure 3H)***. The NY-ESO-1_{87-99} specific cells were
268 predominantly of a naïve (N) phenotype ***(Figure 3I)***. Further, the HDs showed low frequencies of
269 $HA_{307-319}$ specific cells with a mixed differentiation phenotype. Overall, mostly effector memory (EM)
270 and central memory (CM) cells were stained with the standard NY-ESO-1_{87-99} or $HA_{307-319}$ specific
271 multimer staining ***(Figure 3F-I)***. A larger proportion of N cells as well as CM and EM and terminally
272 differentiated effector memory cells (EMRA) were detected with the OSP. NY-ESO-1_{87-99} specific cells
273 displayed an evolution from mostly N cells pre-vaccination in patients' samples towards more CM and
274 EM differentiated cells post-vaccination ***(Figure 3F)***.

275 Overall, these results confirm the efficacy of OSP monitoring of antigen-specific CD4 T cells, also
276 directly *ex-vivo* in HD and patient peripheral blood samples.

277 **Combinatorial labelling of antigen-specific CD4 and CD8 T cells using OSP in patient**
278 **samples**

279 Due to the limited amount of biological material available from patients, it would be advantageous if
280 multiple specificities could be investigated within the same individual sample. For this purpose, a

cocktail of pMHCI and pMHCII multimers labelled with either one or a combination of two fluorochromes as described in ***Figure 4A***, was used. First, the feasibility of combinatorial staining for CD4 and CD8 T cells was verified by spiking CD4 and CD8 T cell clones of the specificities indicated in ***Figure 4A***, into PBMCs. All the specific clones could be detected with the combination of multimers (***Figure 4B***). The OSP allowed for a much sharper discrimination between specific and negative cells in the CD4 T cell population than the standard labeling procedure (***Figure 4B and C***). For CD8 T cells the optimization was effective in the detection of $EBV_{280-288}$, Flu_{58-66} and Melan-A_{26-35} specific cells but not in the case of $CMV_{495-503}$ and NY-ESO-$1_{157-165}$ specific cells (***Figure 4B and C***).

Peripheral blood lymphocyte samples from HLA-$DR7^{+}$, HLA-$DP4^{+}$ and HLA-$A2^{+}$ melanoma patients were used to evaluate the efficiency of combinatorial multimer labeling with and without the optimization procedure directly on *ex-vivo* cells. Multiple antigen specificities were detected within the samples which benefited from the optimization, with a higher frequency of specific cells detected and a higher staining intensity achieved when using the OSP ***(Figure 4D***). These results demonstrate the feasibility of integrating the OSP with combinatorial multimer labelling for sensitive detection of both class I and class II-restricted T cells of multiple specificities within a single patient sample.

The usage of reversible multimers improves cell viability of tumor-specific CD4 T cells upon subsequent expansion

Besides its applicability for direct *ex-vivo* immune monitoring, the OSP might be advantageous in sorting specific cells for in vitro expansion for adoptive cell transfer therapy. In this regard, the impact of the OSP on CD4 T cell viability was evaluated using HLA-DP4/MAGE-$A3_{243-258}$ restricted clones with either an intermediate or high MFI (***Figure 5A***). Once the labeling procedure was complete, the cells from each condition were seeded and cultured for periods of 6 hours, 24 hours and 48 hours before viability assessment. With the intermediate MFI clones, substantial cell death was apparent in cloned T cells after OSP treatment, irrespective of the presence of the multimer (***Figure 5B***). In contrast, the cloned T cells with high MFI exhibited a reduction in the frequency of dead cells following the OSP in the absence of the multimer, suggesting that the persistence of the multimers may have a negative impact on cell viability. To evaluate which molecule in the OSP was causing an increase in cell

mortality, PBMC from healthy donors were treated with LacNAc, dasatinib, neuraminidase, or a combination of all three followed by culture during 6 hours, 24 hours and 48 hours before cell viability assessment. The addition of LacNAc did not affect cell survival (***Figure 5C***) and dasatinib only impacted cell viability of CD4 T cells, at later time points. In contrast, neuraminidase had a strong negative impact on viability by the 6-hour time point either alone or in combination with the other compounds (***Figure 5C***). Altogether, these results suggest that neuraminidase should be avoided to preserve the viability of specific CD4 T cells when using the OSP in settings of in vitro T cell expansion. The mechanism behind this loss in cell viability with the OSP seems to be linked to the improved binding of multimers to TCRs, potentially leading to activation-induced cell death (AICD).

To address this possibility, reversible multimers (NTAmers), which consist of pMHCII monomers linked by a Ni^{2+}-nitrilotriacetic acid (NTA)-His tag-containing scaffold (***Figure 6A***) were generated and compared to the design multimers used thus far in this work. Upon addition of a nontoxic low concentration of imidazole, the NTAmers decay within seconds into pMHCII monomers and PE-labelled streptavidin NTA_4 molecules, causing dissociation of the pMHCII-TCR complex (***Figure 6B and C***). HLA-DP4/MAGE-$A3_{243-258}$ cloned T cells of high staining intensity were labeled using the same conditions as in ***Figure 5B*** but replacing the multimer with the NTAmer. An increase in cell viability was apparent when using NTAmers, which was comparable to that observed using the OSP in the absence of multimers (***Figure 6D***). As expected, viability was further improved by removing neuraminidase from the staining procedure (***Figure 6E***) with maintained superior staining intensity compared to the standard protocol (***Figure 6F***).

To confirm the feasibility of using the above described conditions for subsequent cell culture and functional evaluation, aliquots of cells generated by the *in vitro* stimulation depicted in ***Figure 3G*** were sorted with the standard protocol or the OSP and seeded in single cell cultures. Clonal efficiency was calculated for each patient and for both antigens (***Figure 6G)***. In regards to the NY-ESO-1_{87-99} specificity no major difference was observed between cells sorted with the standard protocol or the OSP. However, since the initial number of NY-ESO-1_{87-99} specific cells detected using the OSP in patients Lau 1293 and 1352 was on average 3.7-fold greater than with the standard protocol, many more

clones could be generated (***Figure 6G***). $HA_{307-319}$ specific cells gave more positive wells with the standard protocol compared to the OSP but when screening for multimer positive clones they resulted to be non-specific for $HA_{307-319}$ (***Figure 6H***), in contrast to the clones issued from the OSP sorted cells. For the NY-ESO-1_{87-99} specificity most clones were positively stained by the specific multimer. Finally, we excluded any functional impairment in OSP sorted clones as upon specific peptide stimulation we observed significant expression of both IFNγ and TNFα (***Figure 6I and J***).

Together, these results suggest that specific T cell viability and functionality can be efficiently preserved by replacing standard multimers with reversible NTAmers and with the removal of neuraminidase to the optimization combo for efficient tumor-specific CD4 T cell expansion.

Discussion

Peptide-MHC multimers have been widely used since their first description back in 1996 (22) and have been an invaluable tool for the detection of specific T cells. In this study, we have developed and validated novel combinatorial pMHC class II multimer staining procedures to detect human antigen-specific CD4 T cells, in *ex-vivo* patient samples. In addition, we show innovative solutions to enhance the yields of viable antigen-specific CD4 T cells after multimer-guided, flow cytometry-based cell sorting.

Despite the clear above described benefits of the OSP staining as compared to the standard procedure, a reduced cell viability was observed using OSP, which could hamper the adoption of this methodology for cell expansion in the context of ACT. We identified in the neuraminidase treatment the main cause of this cell mortality, in line with previous studies documenting its toxicity (28,29). To a lesser extent we also observed a reduction in cell viability by dasatinib treatment. Despite this fact, dasatinib has been implemented in several tetramer staining procedures for CD8 T cell identification, without mention of any negative impact on cell fitness (30,31,21). Additionally, by performing the optimized staining in the absence of the multimer we observed an increase in cell viability, confirming a direct impact of the TCR-pMHC class II multimer binding on cell survival. This has already been described in antigen-specific CD8 T cells, possibly due to the AICD induced by the TCR and pMHCI interaction

(32). In line with this observation in CD8 T cells, our results using the Amnis Imager show increased TCR clustering and enhanced interaction between TCR and pMHCII complexes during the OSP, supporting the concept of AICD induction also in CD4 T cells. Further, in this study we mention for the first time the use of pMHCII NTAmers to successfully reduce cell mortality in isolated CD4 T cells. In the future, this technology could be used also for other applications, such as the measurement of TCR affinities and of the constant of TCR dissociation (K_{off}) as reported for CD8 T cells (15). For this endeavor, the use of the OSP might be key to ensure strong initial pMHCII NTAmer binding to TCRs of low affine tumor-specific T cells.

In an era of personalized immunotherapy, it has become vital to monitor patient responses to therapies (23,24). The use of CD4 T cells as part of cancer therapy is coming of age, yet their monitoring remains elusive. Being able to follow the evolution of such cells is key for vaccination and adoptive cell-transfer based therapies. The large difference in percentages and phenotpye of cells detected using the standard or the optimized staining reflects discrepancies previously reported by others using other technologies (25). The combination of different peptide-MHC multimers and the evaluation of phenotypic markers is expected to generate clues as to CD4 T cell differentiation and polarization in CD4 T cells, at the antigen specific level. Furthermore, TCR affinity studies will be possible, either using the 2D binding methodology or new highly sensitive methods such as the whole cell surface plasmon resonance. (26). Another key aspect will be the improvement and implementation of the expanded combination of fluorochromes or metals for combinatorial multimer labelling, or the use of DNA barcodes (27), that would allow the concomitant visualization of not only tens of specificities as in our case, but of hundreds or even thousands in one single patient sample. Moreover, the strategy to label samples with antibodies specific for both CD4 and CD8 T cells will allow concomitant visualization and isolation of antigen-specific cells in MHC class I and class II restricted T lymphocytes.

Conclusions

In conclusion we believe this study provides significant advancement in direct human tumor-specific CD4 T cell analysis by pMHC class II multimers. We propose two optimization techniques depending on the reasoning behind the detection of the specific CD4 T cells. If immunomonitoring is the focus (screening the specific cells and sequencing their TCR) then the optimization technique would include the use of LacNAc, dasatinib, neuraminidase, standard multimers as well as the secondary cross-linking Ab. However, if the focus is preserving cell viability after multimer-guided, flow cytometry-based cell sorting for further cell culture or use in cell-based therapies, then reversible NTAmers should be used and neuraminidase omitted. It remains to be shown which TCR affinity levels and TCR repertoire are detected with the optimized protocol compared to the standard one, and if the highest MFI levels correspond to T cells with the highest TCR affinity. We expect that our improved ability to dissect CD4 T cells at an antigen-specific level will decisively help with the successful targeting of these cells in immunotherapy.

Acknowledgements

We would like to thank all the patients for their generous contribution and Anthony Cornu and Brigid MacKenzie for their excellent assistance. We thank Hélène Maby-El-Hajjami for the excellent assistance with clinical data of the patients.

Funding

This study was supported in part by grants from the MEDIC Foundation, the Helmut Horten Foundation, the Swiss National Science Foundation (PR00P3_179727), the Ludwig Institute for Cancer Research and the Stiftung für Krebsbekämpfung. A.C. is recipient of an ISREC fellowship. P.R. was supported in part by grants from the SNSF 31003A_156469 and 310030_182735.

Availability of data and materials

The datasets analyzed during the study are available from the corresponding author upon reasonable request.

Authors contributions

For this study G. A. R., P. G., A. C. and M. S performed experiments. G. A. R., P. G., A. C., J. S., C. J. analyzed the data. D. E. S., G. C., A. H. Provided patient samples and reagents. G. A. R., P. R., J. S., C. J. wrote the manuscript.

Ethics approval and consent to participate

Patients samples were obtained from the Department of Oncology, University Hospital (CHUV), Lausanne, Switzerland, upon written informed consent based on the study protocol (NCT00112242) approved by the IRB and Swissmedic.

Consent for publication

Not applicable.

Competing interests

The authors declare that they have no competing interests.

References

1. Restifo NP, Dudley ME, Rosenberg SA. Adoptive immunotherapy for cancer: harnessing the T cell response. Nat Rev Immunol. 2012 Mar 22;12(4):269–81.

2. Spitzer MH, Carmi Y, Reticker-Flynn NE, Kwek SS, Madhireddy D, Martins MM, et al. Systemic Immunity Is Required for Effective Cancer Immunotherapy. Cell. 2017 26;168(3):487-502.e15.

3. Baumgaertner P, Costa Nunes C, Cachot A, Maby-El Hajjami H, Cagnon L, Braun M, et al. Vaccination of stage III/IV melanoma patients with long NY-ESO-1 peptide and CpG-B elicits robust CD8+ and CD4+ T-cell responses with multiple specificities including a novel DR7-restricted epitope. Oncoimmunology. 2016;5(10):e1216290.

4. Ott PA, Hu Z, Keskin DB, Shukla SA, Sun J, Bozym DJ, et al. An immunogenic personal neoantigen vaccine for patients with melanoma. Nature. 2017 Jul 13;547(7662):217–21.

5. Bentzen AK, Marquard AM, Lyngaa R, Saini SK, Ramskov S, Donia M, et al. Large-scale detection of antigen-specific T cells using peptide-MHC-I multimers labeled with DNA barcodes. Nat Biotechnol. 2016 Oct;34(10):1037–45.

6. Cole DK, Pumphrey NJ, Boulter JM, Sami M, Bell JI, Gostick E, et al. Human TCR-Binding Affinity is Governed by MHC Class Restriction. The Journal of Immunology. 2007 May 1;178(9):5727–34.

7. Hamad AR, O'Herrin SM, Lebowitz MS, Srikrishnan A, Bieler J, Schneck J, et al. Potent T cell activation with dimeric peptide-major histocompatibility complex class II ligand: the role of CD4 coreceptor. J Exp Med. 1998 Nov 2;188(9):1633–40.

8. Crawford F, Kozono H, White J, Marrack P, Kappler J. Detection of antigen-specific T cells with multivalent soluble class II MHC covalent peptide complexes. Immunity. 1998 Jun;8(6):675–82.

9. Jönsson P, Southcombe JH, Santos AM, Huo J, Fernandes RA, McColl J, et al. Remarkably low affinity of CD4/peptide-major histocompatibility complex class II protein interactions. Proc Natl Acad Sci U S A. 2016 May 17;113(20):5682–7.

10. Schmidt J, Dojcinovic D, Guillaume P, Luescher I. Analysis, Isolation, and Activation of Antigen-Specific CD4(+) and CD8(+) T Cells by Soluble MHC-Peptide Complexes. Front Immunol. 2013;4:218.

11. Kalandadze A, Galleno M, Foncerrada L, Strominger JL, Wucherpfennig KW. Expression of recombinant HLA-DR2 molecules. Replacement of the hydrophobic transmembrane region by a leucine zipper dimerization motif allows the assembly and secretion of soluble DR alpha beta heterodimers. J Biol Chem. 1996 Aug 16;271(33):20156–62.

12. Ayyoub M, Dojcinovic D, Pignon P, Raimbaud I, Schmidt J, Luescher I, et al. Monitoring of NY-ESO-1 specific CD4+ T cells using molecularly defined MHC class II/His-tag-peptide tetramers. PNAS. 2010 Mar 27;201001322.

13. Fremont DH, Hendrickson WA, Marrack P, Kappler J. Structures of an MHC class II molecule with covalently bound single peptides. Science. 1996 May 17;272(5264):1001–4.

14. Uchtenhagen H, Rims C, Blahnik G, Chow I-T, Kwok WW, Buckner JH, et al. Efficient ex vivo analysis of CD4+ T-cell responses using combinatorial HLA class II tetramer staining. Nat Commun. 2016 30;7:12614.

15. Hebeisen M, Schmidt J, Guillaume P, Baumgaertner P, Speiser DE, Luescher I, et al. Identification of Rare High-Avidity, Tumor-Reactive CD8+ T Cells by Monomeric TCR–Ligand Off-Rates Measurements on Living Cells. Cancer Res. 2015 May 15;75(10):1983–91.

16. Rabinovich GA, Toscano MA. Turning 'sweet' on immunity: galectin–glycan interactions in immune tolerance and inflammation. Nature Reviews Immunology. 2009 May;9(5):338–52.

17. Demotte N, Stroobant V, Courtoy PJ, Smissen PVD, Colau D, Luescher IF, et al. Restoring the Association of the T Cell Receptor with CD8 Reverses Anergy in Human Tumor-Infiltrating Lymphocytes. Immunity. 2008 Mar 14;28(3):414–24.

18. Petit A-E, Demotte N, Scheid B, Wildmann C, Bigirimana R, Gordon-Alonso M, et al. A major secretory defect of tumour-infiltrating T lymphocytes due to galectin impairing LFA-1-mediated synapse completion. Nature Communications. 2016 Jul 22;7:12242.

19. Lu Y-C, Parker LL, Lu T, Zheng Z, Toomey MA, White DE, et al. Treatment of Patients With Metastatic Cancer Using a Major Histocompatibility Complex Class II-Restricted T-Cell Receptor Targeting the Cancer Germline Antigen MAGE-A3. Journal of clinical oncology : official journal of the American Society of Clinical Oncology. 2017 Oct 10;35(29):3322–9.

20. Mekala DJ, Geiger TL. Functional Segregation of the TCR and Antigen-MHC Complexes on the Surface of CTL. The Journal of Immunology. 2003 Oct 15;171(8):4089–95.

21. Uchtenhagen H, Rims C, Blahnik G, Chow I-T, Kwok WW, Buckner JH, et al. Efficient *ex vivo* analysis of CD4+ T-cell responses using combinatorial HLA class II tetramer staining. Nature Communications. 2016 Aug 30;7:12614.

22. Altman JD, Reay PA, Davis MM. Formation of functional peptide complexes of class II major histocompatibility complex proteins from subunits produced in Escherichia coli. Proc Natl Acad Sci U S A. 1993 Nov 1;90(21):10330–4.

23. Hollingsworth RE, Jansen K. Turning the corner on therapeutic cancer vaccines. npj Vaccines. 2019 Feb 8;4(1):7.

24. Hilf N, Kuttruff-Coqui S, Frenzel K, Bukur V, Stevanović S, Gouttefangeas C, et al. Actively personalized vaccination trial for newly diagnosed glioblastoma. Nature. 2019;565(7738):240–5.

25. Martinez RJ, Andargachew R, Martinez HA, Evavold BD. Low-affinity CD4+ T cells are major responders in the primary immune response. Nat Commun [Internet]. 2016 Dec 15 [cited 2019 Jun 3];7. Available from: https://www.ncbi.nlm.nih.gov/pmc/articles/PMC5234832/

26. Soler M, Li X, John-Herpin A, Schmidt J, Coukos G, Altug H. Two-Dimensional Label-Free Affinity Analysis of Tumor-Specific CD8 T Cells with a Biomimetic Plasmonic Sensor. ACS Sens. 2018 Nov 26;3(11):2286–95.

27. Bentzen AK, Hadrup SR. Evolution of MHC-based technologies used for detection of antigen-responsive T cells. Cancer Immunol Immunother. 2017;66(5):657–66.

28. Kelly R, Greiff D. Toxicity of Pneumococcal Neuraminidase. Infect Immun. 1970 Jul;2(1):115–7.

29. Weiss L. Guest Editorial. J Natl Cancer Inst. 1973 Jan 1;50(1):3–19.

30. Dolton G, Zervoudi E, Rius C, Wall A, Thomas HL, Fuller A, et al. Optimized Peptide–MHC Multimer Protocols for Detection and Isolation of Autoimmune T-Cells. Frontiers in Immunology [Internet]. 2018 Jun 29 [cited 2019 Apr 29];9. Available from: https://www.frontiersin.org/article/10.3389/fimmu.2018.01378/full

31. Jansen DTSL, Ramnoruth N, Loh KL, Rossjohn J, Reid HH, Nel HJ, et al. Flow Cytometric Clinical Immunomonitoring Using Peptide–MHC Class II Tetramers: Optimization of Methods and Protocol Development. Front Immunol [Internet]. 2018 [cited 2019 Jun 4];9. Available from: https://www.frontiersin.org/articles/10.3389/fimmu.2018.00008/full#h3

32. Xu X-N, Purbhoo MA, Chen N, Mongkolsapaya J, Cox JH, Meier U-C, et al. A Novel Approach to Antigen-Specific Deletion of CTL with Minimal Cellular Activation Using α3 Domain Mutants of MHC Class I/Peptide Complex. Immunity. 2001 May 5;14(5):591–602.

Figure legends

Table 1: List of peptides used for cell stimulation and MHC class I and II loading

Figure 1: Temperature optimization for pMHCII multimer staining. A) Basic illustration of pMHCII multimers. Multimers were composed of a fluorochrome backbone (PE in the example, red), an average of 2-3 streptavidin complexes (grey) bound to biotin (black)-labelled pMHC complexes (blue), loaded with the peptide of interest (brown). **B)** Representative dot plots illustrating the impact of the temperature on multimer staining. Staining was performed on specific CD4 T cell clones using an HLA-DR7 multimer loaded with the NY-ESO-$1_{87\text{-}99}$ peptide. Dot plots are gated on live lymphocytes, $CD3^+$. **C-D)** Summary of the results obtained on 3 different clones for the frequency of multimer positive cells (**C**) and the Mean Fluorescent Intensity (MFI) (**D**). **E)** Representative dot plots of criss-cross multimer stainings performed at RT. A HLA-DR7/$HA_{307\text{-}319}$-specific and a HLA-DR7/NY-ESO-$1_{87\text{-}99}$-specific CD4 T cell clone were stained with multimers loaded with either the specific peptide (left plots) or an irrelevant peptide (right plots). **F)** Histogram representation of the Mean Fluorescent Intensities (MFI) obtained using an irrelevant (staining at all temperatures) or the specific multimer (only used at RT). The clone $HA_{307\text{-}319}$ was stained with the specific multimer (in blue) or with the non-specific NY-ESO-$1_{87\text{-}99}$/DR7 multimer (in green). Vice versa, the NY-ESO-$1_{87\text{-}99}$ clone was stained with the specific multimer (in green) and the non-specific $HA_{307\text{-}319}$/DR7 multimer (in blue).

Figure 2: Improvement of the standard pMHCII multimer staining procedure. A) Representative dot plots showing the impact of the indicated molecules tested either individually or in combinations, with or without secondary cross-linking Ab (red) overlaid on the standard staining procedure (green). Optimization was tested on a HLA-DR7/$HA_{307\text{-}319}$ clone (top) and on a HLA-DR7/NY-ESO-$1_{87\text{-}99}$ clone (bottom). Dot plots are gated on live lymphocytes, $CD3^+$. **B)** Fold change representation of the impact on MFI increase by each optimizing condition for both antigen-specificities (n=4). **C)** Representative

dot plots of non-specific multimer binding by a HLA-DR7/NY-ESO-1_{87-99} multimer on a $HA_{307-319}$-specific clone subjected to the optimization treatments. Dot plots are gated on live lymphocytes, $CD3^+$. **D)** MFI representation of non-specific multimer staining in all optimization conditions for all clones $HA_{307-319}$ specific tested (n=3). **E)** Contribution of the LacNAc molecule to the optimization of multimer staining, tested on a HLA-DR7/$HA_{307-319}$-specific clone (left) and on HLA-DR7/NY-ESO-1_{87-99} clone (right). MFI representation of non-specific multimer staining in all optimization conditions is shown on the same clones on the bottom panels. **F)** Imagestream visualization of the increased staining intensity of CD4 T cell clones by multimers under optimization conditions. Clone HLA-DP4/MAGE-$A3_{243-258}$ (left) and HLA-DR7/NY-ESO-1_{87-99} (right) were stained with either standard or with optimized staining procedures. Both MFI and cell images are represented. White arrows illustrate clusters of multimers.

Figure 3: In vitro and *ex-vivo* improvement of multimer staining across multiple specificities. A) Clones specific for HLA-DR7/$HA_{307-319}$ (n=4), HLA-DR7/NY-ESO-1_{87-99} (n=4), HLA-DR4/$HA_{307-319}$ (n=4), HLA-DP4/MAGE-$A3_{111-125}$ (n=3), HLA-DP4/MAGE-$A3_{243-258}$ (n=4), HLA-DP4/$TT_{947-960}$ (n=3) were stained using standard (blue) and optimized staining procedures (red). For negative controls, the staining was performed in the absence of the multimer (black) or with a non-specific multimer (purple). **B)** Representative dot plots of *ex-vivo* staining to detect HLA-DR7/$HA_{307-319}$ (top) and HLA-DR7/NY-ESO-1_{87-99} (bottom) specific CD4 T cells in $DR7^+$ patient samples (left) or in mismatched $DR7^-$ patient samples (right) using standard or the OSP. Dot plots are gated on live lymphocytes, $CD3^+$. **C)** Detection of epitope-specific CD4 T cells in *ex-vivo* samples by standard (blue) and optimized multimer staining (red). Specificities investigated include HLA-DR7/$HA_{307-319}$ (n=17), HLA-DR7/NY-ESO-1_{87-99} (n=15), HLA-DP4/MAGE-$A3_{111-125}$ (n=20), HLA-DP4/MAGE-$A3_{243-258}$ (n=16), HLA-DP4/ $TT_{947-960}$ (n=16). Frequencies of multimer positive cells among total $CD4^+$ $CD3^+$ cells. **D)** HLA-mismatched *ex-vivo* samples were stained using multimers for each one of the previously mentioned specificities, comparing the standard (blue) to the optimized staining procedure (red). Frequencies of multimer positive cells among total $CD4^+$ $CD3^+$ cells (n=3). **E)** Melanoma patient samples pre-vaccination (n=2) or post-4 to 5 vaccinations (n=3) or post-8 vaccinations (n=3) were stained with HLA-DR7/$HA_{307-319}$ or HLA-DR7/NY-ESO-1_{87-99} multimers comparing the standard (blue) to the optimized staining procedure (red).

561 **F)** The phenotype of multimer positive cells in standard stained or optimized multimer stained
562 populations was evaluated with the addition of the CCR7 and CD45RA markers. Naïve (blue), central
563 memory (red), effector memory (green) and terminally differentiated effector memory cells (purple)
564 frequencies were analyzed at the different timepoints during vaccination (n=2, n=3, n=3 respectively
565 for each time point). **G)** Standard multimer staining (blue) or optimized multimer procedure (red) post-
566 *in vitro* stimulation with $HA_{307-319}$ or NY-ESO-1_{87-99} peptides of melanoma patient samples post-
567 vaccination. **H)** HLA-DR7/$HA_{307-319}$ or HLA-DR7/NY-ESO-1_{87-99} multimer staining for the detection
568 of specific cells in two HLA-DR7 healthy donors (n=2). Standard protocol (blue) is compared to the
569 optimized protocol (blue). **I)** Representation of the CD4 T cell phenotype among the multimer positive
570 cells of healthy donors stained with the HLA-DR7/$HA_{307-319}$ or HLA-DR7/NY-ESO-1_{87-99} multimers
571 (n=2). Represented in the pie-chart are the naïve population (blue), central memory (red), effector
572 memory (green) and terminally differentiated effector memory cells (purple).

573 **Figure 4: Combinatorial optimized staining for improved in vitro and *ex-vivo* detection of**
574 **multiple antigen-specificities. A)** Panel of fluorescent multimers used in the experimental mix. On the
575 left list of pMHCII multimers and on the right of pMHCI multimers. **B)** Representative dot plots of the
576 detection of multiple antigen-specific T cells spiked in PBMC stained either with the standard (blue) or
577 optimized multimer procedure (red). Gated on live $CD3^+$ $CD4^+$ or $CD8^+$ cells. **C)** Fold change
578 representation of the increased MFI comparing standard and optimized staining procedures for the
579 different antigen specificities. CD4 T cells are represented on the left and CD8 T cells on the right
580 (n=3). **D)** Representative dot plots of a combinatorial *ex-vivo* multimer staining on HLA-$DR7^+$/HLA-
581 $DP4^+$/HLA-$A2^+$ melanoma patients. Both standard and optimized staining are represented. Gated on
582 live, $CD3^+CD4^+$ or $CD8^+$ cells.

583 **Figure 5: The optimization procedure impacts on cell viability. A)** Dot plots representing HLA-
584 DP4/MAGE-$A3_{243-258}$ CD4 T cell clones of intermediate (left) and high staining intensity (right). Dot
585 plots are gated on live $CD3^+$ $CD4^+$ cells. **B)** Cell viability at time points 6h (blue), 24h (red) and 48h
586 (green) of different HLA-DP4/MAGE-$A3_{243-258}$ CD4 T cell clones. On the left the histogram includes
587 clones of both intermediate and high staining intensity (n=6). In the center are represented only the

intermediate stained clones (n=3) and on the right the high stained clones (n=3). Cells were gated on live, $CD3^+$ $CD4^+$ cells. **C)** The effect on viability of individual or combined molecules at different time points 0h, 6h, 24h and 48h on CD4 and CD8 T cells in healthy donor PBMC.

Figure 6: The use of reversible multimers to prevent activation dependent cell death. A) Basic illustration of pMHCII NTAmers used. NTAmer are based on a fluorochrome backbone here PE (red), an average of 2-3 streptavidin complexes (grey) bound to biotin (black) linked to an imidazole-sensitive Ni^{2+}-NTA_4 moiety. Peptide loaded MHCII monomers (blue) are bound stably to the NTA tag via His tags. **B)** Principle of the NTAmer staining. Upon addition of imidazole (100 mM), NTAmers rapidly decay in pMHC monomers and streptavidin-PE-NTA_4 scaffolds. Monomers subsequently dissociate from cell-associated TCRs. **C)** Representation of cells stained with a NTAmer (left) and the loss of the signal 1 min after dissociation with imidazole (right). **D)** Cell viability at time points 6h (blue), 24h (red) and 48h (green) of HLA-DP4/MAGE-$A3_{243-258}$ clones (n=3) of high staining intensity, stained using the different condition procedures indicated in the Figure. **E)** Cell viability at time points 6h (blue), 24h (red) and 48h (green) of HLA-DP4/MAGE-$A3_{243-258}$ clones (n=3) of high staining intensity, stained using the different condition procedures indicated in the Figure. **F)** Impact on multimer HLA-DR7/NY-ESO-1_{87-99} staining of NY-ESO-1_{87-99} specific clone MFI upon removal of neuraminidase to improve survival. Standard protocol (blue), optimized protocol without neuraminidase (green) and full optimized protocol (red) (n=3). **G)** Cloning efficiency of CD4 T cells isolated from three patients, for both $HA_{307-319}$ and NY-ESO-1_{87-99} specificities, comparing cells sorted using the standard protocol (blue) and the optimized protocol (red). **H)** Screening of growing clones with HLA-DR7/$HA_{307-319}$ or HLA-DR7/NY-ESO-1_{87-99} multimers. Cells were initially sorted using the standard protocol (blue) or the optimized protocol (red). **I)** Dot plot representation of the functionality of a representative HLA-DR7/NY-ESO-1_{87-99} multimer positive clone sorted using the optimized staining procedure. IFNγ and TNFα expression was evaluated in unstimulated cells, after stimulation with an irrelevant ($HA_{307-319}$ peptide) or the specific peptide (NY-ESO-1_{87-99} peptide) (from left to right). **J)** Histogram representation of the functionality of the $HA_{307-319}$ or the NY-ESO-1_{87-99} specific clones initially seeded by sorting using the standard protocol (blue) or the optimized protocol (red) (n=3).

Peptide name	Peptide sequence	Peptide origin	HLA restriction	HLA%
$HA_{307-319}$	PKYVKQNTLKLAT	Haemagglutinin	HLA-DRB1*07:01	25
NY-ESO-1_{87-99}	LLEFYLAMPFATP	New York esophageal squamous cell carcinoma 1	HLA-DRB1*07:01	25
$HA_{307-319}$	PKYVKQNTLKLAT	Haemagglutinin	HLA-DRB1*04:01	24
MAGE-$A3_{111-125}$	RKVAELVHFLLLKYR	Melanoma-associated antigen 3	HLA-DPB1*04:01	75
MAGE-$A3_{243-258}$	KKLLTQHFVQENYLEY	Melanoma-associated antigen 3	HLA-DPB1*04:01	75
$TT_{947-960}$	FNNFTVSFWLRVPK	tetanus toxoid	HLA-DPB1*04:01	75
Melan-$A_{26-35(A27L)}$	ELALIGILTV	MART-1	HLA-A*02:01	44
$EBV_{280-288}$	GLCTLVAML	BMLF-1	HLA-A*02:01	44
$CMV_{495-503}$	NLVPMVATV	pp65	HLA-A*02:01	44
Flu matrix protein$_{58-66}$	GILGFVFTL	Influenza matrix protein H3N2	HLA-A*02:01	44
NY-ESO-$1_{157-165}$	SLLMWITQC	New York esophageal squamous cell carcinoma 1	HLA-A*02:01	44

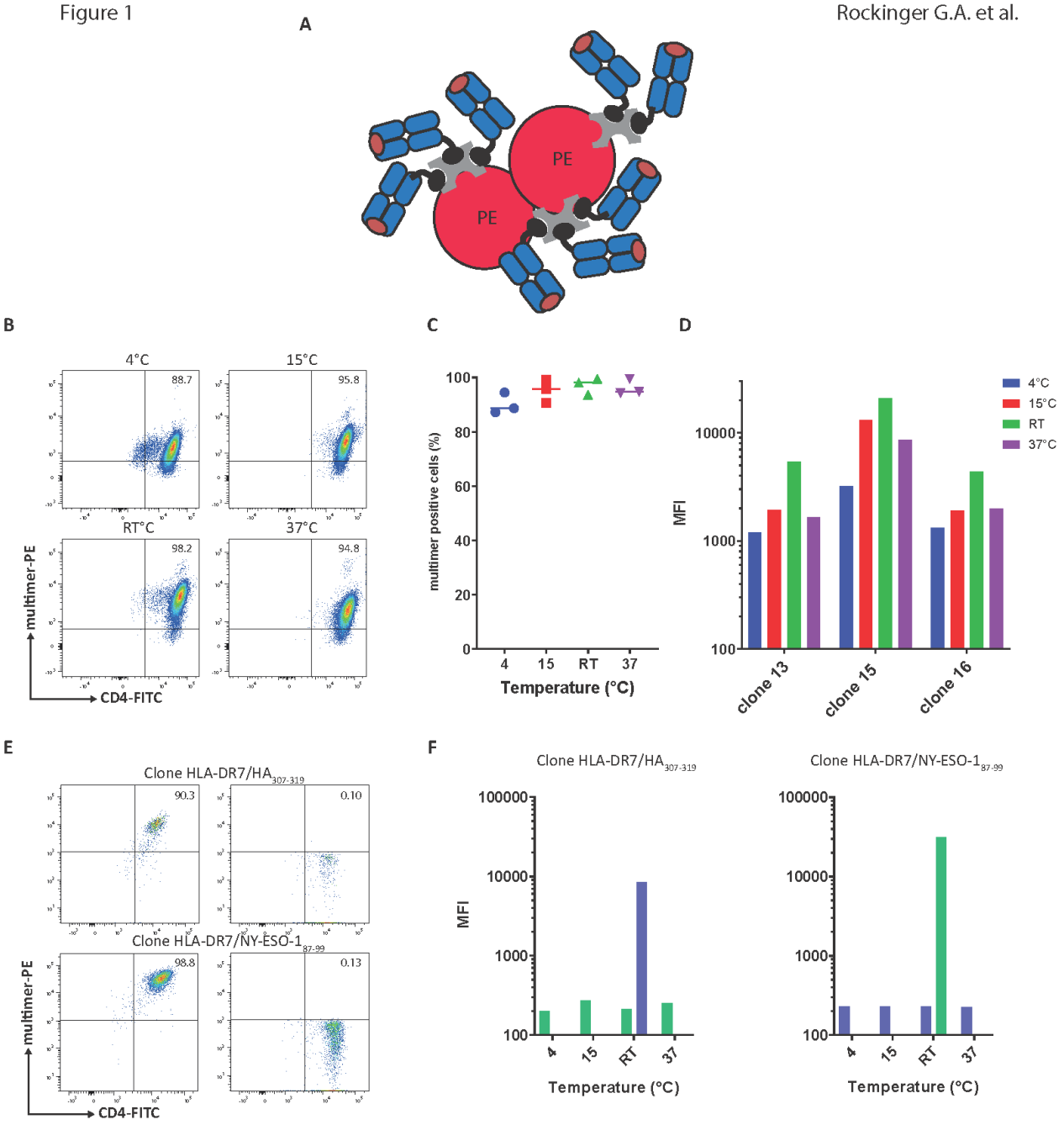
A
PE
PE
B
4°C
15°C
RT°C
37°C
88.7
95.8
98.2
94.8
multimer-PE
CD4-FITC
C
multimer positive cells (%)
Temperature (°C)
4
15
RT
37
D
MFI
4°C
15°C
RT
37°C
clone 13
clone 15
clone 16
E
Clone HLA-DR7/HA307-319
90.3
0.10
Clone HLA-DR7/NY-ESO-187-99
98.8
0.13
multimer-PE
CD4-FITC
F
Clone HLA-DR7/HA307-319
Clone HLA-DR7/NY-ESO-187-99
MFI
Temperature (°C)

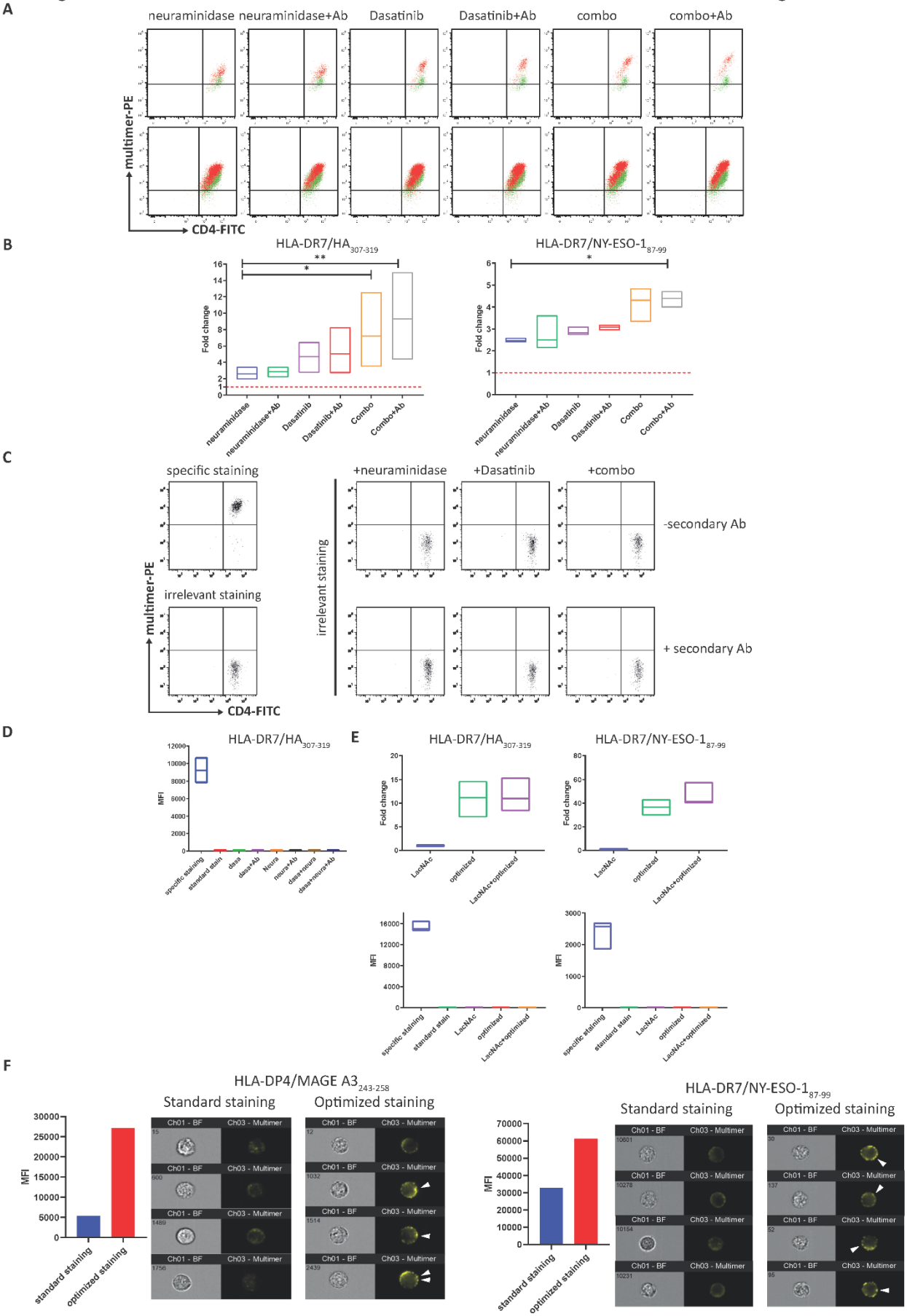
A
neuraminidase
neuraminidase+Ab
Dasatinib
Dasatinib+Ab
combo
combo+Ab
multimer-PE
CD4-FITC
B
HLA-DR7/HA307-319
HLA-DR7/NY-ESO-187-99
Fold change
neuraminidase
neuraminidase+Ab
Dasatinib
Dasatinib+Ab
Combo
Combo+Ab
C
specific staining
+neuraminidase
+Dasatinib
+combo
irrelevant staining
-secondary Ab
+ secondary Ab
multimer-PE
CD4-FITC
D
HLA-DR7/HA307-319
MFI
specific staining
standard stain
dasa
dasa+Ab
Neura
neura+Ab
dasa+neura
dasa+neura+Ab
E
HLA-DR7/HA307-319
HLA-DR7/NY-ESO-187-99
Fold change
LacNAc
optimized
LacNAc+optimized
MFI
F
HLA-DP4/MAGE A3243-258
Standard staining
Optimized staining
MFI
standard staining
optimized staining
Ch01 - BF
Ch03 - Multimer
HLA-DR7/NY-ESO-187-99
Standard staining
Optimized staining

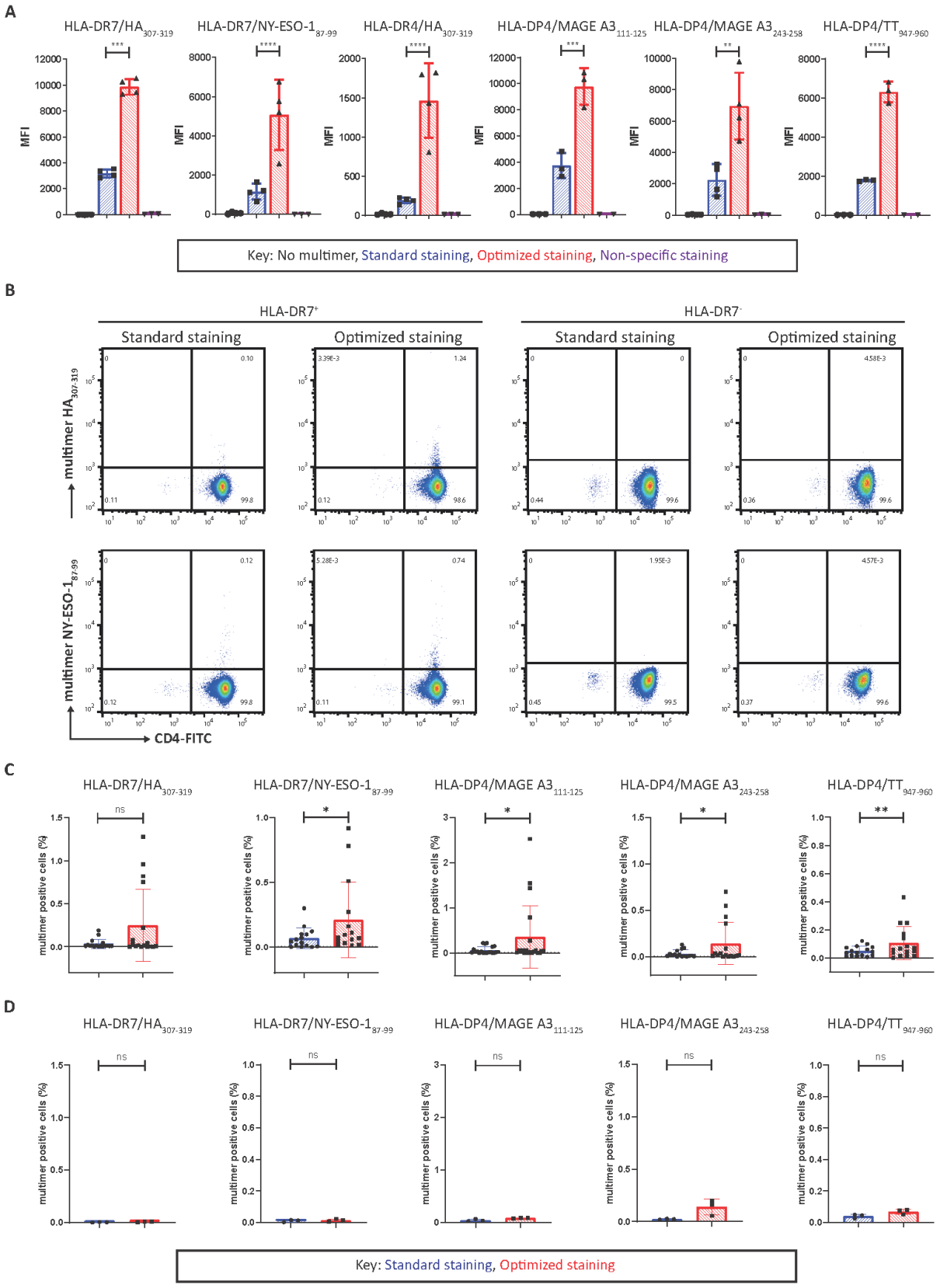
A
HLA-DR7/HA307-319
HLA-DR7/NY-ESO-187-99
HLA-DR4/HA307-319
HLA-DP4/MAGE A3111-125
HLA-DP4/MAGE A3243-258
HLA-DP4/TT947-960
MFI
Key: No multimer, Standard staining, Optimized staining, Non-specific staining
B
HLA-DR7+
HLA-DR7-
Standard staining
Optimized staining
multimer HA307-319
multimer NY-ESO-187-99
CD4-FITC
C
multimer positive cells (%)
ns
D
Key: Standard staining, Optimized staining

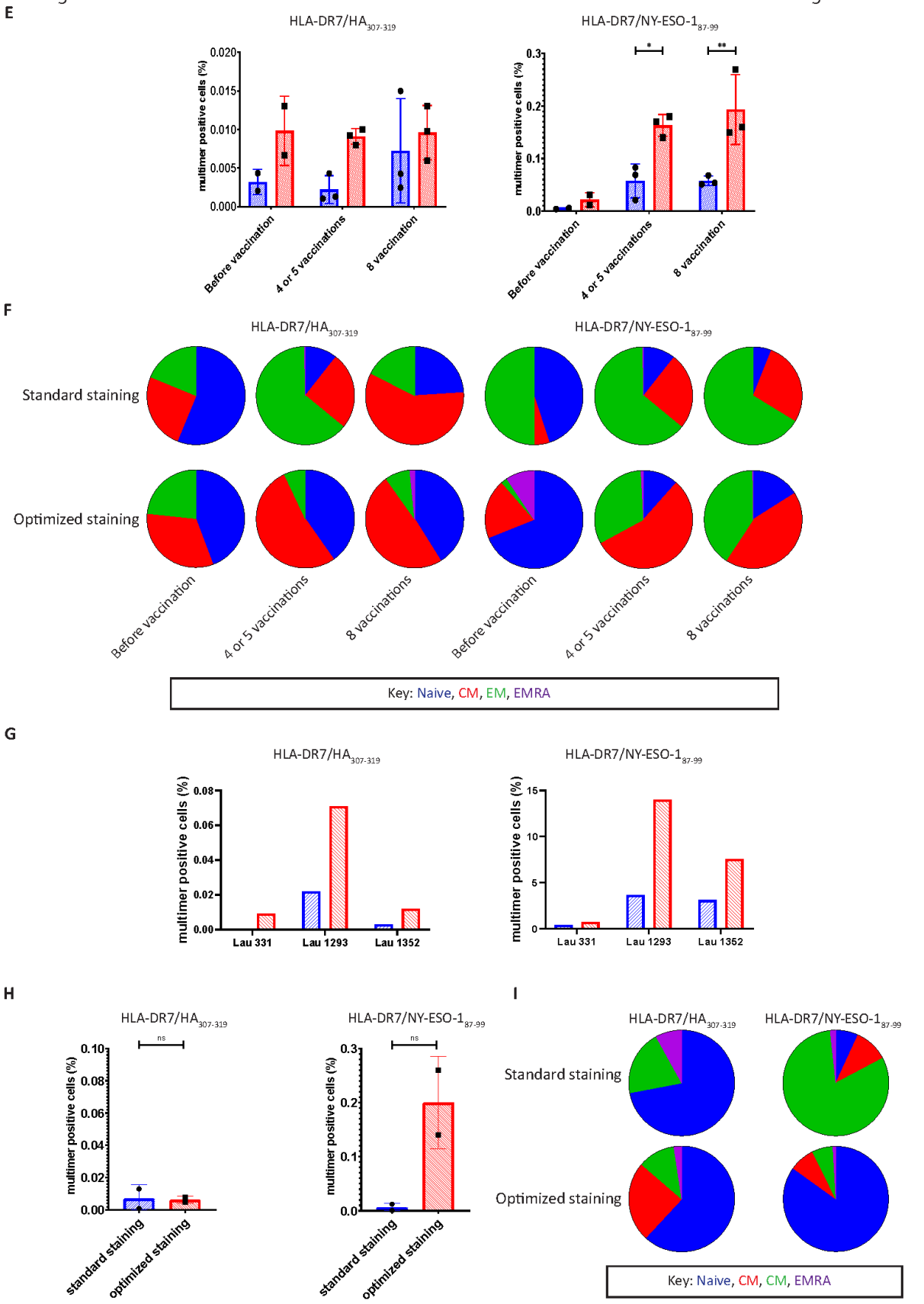
E
HLA-DR7/HA307-319
HLA-DR7/NY-ESO-187-99
multimer positive cells (%)
Before vaccination
4 or 5 vaccinations
8 vaccination
F
HLA-DR7/HA307-319
HLA-DR7/NY-ESO-187-99
Standard staining
Optimized staining
Before vaccination
4 or 5 vaccinations
8 vaccinations
Key: Naive, CM, EM, EMRA
G
HLA-DR7/HA307-319
HLA-DR7/NY-ESO-187-99
multimer positive cells (%)
Lau 331
Lau 1293
Lau 1352
H
HLA-DR7/HA307-319
HLA-DR7/NY-ESO-187-99
ns
multimer positive cells (%)
standard staining
optimized staining
I
HLA-DR7/HA307-319
HLA-DR7/NY-ESO-187-99
Standard staining
Optimized staining
Key: Naive, CM, CM, EMRA

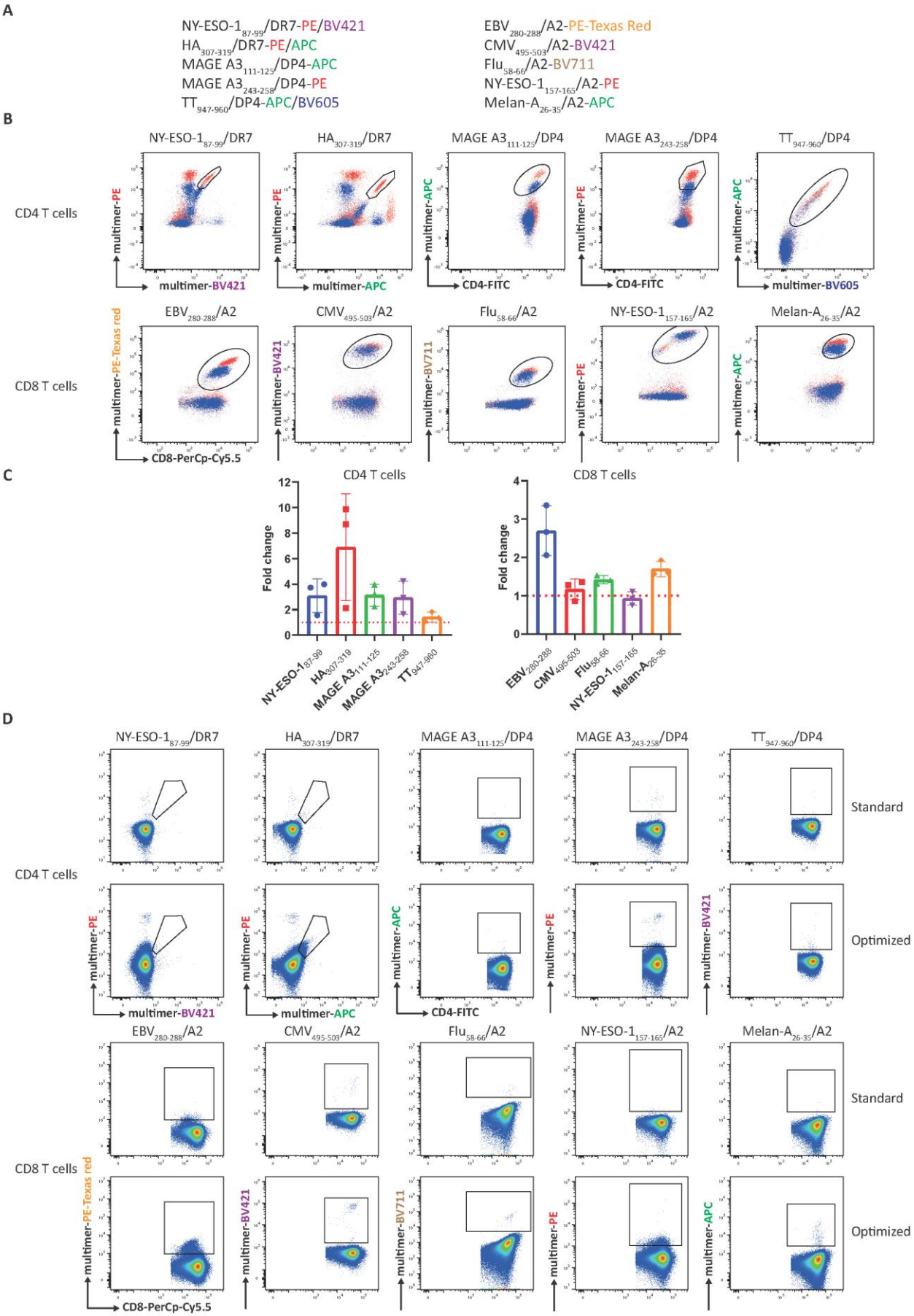
A
NY-ESO-1 87-99/DR7-PE/BV421
HA 307-319/DR7-PE/APC
MAGE A3 111-125/DP4-APC
MAGE A3 243-258/DP4-PE
TT 947-960/DP4-APC/BV605
EBV 280-288/A2-PE-Texas Red
CMV 495-503/A2-BV421
Flu 58-66/A2-BV711
NY-ESO-1 157-165/A2-PE
Melan-A 26-35/A2-APC
B
CD4 T cells
CD8 T cells
multimer-PE
multimer-BV421
multimer-APC
CD4-FITC
multimer-BV605
multimer-PE-Texas red
CD8-PerCp-Cy5.5
multimer-BV711
C
CD4 T cells
CD8 T cells
Fold change
NY-ESO-1 87-99
HA 307-319
MAGE A3 111-125
MAGE A3 243-258
TT 947-960
EBV 280-288
CMV 495-503
Flu 58-66
NY-ESO-1 157-165
Melan-A 26-35
D
Standard
Optimized

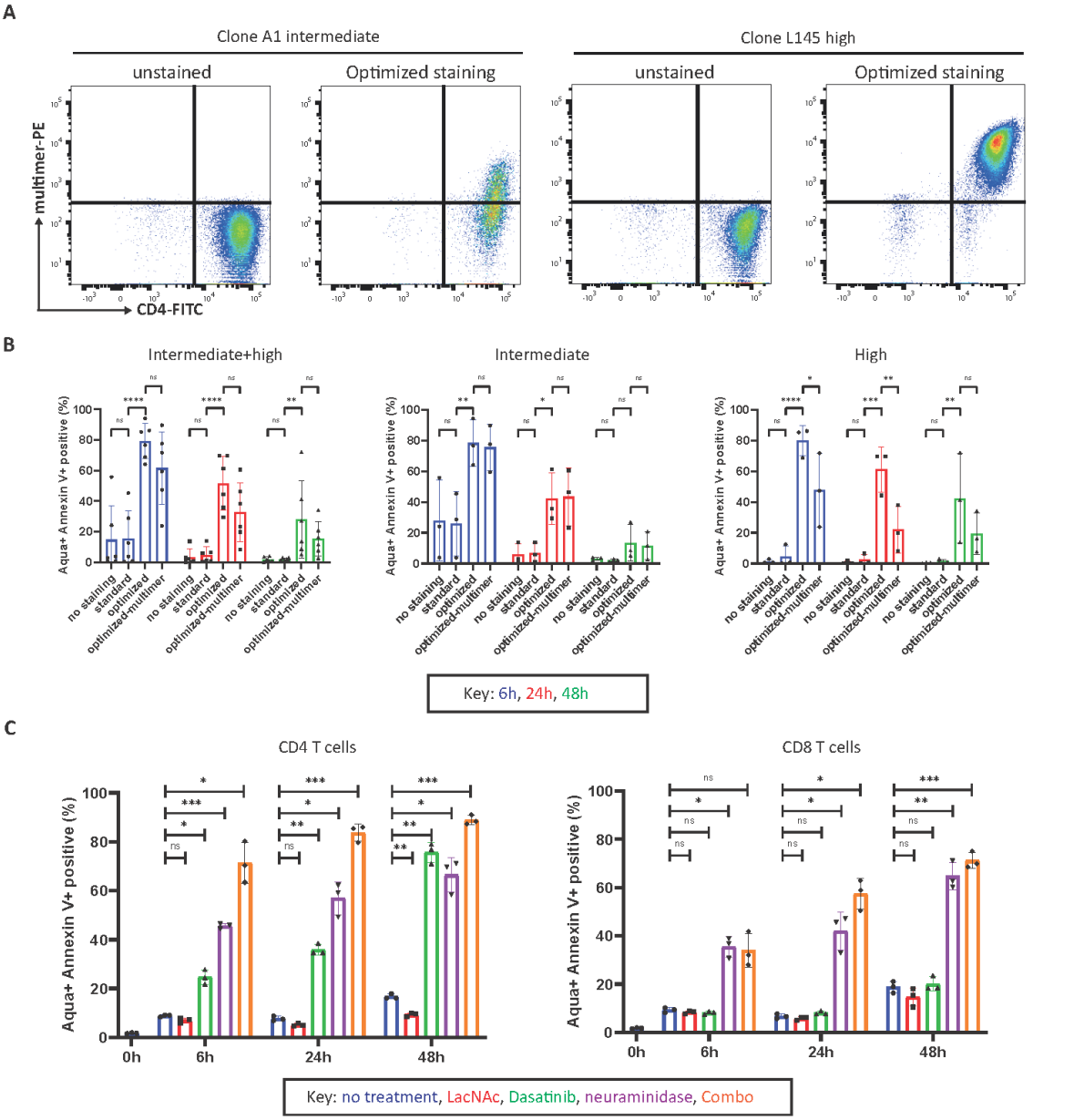
A
Clone A1 intermediate
Clone L145 high
unstained
Optimized staining
unstained
Optimized staining
multimer-PE
CD4-FITC
B
Intermediate+high
Intermediate
High
Aqua+ Annexin V+ positive (%)
no staining
standard
optimized
optimized-multimer
Key: 6h, 24h, 48h
C
CD4 T cells
CD8 T cells
Aqua+ Annexin V+ positive (%)
0h
6h
24h
48h
Key: no treatment, LacNAc, Dasatinib, neuraminidase, Combo

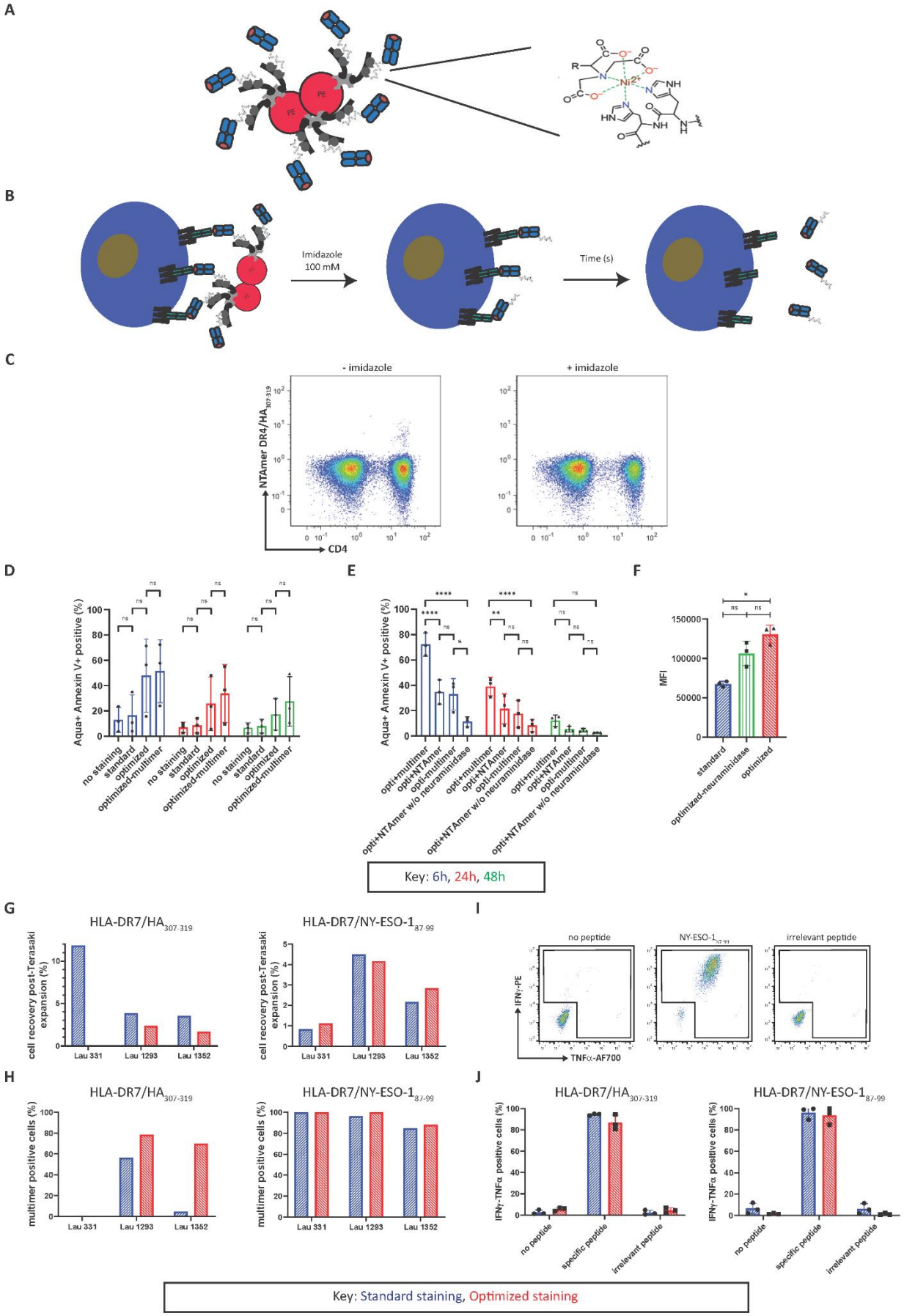
A
PE
PE
B
Imidazole
100 mM
Time (s)
C
- imidazole
+ imidazole
NTAmer DR4/HA307-319
CD4
D
Aqua+ Annexin V+ positive (%)
no staining
standard
optimized
optimized-multimer
E
Aqua+ Annexin V+ positive (%)
opti+multimer
opti+NTAmer
opti-multimer
opti+NTAmer w/o neuraminidase
F
MFI
standard
optimized-neuraminidase
optimized
Key: 6h, 24h, 48h
G
HLA-DR7/HA307-319
HLA-DR7/NY-ESO-187-99
cell recovery post-Terasaki expansion (%)
Lau 331
Lau 1293
Lau 1352
I
no peptide
NY-ESO-187-99
irrelevant peptide
IFNγ-PE
TNFα-AF700
H
HLA-DR7/HA307-319
HLA-DR7/NY-ESO-187-99
multimer positive cells (%)
J
HLA-DR7/HA307-319
HLA-DR7/NY-ESO-187-99
IFNγ-TNFα positive cells (%)
no peptide
specific peptide
irrelevant peptide
Key: Standard staining, Optimized staining

I.5 Discussion

Since the first use of peptide-MHC tetramers, these reagents have represented an invaluable tool for the detection of specific T cells. In a period of personalized immunotherapy, it has become essential to gather as much information as possible on the effects of therapies in patients. As an example, it would be vital in a vaccination trial to be able to monitor the expansion of tumor-specific cells, to isolate them and conduct functional assays to evaluate the efficacy of vaccination, thus improving outcome of clinical trials. pMHC class II multimers would be an excellent tool to move to numerous single cell exploratory analyses of CD4 T cells, as TCR sequencing, transcriptomics, assessment of oligoclonal expansion, and cloning (263). In this study we have used pMHC class II multimers loaded with viral- bacterial- or tumor-specific antigens to detect specific CD4 T cells. Due to a lack of consensus within the field on the optimal temperature for pMHC class II staining (124,263,271) we first started by establishing the ideal temperature for pMHC class II multimer staining and between 4°C,15°C, RT and 22°C, RT resulted as the most favorable temperature. Increasing the temperature of staining did not result in an increase in non-specific binding by our multimers despite this being reported on PBMC (272). Staining with higher temperatures such as a physiologic temperature resulted in a decrease in MFI which could be explained by pMHC class II internalization (273). However, due to the low affinity of pMHC class II for the TCR and high off rate, staining with pMHC class II remains challenging and not yet optimal for immunomonitoring of clinical trials. In this project we investigate a novel and improved methodology to detect as many specific cells as possible and with the brightest staining possible. To do so we introduced an optimized staining procedure (OSP) which uses LacNAc, Dasatinib, neuraminidase as well as an anti-fluorochrome secondary Ab to cross-link pMHC class II multimers at the T-cell surface. With this new procedure we observed a significant increase in specific multimer staining intensity of CD4 T cell clones without an increase in background staining. This increase in cells detected goes in line with the publication from the group of Brian Evavold who has used 2D-binding to evaluate T cell affinity and observed that with conventional tetramer staining a large portion of low affinity cells were not properly detected by tetramers (109). Unfortunately, at the moment the 2D-binding methods still has drawbacks as it is low throughput and time consuming.

In an era where multiple strategies are available for immunotherapy it is vital to time them correctly for an improved response and thus require optimal immunomonitoring (274). We here bring an OSP staining procedure that allows for an improved detection of tumor-, viral- and bacterial-specific cells of *in vitro* cultured cells as well as a detection of higher frequency of cells from *ex vivo* patient samples with little to no background staining. A further longitudinal study of melanoma patient samples pre- and post-vaccination protocol with the 30 amino acid peptide SLP NY-ESO-$1_{79–108}$ (275) showed an increase in NY-ESO-1_{87-99} specific cells detected with our OSP compared to the standard staining procedure showing the feasibility of using the OSP for immunomonitoring. Not only were we able to follow the increase of specific cells post-vaccination

but by adding two supplementary markers CD45RA and CCR7 we could evaluate the differentiation of cells from mostly naïve pre-vaccination transitioning to CM or EM cells post-vaccination. To use this OSP for immunomonitoring, multiple fluorochrome labels were used to label multimers. Single fluorochromes or a combination of two fluorochromes were used to stain clones of multiple specificity both CD4 T cell as well as CD8 T cell all mixed together. Such combinatorial staining with either fluorochromes, metals or DNA barcodes has been performed in the field of CD8 T cells but not yet implemented for CD4 T cells (117). Once more our OSP showed better results compared to the standard staining in the detection of specific cells as well as the frequency of detected cells which was higher with the OSP. Despite our usage of only 10 multimers, the usage of fluorochrome combinations has not been exhausted thus leaving room for the increase of specificities possibly investigated within one sample. Transition towards a DNA based multimer labelling method could also be considered.

As we are probably increasing the affinity of the TCR for pMHC class II molecules with the OSP, there could be reduction in cell viability as described in the CD8 T cell field (276) but not yet reported in the CD4 T cell field. Cells could encounter AICD similarly to the negative selection process in the thymus (61) and we indeed observed such phenomenon. We also observed a certain toxicity on the cells from the use of neuraminidase which had been documented (277,278). We also observed to a lesser extent a reduction of cell viability due to Dasatinib treatment yet we did not find any further proof in literature, on the contrary Dasatinib has been implemented in several tetramer staining procedures without mention of negative impact upon cells (124,263,266). To alleviate the impact on cell survival of TCR-pMHC class II binding we used reversible multimers also known as NTAmers which have the capacity to dissociate the pMHC monomers to the fluorescent backbone upon the addition of imidazole. Following the separation of the backbone from the individual pMHC class II monomers resulted in a rapid dissociation of pMHC class II from the TCR reducing the activation signals sent to the cell (108). When using the NTAmer we observed an increase in cell viability further proving our claim where increased interaction between TCR and pMHC class II complex increased cell mortality.

This study shows the usefulness of using class II multimers for immunomonitoring in combination to the OSP for improved staining performances. In this study we propose two optimization techniques: 1) a first optimization staining procedure for the detection of specific CD4 T cells for an immunomonitoring oriented approach where the focus would be to screen specific cells as well as sequence their TCR. This optimization would include LacNAc, Dasatinib, neuraminidase, standard multimers as well as secondary Ab. This multimer staining can be complemented with any other markers such as CD45RA or CCR7 to evaluate phenotypically the tumor-specific cells. 2) a second optimization staining procedure where the focus would be to preserve cells for further cell culture or use of CD4 T cells in cell-based therapies. In this second procedure we would not use neuraminidase and use reversible multimers as we showed that by using such combination, we

significantly increase cell viability. Despite removing neuraminidase, we still achieve an improved staining upon CD4 T cells. Questions remain to be addressed pertaining to the affinity level of cells that were detected with the optimization protocol but not with the standard protocol as it would be interesting if we were to be able to detect lower affinity cells as they have been described to be major responders in the primary immune response (109). We believe that this optimized staining procedure will help to bring tumor-specific CD4 T further in the spotlight and to an active role within immunotherapy.

J Robust prediction of HLA class II epitopes by deep motif deconvolution of immunopeptidomes

J.1 Introduction

Part of the tumor immunity cycle consist in APC cells taking up antigens of tumor cells upon their death. Following this process APC cells will migrate to the lymph nodes where they will present fragments of the peptides to T cells via the MHC class I and II molecules, resulting in the subsequent activation of the lymphocytes (180). Upon activation, T cells will migrate to the tumor bed where CD8 T cells will kill tumor cells. Due to this fact, CD8 T cells are considered the main actor however, to have an effective and durable anti-tumor immunity, CD4 T cells are key even more so than CD8 T cells. CD4 T enhance antigen presentation, co- stimulation, T cell homing, T cell activation, and effector functions (279). These effects are targeted by cancer vaccine approaches with promising clinical activity (280). Yet the limited accuracy or current predictors of epitopes potentially presented by MHC class II molecules has restricted vaccination and therapy designs targeting this cell type.

Hurdles in this field have been similar to the ones encountered in the generation and usage of pMHC class II multimers. Once more the high polymorphism of MHC class II molecules as well as the extended length of peptides presented in the MHC class II groove, result in difficulties to determine the core binding region of HLA class II ligands. Further complications arise from the knowledge that usually nine amino acids are found in the peptide binding groove of MHC class II molecules and are anchored via the residues at position P1, P4, P6 and P9. Since MHC class II molecules in nature bind peptides between 13 and 25 residues it implicates that several residues are outside of the groove. Despite the main affinity being dictated by the binding core, flanking peptides affect peptide-MHC binding and therefore influence immunogenicity (281). These flanking regions complexify the prediction of peptide binding affinities.

Several prediction methods had been developed such as NetMHCII and NetMHCIIpan, both relying heavily on the amount of peptide binding data generated with high-throughput peptidomics (282,283). Other methods have also been developed but NetMHCII and NetMHCIIpan remained the best methods for predicting binding affinities to MHC class II molecules (284,285). In this study unbiased mass spectrometry was combined with a motif deconvolution algorithm to profile and analyze a total of 99,265 unique peptides eluted from HLA-II molecules. This made this set of data one of the largest datasets of HLA-II ligands available to date. The motif deconvolution algorithm (MoDec) relies on motif to be found anywhere on the peptide instead of attempting to align on peptide residues. MoDec can learn the motifs from peptides, identify their preferred binding core position offsets and their weight. MoDec was then applied to known melanoma-associated antigens and viral and bacterial proteins. The top predictions from both MixMHC2pred (MoDec)

and the currently used NetMHCIIpan were tested for their immunogenicity in melanoma patients and healthy donors to compare their performance as accurate predictor for MHC class II antigen binders.

J.2 Aim

The aim of this project was to develop a new program capable of predicting the binding strengths of epitopes to MHC class II molecules. Our goal was to test the immunogenicity of top predicted peptides from both MixMHC2pred and NetMHCIIpan in melanoma patient samples and healthy donor samples and determine the performance of MixMHC2pred in comparison to NetMHCIIpan.

J.3 Co-author contribution

This work is presented in an article published on the 11.2019 in the journal Nature Biotechnology. For this study I performed the in vitro validation of the predicted viral and tumor antigens, I analysed the data and I wrote the material and method and result section concerning the experimental work that I performed. I discussed the results with my supervisor and with our collaborators in the group of Prof D. Gfeller.

Table 4a and b	Georg Alexander Rockinger and Camilla Jandus generated the table
Figure 2C	I designed and performed the experiment.
Supplementary Figure 9	I designed and performed the experiment.

nature biotechnology

BRIEF COMMUNICATION

https://doi.org/10.1038/s41587-019-0289-6

Robust prediction of HLA class II epitopes by deep motif deconvolution of immunopeptidomes

Julien Racle[1,2], Justine Michaux[1,3], Georg Alexander Rockinger[1], Marion Arnaud[1,3], Sara Bobisse[1,3], Chloe Chong[1,3], Philippe Guillaume[1,3], George Coukos[1,3], Alexandre Harari[1,3], Camilla Jandus[1], Michal Bassani-Sternberg[1,3]* and David Gfeller[1,2]*

Predictions of epitopes presented by class II human leukocyte antigen molecules (HLA-II) have limited accuracy, restricting vaccine and therapy design. Here we combined unbiased mass spectrometry with a motif deconvolution algorithm to profile and analyze a total of 99,265 unique peptides eluted from HLA-II molecules. We then trained an epitope prediction algorithm with these data and improved prediction of pathogen and tumor-associated class II neoepitopes.

Antigen-presenting cells (APCs) display peptides bound to HLA-II on their surface. In infections or cancer, interactions between the T cell receptor on CD4+ T cells and HLA-II–peptide complex on APCs, presenting non-self peptides or tumor-associated antigens, are key to initiate and sustain an immune response[1–4]. Prediction and analysis of HLA-II epitopes is critical to vaccine design and targeted therapy development in immunology and cancer immunotherapy, but is challenging because HLA-II are highly polymorphic and the size of the peptides presented varies. For this reason, the core binding region of HLA-II ligands is difficult to determine, especially in mass spectrometry (MS) datasets of peptides eluted from HLA-II, as peptides from the same sample come from multiple HLA-II alleles. This issue becomes important when training HLA-II epitope prediction algorithms, which display low accuracy[5,6]. Recent developments in HLA peptidomics[7–9], allowing fast and reliable measurements of thousands of HLA ligands per sample, can improve epitope predictions, as shown for HLA-I molecules[10–14]. However, similar improvements have not been observed for HLA-II, and previous studies based on high-throughput peptidomics have been restricted to a few HLA-II alleles[8,15] or failed to demonstrate improvements in epitope predictions[16].

Here we profiled the HLA-II peptidome of 13 different cell lines or tissue samples and identified 40,864 unique HLA-II ligands. We combined this dataset with another one recently generated by our lab[7] to reach a total of 77,189 unique peptides from 23 different samples (Methods; Fig. 1a, Supplementary Table 1 and Supplementary Data 1), making it the largest dataset of HLA-II ligands available to date. To analyze these data, we developed MoDec, a motif deconvolution algorithm (Methods; Supplementary Code 1). Unlike previous approaches that attempted to align peptides[17,18], MoDec is a fully probabilistic framework that allows motifs to be found everywhere on the peptide sequences and learns both the motifs as well as their weights and preferred binding core position offsets (Fig. 1b). MoDec shows conceptual similarity with convolutional neural networks (each motif can be thought of as a filter) but provides direct interpretation and visualization of the results as sequence logos (Fig. 1b).

Applying MoDec to our data, we found many motifs (Supplementary Fig. 1). HLA-II motifs identified across samples with shared HLA-II alleles displayed high similarity (Fig. 1c and Supplementary Fig. 2). This demonstrates high reproducibility of our motif deconvolution approach and enabled us to unambiguously annotate the different motifs to their respective alleles (Supplementary Fig. 2; Methods). Comparison with motifs from the Immune Epitope Database (IEDB)[19] or predictions from NetMHCIIpan[20] showed some similarity but also some important differences, including clearer anchor residues (Supplementary Fig. 2).

The most frequent motifs that we identified corresponded to HLA-DR alleles. To further validate them, we sequentially purified the HLA-DR molecules with an anti-HLA-DR antibody and then the remaining HLA-II molecules with a pan-HLA-II antibody (42,903 and 27,692 peptides, respectively, for a total of 99,265 unique peptides across all our samples; Supplementary Data 2). We observed that the motifs deconvolved from HLA-DR peptidomes are identical to those assigned to HLA-DR alleles from the pan-HLA-II peptidomes (Fig. 1d and Supplementary Fig. 3). In addition, in the HLA-DR-depleted samples, all motifs previously predicted to correspond to HLA-DP or HLA-DQ alleles could be found, indicating that our motif deconvolution approach is not restricted to HLA-DR motifs (Fig. 1d and Supplementary Fig. 3). In comparison to other motif deconvolution methods[18,21], MoDec shows improved resolution and is 100–10,000 times faster (Supplementary Fig. 4), making it particularly appropriate for large HLA-II peptidomics datasets.

We next investigated properties of naturally presented HLA-II ligands beyond the specificity of HLA-II alleles. We first grouped all of our HLA-II ligands and used MoDec to identify motifs occurring three amino acids upstream and downstream of the N or C terminus (Methods). Multiple motifs appeared with a specificity that was in general stronger for amino acids inside the peptides (Supplementary Fig. 5a,b). Some of these amino acid preferences had been suggested to represent different peptide processing and cleavage pathways[15,22,23], such as aminopeptidase trimming of class II ligands with a preference for proline near the N terminus[22]. All alleles showed proline enrichment two residues downstream of the N terminus and upstream of the C terminus (Supplementary Fig. 5c,d). Binding assays demonstrated similar binding between peptides containing proline or alanine at the second position (Supplementary Fig. 5e), validating the hypothesis that proline enrichment reflects peptide processing and loading[22]. We also observed conserved peptide length distributions across HLA-II alleles (Supplementary Fig. 6a),

[1]Department of Oncology UNIL CHUV, Ludwig Institute for Cancer Research, University of Lausanne, Lausanne, Switzerland. [2]Swiss Institute of Bioinformatics (SIB), Lausanne, Switzerland. [3]Department of Oncology UNIL CHUV, Ludwig Institute for Cancer Research, University Hospital of Lausanne, Lausanne, Switzerland. *e-mail: michal.bassani@chuv.ch; david.gfeller@unil.ch

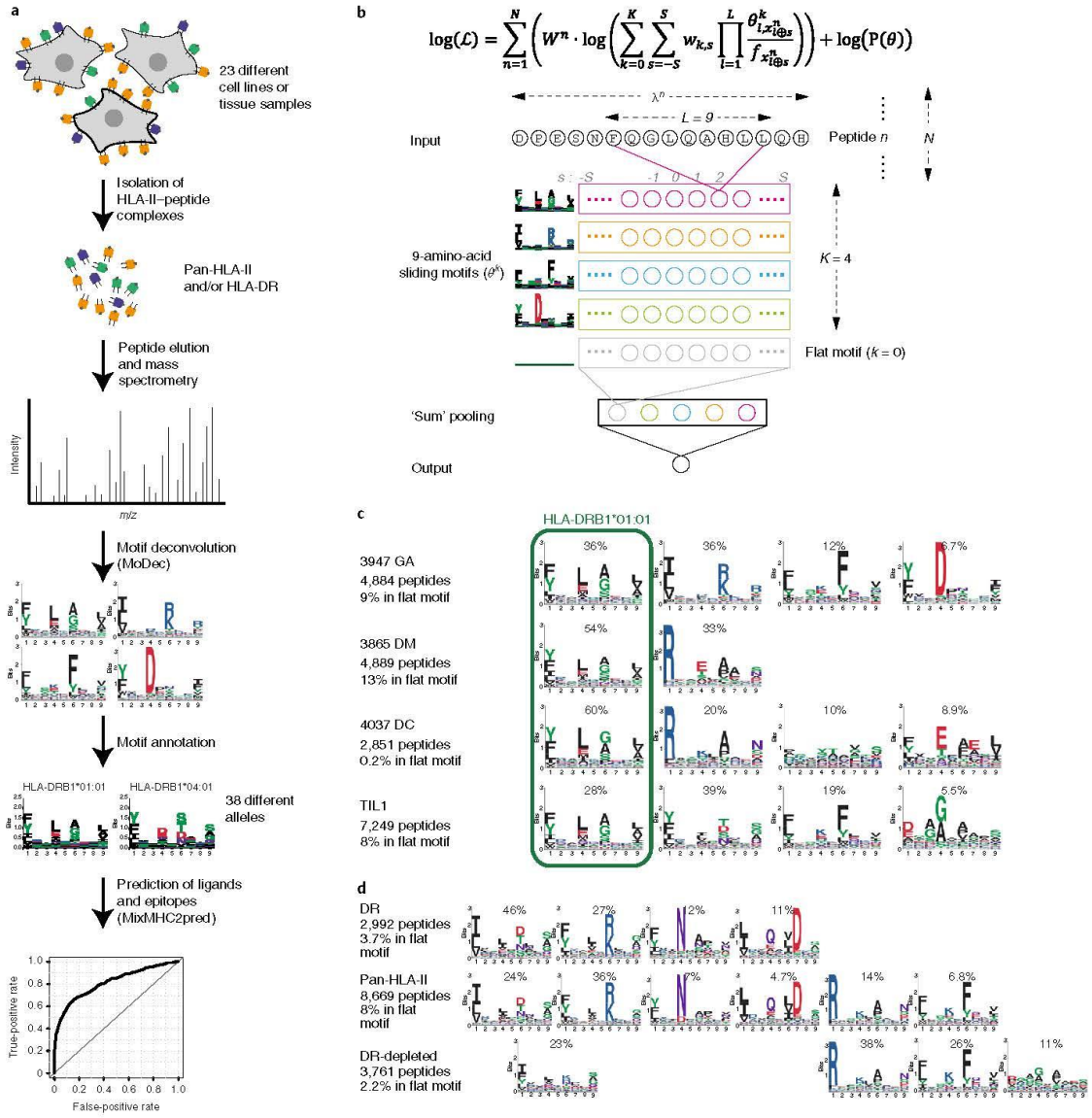

Fig. 1 | Motif deconvolution in HLA-II peptidomics data. a, Description of our pipeline for HLA-II ligand isolation, motif deconvolution and training of an HLA-II ligand predictor. **b**, Top: log-likelihood optimized in MoDec (Methods). Bottom: a graphical interpretation of the model, including *K* sliding 9-amino-acid motifs (θ^k) and a sum pooling step over all positions (*s*). **c**, Motifs identified in four samples sharing exactly one allele (HLA-DRB1*01:01) and showing exactly one highly conserved motif. **d**, A comparison of the motifs found in HLA-II peptidomics, HLA-DR peptidomics and HLA-DR-depleted peptidomics in the same sample (3830-NJF).

unlike for HLA-I alleles[34], and conserved binding core offsets (Supplementary Fig. 6b).

We then took advantage of our deconvolved HLA-II peptidomics datasets to train a predictor of HLA-II ligands (MixMHC2pred; Methods; Supplementary Code 2). This predictor combines allele-specific motifs and allele-independent peptide N- and C-terminal motifs, peptide length and binding core offset preferences (Methods). We first performed predictions on multiple HLA-II peptidomics datasets from independent studies (Supplementary Table 2) and observed improved accuracy as compared to NetMHCIIpan[20] (Fig. 2a and Supplementary Fig. 7). The improvement of our predictor was particularly compelling when considering the positive predictive value for the top 2% of predictions, with an average of 0.90 for MixMHC2pred versus 0.67 for NetMHCIIpan (Supplementary Fig. 7). These results also show the superiority of the full predictor that combines the HLA-II motifs, N- and

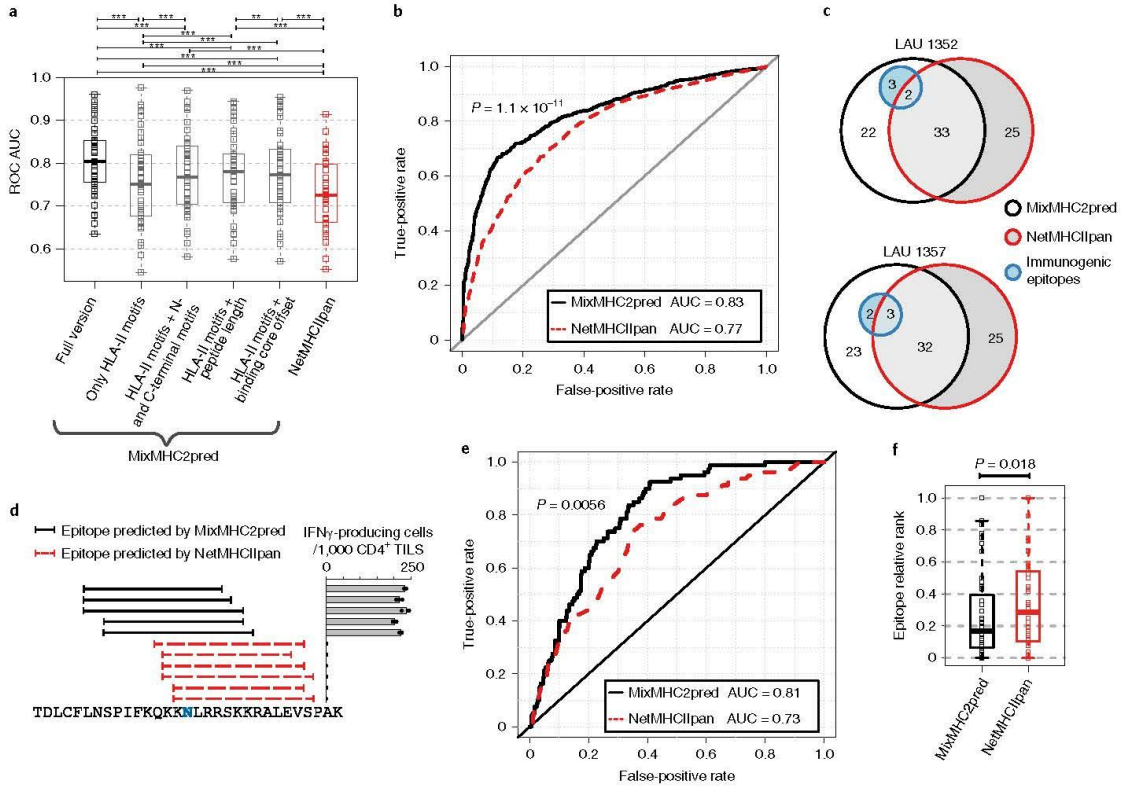

Fig. 2 | MixMHC2pred improves class II epitope prediction. a, Comparison of prediction accuracy of MixMHC2pred (and multiple variants) and NetMHCIIpan for HLA-II ligands ($n = 41$ biologically independent samples). **b**, Receiver operating characteristic (ROC) curve for the predictions of all class II epitopes from CD4+ T cell tetramer assays ($n = 2,359$ positive and negative epitopes). **c**, Euler diagram showing the number of tested and validated (blue circle) epitopes from viral, bacterial and melanoma-associated antigens in two patients with melanoma. **d**, Predictions of epitopes in a minigene encoding an ovarian cancer class II immunogenic mutation ($SGOL1_{D246N}$). The bar plot shows CD4+ T cell responses toward these peptides (mean values from $n = 3$ technical repeats, overlaid with each data point). **e**–**f**, Benchmarking of neoepitope predictions (Supplementary Data 3), based on ROC (**e**, $n = 929$ tested peptides from 13 different patients) and the epitope relative rank (**f**, $n = 80$ independent neoepitopes from 13 different patients). In **a** and **f**, box plots indicate the median, upper and lower quartiles; the results of a paired two-sided Wilcoxon signed rank-test are indicated (**$P < 0.01$, ***$P < 0.001$). In **b** and **e**, P values are based on a two-sided DeLong's test.

C-terminal motifs, peptide length and binding core offset, as compared to a predictor based only on the HLA-II motifs or a combination of the HLA-II motifs with any of the other allele-independent characteristics (Fig. 2a and Supplementary Fig. 7). To investigate whether MixMHC2pred was also appropriate for class II epitopes, we compiled all CD4+ T cell tetramer assays from the IEDB[19]. MixMHC2pred was significantly more accurate than NetMHCIIpan ($P = 1.1 \times 10^{-11}$; Fig. 2b and Supplementary Fig. 8a). The use of neural networks did not improve predictions, which is consistent with the very few interactions observed between positions in the binding core of HLA-II ligands (Supplementary Fig. 8b, Supplementary Table 3 and Supplementary Note). We further surveyed known melanoma-associated antigens and viral and bacterial proteins (Supplementary Table 4a). Top hits from MixMHC2pred and from NetMHCIIpan were tested for class II immunogenicity in two patients with melanoma (Supplementary Table 4b). Our results show a higher fraction of true positives among the predictions of MixMHC2pred versus NetMHCIIpan (Fig. 2c; Matthews correlation coefficients of 0.16 and 0.16 for MixMHC2pred versus −0.17 and −0.058 for NetMHCIIpan). The same peptides were also tested with CD4+ T cells from a healthy donor resulting in many correctly predicted epitopes and similar yield between the two predictors (Supplementary Fig. 9a). We next took advantage of a class II immunogenic substitution (D246N in SGOL1) that was recently identified in a patient with ovarian cancer by screening tumor-infiltrating lymphocytes (TILs) with minigenes (Methods; Supplementary Fig. 10). To determine the actual epitope, we applied MixMHC2pred and NetMHCIIpan on the 31-amino-acid oligomer encoded by the minigene. The results indicate that MixMHC2pred could predict the actual epitope (Fig. 2d and Supplementary Fig. 11). To further assess the use of MixMHC2pred for neoepitope predictions, we compiled recent class II neoantigen studies with available HLA-II typing (Supplementary Data 3). Here again, we observed significant improvements in predictions (Fig. 2e; $P = 0.0056$), with true epitopes in general in the top 16.7% relative to the tested non-immunogenic peptides for MixMHC2pred, but only in the top 28.6% for NetMHCIIpan (Fig. 2f and Supplementary Fig. 12; Methods).

By combining in-depth HLA-II peptidomics with a motif deconvolution algorithm, we could capitalize on unbiased MS profiling of HLA-II ligands for class II epitope predictions. The very high

similarity between HLA-DR motifs identified in pan-HLA-II and HLA-DR peptidomes shows that HLA-DR motifs can be accurately resolved in the pan-HLA-II samples with MoDec. This suggests that monoallelic samples are not needed to determine HLA-DR motifs. Whether increased detection efficacy could be obtained by using anti-HLA-DP and anti-HLA-DQ antibodies remains to be seen, and our motif deconvolution tool may prove highly valuable to analyze such data. Our approach may not capture the full complexity of class II antigen presentation[1], and does not include any information about immunogenicity. Moreover, we cannot exclude the possibility that the use of ligand data also has impacts on our definition of HLA-II motifs, and the latter may therefore not perfectly model the experimental binding stability of peptides, which is important for immunogenicity[25]. This may explain the remaining false positives in our predictions. Despite these limitations, the use of MS data enabled us to integrate unbiased HLA-II motifs together with N- and C-terminal motifs, as well as peptide length and binding core offset preferences, which led to enrichment in true positives among candidate epitopes. The large allele coverage (especially for HLA-DR) makes our predictor suitable for a wide range of applications in infectious diseases, autoimmunity and cancer immunotherapy.

Online content

Any methods, additional references, Nature Research reporting summaries, source data, statements of code and data availability and associated accession codes are available at https://doi.org/10.1038/s41587-019-0289-6.

Received: 15 February 2019; Accepted: 11 September 2019;
Published online: 14 October 2019

References

1. Neefjes, J., Jongsma, M. L. M., Paul, P. & Bakke, O. *Nat. Rev. Immunol.* **11**, 823–836 (2011).
2. Khodadoust, M. S. et al. *Nature* **543**, 723–727 (2017).
3. Linnemann, C. et al. *Nat. Med.* **21**, 81–85 (2015).
4. Kreiter, S. et al. *Nature* **520**, 692–696 (2015).
5. Andreatta, M. et al. *Immunogenetics* **67**, 641–650 (2015).
6. Andreatta, M. et al. *Bioinformatics* **34**, 1522–1528 (2018).
7. Chong, C. et al. *Mol. Cell. Proteomics* **17**, 533–548 (2018).
8. Ritz, D. et al. *Proteomics* **18**, 1700246 (2018).
9. Bassani-Sternberg, M. et al. *Nat. Commun.* **7**, 13404 (2016).
10. Bassani-Sternberg, M. & Gfeller, D. *J. Immunol.* **197**, 2492–2499 (2016).
11. Bassani-Sternberg, M. et al. *PLoS Comput. Biol.* **13**, e1005725 (2017).
12. Abelin, J. G. et al. *Immunity* **46**, 315–326 (2017).
13. Jurtz, V. et al. *J. Immunol.* **199**, 3360–3368 (2017).
14. Bulik-Sullivan, B. et al. *Nat. Biotechnol.* **37**, 55–63 (2019).
15. Barra, C. et al. *Genome Med.* **10**, 84 (2018).
16. Garde, C. et al. *Immunogenetics* **71**, 445–454 (2019).
17. Nielsen, M. & Andreatta, M. *Nucleic Acids Res.* **45**, W344–W349 (2017).
18. Andreatta, M., Alvarez, B. & Nielsen, M. *Nucleic Acids Res.* **45**, W458–W463 (2017).
19. Vita, R. et al. *Nucleic Acids Res.* **47**, D339–D343 (2019).
20. Jensen, K. K. et al. *Immunology* **154**, 394–406 (2018).
21. Bailey, T. L. & Elkan, C. Fitting a mixture model by expectation maximization to discover motifs in biopolymers. in *Proc. Second International Conference on Intelligent Systems for Molecular Biology* (eds Altman, R., Brutlag, D., Karp, P., Lathrop, R., & Searls, D.) 28–36 (AAAI, 1994).
22. Falk, K., Rötzschke, O., Stevanović, S., Jung, G. & Rammensee, H.-G. *Immunogenetics* **39**, 230–242 (1994).
23. Ciudad, M. T. et al. *J. Leukoc. Biol.* **101**, 15–27 (2017).
24. Gfeller, D. et al. *J. Immunol.* **201**, 3705–3716 (2018).
25. Yin, L., Calvo-Calle, J. M., Dominguez-Amorocho, O. & Stern, L. J. *J. Immunol.* **189**, 3983–3994 (2012).

Acknowledgements

We thank the Center of Experimental Therapeutics team for providing us with the patient-derived tissue samples and T cells. We thank P. Romero from the University of Lausanne for sharing the B cell lines with us. We thank R. T. Daniel and M. Hegi from the University Hospital of Lausanne for providing us with the collection of meningioma tissues. We thank M. Solleder for help with the visualization of motifs with ggseqlogo, F. Marino for technical support with sample preparation, H.-S. Pak for MS measurements and R. Genolet for HLA typing. This work was supported by the Swiss Cancer League (grant KFS-4104-02-2017 to D.G. and J.R.), the Ludwig Institute for Cancer Research, the ISREC Foundation thanks to a donation from the Biltema Foundation (to J.M., C.C. and M.B.-S.) and by the MEDIC foundation (to G.A.R. and C.J.).

Author contributions

J.R. developed the computational methods; J.R. and D.G. analyzed the data; J.M., C.C. and M.B.-S. generated the MS peptidomics data; G.A.R., M.A., S.B., P.G., A.H. and C.J. performed the binding and T cell assays; G.C., A.H., C.J. and M.B.-S. provided reagents; J.R., M.B.-S. and D.G. designed the study; and J.R., M.B.S. and D.G. wrote the paper.

Competing interests

The authors declare no competing interests.

Additional information

Supplementary information is available for this paper at https://doi.org/10.1038/s41587-019-0289-6.

Correspondence and requests for materials should be addressed to M.B.-S. or D.G.

Reprints and permissions information is available at www.nature.com/reprints.

Publisher's note Springer Nature remains neutral with regard to jurisdictional claims in published maps and institutional affiliations.

Methods

Cells and patient material. Epstein–Barr-virus-transformed human B-cell lines JY (ATCC, 77442), CD165, PD42, CM467, RA957, BP455, GD149 (a gift from P. Romero (Ludwig Cancer Research Lausanne)), were maintained in RPMI-1640 + GlutaMAX medium (Life Technologies) supplemented with 10% heat-inactivated FBS (Dominique Dutscher) and 1% penicillin–streptomycin solution (BioConcept). Cells were grown to the required cell numbers, collected by centrifugation at 1,200 rpm for 5 min, washed twice with ice cold PBS and stored as dry cell pellets at −20 °C until use.

T cells were expanded from two melanoma tumors as previously described[7,11] and following established protocols[26,27]. In brief, fresh tumor samples were cut in small fragments and placed in 24-well plates containing RPMI CTS grade (Life Technologies), 10% human serum (Valley Biomedical), 0.025 M HEPES (Life Technologies), 55 μmol l^{-1} 2-mercaptoethanol (Life Technologies) and supplemented with a high concentration of interleukin (IL)-2 (Proleukin, 6,000 IU ml^{-1}; Novartis) for 3–5 weeks. TILs (25×10^6) were stimulated with irradiated feeder cells, anti-CD3 (OKT3, 30 ng ml^{-1}; Miltenyi biotec) and high-dose IL-2 (3,000 IU ml^{-1}) for 14 d. The cells were washed using a cell harvester (LoVo, Fresenius Kabi). Finally, the cells were washed with PBS on ice, aliquoted to a cell count of 1×10^8 and stored as dry pellets at −80 °C until use.

Snap-frozen meningioma tissues from patients (3808-HMC, 3830-NJE, 3849-BR, 3865-DM, 3869-GA, 3911-ME, 3912-BAM, 3947-GA, 3971-ORA, 3993, 4001, 4021, 4037-DC and 4052-BA) were obtained from the Centre Hospitalier Universitaire Vaudois (CHUV, Lausanne, Switzerland). Informed consent of the participants was obtained following requirements of the Institutional Review Board (Ethics Commission, CHUV). Protocol F-25/99 has been approved by the local ethics committee and the biobank of the Lab of Brain Tumor Biology and Genetics. Protocol 2017-00305 for antigen and T cell discovery in tumors has been approved by the local ethics committee.

HLA typing. Genomic DNA was extracted using DNeasy kit from Qiagen and 500 ng of genomic DNA was used to amplify HLA genes by PCR. High-resolution 4-digit HLA typing was performed with the TruSight HLA v2 Sequencing Panel from Illumina on a MiniSeq instrument (Illumina). Sequencing data were analyzed with the Assign TruSight HLA v.2.1 software (Illumina) and are provided as Supplementary Table 1.

Generation of antibody-crosslinked beads. Anti-pan-HLA-II and anti-HLA-DR monoclonal antibodies were purified from the supernatant of HB145 (ATCC, HB-145) and HB298 cells (ATCC, HB-298), respectively, grown in CELLLine CL-1000 flasks (Sigma-Aldrich) using protein A-sepharose 4B beads (pro-A beads; Invitrogen). Antibodies were crosslinked to pro-A beads at a concentration of 5 mg of antibodies per milliliter of beads. For this purpose, the antibodies were incubated with pro-A beads for 1 h at room temperature. Chemical crosslinking was performed by addition of dimethyl pimelimidate dihydrochloride (Sigma-Aldrich) in 0.2 M sodium borate buffer, pH 9 (Sigma-Aldrich) at a final concentration of 20 mM for 30 min. The reaction was quenched by incubation with 0.2 M ethanolamine, pH 8 (Sigma-Aldrich) for 2 h. Crosslinked antibodies were kept at 4 °C until use.

Purification of HLA-II and HLA-DR peptides. Cells were lysed in PBS containing 0.25% sodium deoxycholate (Sigma-Aldrich), 0.2 mM iodoacetamide (Sigma-Aldrich), 1 mM EDTA, 1:200 protease inhibitors cocktail (Sigma-Aldrich), 1 mM phenylmethylsulfonylfluoride (Roche) and 1% octyl-beta-D-glucopyranoside (Sigma-Aldrich) at 4 °C for 1 h. The lysis buffer was added to cells at a concentration of 1×10^8 cells per milliliter. Cell lysates were cleared by centrifugation with a table-top centrifuge (Eppendorf Centrifuge) at 4 °C and 14,200 rpm for 50 min. Meningioma tissues were placed in tubes containing the same lysis buffer and homogenized on ice in three to five short intervals of 5 s each using an Ultra Turrax homogenizer (IKA) at maximum speed. For 1 g of tissue, 10–12 ml of lysis buffer was required. Cell lysis was performed at 4 °C for 1 h. Tissue lysates were cleared by centrifugation at 20,000 rpm in a high-speed centrifuge (Beckman Coulter, JSS15314) at 4 °C for 50 min. The cells and tissue lysates were loaded on stacked 96-well single-use microplates (3-μm glass fiber, 10-μm polypropylene membranes; cat no. 360063, Seahorse Bioscience). Purification of pan-HLA-II peptides was performed following depletion of HLA-I as previously described[7]. For the sequential purification of HLA-DR and HLA-II from tissues, three plates were used. The first plate contained pro-A beads (Invitrogen) for depletion of antibodies (pre-clear plate), the second plate contained the same beads crosslinked to the anti-HLA-DR monoclonal antibodies and the third plate contained the beads crosslinked to anti-HLA-II monoclonal antibodies. For the sequential purification of HLA-DR and HLA-II from cells, only the last two plates were used. The Waters Positive Pressure-96 processor (Waters) was employed. The second and third plates were washed separately four times with 2 ml of 150 mM sodium chloride (Carlo-Erba) in 20 mM Tris-HCl, pH 8, four times with 2 ml of 400 mM NaCl in 20 mM Tris-HCl, pH 8 and four times again with 2 ml of 150 mM NaCl in 20 mM Tris-HCl, pH 8. Finally, the plates were washed twice with 2 ml of 20 mM Tris-HCl, pH 8. Each affinity plate was stacked on top of a Sep-Pak tC_{18} 100 mg Sorbent 96-well plate (cat. no. 186002321, Waters) pre-equilibrated with 1 ml of 80% acetonitrile (ACN) in 0.1 % trifluoroacetic acid (TFA) and with 2 ml of 0.1% TFA. The HLA and peptides were eluted with 500 μl of 1% TFA into the Sep-Pak plate and then we washed this plate with 2 ml of 0.1% TFA. Thereafter, HLA-II and HLA-DR peptides were eluted with 500 μl of 32% ACN in 0.1% TFA into a collection plate. Recovered HLA-II and HLA-DR peptides were dried using vacuum centrifugation (Concentrator plus, Eppendorf) and stored at −20 °C.

The data from the third plate in the sequential purification (that we termed 'HLA-DR-depleted') are meant to be enriched in HLA-DP- and HLA-DQ-bound peptides, but not to lead to a full depletion of HLA-DR-bound peptides owing to the amount of antibodies used in the purification and the incubation time during the affinity purification. This is confirmed by the clear presence of HLA-DR motifs in the deconvolution (Supplementary Fig. 3).

LC–MS/MS analyses of HLA-II peptides. Before MS analysis, HLA-II and HLA-DR peptide samples were resuspended in 10 μl of 2% ACN in 0.1% formic acid (FA) and aliquots of 3 μl for each MS run were placed in the Ultra HPLC autosampler. HLA peptides were separated by nanoflow HPLC (Proxeon Biosystems, Thermo Fisher Scientific) coupled on-line to a Q Exactive HF or HFX mass spectrometers (Thermo Fisher Scientific) with a nanoelectrospray ion source (Proxeon Biosystems). We packed a 20-cm-long, 75-μm-inner-diameter column with ReproSil-Pur C18-AQ 1.9 μm resin (Dr. Maisch GmbH) in buffer A (0.5% acetic acid). Peptides were eluted with a linear gradient of 2–30% buffer B (80% ACN and 0.5% acetic acid) at a flow rate of 250 nl min^{-1} over 90 min. Data were acquired using a data-dependent 'top 10' method. Full-scan MS spectra were acquired at a resolution of 70,000 at 200 m/z with an auto gain control (AGC) target value of 3×10^6 ions. The ten most abundant ions were sequentially isolated, activated by higher-energy collisional dissociation and accumulated to an AGC target value of 1×10^5 with a maximum injection time of 120 ms. In the case of assigned precursor ion charge states of one, and from six and above, no fragmentation was performed. MS/MS resolution was set to 17,500 at 200 m/z. Selected ions were dynamically excluded for additional fragmentation for 20 s. The peptide match option was disabled. The raw files and MaxQuant output tables have been deposited to the ProteomeXchange Consortium via the PRIDE[28] partner repository with the dataset identifier PXD012308.

Peptide identification. We employed the MaxQuant platform[29] v.1.5.5.1 to search the peak lists against a fasta file containing the human proteome (Homo_sapiens_UP000005640_9606, the reviewed part of UniProt, with no isoforms, including 21,026 entries downloaded in March 2017) and a list of 247 frequently observed contaminants. Peptides with a length between 8 and 25 amino acids were allowed. The second peptide identification option in Andromeda was enabled. The enzyme specificity was set as unspecific. A false-discovery rate of 1% was required for peptides and no protein false-discovery rate was set. The initial allowed mass deviation of the precursor ion was set to 6 ppm and the maximum fragment mass deviation was set to 20 ppm. Methionine oxidation and N-terminal acetylation were set as variable modifications. The peptide output files summarizing MaxQuant result files are provided as Supplementary Data 1 and 2.

Motif deconvolution algorithm for HLA-II peptidomics. In HLA-II peptidomics data, the HLA-II ligands are coming from different alleles, are of different lengths and their binding core positions are a priori unknown. To account for this, and building upon the successful application of the mixture model to HLA-I peptidomics[10], we developed a probabilistic framework able to learn multiple motifs anywhere on the peptides, as well as the weights and binding core offsets of these motifs. The log-likelihood is given by the following equation (see also Fig. 1b):

$$\log(\mathcal{L}) = \sum_{n=1}^{N}\left(W^n \cdot \log\left(\sum_{k=0}^{K}\sum_{s=-S}^{S} w_{k,s}\prod_{l=1}^{L}\frac{\theta^k_{l,x^n_{l+s}}}{f_{x^n_{l+s}}}\right)\right) + \log(P(\theta)) \qquad (1)$$

where N is the number of peptides; W^n is the similarity weight of the nth peptide (see below); K is the number of motifs; S is the maximal binding core offset ($S = \left\lfloor\frac{max_n(\lambda^n)-L}{2}\right\rfloor$, where λ^n is the length of the nth peptide); $w_{k,s}$ is the weight of motif k with binding core offset s ($\sum_k\sum_s w_{k,s} = 1$); L is the motif length (equal to nine here as HLA-II ligands are known to bind with a 9-amino-acid core (Supplementary Note and Supplementary Fig. 13)); $\theta^k_{i,i}$ represents the motifs (with $\sum_i \theta^k_{i,i} = 1$; $k = 0$ is a special case of a flat motif, $\theta^0_{i,i}$def$=h_i$, where h_i are the amino acid frequencies in the human proteome (this motif is used to model potential contaminant peptides)); x^n_j indicates which amino acid is found in peptide n at the position j (when x^n_j is not defined (that is, $j < 1$ or $j > \lambda^n$), then θ^k_{l,x^n_j}def$=0$); f_i is the expected background frequency in HLA-II peptidomics data for amino acid i; and $P(\theta)$ is a Dirichlet prior term (with the hyperparameter equal to 0.1)[30]. The '$l \oplus s$' in $x^n_{l\oplus s}$ is a 'special sum' that ensures that the binding core offsets are symmetric around 0 for each peptide (see Supplementary Note). A peptide similarity weight is given by $W^n = 1/S^n_{sim}$, where S^n_{sim} represents the average number of times each 9-amino-acid oligomer from the nth peptide is observed in the full dataset. This is useful as multiple overlapping HLA-II ligands from the same source region are typically found by MS.

Unlike the previous approaches for HLA-I[10,11], our model does not need previous peptide alignment, learns the binding core offsets of the motifs and includes peptide similarity weights. MoDec estimates the parameters θ and w based on expectation maximization (Supplementary Note). Although our framework is fully probabilistic, peptide responsibilities are derived during the expectation maximization, and these can be used to predict to which motif each peptide is most likely associated and with which binding core offset. Multiple runs (250 in this study) are performed by MoDec to optimize the log-likelihood of equation (1), starting from different initial conditions, considering all peptides of length 12 or more. As HLA-DR ligands have preference for hydrophobic amino acids at position 1, we implemented the possibility to include such a bias in a subset of the initial conditions used in the optimization by MoDec.

HLA-II motifs determined by MoDec are visualized with ggseqlogo[31].

The optimal number of motifs (K) was first determined using the Akaike information criterion (AIC):

$$\begin{aligned}\mathrm{AIC} = 2 \cdot n_{\mathrm{params}} - 2 \cdot \log(\mathcal{L}) = 2 \cdot (K \cdot (n_{\mathrm{aa}} - 1) \cdot L \\ +(2 \cdot S + 1) \cdot (K + 1) - 1) - 2 \cdot \log(\mathcal{L})\end{aligned} \quad (2)$$

where n_{params} is the number of free parameters, n_{aa} is the number of different amino acids (20) and the other parameters have been defined earlier. This AIC is commonly used in information theory to determine the information gained from using a model with more parameters over a simpler model (the smaller the AIC value the better). However, as with HLA-I peptidomics data[10] (and more generally with many clustering approaches), the optimal number of motifs is difficult to determine in a fully unsupervised way. We therefore explored additional motifs, tried further splitting specific motifs and manually curated each dataset for consistency across samples. Comparison between the numbers of motifs manually curated or determined by the AIC showed that in most cases the correct number of motifs would have been found with the AIC and in 80% of the cases the error when using this criterion would be at most of one motif (Supplementary Fig. 14), suggesting that AIC is a good starting point for the selection of the optimal number of motifs.

Assignment of motifs to alleles. To annotate the different motifs to their respective alleles, we used an iterative approach: we considered all samples that share a given allele and determined whether a motif was shared between all these samples. To decide which motifs are shared, we used the Kullback–Leibler divergence (KLD) between the motifs $\left(\mathrm{KLD}(k,m) = -\sum_l \sum_i \theta^k_{l,i} \cdot \log\left(\frac{\theta^m_{l,i}}{\theta^k_{l,i}}\right) < \mathrm{KLD}_{\mathrm{thr}}\right)$ for a given threshold ($\mathrm{KLD}_{\mathrm{thr}}$ varied between 1 and 1.75 depending on the iteration). Each iteration consists of checking for each allele, one after the other, if we can assign a motif to this allele. In the first five iterations, at least 75% of the samples containing the given allele had to share a motif to assign this motif to the given allele (in later iterations, the threshold of samples is decreased to 60%), with the additional requirement that no other allele was shared by these samples. By repeating these iterations multiple times, various motifs could be annotated to their respective allele. All annotations were further manually curated, allowing, for example, the annotation of HLA-DRB1*01:02, which is highly similar to HLA-DRB1*01:01 but with only the PD42 sample expressing this allele (Supplementary Fig. 2). We could then observe that the KLDs between each pair of motifs was significantly lower between motifs of the same allele or allele supertype than between different alleles (Supplementary Fig. 15a; $P < 0.001$).

We also explored an alternative approach to determine the motif corresponding to each allele, merging the data from multiple samples sharing a given allele together instead of using MoDec on each sample separately. Although this alternative approach allows more peptides per allele, it also requires deconvolving a larger number of specificities, which adds complexity to the deconvolution. In practice, we could nicely recover most of the HLA-DR motifs, but failed to accurately identify most HLA-DP and HLA-DQ motifs, and did not find any additional or improved motifs (Supplementary Note and Supplementary Fig. 15b).

For the binding motifs from the IEDB[19] database, we downloaded the full MHC ligand data (http://www.iedb.org/database_export_v3.php, 28 January 2018) and filtered this data to remove peptides obtained from MS (as for many of them, allele restriction information is based on predictions) and keep only the peptides described as 'Positive-High' binders. MoDec was run considering a single motif on the resulting list of peptides per allele. The corresponding motifs are shown in Supplementary Fig. 2.

Binding motifs from NetMHCIIpan[20] were determined in the following way: 16,000 random human peptides (2,000 of each length between 12 and 19 amino acids) were input into NetMHCIIpan. For each allele, the peptides with a '%Rank' better than five were kept and ggseqlogo[31] was used to draw the motifs from the corresponding 'Core' sequences returned by NetMHCIIpan.

Comparison to other motif deconvolution methods. We compared the motifs found by MoDec with those predicted by Gibbscluster (v.2.0 (ref. [13])) and MEME v.4.12 (ref. [21]) (Supplementary Fig. 4). For a comparison of the timing, the tools were launched on a single 3.3 GHz CPU with 2 GB of RAM, searching for one to eight motifs in various samples.

Gibbscluster was run with the recommended parameters for HLA-II (five seeds for the initial conditions, an initial MC temperature of 1.5, using a trash cluster with a threshold of two for this cluster, the rest being left unchanged). Gibbscluster suggests using a Kullback–Leibler criterion to select the optimal number of clusters from their deconvolution. In some cases, manual curation allowed us to find additional clusters that had similarity with known HLA-II motifs, and we show the results of Gibbscluster including these additional clusters in Supplementary Fig. 4.

MEME was run setting a motif width of nine, a maximum dataset size of 10,000,000 (needed owing to the size of the samples) and the rest was left at default.

Investigation of the properties of HLA-II ligands other than binding specificity. Analysis of N- and C-terminal flanking motifs was done with MoDec by taking the three amino acids upstream and downstream of the N and C termini of the peptides that could be assigned to alleles (that is, the peptides were extended on the basis of their protein of origin to include the three amino acids upstream of the N terminus and downstream of the C terminus).

The peptide length distributions, binding core offset distributions and frequencies of proline two residues downstream of the N terminus and upstream of the C terminus, were computed for all peptides associated to each allele.

Binding affinity assays. Peptide binding affinity (Supplementary Fig. 5e) was assessed by peptide competition assay. For each peptide, eight wells of a v-bottom 96-well plate (Greiner Bio-One) were filled with 100 µl of each recombinant 'empty' DR1, DR4 or DR7 protein (1 µg) in a citrate saline buffer (100 mM citrate, pH 6.0), with 0.2% β-octyl-glucopyranoside (Calbiochem), 1× complete protease inhibitors (Roche) and 2 µM FLAG-$\mathrm{HA}_{307-319}$ peptide. Competitor peptides (10 mM DMSO solution) were added to each well to a final concentration of 100, 33, 11, 3.7, 1.2, 0.4, 0.1 and 0 µM for DR1 and DR4 or 100, 33, 11, 3.7, 1.2, 0.4, 0.1 and 0 nM for DR7. After incubation at 37 °C overnight, 100 µl was transferred to a plate coated with avidin (2 µg ml^{-1}) and previously blocked. After 1 h of incubation at room temperature and three washes with 1× PBS, pH 7.4 and 0.05% Tween 20, anti-FLAG-alkaline phosphatase conjugate (Sigma) was added as 1:5,000. After 1 h, the plate was washed as previously described and developed with pNPP SigmaFAST substrate and absorbance was read with a 405-nm filter.

MixMHC2pred, a predictor of HLA-II ligands. We trained a predictor of HLA-II ligands (MixMHC2pred) using all our HLA-II peptidomics data (including the pan-HLA-II, HLA-DR and HLA-DR-depleted peptidomics data). For a given allele, a, and peptide, n, the binding score is given by:

$$B^a_n = \left(\sum_{s=-S}^{S} w_s \prod_{l=1}^{L} \frac{\theta^a_{l,n_{l+s}}}{f_{n_{l+s}}}\right) \cdot \left(\sum_{k=0}^{3} w^N_k \prod_{l=1}^{3} \frac{\iota^k_{l,n^n_l}}{f_{n^n_l}}\right) \cdot \left(\sum_{k=0}^{3} w^C_k \prod_{l=\lambda^n-2}^{\lambda^n} \frac{\gamma^k_{l,n^n_l}}{f_{n^n_l}}\right) \quad (3)$$

where w_s represents the global binding core offset preference (computed by combining all peptides associated to an allele); $\theta^a_{l,i}$ is the position probability matrix for allele a (computed from all peptides associated to this allele with their respective binding core offset on the basis of the highest responsibility value, and adding pseudocounts on the basis of the BLOSUM62 substitution matrix with a parameter $\beta = 200$ (ref. [32])); $\iota^k_{l,i}$ and $\gamma^k_{l,i}$ are similar matrices representing the N- and C-terminal motifs (Supplementary Fig. 5a,b; including here only the amino acids within the peptides); w^N_k and w^C_k represent the relative contributions of the N- and C-terminal motifs (that is, the fraction of peptides assigned to each of these motifs). See equation (1) for the definition of other terms.

This binding score is then transformed to a percentile rank per peptide length by comparing it to the score of 10,000 random human peptides of the same length, and then further transformed to a global percentile rank by ensuring that the top 1% of random human peptides follow the same peptide length distribution as the global peptide length distribution observed in our HLA-II peptidomics data. Finally, when the score among multiple alleles is requested, the score from each peptide is taken as its best percentile rank among all the alleles.

Benchmarking HLA-II ligand predictions. The accuracy of MixMHC2pred was tested in 41 samples from seven independent HLA-II peptidomics datasets[2,8,33–37] (Supplementary Table 2). The positives were the peptides of lengths between 12 and 19 amino acids observed in these samples (removing all the peptides that were also part of the training data from MixMHC2pred for any of the alleles from a given sample). For each sample we then added four times more negatives by randomly sampling human peptides of lengths between 12 and 19 amino acids.

Predictions from MixMHC2pred and its different variants (see Fig. 2a) were compared with those from NetMHCIIpan (v.3.2 (ref. [20]) with default parameters) on the basis of the HLA-II typing provided in these studies (Supplementary Table 2). The area under the curve (AUC) of the receiver operating characteristic (ROC) curve was computed for each sample separately (Fig. 2a and Supplementary Fig. 7). The positive predictive value for the top x% of predictions ($\mathrm{PPV}_{x\%}$) was also computed for each sample (Supplementary Fig. 7; computed for $x = 2\%$ and $x = 20\%$). For this, a threshold was determined for the predictor score to have x% of peptides considered to be ligands. PPV at this threshold was then obtained as $\mathrm{PPV}_{x\%} = \frac{\mathrm{True\ positives}_{x\%}}{\mathrm{True\ positives}_{x\%} + \mathrm{False\ positives}_{x\%}}$.

In addition to the HLA-II peptidomics data, we tested the predictors on binding affinity data. This included all binding affinity data obtained from the IEDB database[19] (as of 5 May 2019). These data was filtered to remove peptides with non-standard amino acids or that were tested against an allele absent from MixMHC2pred. Only data from 2017 onward was included, because NetMHCIIpan had been trained on all the binding affinity data up to 2016. This analysis showed that the motifs obtained from HLA-II peptidomics data also helped in predicting binding affinities (Supplementary Fig. 16a,b). Other features than HLA-II motifs did not help here (Supplementary Fig. 16), which is expected as these characteristics would be more related to processing and cleavage biases than binding affinities.

Benchmarking predictions of epitopes from tetramer assays. All the multimer and tetramer assay data for human CD4+ T cells from the IEDB database[19] were downloaded (as of 20 July 2018). We then filtered these data to remove peptides with non-standard amino acids and to keep peptides of length 12 and longer that were associated to a known allele based on the following 'Allele evidence codes': 'MHC binding assay' or 'T cell assay -Single MHC type present'. Only interactions involving alleles available in MixMHC2pred were considered.

Predictions with MixMHC2pred and NetMHCIIpan v.3.2 (ref. [20]) were performed for each peptide with its associated HLA-II allele, both for the positive (1,319 peptides) and the negative (1,040 peptides) cases. The corresponding ROC curve and its AUC are shown in Fig. 2b. The epitope relative rank is defined as the fraction of negative peptides in the dataset that had a better predicted score than a given true epitope, and was computed separately for each true epitope (Supplementary Fig. 8a).

Selection of candidate viral, bacterial and tumor-associated epitopes. To further benchmark MixMHC2pred, we retrieved a list of known viral, bacterial and melanoma-associated proteins (Supplementary Table 4a) and tested their immunogenicity in two HLA-DRB1*07:01-positive patients with melanoma and one HLA-DRB1*07:01-positive healthy donor. Each protein was cut into 20-amino-acid oligomers overlapping by 10 amino acids to cover all possible 9-amino-acid cores. These 20-amino-acid peptides were then ranked according to the predicted affinity to HLA-DRB1*07:01 (considering the highest predicted affinity from the 15-amino-acid subsequences in each peptide). We then selected the 30 best scoring potential epitopes from the viral and bacterial proteins and the 30 best scoring potential epitopes from the tumor-associated antigens for experimental validation, both for the predictions from MixMHC2pred and NetMHCIIpan.

Matthews correlation coefficients were computed on the basis of the epitopes tested experimentally (for example, the true negatives from MixMHC2pred are the peptides that had been predicted in the top 60 by NetMHCIIpan but not by MixMHC2pred and that are not immunogenic).

Peptide synthesis. Peptides were synthesized at the Protein and Peptide Chemistry Facility at the University of Lausanne by standard solid phase chemistry on a multiple peptide synthesizer (Applied Biosystem). All peptides were >90% pure as indicated by analytic HPLC. Lyophilized peptides were diluted in pure DMSO at 10 mg ml^{-1} and aliquots at 1 mg ml^{-1} in 10% DMSO were prepared and stored at −80 °C.

In vitro peptide stimulation. Peripheral blood mononuclear cells (PBMCs) from two HLA-DRB1*07:01-positive patients with malignant melanoma and from one HLA-DRB1*07:01-positive healthy donor were thawed and CD4+ T cells were enriched using anti-CD4 microbeads and MiniMACS magnetic separation columns (Miltenyi Biotec). CD4+ T cells were resuspended in RPMI 1640 (Gibco) supplemented with 2 mM glutamine, 1% (vol/vol) non-essential amino acids, 50 μM 2-β-mercaptoethanol, penicillin (50 U ml^{-1}) and streptomycin (50 μg ml^{-1}) (Gibco), and 8% human serum (Blood Transfusion Center, Bern) (complete medium) and seeded (0.5×10^6/well) in 48-well plates to which autologous irradiated (30grey) CD4− T cells were added at a 1:1 ratio. Pools of the selected viral, bacterial or tumor-associated peptides (20-amino-acid oligomers; Supplementary Table 4b) were added to the wells at a final concentration of 2 μM each. After an overnight period in culture, 500 μl of medium was replaced by fresh medium containing 100 IU ml^{-1} final of human recombinant IL-2. Every 2 d the medium was refreshed. After 10 d of in vitro expansion, cultures were tested for the presence of antigen-reactive CD4+ T cells. Aliquots of 10^5 cells were transferred to individual wells of a 96-well plate and stimulated overnight with a mix of multiple peptides distributed in different pools according to a specific matrix (Supplementary Fig. 9b). Brefeldin A at 2.5 μg ml^{-1} (Sigma-Aldrich) was added to each well. A non-stimulated control was added as well as a positive control where cells were stimulated with phorbol 12-myristate 13-acetate (PMA) (Sigma-Aldrich) and ionomycine (Sigma-Aldrich) at 50 ng ml^{-1} and 500 ng ml^{-1}, respectively. The following day, cells were collected and stained using anti-CD3-APC (clone UCHT1, Beckman Coulter), anti-CD4-FITC antibodies (clone RPA-T4, Biolegend) and live–dead feasible Aqua dead-cell stain (Invitrogen) for 20 min at 4 °C. Cells were then washed with PBS, fixed and permeabilized using the FOXP3/transcription kit (Invitrogen) for 30 min at room temperature. Finally, the cells were stained for intracellular markers using anti-interferon-γ (IFNγ)-PE (clone 4SB3, BD Biosciences) and anti-tumor necrosis factor-α (TNFα)-AF700 antibodies (clone Mab11, BD Biosciences) for 20 min at 4 °C. Cells were acquired with the CYTOFLEX analyzer (Beckman Coulter) and data were analyzed with Flowjo software. Positive wells for IFNγ and/or TNFα were identified (Supplementary Fig. 9c,d). As each individual peptide was only contained in two different pools, by matching the positive wells in the matrix, individual immunogenic peptide were selected and evaluated individually. In a similar procedure that was used to evaluate multiple peptides in a matrix format, individual selected peptides were added to newly seeded CD4+ T cells and after an overnight incubation the cells were evaluated for their expression of IFNγ and TNFα using the same method as described above (Supplementary Fig. 9e–f).

Patient and neoantigen description. Patient CTE-0007 is a patient with recurrent ovarian cancer. Clinical data and all methodologies for the identification of non-synonymous somatic mutations were already described[38].

Identification and validation of neoepitope-specific CD4+ TILs. Neoantigen (mutation D246N in SGOL1)-specific CD4+ TILs were identified in patient CTE-0007 upon co-culture with tandem-minigene-transfected autologous B cells. TILs were derived from tumor single-cell suspensions and expanded with high-dose IL-2 (Proleukin, 6,000 IU ml^{-1}) for 15 d as previously reported[38]. In parallel, CD19+ cells were isolated from PBMCs using magnetic beads (Miltenyi) and expanded for 14 d with multimeric CD40L (Adipogen; 1 μg ml^{-1}) and IL-4 (Miltenyi; 200 IU ml^{-1}). CD40-activated B cells were electroporated using a Neon system (Invitrogen) with 1 μg of in vitro transcribed RNA (Ambion) coding for 31-amino-acid oligomers centered on the specific mutations. Following 16 h of resting after electroporation, 10^5 cells per well of RNA-transfected B cells were co-cultured with TILs at a ratio of 1:1 and incubated overnight in precoated enzyme-linked immune absorbent spot (ELISpot) plates (Mabtech). Subsequently, T cell activation was validated by intracellular cytokine staining as described[38]. Either RNA-transfected B cells or B cells loaded with peptides were used as APCs. Neoepitope-reactive CD4+ TILs were sorted using a FACSAria IIu, on the basis of CD154 upregulation, as described[39]. CD154-sorted cells were expanded with irradiated feeder cells (PBMCs from two donors) in the presence of OKT3 (Miltenyi; 30 ng ml^{-1}) and IL-2 and further interrogated to identify the predicted candidate epitopes by IFNγ ELISpot. Additionally, HLA-DR-blocking (clone L243, in-house production) antibody was added together with cognate peptides. For HLA-restriction analysis, HLA-matched or mismatched CD40-activated B cells were loaded with 2 μM peptide SPIFKQKKNLRRS for 2 h before co-culture.

The candidate epitopes have been selected on the basis of the top five predictions from MixMHC2pred and NetMHCIIpan among all 13- to 16-amino-acid oligomers of the minigene (TDLCFLNSPIFKQKKNLRRSKKRALEVSPAK).

Benchmarking neoepitope predictions. The list of neoantigens that were tested experimentally for CD4+ T cell immunogenicity was retrieved from the literature[40–46]. All patients for which HLA typing was publicly available and that had allele(s) defined in MixMHC2pred were included in the benchmark (Fig. 2e–f and Supplementary Data 3). Neoantigens tested experimentally were usually sequences of 20–25 amino acids. We gave a score to these sequences on the basis of the highest score from their 15-amino-acid oligomer subsequences with either MixMHC2pred or NetMHCIIpan. We then computed the ROC curve and corresponding AUC considering only the peptides tested experimentally for each patient (that is, no artificial negatives). Figure 2e shows the results obtained by grouping the data from all patients and Supplementary Fig. 12 shows the data for each patient separately. Additionally, for each neoepitope, we determined its epitope relative rank (that is, the fraction of negative antigens tested experimentally for a given patient that had a better predicted score than a given true epitope; Fig. 2f).

Statistics. The relevant statistical test, sample size, replicate type and *P* values for each figure and table are found in the figure or table and/or the corresponding figure or table legends. Statistical analyses were performed with R.

Reporting Summary. Further information on research design is available in the Nature Research Reporting Summary linked to this article.

Data availability

The raw datasets generated during the current study are available in the ProteomeXchange Consortium via the PRIDE partner repository with the dataset identifier PXD012308 and the corresponding peptide output files are provided as Supplementary Data 1 and 2. Additional datasets generated during the current study are available as Supplementary Tables 1 and 4. In addition, public datasets were analyzed in this study, obtained from the IEDB database[19] and from the studies listed in Supplementary Table 2, as well as from multiple neoantigen studies listed in Supplementary Data 3.

Code availability

MoDec and MixMHC2pred are freely available as C++ executables (https://github.com/GfellerLab/ and Supplementary Code 1 and 2) for academic non-commercial

research purposes. MixMHC2pred is also freely available for academic non-commercial research purposes as a web application (http://mixmhc2pred.gfellerlab.org/).

References

26. Dudley, M. E. et al. *Clin. Cancer Res.* **16**, 6122–6131 (2010).
27. Donia, M., Larsen, S. M., Met, Ö. & Svane, I. M. *Cytotherapy* **16**, 1117–1120 (2014).
28. Vizcaíno, J. A. et al. *Nucleic Acids Res.* **44**, D447–D456 (2016).
29. Cox, J. & Mann, M. *Nat. Biotechnol.* **26**, 1367–1372 (2008).
30. Gfeller, D. et al. *Mol. Syst. Biol.* **7**, 484 (2011).
31. Wagih, O. *Bioinformatics* **33**, 3645–3647 (2017).
32. Nielsen, M. et al. *Bioinformatics* **20**, 1388–1397 (2004).
33. Clement, C. C. et al. *J. Biol. Chem.* **291**, 5576–5595 (2016).
34. Collado, J. A. et al. *Eur. J. Immunol.* **43**, 2273–2282 (2013).
35. Ooi, J. D. et al. *Nature* **545**, 243–247 (2017).
36. Wang, Q. et al. *J. Proteome Res.* **16**, 122–136 (2017).
37. Bergseng, E. et al. *Immunogenetics* **67**, 73–84 (2015).
38. Bobisse, S. et al. *Nat. Commun.* **9**, 1092 (2018).
39. Chattopadhyay, P. K., Yu, J. & Roederer, M. *Nat. Protoc.* **1**, 1–6 (2006).
40. Ott, P. A. et al. *Nature* **547**, 217–221 (2017).
41. Tran, E. et al. *Science* **350**, 1387–1390 (2015).
42. Veatch, J. R. et al. *J. Clin. Invest.* **128**, 1563–1568 (2018).
43. Veatch, J. R et al. *Cancer Immunol. Res.* **7**, 910–922 (2019).
44. Yossef, R et al. *JCI Insight* **3**, e122467 (2018).
45. Zacharakis, N. et al. *Nat. Med.* **24**, 724–730 (2018).
46. Sahin, U. et al. *Nature* **547**, 222–226 (2017).

Antigen	Antigen type	Sequence
CMV pp65	Viral	MESRGRRCPEMISVLGPISGHVLKAVFSRGDTPVLPHETRLLQTGIHVRVSQPSLILVSQYTPDSTPCHRGDNQLQVQHTYFTGSEVENVSVNVHNPTGRSICPSQEPMSIYVYALPLKMLNIPSINVHHYPSAAERKHRHLPVADAVIHASGKQMWQARLTVSGLAWTRQQNQWKEPDVYYTSAFVFPTKDVALRHVVCAHELVCSMENTRATKMQVIGDQYVKVYLESFCEDVPSGKLFMHVTLGSDVEEDLTMTRNPQPFMRPHERNGFTVLCPKNMIIKPGKISHIMLDVAFTSHEHFGLLCPKSIPGLSISGNLLMNGQQIFLEVQAIRETVELRQYDPVAALFFFDIDLLLQRGPQYSEHPTFTSQYRIQGKLEYRHTWDRHDEGAAQGDDDVWTSGSDSDEELVTTERKTPRVTGGGAMAGASTSAGRKRKSASSATACTSGVMTRGRLKAESTVAPEEDTDEDSDNEIHNPAVFTWPPWQAGILARNLVPMVATVQGQNLKYQEFFWDANDIYRIFAELEGVWQPAAQPKRRRHRQDALPGPCIASTPKKHRG
EBV, BMLF-1	Viral	MVPSQRLSRTSSISSNEDPAESHILELEAVSDTNTDCDLDPMEGSEEHSTDGEISSSEEEDEDPTPAHAIPARPSSVVITPTSASFVIPRKKWDLQDKTVTLHRSPLCRDEDEKEETGNSSYTRGHKRRRGEVHGCTDESYGKRRHLPPGARAPRAPRAPRVPRAPRSPRAPRSRNRATRGPRSESRGAGRSTRKQARQERSQRPLPNKPWFDMSLVKPVSKITFVTLPSPLASLTLEPIQDPFLQSMLAVAAHPEIGAWQKVQPRHELRRSYKTLREFFTKSTNKDTWLDARMQAIQNAGLCTLVAMLEETIFWLQEITYHGDLPLAPAEDILLACAMSLSKVITKLKELAPCFLPNTRDYNFVKQLFYITCATARQNKVVETLSSSYVKQPLCLLAAYAAVAPAYINANCRRRHDEVEFLGHYIKNYNPGTLSSLLTEAVETHTRDCRSASCSRLVRAILSPGTGSLGLFFVPGLNQ
Flu H3NA, HA	Viral	MKTIIALSYIFCLVFAQKLPGNDNSTATLCLGHHAVPNGTLVKTITNDQIEVTNATELVQSSSTGRICDSPHRILDGKNCTLIDALLGDPHCDGFQNEKWDLFVERSKAFSNCYPYDVPDYASLRSLVASSGTLEFINEEFNWTGVTQSGGSYACKRGSVNSFFSRLNWLYKSEYKYPALNVTMPNNGRFDKLYIWGVHHPSTDREQTNLYVRASGRVTVSTKRSQQTVIPNIGPRPWVRGLSSRISIYWTIVKPGDILLINSTGNLIAPRGYFKIHTGKSSIMRSDAPIGTCSSECITPNGSIPNDKPFQNVNKITYGACPRYVKQNTLKLATGMRNVPEKQTRGIFGAIAGFIENGWEGMVDGWYGFRHQNSEGTGQAADLKSTQAAIDQINGKLNRLIEKTNEKFHQIEKEFSEVEGRIQDLEKYVEDTKIDLWSYNAEVLVALENQHTIDLTDSEMNKLFEKTRKQLRENAEDMGNGCFKIYHKCDNACIGSIRNGTYDHDVYRDEALNNRFQIKGVELKSGYKDWILWISFAISCFLLCVVLLGFIMWACQKGNIRCNICI
HA-1 (first 300 aa)	Viral	MFSRKKRELMKTPSISKKNRAGSPSPQPSGELPRKDGADAVFPGPSLEPPAGSSGVKATGTLKRPTSLSRHASAAGFPLSGAASWTLGRSHRSPLTAASPGELPTEGAGPDVVEDISHLLADVARFAEGLEKLKECVLHDDLLEARRPRAHECLGEALRVVMHQISKYPLLNTVETLTAAGTLIAKVKAFHYESNNDLEKQEFEKALETIAVAFSSTVSEFLMGEVDSSTLLAVPPGDSSQSMESLYGPGSEGTPPSLEDCDAGCLPAEEVDVLLQRCEGGVDAALLYAKNMAKYMKDLI
Tetanus toxoid (aa 5	Bacterial	SVDDALINSTKIYSYFPSVISKVNQGAQGILFLQWVRDIIDDFTNESSQKTTIDKISDVSTIVPYIGPALNIVKQGYEGNFIGALETTGVVLLLEYIPEITLPVIAALSIAESSTQKEKIIKTIDNFLEKRYEKWIEVYKLVKAKWLGTVNTQFQKRSYQMVRSLEYQVDAIKKIIDYEYKISGPDKEQIADEINNLKNKLEEKANKAMININIFMRESSRSFLVNQMINEAKKQLLEFDTQSKNILMQYIKANSKFIGITELKKLESKINKVFSTPIPFSYSKNLDCWVNEEDIDVILKKSTILNLDINNDIISDISGFNSSVITYPDAQLVPGINGKAIHLVNNESSEVIVHKAMDIEYNDMFNNFTVSFWLRVPKVSASHLEQYGTNEYSIISSM
CAMEL	Tumor-associated	MLMAQEALAFLMAQGAMLAAQERRVPRAAEVPGAQGQQGPRGREEAPRGVRMAVPLLRRMEGAPAGPGGRTAACFSCTSRCLSRRPWKRSWSAGSCPGMPHLSPDQGRF
Gp-100	Tumor-associated	MDLVLKRCLLHLAVIGALLAVGATKVPRNQDWLGVSRQLRTKAWNRQLYPEWTEAQRLDCWRGGQVSLKVSNDGPTLIGANASFSIALNFPGSQKVLPDGQVIWVNNTIINGSQVWGGQPVYPQETDDACIFPDGGPCPSGSWSQKRSFVYVWKTWGQYWQVLGGPVSGLSIGTGRAMLGTHTMEVTVYHRRGSRSYVPLAHSSSAFTITDQVPFSVSVSQLRALDGGNKHFLRNQPLTFALQLHDPSGYLAEADLSYTWDFGDSSGTLISRALVVTHTYLEPGPVTAQVVLQAAIPLTSCGSSPVPGTTDGHRPTAEAPNTTAGQVPTTEVVGTTPGQAPTAEPSGTTSVQVPTTEVISTAPVQMPTAESTGMTPEKVPVSEVMGTTLAEMSTPEATGMTPAEVSIVVLSGTTAAQVTTTEWVETTARELPIPEPEGPDASSIMSTESITGSLGPLLDGTATLRLVKRQVPLDCVLYRYGSFSVTLDIVQGIESAEILQAVPSGEGDAFELTVSCQGGLPKEACMEISSPGCQPPAQRLCQPVLPSPACQLVLHQILKGGSGTYCLNVSLADTNSLAVVSTQLIMPGQEAGLGQVPLIVGILLVLMAVVLASLIYRRRLMKQDFSVPQLPHSSSHWLRLPRIFCSCPIGENSPLLSGQQV
MAGE-A1	Tumor-associated	MSLEQRSLHCKPEEALEAQQEALGLVCVQAATSSSSPLVLGTLEEVPTAGSTDPPQSPQGASAFPTTINFTRQRQPSEGSSSREEEGPSTSCILESLFRAVITKKVADLVGFLLLKYRAREPVTKAEMLESVIKNYKHCFPEIFGKASESLQLVFGIDVKEADPTGHSYVLVTCLGLSYDGLLGDNQIMPKTGFLIIVLVMIAMEGGHAPEEEIWEELSVMEVYDGREHSAYGEPRKLLTQDLVQEKYLEYRQVPDSDPARYEFLWGPRALAETSYVKVLEYVIKVSARVRFFFPSLREAALREEEEGV
MAGE-A12	Tumor-associated	MPLEQRSQHCKPEEGLEAQGEALGLVGAQAPATEEQETASSSSTLVEVTLREVPAAESPSPPHSPQGASTLPTTINYTLWSQSDEGSSNEEQEGPSTFPDLETSFQVALSRKMAELVHFLLLKYRAREPVTKAEMLGSVIRNFQDFFPVIFSKASEYLQLVFGIEVVEVVPISHLYILVTCLGLSYDGLLGDNQIVPKTGLLIIVLAIIAKEGDCAPEEKIWEELSVLEAFDGREDSVFAHPRKLLTQDLVQENYLEYRQVPGSDPACYEFLWGPRALVETSYVKVLHHLLKISGGPHISYPPLHEWAFREGEE
Melan-A	Tumor-associated	MPREDAHFIYGYPKKGHGHSYTTAEEAAGIGILTVILGVLLLICGCWYCRRRNGYRALMDKSLHVGTQCALTRRCPQEGFDHRDSKVSLQEKNCEPVVPNAPPAYEKLSAEQSPPPYSP
NY-ESO1	Tumor-associated	MQAEGRGTGGSTGDADGPGGPGIPDGPGGNAGGPGEAGATGGRGPRGAGAARASGPGGGAPRGPHGGAASGLNGCCRCGARGPESRLLEFYLAMPFATPMEAELARRSLAQDAPPLPVPGVLLKEFTVSGNILTIRLTAADHRQLQLSISSCLQQLSLLMWITQCFLPVFLAQPPSGQRR
Trp-2	Tumor-associated	VLHSFTDAIFDEVMKRFNPPADAWPQELAPIGHNRMVNMVPFFPPVTNEELFLTSDQLGYSYAIDLPVSVEETPGWPTTLLVVMGTLVALVGLFVLLAFLQYRRLRKGYTPLMETHLSSKRYTEEA
Tyrosinase	Tumor-associated	MLLAVLYCLLWSFQTSAGHFPRACVSSKNLMEKECCPPWSGDRSPCGQLSGRGSCQNILLSNAPLGPQFPFTGVDDRESWPSVFYNRTCQCSGNFMGFNCGNCKFGFWGPNCTERRLLVRRNIFDLSAPEKDKFFAYLTLAKHTISSDYVIPIGTYGQMKNGSTPMFNDINIYDLFVWMHYYVSMDALLGGSEIWRDIDFAHEAPAFLPWHRLFLLRWEQEIQKLTGDENFTIPYWDWRDAEKCDICTDEYMGGQHPTNPNLLSPASFFSSWQIVCSRLEEYNSHQSLCNGTPEGPLRRNPGNHDKSRTPRLPSSADVEFCLSLTQYESGSMDKAANFSFRNTLEGFASPLTGIADASQSSMHNALHIYMNGTMSQVQGSANDPIFLLHHAFVDSIFEQWLRRHRPLQEVYPEANAPIGHNRESYMVPFIPLYRNGDFFISSKDLGYDYSYLQDSDPDSFQDYIKSYLEQASRIWSWLLGAAMVGAVLTALLAGLVSLLCRHKRKQLPEEKQPLLMEKEDYHSLYQSHL

Supplementary Table 4. Viral, bacterial and tumor-associated epitopes. (a) List and full sequence of the viral, bacterial and tumor-associated antigens included in the experiment.

				(x: immunogenic epitopes; NA: peptide that could not be tested)		
Type	**Gene**	**Peptide**	**Predicted_by**	**Lau_1352_Immunogen**	**Lau_1357_Immunogen**	**HD_Immunogen**
Viral/bacterial	CMV_pp65_(101-120)	SICPSQEPMSIYVYALPLKM	netMHCIIpan			
Viral/bacterial	CMV_pp65_(111-130)	IYVYALPLKMLNIPSINVHH	Both	x	x	x
Viral/bacterial	CMV_pp65_(171-190)	QQNQWKEPDVYYTSAFVFPT	Both			
Viral/bacterial	CMV_pp65_(181-200)	YYTSAFVFPTKDVALRHVVC	MixMHC2pred			
Viral/bacterial	CMV_pp65_(341-360)	QYDPVAALFFFDIDLLLQRG	MixMHC2pred	x	x	
Viral/bacterial	CMV_pp65_(41-60)	LLQTGIHVRVSQPSLILVSQ	netMHCIIpan			
Viral/bacterial	EBV_BMLF_1_(1-20)	MVPSQRLSRTSSISSNEDPA	MixMHC2pred			
Viral/bacterial	EBV_BMLF_1_(201-220)	SQRPLPNKPWFDMSLVKPVS	netMHCIIpan			
Viral/bacterial	EBV_BMLF_1_(211-230)	FDMSLVKPVSKITFVTLPSP	Both			
Viral/bacterial	EBV_BMLF_1_(221-240)	KITFVTLPSPLASLTLEPIQ	netMHCIIpan			
Viral/bacterial	EBV_BMLF_1_(311-330)	TIFWLQELTYHGDLPLAPAE	MixMHC2pred	NA	NA	NA
Viral/bacterial	EBV_BMLF_1_(321-340)	HGDLPLAPAEDILLACAMSL	netMHCIIpan			
Viral/bacterial	EBV_BMLF_1_(331-350)	DILLACAMSLSKVILTKLKE	Both			
Viral/bacterial	EBV_BMLF_1_(361-380)	DYNFVKQLFYITCATARQNK	netMHCIIpan			
Viral/bacterial	EBV_BMLF_1_(391-410)	KQPLCLLAAYAAVAPAYINA	Both			
Viral/bacterial	EBV_BMLF_1_(71-90)	PARPSSVVITPTSASFVIPR	Both			
Viral/bacterial	Flu_H3N2_HA_(1-20)	MKTIIALSYIFCLVFAQKLP	Both			
Viral/bacterial	Flu_H3N2_HA_(121-140)	YASLRSLVASSGTLEFINEE	netMHCIIpan			
Viral/bacterial	Flu_H3N2_HA_(201-220)	PSTDREQTNLYVRASGRVTV	netMHCIIpan			
Viral/bacterial	Flu_H3N2_HA_(231-250)	PNIGPRPWVRGLSSRISIYW	netMHCIIpan			x
Viral/bacterial	Flu_H3N2_HA_(241-260)	GLSSRISIYWTIVKPGDILL	Both			x
Viral/bacterial	Flu_H3N2_HA_(251-270)	TIVKPGDILLINSTGNLIAP	Both			
Viral/bacterial	Flu_H3N2_HA_(271-290)	RGYFKIHTGKSSIMRSDAPI	netMHCIIpan			
Viral/bacterial	Flu_H3N2_HA_(41-60)	LVKTITNDQIEVTNATELVQ	MixMHC2pred			
Viral/bacterial	Flu_H3N2_HA_(521-540)	VELKSGYKDWILWISFAISC	MixMHC2pred			
Viral/bacterial	HA_1_(181-200)	GTLIAKVKAFHYESNNDLEK	Both			
Viral/bacterial	HA_1_(201-220)	QEFEKALETIAVAFSSTVSE	MixMHC2pred			
Viral/bacterial	HA_1_(211-230)	AVAFSSTVSEFLMGEVDSST	Both			
Viral/bacterial	HA_1_(71-90)	HASAAGFPLSGAASWTLGRS	MixMHC2pred			
Viral/bacterial	TT_(591-610)	KIYSYFPSVISKVNQGAQGI	Both	x	x	
Viral/bacterial	TT_(661-680)	FIGALETTGVVLLLEYIPEI	MixMHC2pred			
Viral/bacterial	TT_(671-690)	VLLLEYIPEITLPVIAALSI	Both			x
Viral/bacterial	TT_(691-710)	AESSTQKEKIIKTIDNFLEK	MixMHC2pred			
Viral/bacterial	TT_(711-730)	RYEKWIEVYKLVKAKWLGTV	Both			
Viral/bacterial	TT_(721-740)	LVKAKWLGTVNTQFQKRSYQ	MixMHC2pred	x	x	x
Viral/bacterial	TT_(731-750)	NTQFQKRSYQMVRSLEYQVD	netMHCIIpan			
Viral/bacterial	TT_(791-810)	INLNIFMRESSRSFLVNQMI	Both			x
Viral/bacterial	TT_(821-840)	DTQSKNILMQYIKANSKFIG	Both			
Viral/bacterial	TT_(841-860)	ITELKKLESKINKVFSTPIP	Both			x
Viral/bacterial	TT_(851-870)	INKVFSTPIPFSYSKNLDCW	netMHCIIpan			x
Viral/bacterial	TT_(891-910)	INNDIISDISGFNSSVITYP	MixMHC2pred			
Viral/bacterial	TT_(941-960)	IEYNDMFNNFTVSFWLRVPK	Both			x
Tumor-associated antigen	CAMEL_(1-20)	MLMAQEALAFLMVQGAMLAA	Both			
Tumor-associated antigen	Gp_100_(1-20)	MDLVLKRCLLHLAVIGALLA	netMHCIIpan			
Tumor-associated antigen	Gp_100_(11-30)	HLAVIGALLAVGATKVPRNQ	Both			
Tumor-associated antigen	Gp_100_(151-170)	YVWKTWGQYWQVLGGPVSGL	Both			
Tumor-associated antigen	Gp_100_(171-190)	SIGTGRAMLGTHTMEVTVYH	MixMHC2pred			
Tumor-associated antigen	Gp_100_(191-210)	RRGSRSYVPLAHSSSAFTIT	netMHCIIpan			
Tumor-associated antigen	Gp_100_(201-220)	AHSSSAFTITDQVPFSVSVS	Both			
Tumor-associated antigen	Gp_100_(211-230)	DQVPFSVSVSQLRALDGGNK	Both			
Tumor-associated antigen	Gp_100_(221-240)	QLRALDGGNKHFLRNQPLTF	netMHCIIpan			
Tumor-associated antigen	Gp_100_(231-250)	HFLRNQPLTFALQLHDPSGY	netMHCIIpan			
Tumor-associated antigen	Gp_100_(261-280)	DFGDSSGTLISRALVVTHTY	netMHCIIpan			
Tumor-associated antigen	Gp_100_(401-420)	TPAEVSIVVLSGTTAAQVTT	Both			
Tumor-associated antigen	Gp_100_(421-440)	TEWVETTARELPIPEPEGPD	MixMHC2pred			
Tumor-associated antigen	Gp_100_(441-460)	ASSIMSTESITGSLGPLLDG	MixMHC2pred			
Tumor-associated antigen	Gp_100_(451-470)	TGSLGPLLDGTATLRLVKRQ	MixMHC2pred			
Tumor-associated antigen	Gp_100_(471-490)	VPLDCVLYRYGSFSVTLDIV	netMHCIIpan			
Tumor-associated antigen	Gp_100_(571-590)	LADTNSLAVVSTQLIMPGQE	Both			
Tumor-associated antigen	Gp_100_(601-620)	GILLVLMAVVLASLIYRRRL	MixMHC2pred			
Tumor-associated antigen	Gp_100_(71-90)	SNDGPTLIGANASFSIALNF	netMHCIIpan			x
Tumor-associated antigen	Gp_100_(81-100)	NASFSIALNFPGSQKVLPDG	netMHCIIpan			
Tumor-associated antigen	MAGE_A1_(161-180)	EADPTGHSYVLVTCLGLSYD	MixMHC2pred			
Tumor-associated antigen	MAGE_A1_(271-290)	LAETSYVKVLEYVIKVSARV	Both			x
Tumor-associated antigen	MAGE_A1_(281-300)	EYVIKVSARVRFFFPSLREA	netMHCIIpan			
Tumor-associated antigen	MAGE_A1_(91-110)	SCILESLFRAVITKKVADLV	Both			
Tumor-associated antigen	MAGE_A12_(101-120)	LETSFQVALSRKMAELVHFL	Both			
Tumor-associated antigen	MAGE_A12_(141-160)	RNFQDFFPVIFSKASEYLQL	Both			
Tumor-associated antigen	MAGE_A12_(151-170)	FSKASEYLQLVFGIEVVEVV	MixMHC2pred			
Tumor-associated antigen	MAGE_A12_(171-190)	RIGHLYILVTCLGLSYDGLL	MixMHC2pred			
Tumor-associated antigen	MAGE_A12_(271-290)	FLWGPRALVETSYVKVLHHL	MixMHC2pred	x		x
Tumor-associated antigen	MAGE_A12_(281-300)	TSYVKVLHHLLKISGCPHIS	netMHCIIpan			
Tumor-associated antigen	MAGE_A12_(91-110)	EQEGPSTFPDLETSFQVALS	MixMHC2pred			
Tumor-associated antigen	NY_ESO_1_(121-140)	VLLKEFTVSGNILTIRLTAA	Both			
Tumor-associated antigen	NY_ESO_1_(141-160)	DHRQLQLSISSCLQQLSLLM	Both			
Tumor-associated antigen	NY_ESO_1_(81-100)	RGPESRLLEFYLAMPFATPM	Both		x	
Tumor-associated antigen	Trp_2_(51-70)	LFLTSDQLGYSYAIDLPVSV	Both			
Tumor-associated antigen	Trp_2_(71-90)	EETPGWPTTLLVVMGTLVAL	MixMHC2pred			
Tumor-associated antigen	Tyrosinase_(1-20)	MLLAVLYCLLWSFQTSAGHF	netMHCIIpan			
Tumor-associated antigen	Tyrosinase_(131-150)	KDKFFAYLTLAKHTISSDYV	netMHCIIpan			
Tumor-associated antigen	Tyrosinase_(171-190)	NIYDLFVWMHYYVSMDALLG	Both			
Tumor-associated antigen	Tyrosinase_(201-220)	AHEAPAFLPWHRLFLLRWEQ	MixMHC2pred			
Tumor-associated antigen	Tyrosinase_(381-400)	ANDPIFLLHHAFVDSIFEQW	Both			
Tumor-associated antigen	Tyrosinase_(431-450)	PLYRNGDFFISSKDLGYDYS	MixMHC2pred			
Tumor-associated antigen	Tyrosinase_(471-490)	ASRIWSWLLGAAMVGAVLTA	netMHCIIpan			

Supplementary Table 4. Viral, bacterial and tumor-associated epitopes. (b) Best scoring candidate epitopes predicted by MixMHC2pred or NetMHC2pan that were tested for immunogenicity in two melanoma patients (LAU1352 and LAU1357) and a healthy donor (HD).

nature biotechnology

SUPPLEMENTARY INFORMATION

https://doi.org/10.1038/s41587-019-0289-6

In the format provided by the authors and unedited.

Robust prediction of HLA class II epitopes by deep motif deconvolution of immunopeptidomes

Julien Racle[1,2], Justine Michaux[1,3], Georg Alexander Rockinger[1], Marion Arnaud[1,3], Sara Bobisse[1,3], Chloe Chong[1,3], Philippe Guillaume[1,3], George Coukos[1,3], Alexandre Harari[1,3], Camilla Jandus[1], Michal Bassani-Sternberg[1,3]* and David Gfeller[1,2]*

[1]Department of Oncology UNIL CHUV, Ludwig Institute for Cancer Research, University of Lausanne, Lausanne, Switzerland. [2]Swiss Institute of Bioinformatics (SIB), Lausanne, Switzerland. [3]Department of Oncology UNIL CHUV, Ludwig Institute for Cancer Research, University Hospital of Lausanne, Lausanne, Switzerland. *e-mail: michal.bassani@chuv.ch; david.gfeller@unil.ch

Supplementary Figures

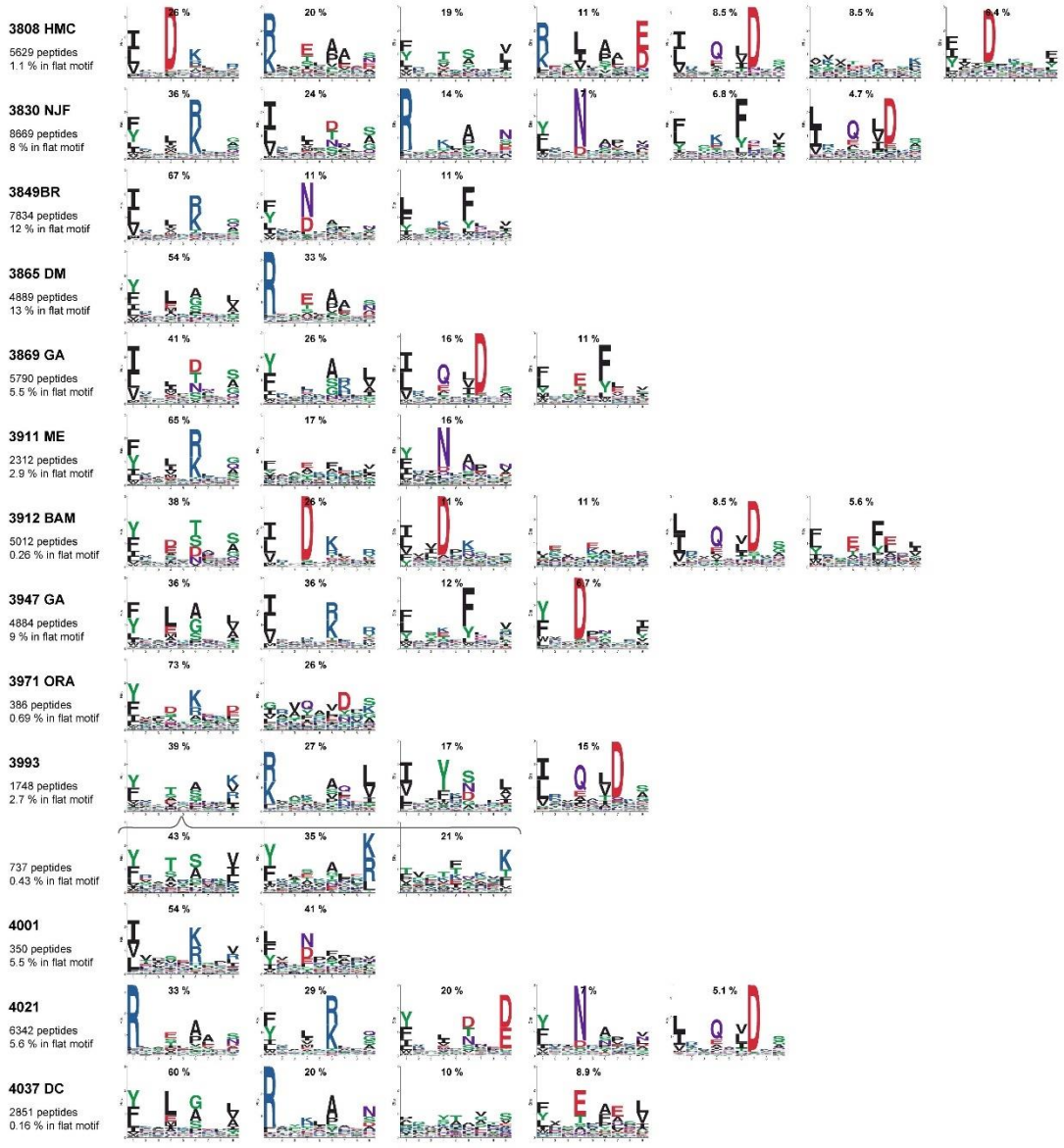

Supplementary Figure 1 (continued on next page).

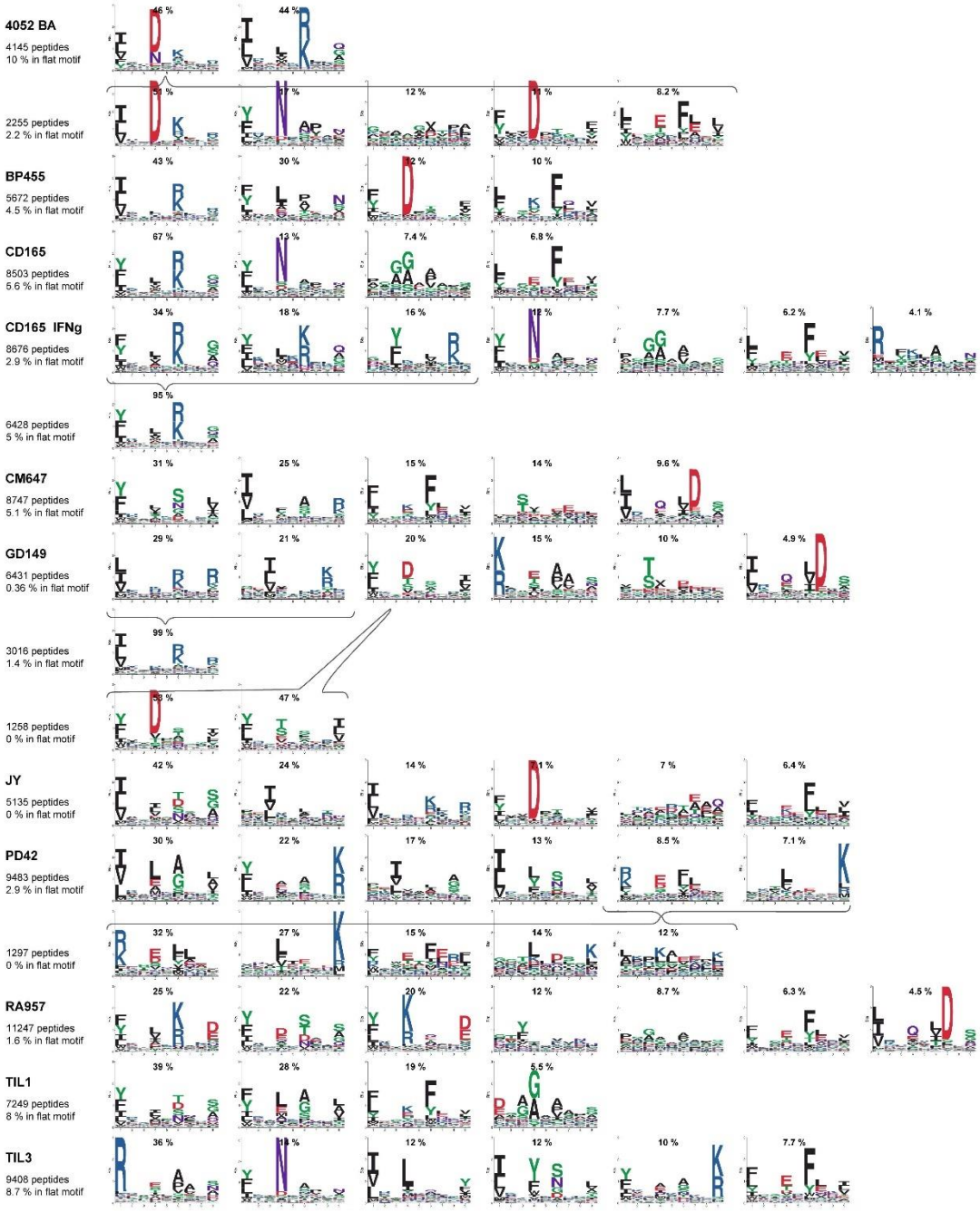

Supplementary Figure 1. Motifs found by MoDec in the HLA-II peptidomics data.

Each row corresponds to a different deconvolution. Sample name and number of peptides are indicated in the first column as well as the percentage of peptides that

best represent false positives (flat motif). Numbers above each motif indicate the percentage of peptides assigned to this motif from the sample. In few cases when a motif seemed to combine multiple specificities, we split it further with MoDec as indicated by the accolades under and above the respective motifs.

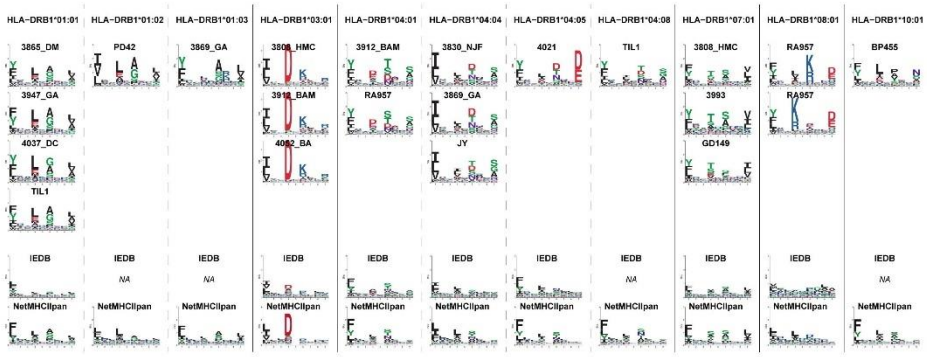

Supplementary Figure 2 (continued on next page)

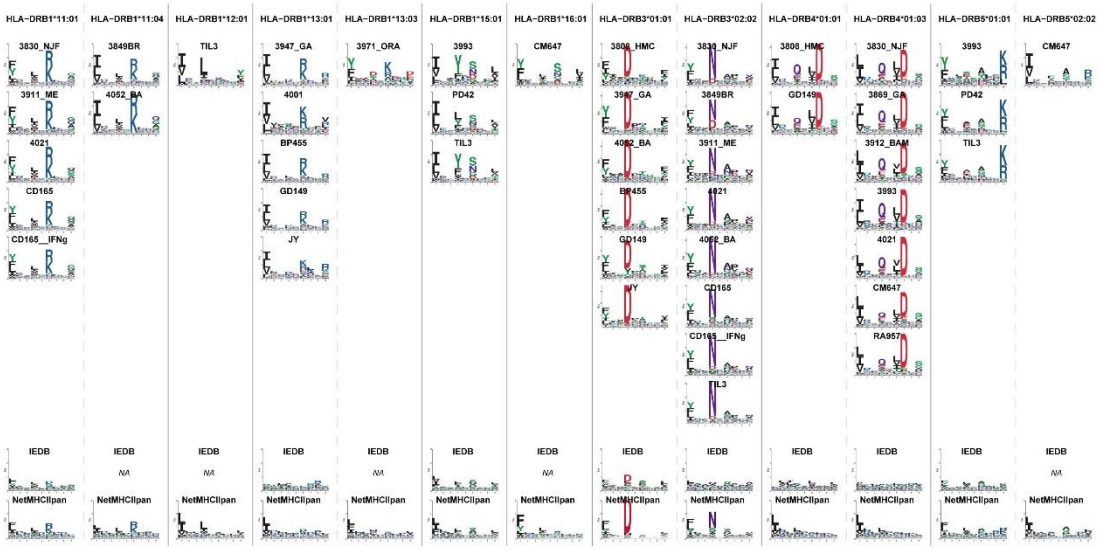

Supplementary Figure 2 (continued on next page)

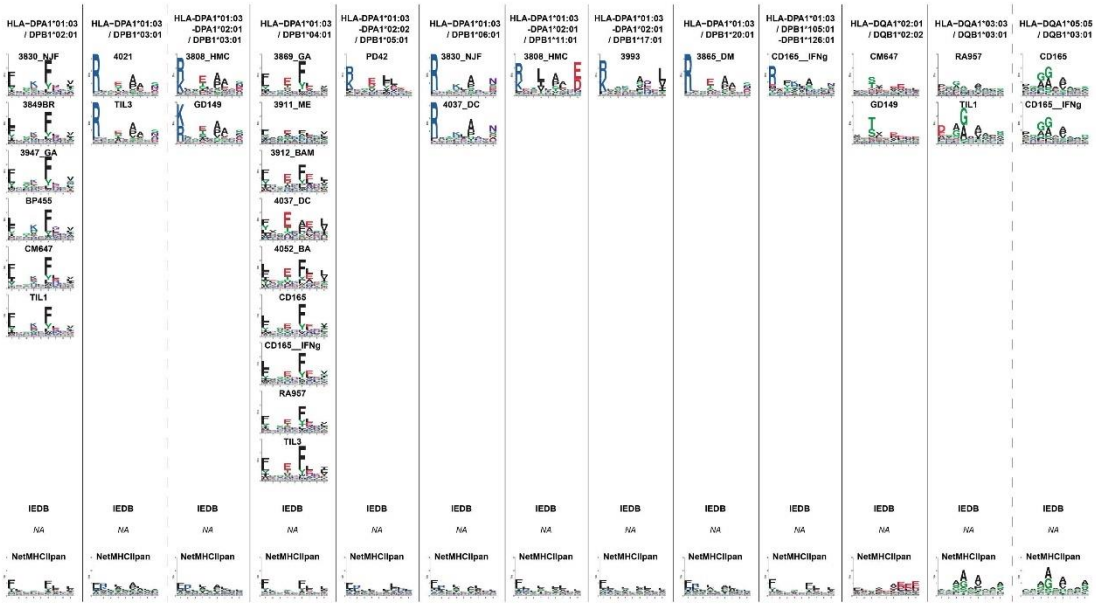

Supplementary Figure 2. Motifs are highly similar between cell lines and tissues sharing a same allele – the corresponding allele is annotated on top of each column. The name of the cell line or tissue is indicated above each motif. The last two rows show the motifs obtained from IEDB positive-high data for the respective allele (if such data is available for this allele) and the motif determined from NetMHCIIpan (see Methods). DPA1*02:01 only appears in cell lines and tissues also containing DPA1*03:01, which explains why the two alleles are listed with the corresponding motifs.

6

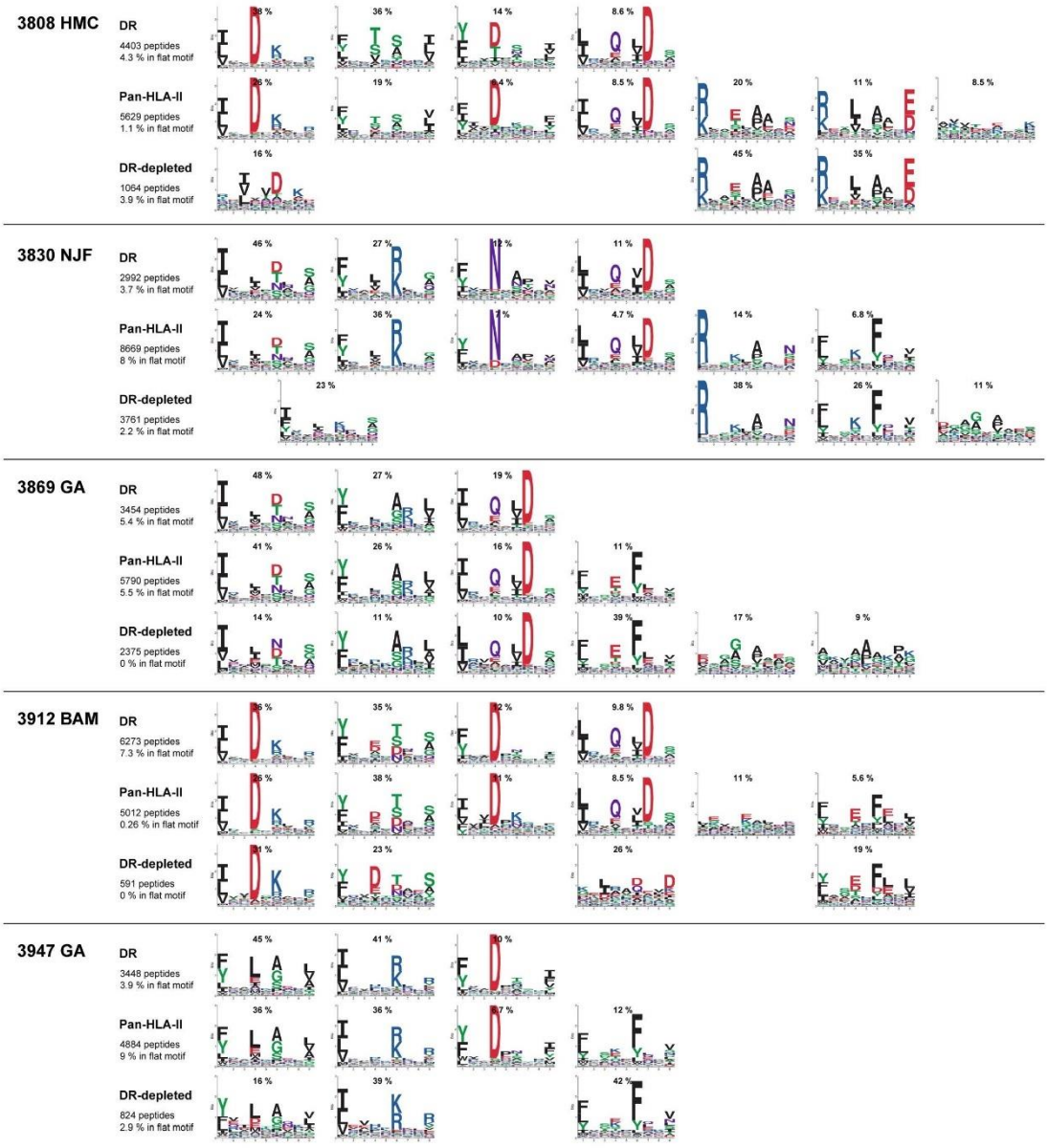

Supplementary Figure 3 (continued on next page).

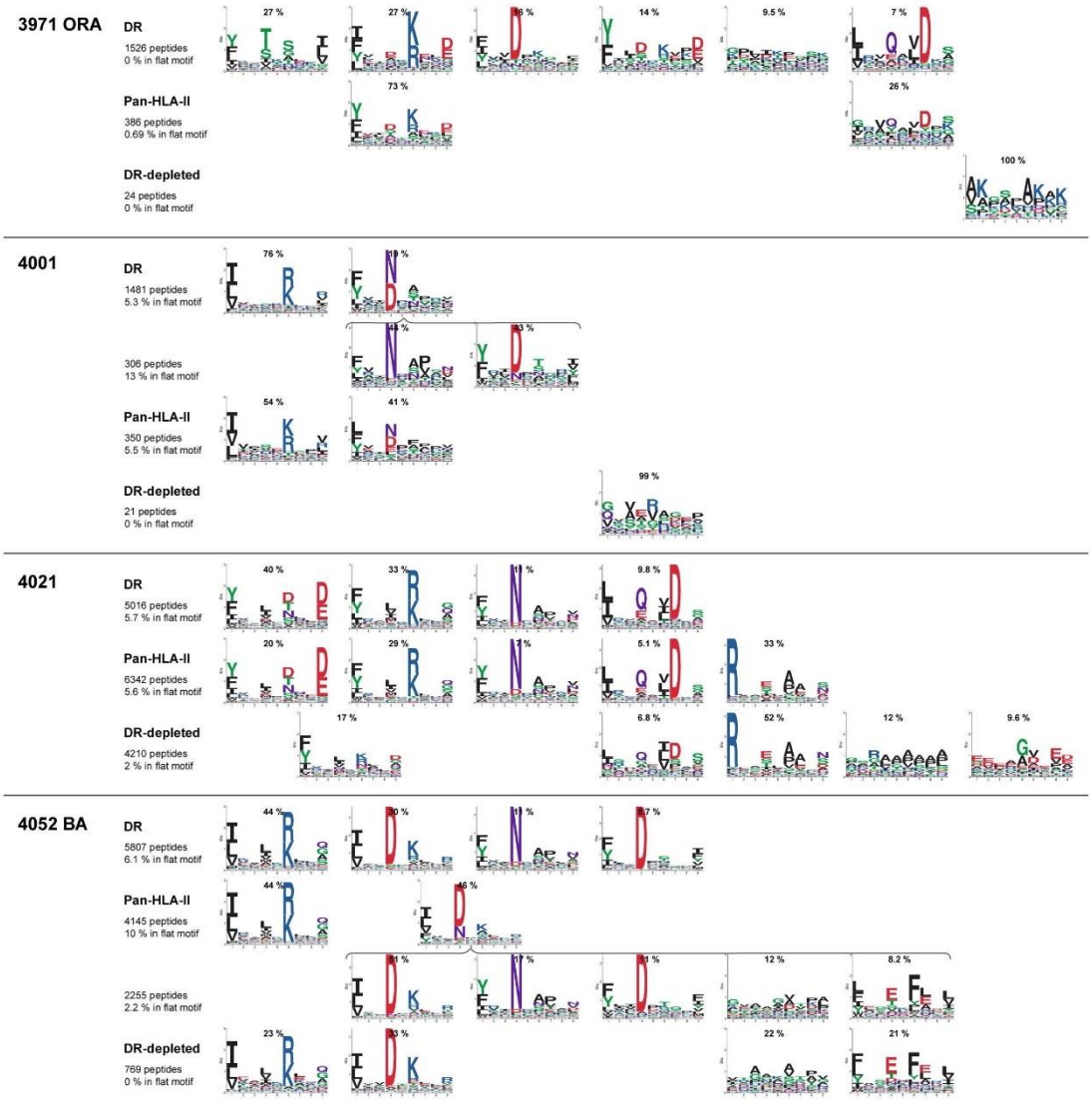

Supplementary Figure 3 (continued on next page).

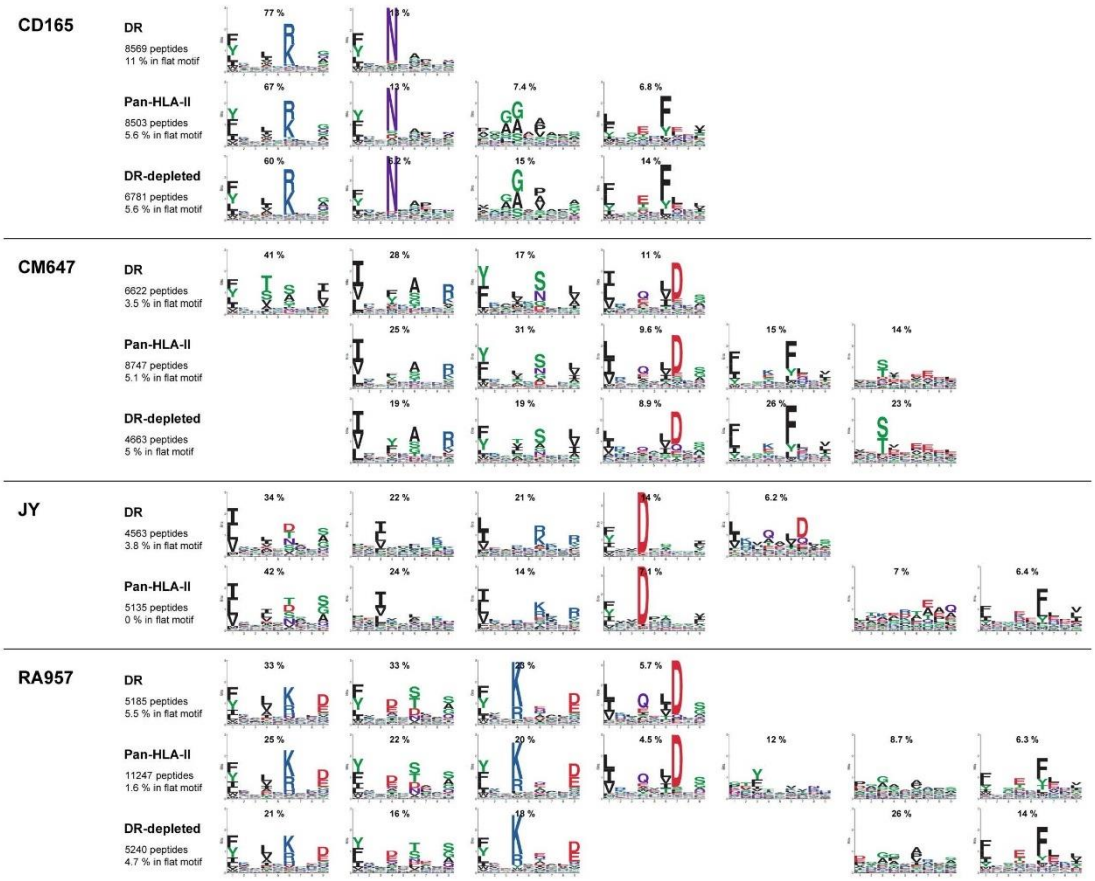

Supplementary Figure 3. Similar to Supplementary Fig. 1, showing here a comparison of the motifs found with MoDec in HLA-II, HLA-DR and HLA-DR-depleted peptidomics on a same cell line or tissue.

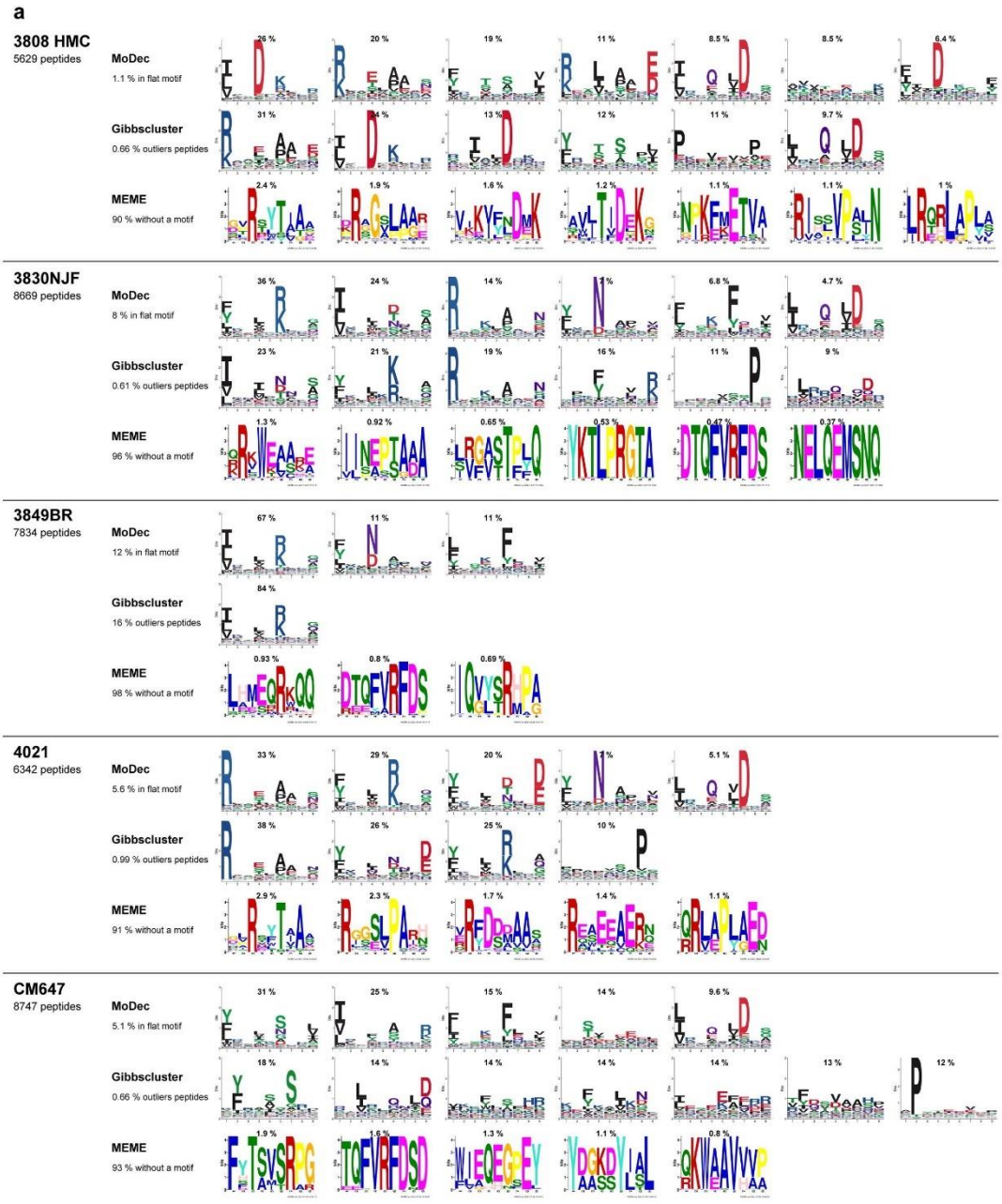

Supplementary Figure 4 (continued on next page).

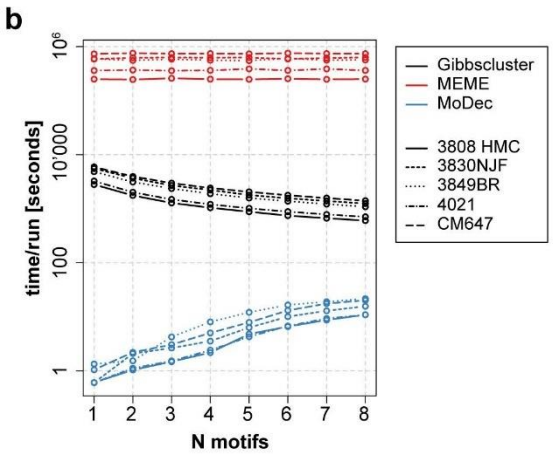

Supplementary Figure 4. MoDec has a better resolution and is faster than other deconvolution methods. (a) Comparison of the motifs found by MoDec, Gibbscluster and MEME in 5 different cell lines or tissue samples. MoDec and Gibbscluster both find the motifs containing many peptides, but MoDec finds additional well-defined motifs containing fewer peptides. **(b)** Timing comparison of the 3 methods in function of the number of motifs searched.

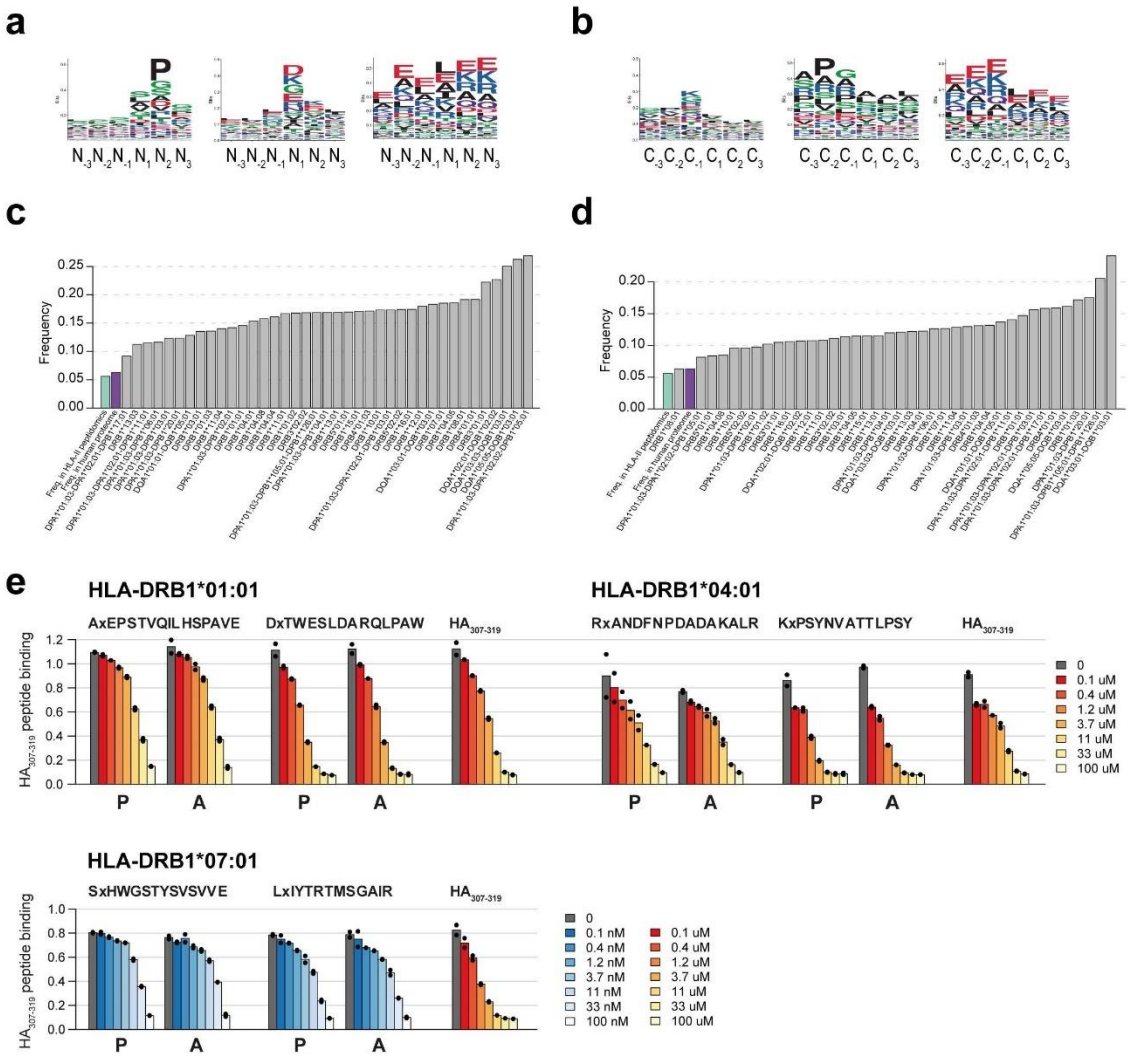

Supplementary Figure 5. Characteristics of the N- / C-terminus region of the peptides. (a-b) Motifs determined by MoDec for the three amino acids upstream and downstream of the N-terminus (a) or C-terminus (b) when grouping all HLA-II peptidomics data. **(c-d)** Frequency of proline at the 2nd position downstream of N-terminus (c) or 2nd position upstream of C-terminus (d) of the peptide in function of the allele to which the peptide is associated. Colored bars represent the proline frequency in the human proteome and the proline frequency at any position in HLA-II peptidomics. **(e)** Competition assays for different alleles between $HA_{307-319}$ and various peptide variants containing proline at the 2nd position or alanine (the "x" in

the peptide sequences is replaced by proline or alanine as indicated below the bars; $HA_{307-319}$ is used as a control). Data from two technical repeats are showed.

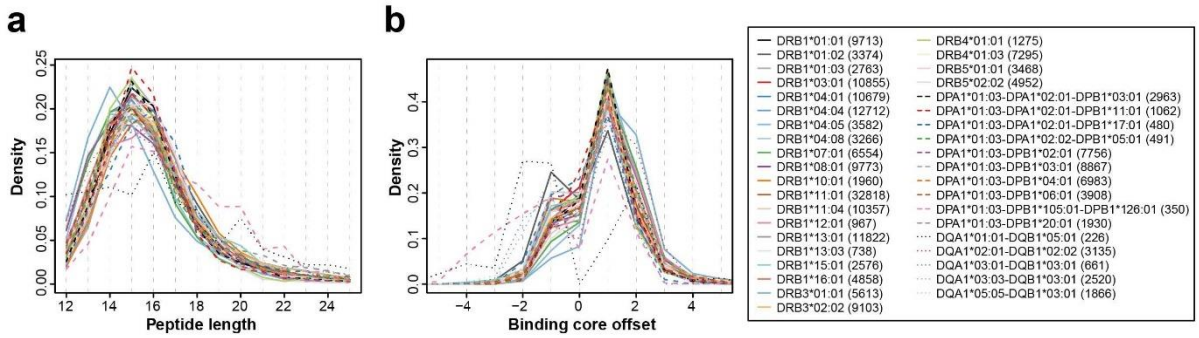

Supplementary Figure 6. Peptide length (a) and binding core offset (b) are independent of the allele. Number of peptides associated to each allele is indicated in parenthesis. The outliers' distributions are those from alleles with too few peptides for robust statistics.

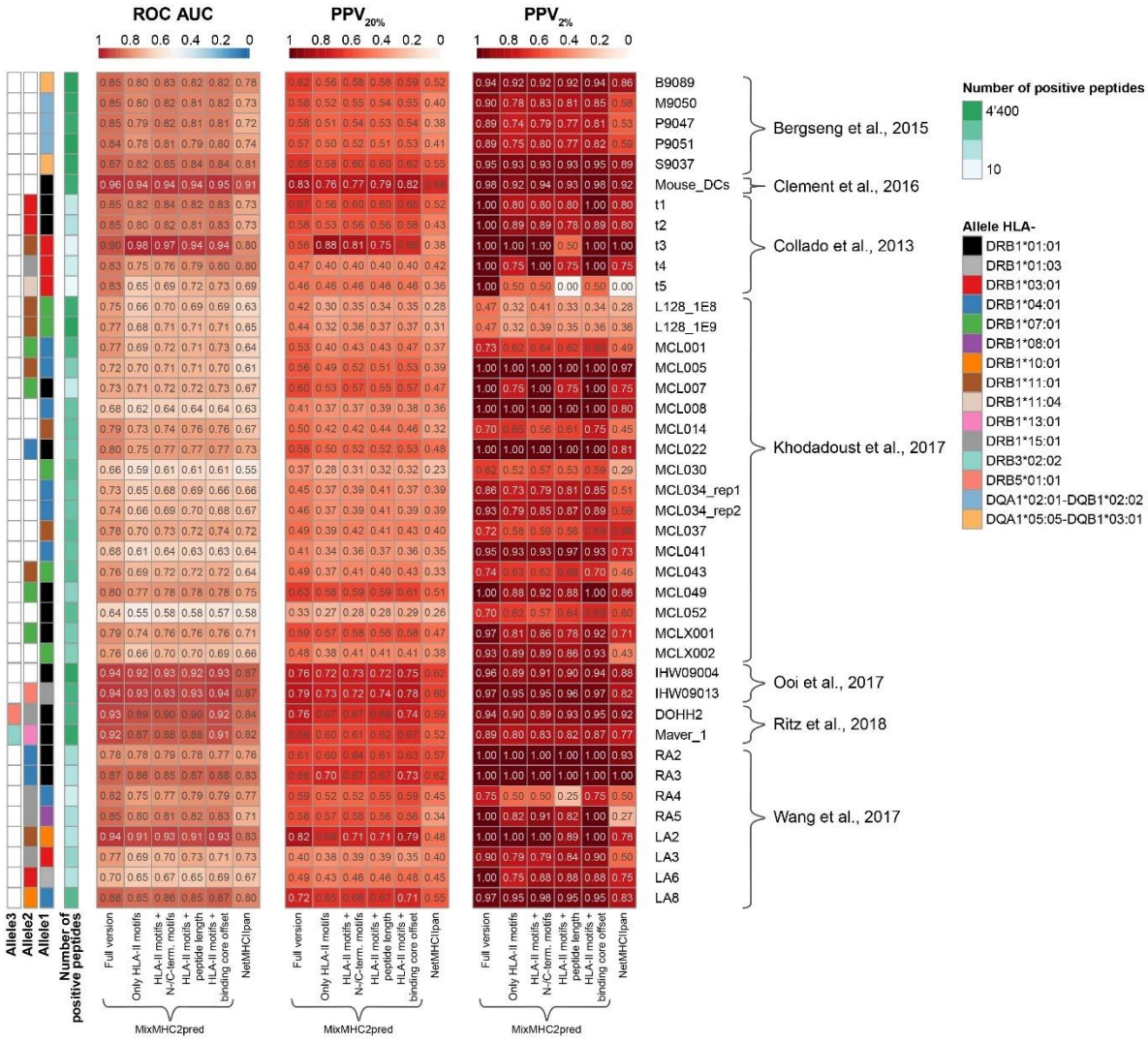

Supplementary Figure 7. Detailed results from the comparison of the predictors on independent HLA-II ligand data, showing the ROC AUC, the positive predictive value (PPV) corresponding to the top 20% predictions and the PPV for the top 2% predictions from each sample.

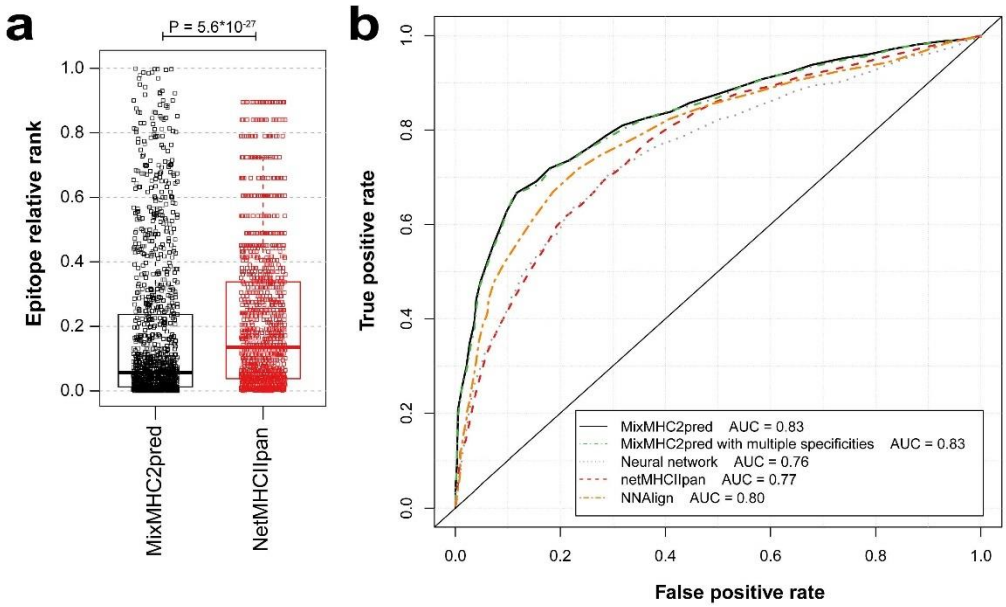

Supplementary Figure 8. Accuracy of predictors on IEDB tetramer data. (a) Epitope relative rank of the true epitopes (i.e. the fraction of negative peptides in the test data that had a better predicted score than a given true epitope). Box plots indicate the median, upper and lower quartiles. Paired two-sided Wilcoxon signed-rank test P value is indicated (n = 1319 positive epitopes). **(b)** Similar to Fig. 2b including various additional predictors (n = 2359 positive and negative epitopes).

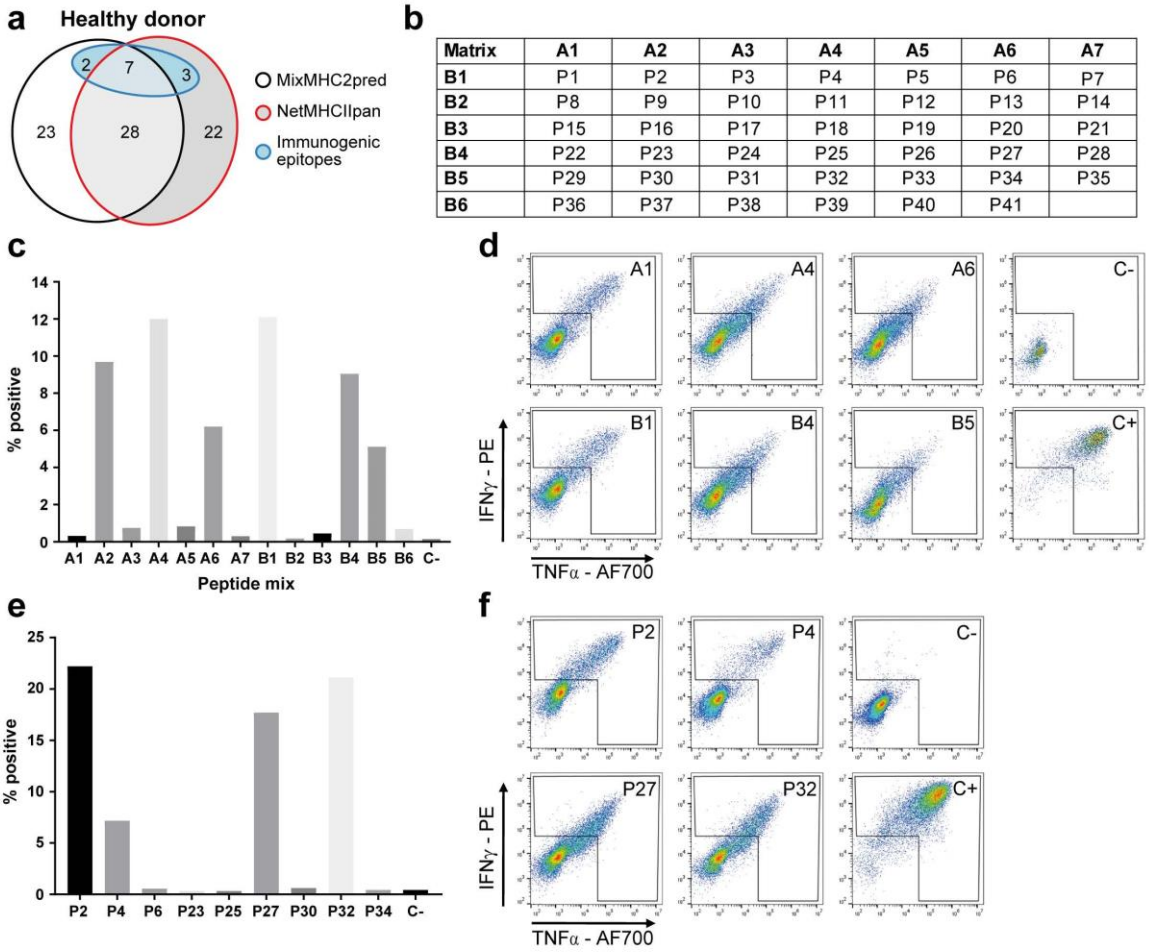

Matrix	A1	A2	A3	A4	A5	A6	A7
B1	P1	P2	P3	P4	P5	P6	P7
B2	P8	P9	P10	P11	P12	P13	P14
B3	P15	P16	P17	P18	P19	P20	P21
B4	P22	P23	P24	P25	P26	P27	P28
B5	P29	P30	P31	P32	P33	P34	P35
B6	P36	P37	P38	P39	P40	P41	

Supplementary Figure 9. Determining class II immunogenic epitopes from viral, bacterial and tumor-associated antigens. (a) Similar to Fig. 2c with the results from a healthy donor (MCC of 0.039 for MixMHC2pred and 0.11 for NetMHCIIpan). **(b-f)** Representative example of the immunogenicity screening procedure, showing the results from the viral/bacterial epitopes of the melanoma patient LAU 1352 (these experiments were repeated independently in three different donors with similar results). (b) Matrix used for the screening of all viral/bacterial peptides. A-labelled mixes from 1 to 7 contain vertically listed peptides and B-labelled mixes from 1 to 6 contain horizontally listed peptides. (c) Readout in % positive cells (positive for intracellular IFNγ and TNFα) following stimulation with the peptide matrix mixes. (d) Dot plot representation of the wells positive for both IFNγ and TNFα, and of the negative (C-) and positive controls (C+). (e) Readout of the single peptides tested

individually (peptides that were selected based on the positive wells from the peptide mixes stimulation). (f) Dot plot representation of the wells reacting to individual peptides and the positive and negative controls.

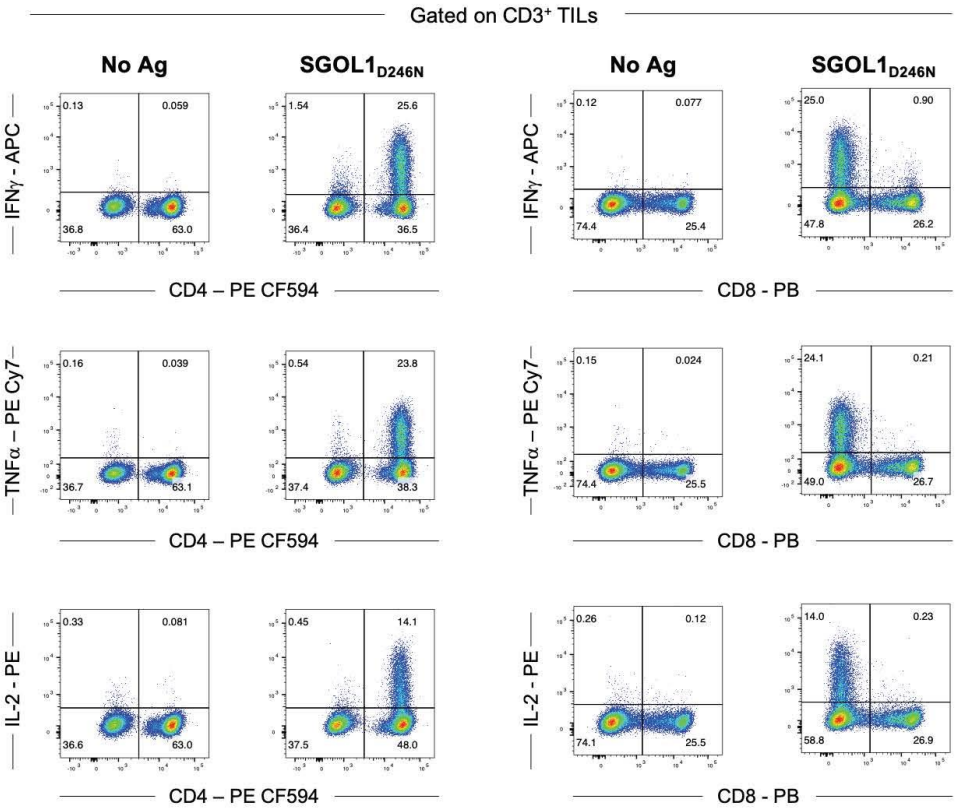

Supplementary Figure 10. *SGOL1$_{D246N}$*-specific tumor infiltrating lymphocytes from patient CTE-0007 are CD4+ T cells. Intracellular cytokine staining showing the frequency of viable IFNγ , TNFα, and IL-2 cytokine- producing CD4+ TILs following stimulation with the 31-mer peptide containing the identified neoepitope from *SGOL1$_{D246N}$* gene. Representative plots of n=3 independent experiments with similar results are shown.

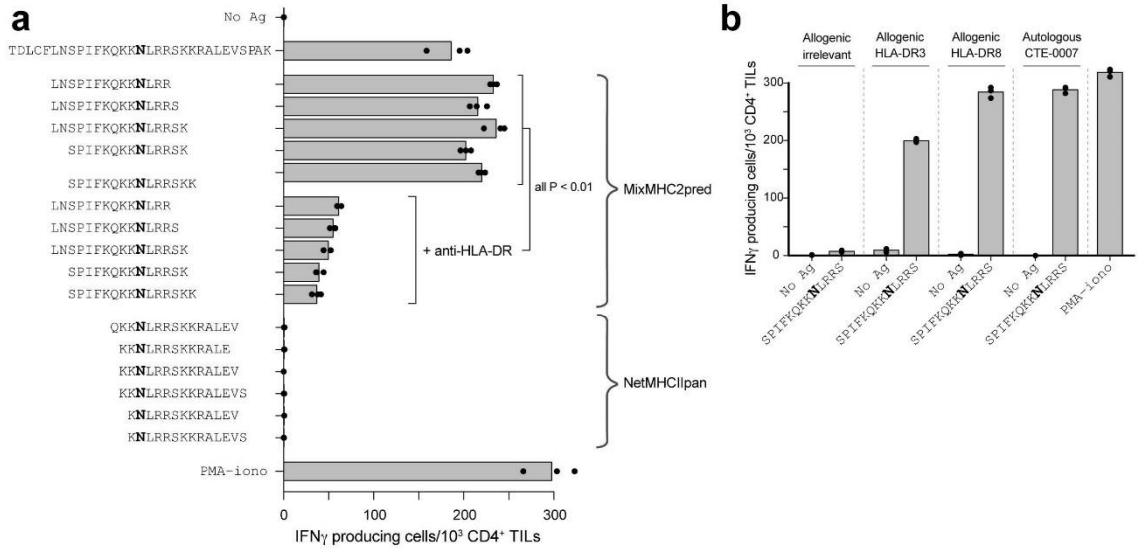

Supplementary Figure 11. Validation of neoepitope and HLA restriction. (a) Neoepitope-specific CD4+ TILs from patient CTE-0007 were isolated based on CD154 upregulation following stimulation with the 31-mer peptide encompassing the neoepitope ($SGOL1_{D246N}$). Neoepitope-specific CD4+ TILs were interrogated by IFNγ ELISpot with the candidate epitopes from MixMHC2pred and NetMHCIIpan (mutation indicated in bold in the peptide sequences). Autologous CD40-activated B cells were used as APCs. T cell stimulation was inhibited in the presence of anti-HLA-DR antibody (clone L243). P values are from one-way ANOVA with multiple comparisons. (n = 3 technical repeats). **(b)** Neoepitope specific CD4+ TILs from patient CTE-0007 were re-challenged with CD40-activated B cells pulsed with 2μM of the peptide SPIFKQKK**N**LRRS. Autologous B cells, allogenic B cells sharing HLA-DRB1-03:01 (DR3) or HLA-DRB1-08:01 (DR8) alleles and irrelevant allogenic B cells (neither DR3 nor DR8) were used as APCs. Screening by IFNγ ELISpot (*PMA-iono*: phorbol-myristate-acetate + ionomycin, *No Ag*: no peptide). Mean values from n = 3 technical repeats are showed, overlaid by each data point.

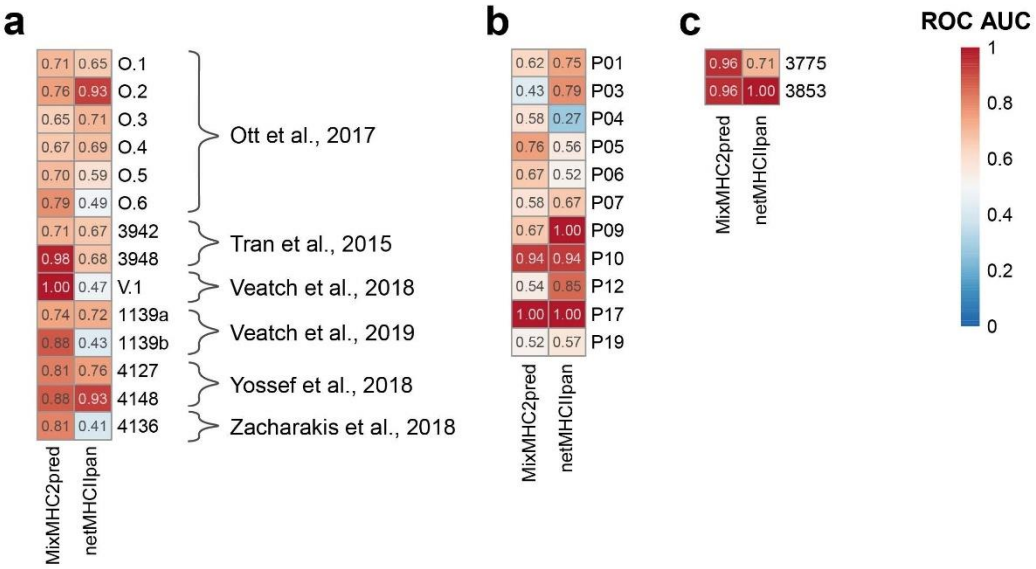

Supplementary Figure 12. Benchmarking of class II neoepitope predictions. (a) Results for class II neoantigen studies selected based on the availability of HLA-II typing information (Supplementary Data 3; n = 13 (O.1), 17 (O.2), 14 (O.3), 19 (O.4), 20 (O.5), 22 (O.6), 144 (3942), 211 (3948), 20 (V.1), 48 (1139a), 43 (1139b), 179 (4127), 108 (4148) and 71 (4136) tested peptides per patient). **(b)** Results on the data from Sahin et al., *Nature*, 2017 (n=10 tested peptides for each patient, except n=8 for P03, n=7 for P07 and n=5 for P09). NetMHCIIpan predictions are slightly better than MixMHC2pred but not significantly (P=0.44 from a paired two-sided Wilcoxon signed rank test between ROC AUC of the n=11 patients) and the results are possibly biased towards NetMHCIIpan because the peptides tested experimentally have been selected partly based on HLA-II binding predictions. HLA-II typing for this study is not publicly available but can be obtained from https://ega-archive.org/datasets/EGAD00001004455 after data access agreement, and was kindly provided to us by the authors of this study. **(c)** Benchmarking on viral (HPV) epitopes identified in Stevanovic et al., *Science*, 2017, for patients with HPV-associated cervical cancer (n=59 (patient 3775) and 24 (patient 3853) tested peptides).

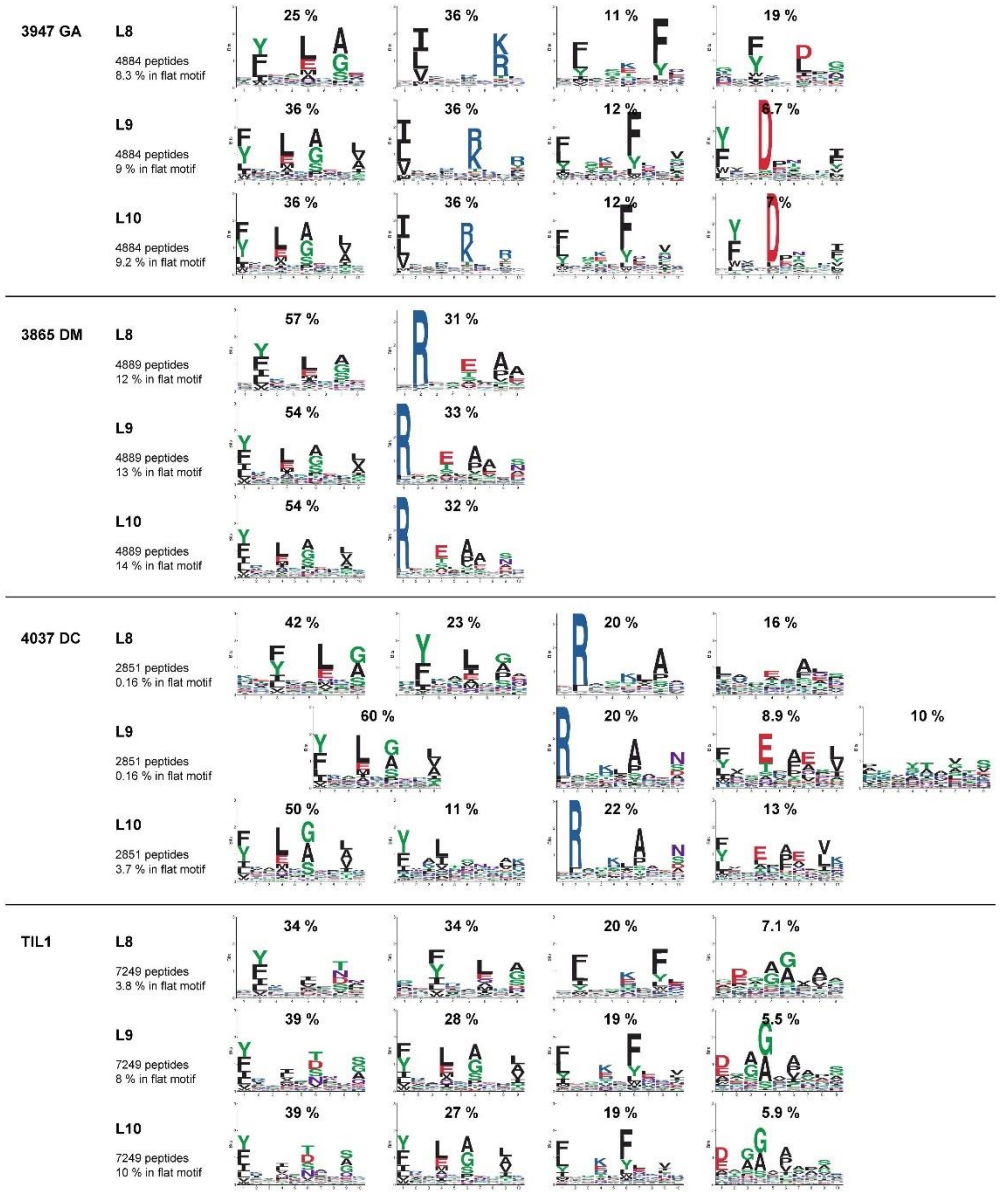

Supplementary Figure 13. Example of motifs obtained with various binding core lengths. The deconvolution was performed by MoDec, asking for a motif length of 8, 9 or 10 amino acids.

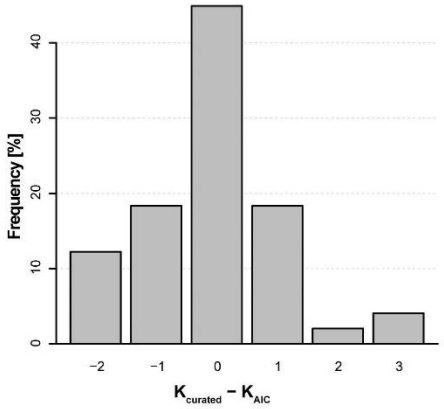

Supplementary Figure 14. Comparison between the number of motifs determined by the AIC and after manual curation. The best number of motifs is most often directly selected by the AIC.

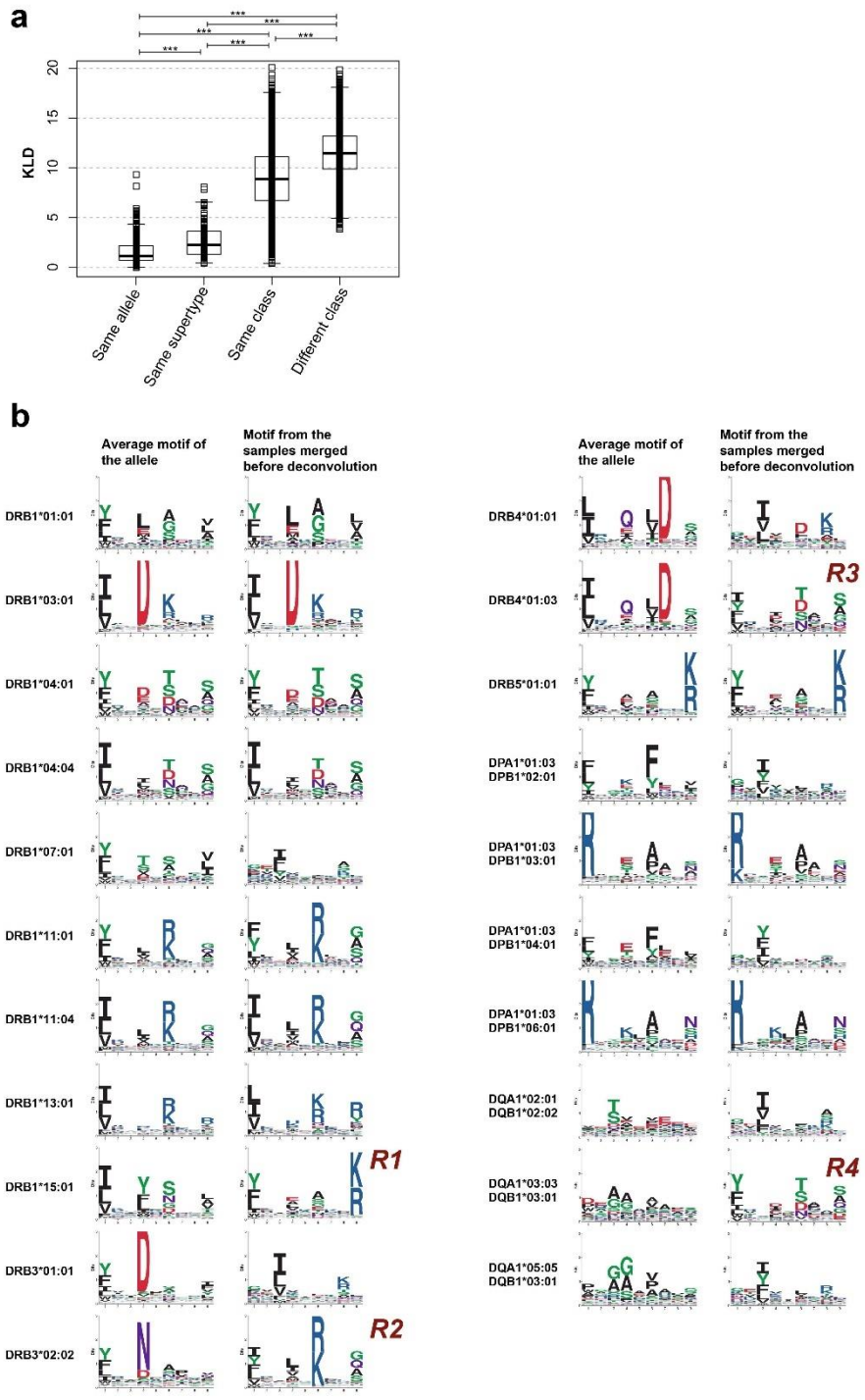

Supplementary Figure 15. Analysis of the motif annotations. (a) Kullback-Leibler divergence between all pairs of motifs that could be assigned to a given allele,

grouping pairs of motifs coming from a same allele, a same allele supertype (e.g. DRB1*01:01 and DRB1*01:03), a same class (e.g. DRB1*01:01 and DRB1*04:01) or different class (e.g. DRB1*01:01 and DPA1*01:03-DPB1*02:01). Box plots indicate the median, upper and lower quartiles. Two-sided Wilcoxon signed-rank test with Holm's correction for multiple testing was performed between groups (***: $P < 0.001$; n = 332 (same allele), 126 (same supertype), 4644 (same class) and 4600 (different class) pairs of motifs). **(b)** Motif obtained either by combining the peptides that had been assigned to each allele per sample (i.e. "averaging" the motifs from Supplementary Fig. 2) or obtained by doing the deconvolution on the data merged from multiple samples sharing an allele and annotating the motif most likely representing the allele by determining which motif was shared by all samples of origin (see Supplementary Note). Alleles that were present in a single sample could not be determined by the alternative approach and are not showed here Note the following remarks concerning the motifs obtained by the alternative approach: R1: the motif corresponds to DRB5*01:01, an allele genetically linked to DRB1*15:01 (i.e. both alleles were always present in the samples containing DRB1*15:01); R2: similarly, this motif corresponds to DRB1*11:01 / DRB1*11:04, which were present in most samples containing DRB3*02:02; R3 and R4: these motifs correspond to DRB1*04:xx that were present in most samples containing DRB4*01:03 or DQA1*03:03-DQB1*03:01.

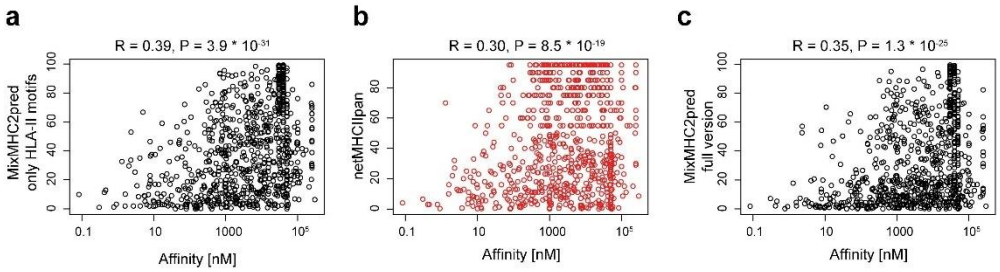

Supplementary Figure 16. Correlation between measured binding affinity and predictions of (a) the HLA-II motifs from MixMHC2pred, (b) NetMHCIIpan, (c) the full version of MixMHC2pred. Spearman rank correlations are given on top of each figure (n = 818 binding affinity measures, P values are from a two sided test from the asymptotic t approximation).

Supplementary Tables

Supplementary Table 1. HLA-II typing from the cell lines and tissue samples used in our HLA-II peptidomics experiments. In case of ambiguous allele assignment, the other allele name is given in parentheses.

ID	HLA-DRB1		HLA-DRB3/4/5		HLA-DPA1		HLA-DPB1		HLA-DQA1		HLA-DQB1	
3808_HMC	DRB1*03:01	DRB1*07:01	DRB3*01:01	DRB4*01:01	DPA1*01:03	DPA1*02:01	DPB1*03:01	DPB1*11:01	DQA1*02:01	DQA1*05:01	DQB1*02:01	DQB1*02:02
3830_NJF	DRB1*04:04	DRB1*11:01	DRB3*02:02	DRB4*01:03	DPA1*01:03		DPB1*02:01	DPB1*06:01	DQA1*03:01	DQA1*05:05	DQB1*03:01	DQB1*03:02
3849BR	DRB1*11:04		DRB3*02:02		DPA1*01:03		DPB1*02:01	DPB1*04:01	DQA1*05:05		DQB1*03:01	
3865_DM	DRB1*01:01	DRB1*07:01	DRB4*01:03		DPA1*01:03		DPB1*04:01	DPB1*20:01	DQA1*01:01	DQA1*02:01	DQB1*03:03	DQB1*05:01
3869_GA	DRB1*01:03	DRB1*04:04	DRB4*01:03		DPA1*01:03		DPB1*04:01 (DPB1*04:02)	DPB1*126:01 (DPB1*105:01)	DQA1*03:01	DQA1*05:05	DQB1*03:01	DQB1*03:02
3911_ME	DRB1*11:01		DRB3*02:02		DPA1*01:03		DPB1*04:01		DQA1*05:05		DQB1*03:01	
3912_BAM	DRB1*03:01	DRB1*04:01	DRB3*01:01	DRB4*01:03	DPA1*01:03		DPB1*04:01		DQA1*03:01	DQA1*05:01	DQB1*02:01	DQB1*03:02
3947_GA	DRB1*01:01	DRB1*13:01	DRB3*01:01		DPA1*01:03		DPB1*02:01 (DPB1*416:01)	DPB1*04:02 (DPB1*105:01)	DQA1*01:01	DQA1*01:03	DQB1*05:01	DQB1*06:03
3971_ORA	DRB1*13:03	DRB1*07:01	DRB3*01:01	DRB4*01:01	DPA1*01:03	DPA1*02:02	DPB1*04:01		DQA1*02:01	DQA1*05:05	DQB1*02:02	DQB1*03:01
3993	DRB1*07:01	DRB1*15:01	DRB4*01:03	DRB5*01:01	DPA1*01:03	DPA1*02:01	DPB1*04:01	DPB1*17:01	DQA1*01:02	DQA1*02:01	DQB1*02:02	DQB1*06:02
4001	DRB1*13:01	DRB1*14:01	DRB3*01:01	DRB3*02:02	DPA1*01:03		DPB1*04:01 (DPB1*126:01)	DPB1*04:02 (DPB1*105:01)	DQA1*01:03	DQA1*01:04	DQB1*05:03	DQB1*06:03
4021	DRB1*11:01	DRB1*04:05	DRB3*02:02	DRB4*01:03	DPA1*01:03		DPB1*03:01	DPB1*104:01	DQA1*03:03	DQA1*05:05	DQB1*02:02	DQB1*03:01
4037_DC	DRB1*01:01				DPA1*01:03		DPB1*04:01	DPB1*06:01	DQA1*01:01		DQB1*05:01	
4052_BA	DRB1*03:01	DRB1*11:04	DRB3*01:01	DRB3*02:02	DPA1*01:03		DPB1*04:01		DQA1*05:01	DQA1*05:05	DQB1*02:01	DQB1*03:01
BP455	DRB1*10:01	DRB1*13:01	DRB3*01:01		DPA1*01:03		DPB1*02:01		DQA1*01:05	DQA1*01:10	DQB1*05:01	DQB1*06:03
CD165	DRB1*11:01		DRB3*02:02		DPA1*01:03		DPB1*04:01 (DPB1*105:01)	DPB1*04:02 (DPB1*126:01)	DQA1*05:05		DQB1*03:01	
CM647	DRB1*07:01	DRB1*16:01	DRB4*01:03	DRB5*02:02	DPA1*01:03		DPB1*02:01	DPB1*23:01	DQA1*01:02	DQA1*02:01	DQB1*02:02	DQB1*05:02
GD149	DRB1*07:01	DRB1*13:01	DRB3*01:01	DRB4*01:01	DPA1*01:03	DPA1*02:01	DPB1*03:01 (DPB1*124:01)	DPB1*04:01 (DPB1*350:01)	DQA1*01:10	DQA1*02:01	DQB1*02:02	DQB1*06:03
JY	DRB1*04:04	DRB1*13:01	DRB3*01:01	DRB4*01:03	DPA1*01:03		DPB1*02:01	DPB1*04:01	DQA1*01:03	DQA1*03:01	DQB1*03:02	DQB1*06:03
PD42	DRB1*01:02	DRB1*15:01	DRB5*01:01		DPA1*01:03	DPA1*02:02	DPB1*04:01	DPB1*05:01	DQA1*01:01	DQA1*01:02	DQB1*05:01	DQB1*06:02
RA957	DRB1*04:01	DRB1*08:01	DRB4*01:03		DPA1*01:03		DPB1*04:01 (DPB1*105:01)	DPB1*04:02 (DPB1*126:01)	DQA1*03:03	DQA1*04:01	DQB1*03:01	DQB1*04:02
TIL1	DRB1*01:01	DRB1*04:08	DRB4*01:03		DPA1*01:03		DPB1*02:01	DPB1*04:01	DQA1*01:01	DQA1*03:03	DQB1*03:01	DQB1*05:01
TIL3	DRB1*12:01 (DRB1*12:10)	DRB1*15:01	DRB3*02:02	DRB5*01:01	DPA1*01:03		DPB1*03:01 (DPB1*124:01)	DPB1*04:01 (DPB1*350:01)	DQA1*01:02	DQA1*05:05	DQB1*03:01	DQB1*05:02

Supplementary Table 2. HLA-II typing and number of peptides from the independent public HLA-II peptidomics samples used to benchmark MixMHC2pred.

ID	Reference	HLA-			# peptides
B9089	Bergseng et al., 2015	DQA1*05:05	DQB1*03:01		4396
M9050	Bergseng et al., 2015	DQA1*02:01	DQB1*02:02		3425
P9047	Bergseng et al., 2015	DQA1*02:01	DQB1*02:02		2596
P9051	Bergseng et al., 2015	DQA1*02:01	DQB1*02:02		4100
S9037	Bergseng et al., 2015	DQA1*05:05	DQB1*03:01		3337
Mouse_DC	Clement et al., 2016	DRB1*01:01			2559
t1	Collado et al., 2013	DRB1*01:01	DRB1*03:01		48
t2	Collado et al., 2013	DRB1*01:01	DRB1*03:01		81
t3	Collado et al., 2013	DRB1*03:01	DRB1*11:01		16
t4	Collado et al., 2013	DRB1*03:01	DRB1*15:01		30
t5	Collado et al., 2013	DRB1*03:01	DRB1*11:04		11
L128_1E8	Khodadoust et al., 2017	DRB1*07:01	DRB1*11:01		2210
L128_1E9	Khodadoust et al., 2017	DRB1*07:01	DRB1*11:01		3976
MCL001	Khodadoust et al., 2017	DRB1*04:01	DRB1*07:01		1449
MCL005	Khodadoust et al., 2017	DRB1*04:01	DRB1*11:01		320
MCL007	Khodadoust et al., 2017	DRB1*01:01	DRB1*07:01		40
MCL008	Khodadoust et al., 2017	DRB1*04:01			543
MCL014	Khodadoust et al., 2017	DRB1*11:01			684
MCL022	Khodadoust et al., 2017	DRB1*01:01	DRB1*04:01		511
MCL030	Khodadoust et al., 2017	DRB1*07:01			1008
MCL034_rep1	Khodadoust et al., 2017	DRB1*04:01			514
MCL034_rep2	Khodadoust et al., 2017	DRB1*04:01			522
MCL037	Khodadoust et al., 2017	DRB1*11:01			911
MCL041	Khodadoust et al., 2017	DRB1*04:01			588
MCL043	Khodadoust et al., 2017	DRB1*07:01	DRB1*11:01		839
MCL049	Khodadoust et al., 2017	DRB1*01:01	DRB1*07:01		231
MCL052	Khodadoust et al., 2017	DRB1*01:01			871
MCLX001	Khodadoust et al., 2017	DRB1*01:01	DRB1*07:01		362
MCLX002	Khodadoust et al., 2017	DRB1*07:01			276
IHW09004	Ooi et al., 2017	DRB1*01:01			3543
IHW09013	Ooi et al., 2017	DRB1*15:01	DRB5*01:01		1526
DOHH2	Ritz et al., 2018	DRB1*01:01	DRB1*15:01	DRB5*01:01	1464
Maver_1	Ritz et al., 2018	DRB1*01:01	DRB1*13:01	DRB3*02:02	2904
LA2	Wang et al., 2017	DRB1*10:01	DRB1*11:01		84
LA3	Wang et al., 2017	DRB1*03:01	DRB1*15:01		178
LA6	Wang et al., 2017	DRB1*01:03	DRB1*03:01		77
LA8	Wang et al., 2017	DRB1*04:01	DRB1*10:01		1042
RA2	Wang et al., 2017	DRB1*01:01	DRB1*04:01		115
RA3	Wang et al., 2017	DRB1*01:01	DRB1*04:01		84
RA4	Wang et al., 2017	DRB1*04:01	DRB1*15:01		29
RA5	Wang et al., 2017	DRB1*08:01	DRB1*15:01		104

Supplementary Table 3. Interactions between the positions in the core binding region of the peptides. Alleles with a significant mutual information between two positions are listed (threshold for significance: Holm's adjusted P < 0.05; P values were obtained from the one-sided comparison of the MI against n = 10^5 random MI values from the null model, see Supplementary Note for details).

Allele	Core positions	P.adj
DRB1*04:01	P3 – P5	0.00324
DRB1*04:04	P3 – P5	0.03024
DRB1*08:01	P4 – P6	< 0.001
DRB1*11:01	P3 – P5	0.0035
	P5 – P7	0.00324
	P7 – P8	0.0085
DRB1*13:01	P4 – P7	0.0224
	P4 – P9	< 0.001

Supplementary Table 4 (provided as a separate .xlsx file)**. Viral, bacterial and tumor-associated epitopes. (a)** List and full sequence of the viral, bacterial and tumor-associated antigens included in the experiment. **(b)** Best scoring candidate epitopes predicted by MixMHC2pred or NetMHCIIpan that were tested for immunogenicity in two melanoma patients (LAU1352 and LAU1357) and a healthy donor.

Supplementary Note

Further details on MoDec framework

Binding motif length

In our deconvolution with MoDec, we assumed a binding motif length of 9 amino acids. This is what is observed in all currently available crystal structures for class II. In view of a recent computational study, approximately 2% of peptides could nonetheless have a shorter or longer binding core[1]. For this reason, we investigated the importance of the 9-mer core by performing again the deconvolution, using this time a motif length of 8 or 10 (Supplementary Fig. 13). The motifs that we found corresponded nevertheless to the standard 9-mer motifs, either truncated by one amino acid or with an extra flat position at the beginning or end of the 9-mer motif (with main anchors either at 1-4-6-9 or 2-5-7-10). It thus seems that other binding core sizes are not frequent also in our data.

Definition of the special sum

The *special sum* "$l \oplus s$" appearing in equation (1) of the log-likelihood equation solved by MoDec is defined in the following way:

$$(l \oplus s)_n = l + s + \left\lceil \frac{\lambda^n - L}{2} \right\rceil - g(s, \lambda^n, L) \qquad \text{(N1)}$$

with

$$g(s, \lambda^n, L) = \begin{cases} 1, & (\lambda^n - L) \,\%\, 2 \neq 0 \text{ and } s > 0 \\ \infty, & (\lambda^n - L) \,\%\, 2 \neq 0 \text{ and } s = 0 \\ 0, & \text{otherwise} \end{cases} \qquad \text{(N2)}$$

This special sum renders the binding core offsets to be fully symmetric around 0 for each peptide (e.g. only the s values -2, -1, 1 and 2 will be defined for a peptide of length 12 when the motif has a length 9, while a peptide of length 13 would additionally have the offset $s=0$).

Parameter estimation by expectation-maximization

For a fixed number of motifs K, MoDec determines the maximal likelihood from equation (1) through the expectation-maximization algorithm. Similarly to the derivation proposed by Bishop[2], we rewrite equation (1) as

$$\log(\mathcal{L}) = \sum_n \left(W^n \cdot \mathfrak{L}(q^n, \theta, w) + W^n \cdot \mathrm{KL}(q^n \parallel p^n) \right) + \log\left(\mathrm{P}(\theta)\right) \quad \text{(N3)}$$

where $q^n(z^n=(k,s))$ is a normalized distribution defined over some latent variables z^n. q^n can also be referred to as the "responsibility of peptide n towards the motif k and binding core offset s". The other terms of this equation correspond to:

$$\mathfrak{L}(q^n, \theta, w) = \sum_{z^n} q^n(z^n) \cdot \log\left(\frac{\mathrm{P}(x^n, z^n|\theta, w)}{q^n(z^n)}\right) \quad \text{(N4)}$$

$$\mathrm{KL}(q^n \parallel p^n) = -\sum_{z^n} q^n(z^n) \cdot \log\left(\frac{\mathrm{P}(z^n|x^n, \theta, w)}{q^n(z^n)}\right) \quad \text{(N5)}$$

and

$$p^n = \mathrm{P}(z^n|x^n, \theta, w) \quad \text{(N6)}$$

Note that all $\mathrm{KL}(q^n \parallel p^n)$ correspond to Kullback-Leibler divergences and are always positive or 0.

The expectation-maximization then works briefly as follow:

1. Some initial conditions for the θ and w are given.
2. "Expectation step": θ, w are fixed and we search for the peptide responsibilities q^n that make the Kullback-Leibler divergences from equation (N5) to be 0.
3. The next step is the "maximization step": the peptide responsibilities are now fixed to those found in previous step and the lower bound from equation (N3) is maximized over θ and w (i.e. the Kullback-Leibler terms are "removed" as always positives and the other terms are maximized).
4. The steps 2 and 3 are then repeated multiple times until convergence to some maximum.

This algorithm does however not guarantee the convergence towards the global maximum. Therefore, the above iterations starting from different initial conditions are repeated multiple times and the best result is selected.

Alternative approach to determine the motif from each allele

As an alternative approach to determine the motif corresponding to each allele, we merged all samples sharing a given allele, one allele at a time, and performed a deconvolution with MoDec on the merged data. This merged data should contain multiple motifs: one (or more) that contains peptides from all original samples that were merged together (corresponding to the allele(s) that was shared by all these original samples) and multiple other motifs that represent alleles expressed by a subset of the original samples. We thus selected the motif representing the shared allele as the one with the highest Shannon entropy, computed as: $S_k = -\sum_n p_k^n \cdot \log p_k^n$ (with $p_k{}^n$ being the fraction of peptides from the original sample n that were assigned to the motif k).

This alternative approach worked well for most HLA-DR alleles, resulting in the same motifs than what was found by our initial approach (Supplementary Fig. 15b). However, it failed to capture most HLA-DP and -DQ motifs (Supplementary Fig. 15b). These motifs containing fewer peptides, it was more challenging for the deconvolution to find these rarer motifs, in particular because merged samples contained lots of different alleles and thus lots of motifs to build, leading possibly to higher contamination between the motifs.

Overall, our results suggest that there is a trade-off between the number of peptides and the number of HLA-II alleles to deconvolve. In our hands (and considering that most of our samples already have from 2000-5000 peptides), we consistently found that having less alleles is useful for the accuracy of the deconvolution.

Another approach that would nevertheless be worth testing once available is NNAlign_MA[3], where multiple samples are also merged together but information on previous estimates from the allele motifs is used to help for the deconvolution.

Accounting for interactions between binding core positions

The binding term from MixMHC2pred is computed based on position weight matrices (PWM), which does not account per se for possible interactions between the positions in the binding core. This is consistent with existing crystal structures, which show that the

binding of HLA-II ligands is mainly linear (unlike HLA-I ligands that can bulge out) and that amino acids along the peptides are not physically interacting much with each other.

We nevertheless further investigated if accounting for such interactions could still be important for the predictions. We first determined if such interactions were present in our data with help of mutual information (MI). Briefly, we computed the MI between each pair of positions within the binding core of an allele, considering all peptides that had been assigned to the given allele. We then compared this MI against a null model of random 9-mer peptides sampled from the human proteome: random MI values were computed considering the same number of random 9-mers that the number of peptides that had been assigned to the given allele, and this computation of random MI values was repeated multiple times in order to determine a P value for the test that the observed MI value of the allele between two given positions was significantly greater than would be for random peptides. P values were adjusted based on Holm's multiple testing correction (for each allele independently). Based on this analysis, we determined that five alleles possessed interactions between the positions (Supplementary Table 3).

We accounted for these interactions by modeling the binding through PWMs with multiple specificities, in a similar manner than in ref.[4]. Notably, the interactions between positions 4 and 6 from DRB1*08:01 had directly been observed by MoDec in the initial deconvolution, splitting its motif into two distinct sub-motifs (Supplementary Fig. 2).

This model (termed "multiple specificities") did nevertheless not perform better than MixMHC2pred (Supplementary Fig. 8b).

Neural network predictors

As an alternative approach that could capture interactions between amino acids, as well as other hidden features, we built two neural network predictors. Indeed, in multiple settings, predictions based on neural networks have been showed to be of greater accuracy than PWM based approaches[5,6]. Yet, a recent study revealed that PWM based approaches had higher accuracy in predicting class-I epitopes[7]. We thus also tested such predictors here for comparison of the accuracy.

Firstly, we used NNalign[8], version 2.1, which is the state-of-the-art neural network predictor for HLA predictions. We trained this predictor for each allele separately, based on the peptides that had been assigned to this allele by our deconvolution (i.e. the same peptides than what is used in our training set to build MixMHC2pred). Negative peptides were added to the training data, adding five times more negative peptides than there are ligands for a given allele, and considering a uniform distribution of the negative peptides (of sizes 12–19 aa). The addition of negative peptides is needed for neural network predictors. The true ligands were given a value of 1 and the negative a value of 0 in the training data input. Following options were defined to NNalign for the training: "-rescale 2 -seeds 10 -nh 2,10,20,40,60 -eplen 15 -p1a -burn 2 -split 2 -thrCM 9 -stop".

Secondly, we built a neural network predictor encoding the same features than MixMHC2pred, training such a predictor for each allele separately. Here the binding core of the true ligands was obtained from the results of our deconvolution. For the negative peptides (the same as described above for NNalign), we used a binding core offset that was drawn from a random uniform distribution and we used the corresponding binding core sequence. The binding core sequence as well as the 3 amino acids on the N-/C-terminus of the peptide were encoded through a one-hot encoding. In addition, the peptide length was encoded through a one-hot encoding for the sizes between 12 and 19. Similarly, a one-hot encoding was used for the binding core offset, considering the classes between an offset of -4 to +4. This resulted in a vector of size 317 encoding each peptide. The true ligands were given a value of 1 and the negative peptides a value of 0. The neural network was trained with help of the R-package *neuralnet*[9] version 1.44.2, considering a logistic activation function, a non-linear output function and a single hidden layer with 60 hidden nodes. For each allele, we repeated the training 10 times and kept the 3 best performing models. For predictions, the score was then the average between these 3 models.

We then tested these two neural network predictors on the tetramer data from IEDB and observed that they displayed a lower accuracy than MixMHC2pred (Supplementary Fig. 8b).

Supplementary references

1. Massimo Andreatta et al. *Immunology* **152**, 255–264 (2017).
2. Bishop, C. (Springer-Verlag: New York, 2006).at <www.springer.com/us/book/9780387310732>
3. Alvarez, B. et al. *bioRxiv* 550673 (2019).
4. Gfeller, D. et al. *J. Immunol.* **201**, 3705–3716 (2018).
5. Zhao, W. & Sher, X. *PLOS Comput. Biol.* **14**, e1006457 (2018).
6. Bulik-Sullivan, B. et al. *Nat. Biotechnol.* **37**, 55–63 (2019).
7. Mei, S. et al. *Brief. Bioinform.* bbz051 (2019).
8. Nielsen, M. & Andreatta, M. *Nucleic Acids Res.* **45**, W344–W349 (2017).
9. Fritsch, S., Guenther, F., Wright, M.N., Suling, M. & Mueller, S.M. (2019).at <https://CRAN.R-project.org/package=neuralnet>

J.5 Discussion

In cancer immunotherapy there has always been a deep interest in the identification of antigens which could be associated with one particular cancer type and exploited therapeutically. The knowledge of cell specificity has brought great advances in the medical field in the form of vaccination for infectious diseases and cancer. Vaccination has been most effective for cancers of infectious (viral) etiology as the target antigen is only present on diseased cells (286). However, for cancers of non-viral origin the finding of a good target remains complicated. Currently, the field of tumor immunology is moving towards a more personalized approach, particularly by exploiting neoantigens which are resulting from unique mutations due to errors in the DNA replication and repair processes in cancer cells. Neoantigens represents new attractive targets for vaccination (286). The complication remains to predict which of the neoepitopes will bind adequately to MHC molecules and be immunogenic. Nowadays there are good MHCI peptide predictors such as NetMHC but despite the availability of NetMHCII improvement is needed in the MHC class II peptide binding prediction field.

In this study a large panel of 99265 unique peptides eluted from HLAII molecules were analyzed with a motif deconvolution algorithm (MoDec). The data was then used to train an epitope prediction algorithm. The developed predicting algorithm was called MixMHC2pred and unlike previous prediction programs relies on a probabilistic framework instead of a strict alignment of peptides (287,288). What this entails is an algorithm that detects binding motifs on the whole length of a peptide and not only the supposed binding site. This allows also the learning by the algorithm of the preferred binding core position offsets by the peptide and their weight. Further, one of the limitations of current predictors was their ability to predict peptide binding only to the HLA-DR molecules (283). Advances in this regard were made with the MixMHC2pred algorithm as it was able to predict peptide binding also to HLA-DP or HLA-DQ alleles in addition to HLA-DR ones. This aspect was also addressed by the creators of the NetMHCIIpan-3.0 software back in 2014 and they now offer with the 3.2 version a larger array of HLA alleles (281). In comparison to the other existing motif deconvolution methods, MixMHC2pred resulted in improved resolution and speed needed to resolve interrogations making it particularly useful for large HLA-II peptidomics datasets.

Although our work is not exhaustive in terms of understanding the complexity of MHC class II antigen presentation, it represents an improved tool for the binding prediction of tumor associated antigens as well as neoantigens, to be selected for vaccination trials after proper evaluation of their immunogenicity. To test the MixMHC2pred capacity to predict good MHC binding peptides, known melanoma associated antigens as well as and viral and bacterial proteins were screened with both MixMHC2pred and NetMHCIIpan. The top candidates were tested in immunogenicity assays with melanoma patient samples as well as healthy donor samples. A higher fraction of true positives was predicted by MixMHC2pred compared to NetMHCIIpan. This improved prediction of true epitopes was further confirmed when validating neoepitope binding to MHC class II.

In conclusion MixMHC2pred offers a peptide-binding algorithm which has the capability of predicting higher numbers of true positive binding peptides compared to the existing NetMHCIIpan algorithm. Both have the capacity to predict peptides binding to the multiple common HLA-II alleles -DR, -DP and -DQ but MixMHC2pred can do so faster. However, as other prediction algorithms, MixMHC2pred is not able to predict immunogenicity which still needs to be confirmed experimentally. Furthermore, it does not consider the binding stability of the peptide to the MHC which also can influence peptide immunogenicity.

K Unlocking the anti-tumor CD4 T cell potential by modulating T cell differentiation via miRNA manipulations

K.1 Introduction

Since the discovery of the first miRNA back in 1993 in C. elegans, many others have been discovered in multiple organisms such as plants, mouse and humans (289). They are expressed differently from one tissue to another and even within the same tissue there are significant differences suggesting a role of miRNA in development (290). In fact, miRNA have already been linked with the ability to regulate fat metabolism, insulin secretion, haematopoiesis, muscle development and many other mechanisms. Interestingly, miRNA have been shown to maintain stemness within cells and modulate their differentiation (290). In that regard a large number of miRNAs have been identified in the complex mechanism of haematopoiesis in which blood cells will undergo a series of proliferation and differentiation processes from their original hematopoietic stem cell and give rise to both the myeloid and lymphoid lineages. miRNAs have numerous functions within these cells, the three main being: maintaining hematopoietic stem cell lineage by inhibiting differentiation, specifying commitment to either the myeloid or the lymphoid lineage (such as miR-223 and 181) and supporting differentiation of granulocyte-macrophage precursors and megakaryocyte-erythroid precursors (such as miR-451, miR-16, miR-150, miR-155, miR-221 and miR-222 (291)). miR-221 and miR-222 were linked with targeting KIT and thus preventing erythroid differentiation (292), while miR-99 is a broadly conserved miRNA family who is expressed in hematopoietic stem cells. This miRNA is less known in regard to its function within hematopoietic cells but one study has linked its expression with a capacity to regulate self-renewal of hematopoietic stem cells. miR-99 acts on cell differentiation by inhibiting it and inhibiting the cell cycle entry (293). Further, miR-21 was identified as an important regulator of T cell effector versus memory formation. miR-21 expression was strongly induced and caused changes in the transcriptional network by negative targeting ERK, AP-1, and AKT pathways. These pathways are major signaling pathways and by acting on them miR-21 is also acting on cell differentiation, resulting in an inhibition of the development of a memory transcriptome (294).

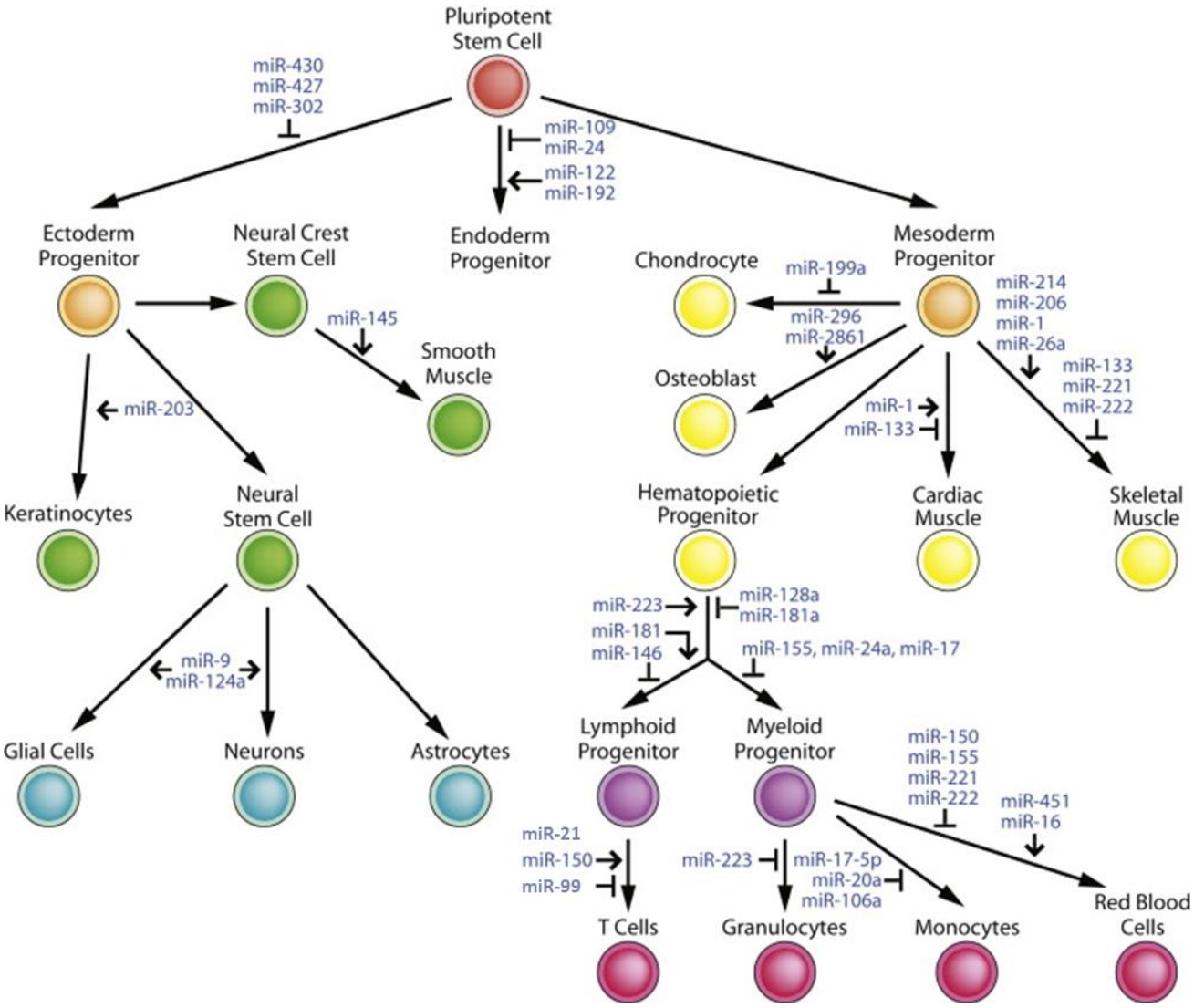

Figure 12: miRNAs regulation of multiple cell types. miRNA can regulate multiple facets of cell differentiation and lineage commitment by inhibiting of promoting cells to assume a distinct fate. Adapted from (295).

Once a T cell has encountered an antigen which it will recognize upon TCR-MHC engagement it will become activated. The T lymphocyte will start proliferating and migrating to the infection site or the tumor bed. Beside T_{EM} and T_{CM}, the existence of another subset of differentiated T cells was recently described and called T_{SCM} cells. These cells were part of viral and tumor-reactive T cell populations which upon activation released cytokines and proliferated in response to IL-15 (296). These cells were mostly studied in the CD8 T cell field. They were first discovered in mice thanks to advances in flow cytometry. T_{SCM} cells expressed high levels of the stem cell antigen-1 (SCA-1) and markers for memory such as IL-2Rβ and chemokine receptor-3 (CXCR3) (164). Their identification in humans and non-human primates was more complicated as there was no human orthologue for SCA-1. The discovery of T_{SCM} cells as a human cell population was the result of the discovery in mice that T_{SCM} could be generated from naïve cells by modulation with the GSK3 inhibitor TWS119. It was thought that Wnt signaling promoted the generation of $CD44^{low}CD62L^{high}Sca\text{-}1^{high}CD122^{high}Bcl\text{-}2^{high}$ multipotent CD8 T cells (297). However, it resulted that the modulation by TWS119 of mTOR1 and not of Wnt

was resulting in the induction of T_{scm} cells. Similarly to the mouse cells the T_{SCM} in human and non-human primate were largely of a naïve-like phenotype with memory marker such as CD95, CXCR3, IL-2Rβ, CD58 and CD11a (132,133). Therefore, T_{SCM} cells were put in the progressive T cell differentiation pathway in between T_N cells and memory T cells (134). T_{SCM} represent only 2-3% of circulating T lymphocytes (296). T_{SCM} cells are linked with long-term persistence within hosts after transfer, great capacity of self-renewal and ability to generate memory cells as well as effector cells. The power of T cell proliferation capacity of less differentiated cells was demonstrated when the group of Dirk H. Busch transferred in normal recipient mice one single antigen-specific naive T cell. It resulted in a broad expansion of specific cells as well as their differentiation into multiple subsets of T cells (298). It was shown early on that the injection of early differentiated CD8 T cells in mice resulted in the eradication of established tumors whereas this was not achievable with late differentiated effector cells (299). Later on these observations were confirmed and even accentuated when T_{SCM} cells were injected in tumor bearing mice, resulting in the best anti-tumoral response even surpassing the use of early differentiated and proliferation capable T_{CM} cells (133). T_{SCM} have not been thoroughly investigated within the CD4 T cell field. Their existence is known and there have been studies in several contexts such as CD4 T cell tropic retrovirus infections such as with HIV-1. T_{SCM} due to their particular nature could support both the transcriptionally-silent form of infection as well as a productive viral replication (300). furthermore the virus can exploit this cell stemness to its advantage and establish a durable, self-renewable viral reservoir (301). Little to no information can be found about the use of CD4 T_{SCM} in an anti-tumor context but a preliminary study demonstrated the possibility of modulating the formation of CD4 T_{SCM} via the modulation of mTOR signaling (163). Despite this limited knowledge in CD4 T_{SCM}, the powerful anti-tumor response encouraged scientists to determine the signaling pathways mediating T_{SCM} induction, since T_{SCM} cells could then be used in anti-tumor therapeutical approaches.

Several attempts have been made to understand the pathway mediating T_{SCM} modulation. One such target is the Wnt signaling cascade whose functions include cell determination and proliferation. Wnt controls the regulation of target genes which upon Wnt aberrant activity will result in uncontrolled cell growth and survival. A malfunctioning Wnt signaling cascade can result in oncogenesis (302). Acting on the Wnt signaling pathway by using the activator TWS119 on T_N cells inhibited the glycogen synthase kinase-3β (GSK-3β). This effect seamed to generate differentiation of T_N cells to T_{SCM} (133). Controversy surrounds these results as ex-vivo T_{SCM} cells were not excluded from the initial T_N population (163). Metabolism might also play an important role in T cell differentiation thus the targeting of the mTOR kinase might be relevant for the generation of T_{SCM} cells. Indeed, mTORC1 appeared to be a target as it was pointed out as a major regulator of CD4 T_{SCM} cell differentiation that could be modulated by the mTORC1 inhibitor TWS119 (163). It was reported that the inhibition of mTORC1 and simultaneous activation of mTORC2 signaling gives rise to T_{SCM} cells independently of Wnt signaling (163).

These observations brought insight in the pharmacological induction of CD4 T_{SCM} cells. But other natural occurring mechanisms cannot be excluded when it comes to the modulation of T_N cells towards the T_{SCM} subset. As miRNA have also been implicated in the maintenance of stemness within hematopoietic stem cells they could be plausible candidates to the T_{SCM} subset generation. Yet, at the present time little is known about miR expression in human T_N, T_{SCM} and T_{CM} cells.

K.2 Aim

The aim of this project is to identify miRNA which are differentially expressed between the various T_N, T_{SCM} and T_{CM} cells subsets and to correlate their expression with those of the mRNA that they are targeting. The goal is to then modulate the expression of the identified miRNA candidates in tumor-specific CD4 T cells to induce a T_{SCM} phenotype, given its great potential in anti-tumor control in mouse models.

K.3 Material and methods

K.3.1 Human T lymphocytes

The peripheral blood mononuclear cells (PBMCs) were isolated from blood of healthy donors obtained from the blood transfusion centre of Lausanne. Blood was diluted with PBS and mononuclear cells were purified by centrifugation over Ficoll-Plaque TM Plus (Amersham Bioscience, Uppsala, Sweden), then washed three times with RPMI 1640. The mononuclear cells were collected and immediately used for cell sorting. Experiments were performed in accordance to the guidelines of the Ethics Commission of the Canton de Vaud.

K.3.2 mRNA sequencing and miRNA array

The mRNA sequencing and the miR array were performed by a former MD-PhD candidate in the group of Prof Pedro Romero. The methods for the mRNA sequencing are included in the publication (163). For the miRNA array the labelled miRNA was hybridized onto a human miR microarray and the assay was run in standard conditions by the company IMGM laboratories GmbH.

K.3.3 Flow cytometry

After isolation from fresh blood samples, cells were immediately stained with the following markers: LIVE/DEAD fixable dead cell stain (Vivid, Invitrogen, CA, united states) diluted 1:800 in PBS, anti-human CD3 AF700 (clone HIT3a, Biolegend, London, UK), anti-human CD4-PE (clone RPA-T4, Biolegend, London, UK), anti-human CD8-APC-Cy7 (clone B9.11, Beckman Coulter, CA, USA), anti-human CCR7-BV421 (clone G043H7, Biolegend, London, UK), anti-human CD45RA-PE-CF594 (clone HL100, BD, NJ, USA), anti-human CD95-APC (clone DX2, Biolegend, London, UK), anti-human CD58-FITC (clone 1C3, BD, NJ, USA). After 30min incubation at RT, cells were washed with PBS and resuspended in PBS at a concentration of 10 million/ml and sorted using either an Aria IIU or the Aria III (Becton Dickinson, NJ, USA). The cells were collected in Eppendorf tubes containing RPMI 1640 containing 8% of human serum, 2 mM glutamine, 1% (vol/vol) nonessential amino

acids, 50µM 2β-mercaptoethanol, penicillin (50 U/ml) and streptomycin (50 µg/ml) (R8 media) and centrifuged at 400g for 5min. The supernatant was collected by pipetting and discarded with care to not disturb the cell pellet. The cells were then either frozen at -80°C as a dry pellet if the miRNA had to be extracted or resuspended in 0.5 mL trizol® reagent (Thermo Fisher scientific, MA, USA) for mRNA extraction. The data from the cell sorting was analysed using FlowJo software (FlowJo).

K.3.4 miRNA extraction and miRNA RT-qPCR

Total RNA was extracted from the dry pellets of the sorted cells conserved at -80°C using the mirVana™ miRNA Isolation Kit, without phenol (Thermo Fisher scientific, MA, USA). The dry pellet was resuspended in 600 µl of lysis binding buffer and mixed well to obtain a homogeneous lysate. 60 µl of homogenate additive was added and vortexed, then kept on ice for 10 min. 600 µl of Acid-Phenol: Chloroform (Thermo Fisher scientific, MA, USA) was added to the samples with caution. The mix was vortexed for 30-60 seconds and then centrifuged at 15'000 rpm for 5 min at RT. Once the interphase was compact, the aqueous upper-phase (approximatively 600 µl) was transferred to a new collecting tube. If the phases are not clear the centrifugation step can be performed once more. 750 µl of absolute ethanol (99.5%pure) (Thermo Fisher scientific, MA, USA) was added to the collected volume, representing 1.25 volumes of the transferred liquid. The mix was mixed up and down a few times. A filter cartridge provided in the kit was placed in a fresh collecting tube and a maximum of 700 µl at the time of the mix was added to the column. The columns were centrifuged for 30 sec at 10'000 rpm to let the liquid pass through the filter. The flow through was discarded and this step was repeated until the totality of the solution has passed. Next, 700 µl of washing solution 1 (containing ethanol) was added to the column and the tube was centrifuged for 30 sec at 10'000 rpm. The flow through was discarded. At this stage 500 µl of washing solution 2/3 was added to the column and the tubes were centrifuged for 30 sec at 10'000 rpm. This washing step was repeated twice. After the last wash, the columns were centrifuged one more time for 1 min to get rid of all liquid on the cartridge. The cartridge was then placed on a clean collection tube and the RNA was eluted with 50 µl of nuclease-free water (Thermo Fisher scientific, MA, USA) warmed up prior to its usage to 95°C. In the case of low cell numbers, a lower volume of H_2O can be used to elute the samples. The tube was then incubated for 2-5 min, then centrifuged at 10'000 rpm for 2 min to elute the sample. The quantity of collected material is then evaluated using Nanodrop one (Thermo Fisher scientific, MA, USA).

After extracting total RNA, the miRNA had to be reverse transcribed (RT) to cDNA. This was done with the TaqMan® Advanced miRNA cDNA Synthesis Kit (Thermo Fisher scientific, MA, USA) which allows for the RT of all miRNA without having to add specific primers at this stage. The protocol includes 4 steps: 1) a poly(A) tailing reaction, 2) an adaptor ligation phase 3) the actual RT reaction and 4) the amplification reaction (miR-Amp). These steps were performed following the manufacturers quick reference guide. Once the miRNA was transformed into cDNA we performed the RT-qPCR which was also detailed in the manufacturers' quick

reference guide and required the usage of the TaqMan® Fast Advanced Master Mix (Thermo Fisher scientific, MA, USA) and of the TaqMan® Advanced MicroRNA Assay (Thermo Fisher scientific, MA, USA). The latter item consisted of the individual miRNA primers chosen to be investigated in this assay. We used the primers for hsa-miR-146a-5p, hsa-miR-155-5p, hsa-miR-21-5p, hsa-miR-221-3p, hsa-miR-222-3p, hsa-miR-99b-5p and hsa-miR-630. Two further miRNA primers were ordered to provide a housekeeping reference. We selected two miRNA which were stably expressed in our miR array dataset, miR were hsa-miR-16-5p and hsa-miR-4428. 15 µl of the RT-qPCR master mix including primers and nuclease-free water were added to a MicroAmp® Fast 96-Well Reaction Plate (0.1mL) plate (Thermo Fisher scientific, MA, USA). The cDNA template was diluted 1:10 according to the manufacture's guidelines and 5 µl were added per well. The plate was then run on an ABI 7500 Real Time PCR System (Thermo Fisher scientific, MA, USA) using the standard Fast RT-qPCR thermal profile and by performing 40 cycles. The data was then collected and analyzed on Excel (Windows, NM, USA) and plotted in graphs via Prism – GraphPad (GRAPHPAD SOFTWARE, LLC, CA, USA).

K.3.5 mRNA extraction and mRNA RT-qPCR

To extract the total RNA from cells frozen in trizol, 100 µl of Roti®-Phenol/Chloroform/Isoamyl alcohol (Carl Roth Gmbh, Karlsruhe, Germany) were added to the thawn samples and vortexed for 5 sec until the samples was of a homogeneous pink. Samples were incubated for 5 min at RT, then centrifuged for 15 min at 12'000 rpm. The supernatant was then harvested (around 200 µl) and transferred to a clean Eppendorf tube where 0.5 µl of Glycogen (Thermo Fisher scientific, MA, USA) were added as well as 250 µl of isopropanol (Thermo Fisher scientific, MA, USA). The samples were incubated for 10 min and then centrifuged at 12'000rpm for 10 min. The supernatant was discarded and 500 µl of 70% ethanol were added to the samples and quickly vortexed. Next, the samples were centrifuged at 12'500rpm for 5 min. The supernatant was discarded and the tube left open until the ethanol was completely evaporated. The RNA pellet was resuspended in 12 µl of nuclease-free water and let stand at 55°C for 15 min at 400rpm. The total RNA was stored at -80°C.

To reverse transcribe the recovered total RNA we used the iScript™ Reverse Transcription Supermix (Bio-Rad, CA, USA). 1 µg of total RNA was added to 4 µl of the iScript RT supermix and the volume was adjusted to 20 µl with nuclease-free water. The reaction was incubated in a T3000 thermocycler (Biometra, Châtel-Saint-Denis, VD, CH) with the following profile: priming for 5 min at 25°C, reverse transcription for 20 min at 46°C and RT inactivation for 1 min at 95°C. The final product was diluted 1:5 in nuclease-Free water and conserved at -20°C.

The RT-qPCR reaction was performed with the KAPA SYBR® FAST qPCR kit (Merck & Co., NJ, USA). For one reaction 5 µl of Sybergreen were added with 2.6 µl of nuclease-free water, 0.2 µl of the forward primer and 0.2 µl of the reverse primer. This mix was plated on 48-well Eco™ Plates (VWR, PA, USA) and 2 µl of diluted cDNA were added to the appropriate wells. The plate was then sealed with Eco™ Adhesive Seals (VWR, PA, USA) and placed in the Illumina Eco Real-time PCR System (Thermo Fisher scientific, MA, USA). The plate was

run for quantification with the standard thermal profile for 40 cycles. The data was then collected and analysed on Excel (Windows, NM, USA) and plotted in graphs via Prism – GraphPad (GRAPHPAD SOFTWARE, LLC, CA, USA).

K.4 Results

K.4.1 Analysis of the miRNA involvement in human CD4 T cell differentiation

A key to CD4 T cell usage in immunotherapy will depend on a better understanding of the regulation of CD4 T cell differentiation, to promote T_{SCM} and central memory T_{CM} phenotypes. We aimed at identifying optimal miR candidates that could be therapeutically targeted to influence the differentiation of naïve CD4 T cells into T_{SCM} or T_{CM} CD4 T cells capable of targeting tumor cells.

Four different CD4 T cell populations were sorted (T_N, T_{SCM}, T_{CM} and T_{EMRA}) from 4 healthy donors' PBMCs using key markers of T cell differentiation such as CD45RA, CCR7, CD95 and CD58 **(Figure 13A)**. Total RNA was extracted including the small RNA fraction. After evaluating RNA concentration and purity the miR were purified and prepared for one-color hybridization. The labelled miRNA was hybridized onto a human miR microarray and the assay was run in standard conditions by the company IMGM laboratories GmbH. By performing a bioinformatics analysis of the miR array data we were able to identify miR that were differentially expressed between differentiated CD4 T cell populations. The most differentially expressed miR were found between the T_N and the T_{CM} population: miR-146a-5p, miR155-5p, miR-21-5p, miR-221-3p, miR-222-3p and miR-99b-5p. Between T_N and T_{SCM} population only miR-630 and finally between T_{CM} and T_{SCM} miR-222-3p and miR-99b-5p were differentially expressed **(Figure 13B)**.

To confirm this differential expression of miR between the differentiated CD4 T cells, we proceeded to sorting highly pure T_N, T_{SCM} and T_{CM} populations from 6 healthy donors, as done for the miR array. In addition, we also decided to sort the T_{EM} population as it represents a later stage of differentiation that could give us further insights into the expression of our candidate miRs across T cell stages. The total RNA including miR was extracted using the same process as in the miRNA array. The miR were then amplified and by performing real-time quantitative PCR (RT-qPCR) we were able to evaluate the level of expression of the target miR. By comparing both datasets, we could observe similar trends **(Figure 13C)**. As an example: in the miR array as with the RT-qPCR, miR-21-5p had increased levels of expression in T_{SCM} and in T_{CM} cells compared to T_N cells. We could also observe the reduced expression of miR-222-3p and miR-99b-5p in T_{SCM} cells compared to T_{CM} cells. The miR-630 is not represented in the data as it was not detected by RT-qPCR probably due to a lack of sensitivity of the assay. This data has brought to light novel miRNA targets other than the extensively investigated miR-146a, -155 and -21.

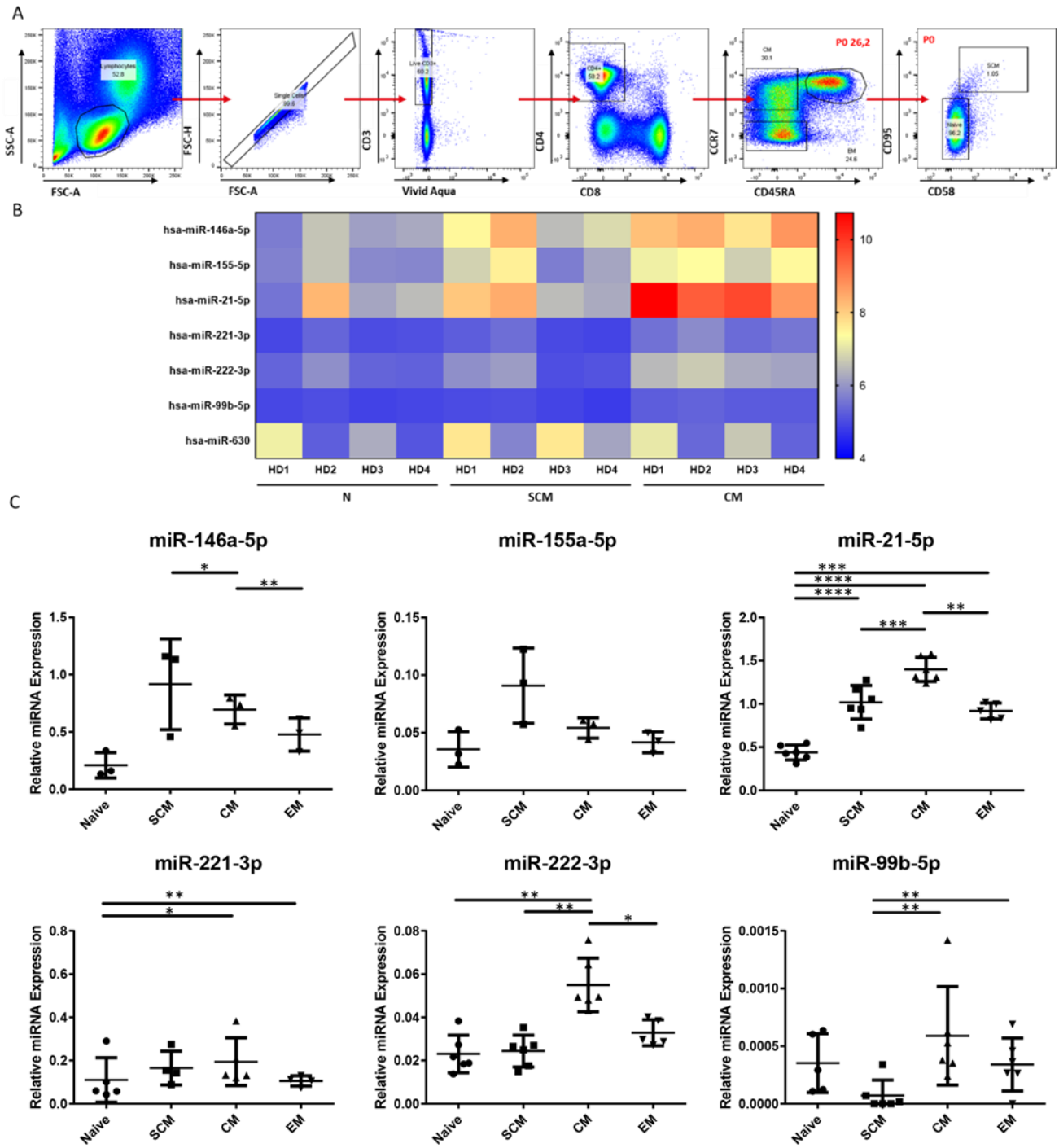

Figure 13: Analysis of miRNA expression in differentiated human CD4 T cells. A) Representative gating strategy for the sorting of differentiated CD4 T cells: T_N, T_{SCM}, T_{CM} and T_{EM}. **B)** Heatmap representation of the differentially expressed miRNA between CD4 T cell populations, as assessed by miR Array on 4 HDs. **C)** RT-qPCR evaluation of the miRNA target expression in the different sorted CD4 T cell populations. T test was used to evaluate the statistical significance $P<0.05$. Results from 6 HDs.

K.4.2 Differentially expressed mRNA targets correlating with different miRNA expression

To link a miR to a cell function, an mRNA sequencing was done on the same samples as the miR array, on 4 human healthy donors. RNA was purified and an amount of 10 ng of total RNA was amplified. The cDNA from the amplification reactions were cut and libraries were generated and sequenced at 100 nucleotides single read mode on an Illumina HiSeq 2000 instrument. Form this data a bioinformatics analysis was performed to

identify genes differentially expressed between the different CD4 T cell subsets. We focused on genes that are predicted and validated targets of the miR that we have identified using the miR array.

We were able to create heat maps of the target genes comparing their expression in two by two populations: T_N vs T_{SCM}, T_N vs T_{CM} and T_{CM} vs T_{SCM} **(Figure 14)**. We were selecting genes that are either downregulated when miRs are expressed (anticorrelated) **(Figure 14A)**, or genes that are upregulated (correlated) **(Figure 14B)** to miR expression as it was reported that despite being known for downregulating gene, miR are also able to act as activators of gene expression (158). We observed that several genes were downregulated between the comparaisons between T_N vs T_{SCM}, T_N vs T_{CM} and T_{CM} vs T_{SCM} but we also observed a greater number of upregulated genes between the same T cell populations and were targets either validated or predicted of the miR-146a, 155, 21, 221, 222, 99b or 630. In fact, when comparing T_N vs T_{SCM} we identified 8 genes as being downregulated and 6 being upregulated when their validated target miRNA expression was changed between the two subsets. Similarly, between T_N vs T_{CM}, 35 genes were downregulated and 118 were upregulated and finally T_{CM} vs T_{SCM} resulted in 6 genes upregulated and 3 were downregulated.

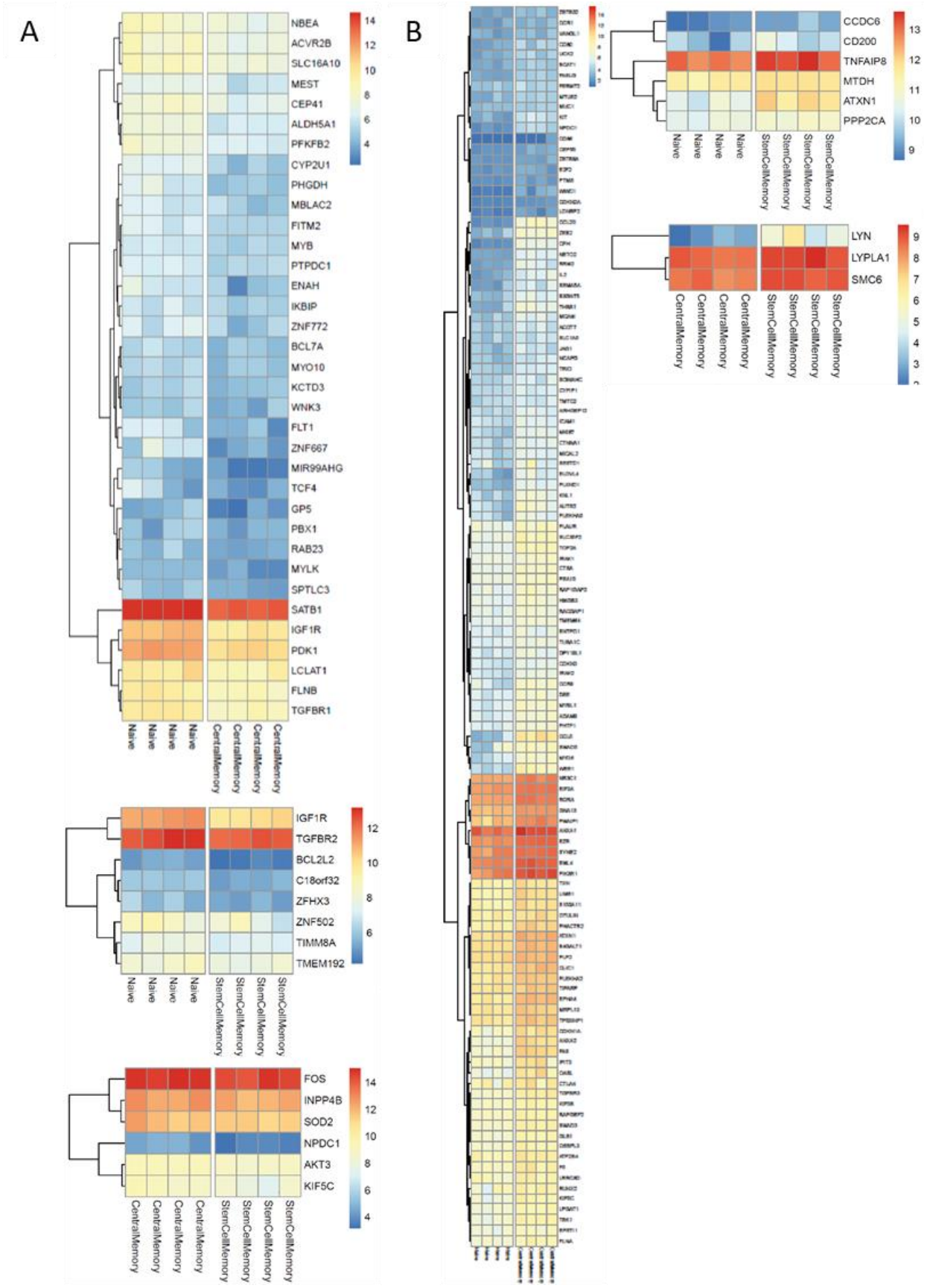

Figure 14: mRNA targets correlating with miRNA expression. Heatmap representation of the mRNA expression within the T_N, T_{SCM} and T_{CM} populations. **A)** Heatmap of the target mRNA anticorrelated with the levels of expression of the miRNA. From top to bottom the heatmaps are comparing T_N vs T_{CM}, T_N vs T_{SCM} and T_{CM} vs T_{SCM}. The scale ranges from genes which are higher expressed in red and lower expressed in blue. **B)** Heatmap of the mRNA positively correlating with the level of expression of miRNA. All mRNA targets represented had an adjusted P value P<0.05 and represent previously validated targets of our miR of interest. On the left

can be seen the comparison between T_N vs T_{CM}. On the top right are represented the T_N vs T_{SCM} comparison and bellow it the one between T_{CM} vs T_{SCM}. The scale color also ranges from higher expression in red to lower expressed in blue.

Since the list of mRNAs either up or down regulated was of a large scale we further refined our selection strategy. The first approach was to focus on the genes which have been predicted or validated to be targeted by our differentially expressed miRNA **(Figure 15)**. In this figure we observe a greater number of validated targets within the various cell types compared to the ones depicted in the previous heatmap. This finding can be explained by two facts. As one mRNA can be targeted by several miRNA, the mRNA target has to be considered as two or more separate targets. Furthermore, the Venn diagram is taking into account mRNA targets both upregulated or downregulated. We observed that the most differentially expressed genes were found in between T_N vs T_{CM} probably due to the fact that most miRNA differentially expressed were found in between these subsets **(Figure 13B)**. Between T_N vs T_{SCM} and T_{CM} vs T_{SCM} less genes were found as differentially expressed and targets of our candidate miRNA. The greater difference between T_N vs T_{CM} compared to the smaller difference between T_N vs T_{SCM} and T_{CM} vs T_{SCM} goes in line with the doctrines of CD4 T cell differentiation (137). Another approach was to look at the genes which were validated or predicted targets only of the miRNA of interest, namely the miR-21-5p, miR-221-3p, miR-222-3p, miR-99b-5p and miR-630, each one individually **(Figure 16)**. This second approach would also restrict further the number of genes to be investigated. We observed similar results obtained with the previous Venn diagrams were most target genes were found between the T_N vs T_{CM} subsets. miR-222-3p had targets differentially expressed between T_N vs T_{CM} and T_{CM} vs T_{SCM}. miR-630 as only differentially expressed between T_N vs T_{SCM} had target genes only in between these T cell subsets. Out of these validated targets represented in the Venn diagrams in **Figure 15** we focused on the top 10% differentially expressed and were targeted by the miRNA represented in the **Figure 16**. We obtained a list of target genes that are reported in **Table 3** with the indication if the gene is either up or down regulated, between which pair of differentiated CD4 T cell subsets, and for which miR it is a predicted/validated target.

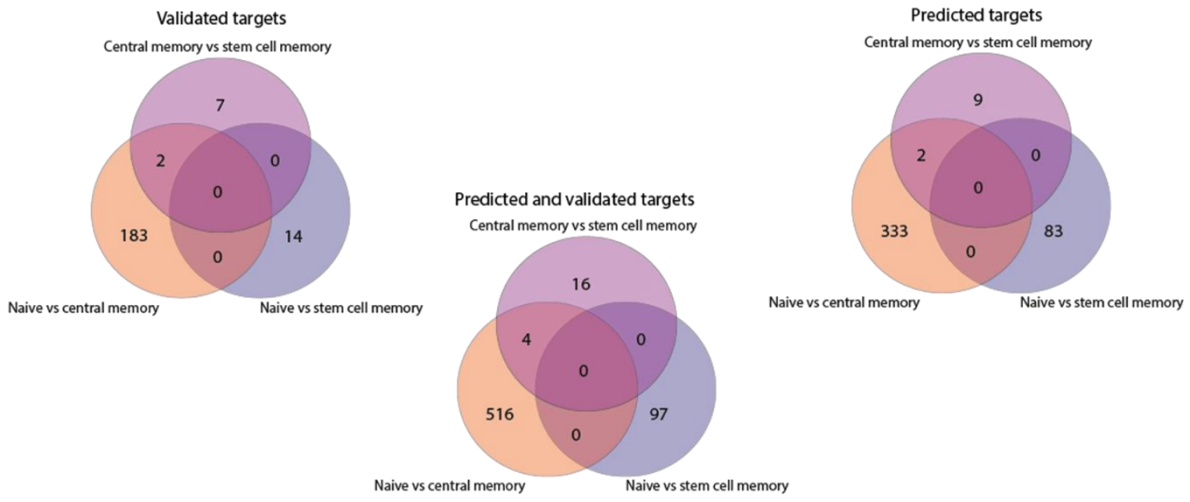

Figure 15: Venn diagram representation of validated and/or predicted target genes of our candidate miRNA.

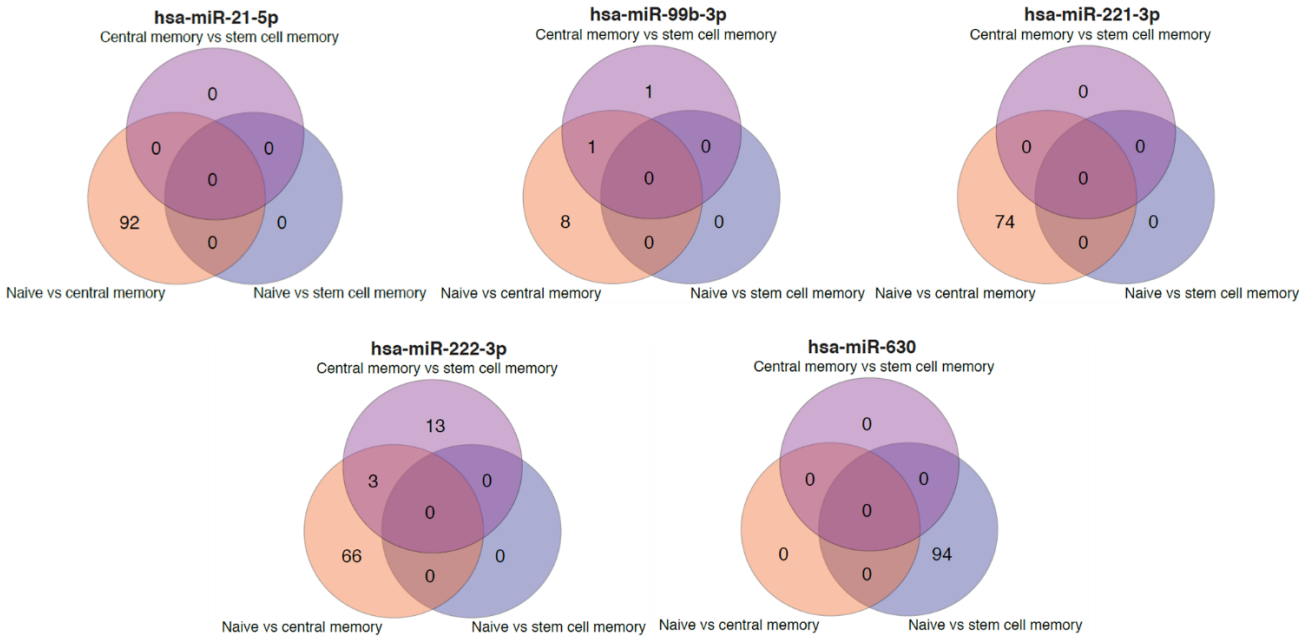

Figure 16: Venn diagram representation of the genes (predicted and validated) targeted by individual miRNA of interest.

T_N Vs T_{SCM}		T_N Vs T_{CM}			T_{CM} Vs T_{SCM}	
Up	Down	Up	Up	Down	Up	Down
CD200	TIMM8A	ZEB2	BCAT1	ZNF772	LYPLAI	NPDC1
CCDC6	BCL2L2	NPDC1	CDKN1A	TCF4	SMC6	INPP4B
PP2CA	IGFIR	AUTS2	TOP2A	ZNF667	LYN	SOD2
ATXN1	ZFHX3	KIT	KNL1	MIR99AHG		AKT3
TNFA1P8	TGFBR2	WEE1	MYO6	GP5		KIF5C
MTDH	TMEM192	THBS1	AUTS2	ENAH		FOS
	C18orf32	RRM2	B3GNT5	IGF1R		
	ZNF502	FAS	ELOVL4	PFKFB2		
		PLXND1	FASLG			
		NETO2	LONRF2			
		CCL20	SEMA5A			
all targets of miR-630		targets of miR-21, 221, 222 or 99b			targets of miR-99b or 222	

Table 3: list of top genes targeted by miRNA. Genes are represented depending on weather they are up or down regulated compared to the different cell types. miRNA which are targeting the genes are indicated at the bottom of the table.

The biological relevance of the genes listed in **Table 3** was evaluated by searching in the literature for known functions in overall cell differentiation, and if available in CD4 T cells. If nothing was found for these 2 criteria, we searched for any overall known role of the gene in cellular biology. Indeed, pertinent information could not be found for several genes such as C18orf32 or ZNF772. Others on the contrary revealed interesting functions. As a few examples ATXN1 has been shown to be involved in the Notch signaling pathway which is controlling a range of developmental processes (303). ATXN1 was also associated to regulate cerebellar biogenetics through the GSK3β-mTOR pathway (304) and its function could be modulated through the use of rapamycin as it would act on the mTOR pathway. Another gene such as LYN encodes for a tyrosine kinase, member of the Src family kinases. It was proposed that Lyn promotes progenitor cell expansion via the erythroid cell-intrinsic mechanism. In fact the absence of Lyn expression in deficient mice resulted in an

impaired proliferation of peripheral B cells (305). Another gene of interest from this list was the AKT3 gene which has been described as responsible for the survival and proliferation of embryonic stem cells as it controls p53 activity. Without AKT3, p53 accumulates in the nucleus which in turn will activate downstream targets such as Mdm2, p21, and Fas resulting ultimately in apoptosis and cell cycle arrest at the G1 phase (306). One last example is the WEE1. It is an oncogenic kinase capable of regulating the cell cycle as a checkpoint of the G2M phase (307). When WEE1 overexpression results in an increased cell proliferation as it was observed in gastric cancer cells (308). These are only a few examples of mRNA targets for miRNA identified in this study. This first approach to identify targets could in the future be extended to the other validated genes and even to the predicted target genes.

K.5 Discussion

This data revealed miR that have been extensively investigated such as miR-146a which expression in CD8 T cells correlates with a memory phenotype and has emerged as a critical regulator of the immune system [62]. miR-155 was reported to contribute to Th17 and Treg cell function by suppressing DNA transcription inhibitors [63]. miR-21 was reported to be a negative modulator of signal transduction downstream of the TCR in T lymphocytes [64], by comparing T_N and T_{CM}. However, our data also gives new insights into novel miR that could potentially influence CD4 T cell differentiation, especially towards the T_{SCM} phenotype, as they have been reported to influence differentiation and control cell cycle of other tissue cells. In fact, miR-221 and 222 are relatively unknown but seem to have an important function in human adipocyte differentiation, since the downregulation of these miR is crucial for this process [65]. Regarding miR-99b, it has been reported to be capable of potentiating endothelial cell differentiation from pluripotent human embryonic stem cells by regulating key genes [66], but nothing is known on the role of these miRs in the differentiation of CD4 T cells.

We have started the evaluation by RT-qPCR of mRNA potentially targeted by the miRNA, as we identified a panel of interesting candidate genes (Table 2). We expect this data to be in line with the data obtained with the RNA sequencing. We plan to modulate, in future experiments, the level of expression of the various miRNA targets in CD4 T cells with either miRNA mimics or inhibitors. To do this, we will be sorting primary human cells of the various subsets investigated here: naïve, central memory and stem cell memory and transfect the cells using the TransIT Transfection Reagent with miRNA identified earlier. Upon physiologic stimulation (CD3-CD28) and an incubation over time cell phenotype will be evaluated using the markers CD45RA, CCR7, CD58, CD95 to assess the cell differentiation. The use of miRNA mimics as well as inhibitors is now widely used (309). The feasibility of using of miRNA mimics as a therapeutic treatment for the enhancement of chemosensitivity in advance prostate cancer is now being investigated, as the use of mimics of miR-217 and miR-181b-5p was observed to increased significantly the apoptosis of the cancerous cells (310). Similarly in the field of neurosurgery it was shown that the inhibition of miR-155 with miRNA inhibitors following cerebral ischemia resulted in improved stroke recovery (311). The use of Antagomirs was possible

in primary T and B cells of human and mice, by employing an Antagomir modified with cholesterol to facilitate the entry into the primary cells in an efficient way. The miRNA resulted as 99.5% inhibited without impacting cell viability (312). Even though miRNA mimics and inhibitors are known to the field they have not been extensively used for the understanding of cell differentiation. One study attempted to use these products to induce mesenchymal stem cell differentiation into neuroblasts or neuroblastomas (313). The combination of inhibitors and mimics for miR-107, 124 and 381 was needed to push mesenchymal stem cells to differentiate probably due to a synergistic effect. Despite these studies, to our knowledge miRNA mimics and inhibitors have not yet been used to modulated CD4 T cell differentiation.

Once the impact on miRNA on T cell differentiation will have been validate in primary CD4 T cells. The miRNA inhibitors or mimics will be used in mice to confirm the impact of these molecules on the differentiation process of CD4 T cell. The functionality of differentiated T_{SCM} and T_{CM} through the use of mimics and inhibitors will have to be evaluated. The use of tumor bearing mice transfused with tumor specific cells made to be SCM or CM like through miRNA modulation could be used to see the feasibility of using such process and cell subtypes to control tumors. Such assays would show the pertinence of these subsets of T cells for tumor control and how to induce them

L General Discussion

For a long time CD4 T cells have been in the shadow casted by the CD8 T cell's capacity to kill tumor cells. Yet CD4 T cells greatly contribute to CD8 T cell responses, in fact more and more studies have investigate the contribution of both CD4 and CD8 T cell responses in tumor immunity (314). Within these studies, one showed the importance of CD4 T presence when the number of CD8 T cells was suboptimal for tumor rejection (315). Tumor-specific CD8 T cells also needed tumor-specific CD4 T cells help to maintain their functionality and to avoid exhaustion (316). The role of CD4 T cells within anti-tumor immunity is now well accepted in the field. The group of Steven Rosenberg performed a safety and efficacy trial on several cancer patients by injecting CD4 T cells retrovirally transduced with a MAGE-A3 specific TCR resulting in several cases of complete or partial responses. This further sediment the potential of using CD4 T in anti-tumor therapies. Yet when using CD4 T one has to be cautious as for their functional plasticity.

L.1 Perspectives in T cell immunomonitoring

The first project covered in this thesis aimed to answer the need of developing better tools for the immunomonitoring of antigen-specific CD4 T cells. Despite the knowledge that pMHC class II multimers could be used to detect CD4 T cells, their implementation has been difficult due to many hurdles in the pMHC class II generation which have been encountered throughout the years (121). This has left the field of CD4 T cells specific detection lagging behind the CD8 T cells field with the nowadays common usage of pMHC class I. In fact some optimization attempts have been made in the CD8 T cells field over the years (265,266), but surprisingly they have not often been implemented in prominent groups using pMHC class I multimers (317–320). We here decided to optimize pMHC class II multimer staining, since standard multimer staining is known to miss a large proportion of cells with low affinity TCRs (109). We decided to use a combination of optimizing molecules such as LacNAc, Dasatinib, neuraminidase and a secondary antibody directed towards the multimer label to improve pMHC class II staining of tumor-specific CD4 T cells. We achieved an improved detection of tumor-specific CD4 T cells with the combination of the previously cited molecules, without increase of background. By using a combination of fluorochromes, multiple specificities can be investigated within one sample. Finally we observed an increase in cell death upon optimized cell staining which was primarily caused by the use of neuraminidase, a known toxic agent (277). We demonstrated for the first time that TCR-pMHC class II improved binding resulted in AICD which was known for CD8 T cells, but not for CD4 T cells (276). Even though we achieved improvement in tumor-specific CD4 T cells staining and detection, several questions remain unanswered such as the TCR affinity (Koff) value of the detected CD4 T cells, as compared to the ones detected with the standard staining procedure. To address this we are developing 2 methods: one relies on the usage of reversible multimers caller NTAmers (321) and the other on a novel methodology of surface plasmon resonance (SPR) performed on whole cell (322). We have encountered difficulties with the usage of NTAmers, but we have obtained initial encouraging results with the use of the

whole cell SPR method in collaboration with the group of Hatice Altug at the EPFL. This novel method consists of using a multiparametric Surface Plasmon Resonance biosensor (MP-SPR). The chip used has been functionalized with a planar lipid bilayer linked to biotin. Streptavidin followed by a biotinylated monomers pMHC class II were run on the chip. This process created a scaffold to which the tumor-specific T cells can bind to and build a TCR-MHC class II synapse (322). The interaction can be measured using the same principal of conventional SPR. In preliminary experiments we could confirm that the optimization procedure improves the detection of low affinity cells which are more likely involved in tumor immunity (323). This method places itself among the rare methods existing up to date to measure the low TCR-pMHC class II affinity with a whole cell (the other one being 2D binding and the not yet functional pMHC class II NTAmers). The capacity to measure CD4 T affinity opens a myriad of possibilities including the possible comparison of the affinity of TCR affinity for viral-, bacterial-, TAA-, and neoantigens. This method could also be used as an immunomonitoring tool for the detection and selection of tumor-specific CD4 T cells after vaccination trials. It could give novel information on the optimal affinity of the clonotypes generated post vaccination trials and thus allow for the harvesting of this cells for clonal expansion and ACT. TCRs with optimal affinity could also be sequenced for the generation genetically modified CD4 T cells expressing the desired TCR. This novel method in combination with the optimization staining procedure can greatly improve our current understanding of CD4 T cells.

Beside TCR affinity studies, the set of cytokines that a CD4 T cell secrete dictates its pro- or anti- tumor response. It is thus important to evaluate the cytokines that are secreted by CD4 T cells that are tumor specific to select the ones with anti-tumor function and discard the ones that would be pro-tumoral. Up to date several techniques exist to study secreted proteins, including i) enzyme-linked immunosorbent assay (ELISA) which evaluates the cytokine concentrations present in cell-free supernatants from culture experiments. The volume needed for this type of assay is usually more than 50 µl thus limiting its sensitivity ii) enzyme-linked immunosorbent spot (ELISpot) where cell-derived cytokines are directly captured on an antibody pre-coated plate and then revealed similarly to ELISA assay (324). Luminex technology works on cell-free supernatants and rely on a mixture of color-coded beads, pre-coated with analyte-specific capture antibodies and a sandwich detection antibody system. The Polystyrene beads are read on a dual-laser flow-based detection instrument (325). And MSD technology which can evaluated up to 10 cytokines in culture supernatants. This technology relies on capture and detection antibodies and an electrochemiluminescence revelation technique (326), iii) cytokine production within cells can be visualized through Intracellular Cytokine Staining (327), providing single-cell resolution of secreted proteins, but implying cell loss due to fixation and permeabilization. Arrays of subnanoliter wells (nanowells) are poorly used but provide a useful system to isolate single cells, analyze their secreted proteins and recover the cell of interest. They offer the advantage to control mechanical and environmental cues compared to traditional assay. Two general approaches have emerged: one that uses open arrays and local capture of secreted proteins as antibodies are usually fixed at the bottom of the wells (328), and a second (called microengraving) that relies on closed with a glass slide

supporting immobilized antibodies arrays to capture secreted proteins, which is subsequently removed from the array (329). As for the future, new platforms are relying on label-free, real-time biosensors such as nanoplasmonic biosensors featuring nanoscale structures as they provide high sensitivity and robustness without the need of complex instrumentation as it was necessary with surface plasmon resonance biosensors (330). In collaboration with the research group at the EPFL led by Prof. H. Altug, we are developing a nanoplasmonic biosensor platform integrated with a microfluidic live cell culture for the real-time monitoring of cellular secretion at the single cell level, without the usage of cellular labels (**Figure 17A and B**). Nanoplasmonic biosensors consisting of gold nanohole arrays (NHAs) (**Figure 17C and D**) support the extraordinary optical transmission (EOT) which allows the NHAs to be highly sensitive to minute local refractive index changes such as when a cytokine binds to its probe (**Figure 17E**). To sense such variations the system relies on a high-resolution spectroscopic imaging of multiple sensor arrays simultaneously by utilizing normal broadband illumination and simple bright field transmission optics (330). The current prototype system consists in a nanoplasmonic biosensor incorporating miniaturized microfluidics chambers on a NHA. The chambers are composed of a cell region unit that captures individual cells, surrounded by a plasmonic unit coated with specific anti-cytokine antibodies. The proof-of concept of the system has been performed using the EL4 lymphoma line secreting IL-2 upon activation (331). We plan to perform In vitro assay with tumor-specific CD4 T clones followed by the analysis of cytokines secreted by *ex vivo* isolated tumor-specific CD4 T cells from patient samples, using the optimized multimer staining procedure. Since cells are maintained alive in the chambers of this system they could be recuperated and either put into culture or their TCR could be sequenced to generated libraries of functional TCR, which could be used to genetically engineer patient cells for ACT. This approach would bring further depth in the capacity to monitor CD4 T cells in cell-based cancer therapies.

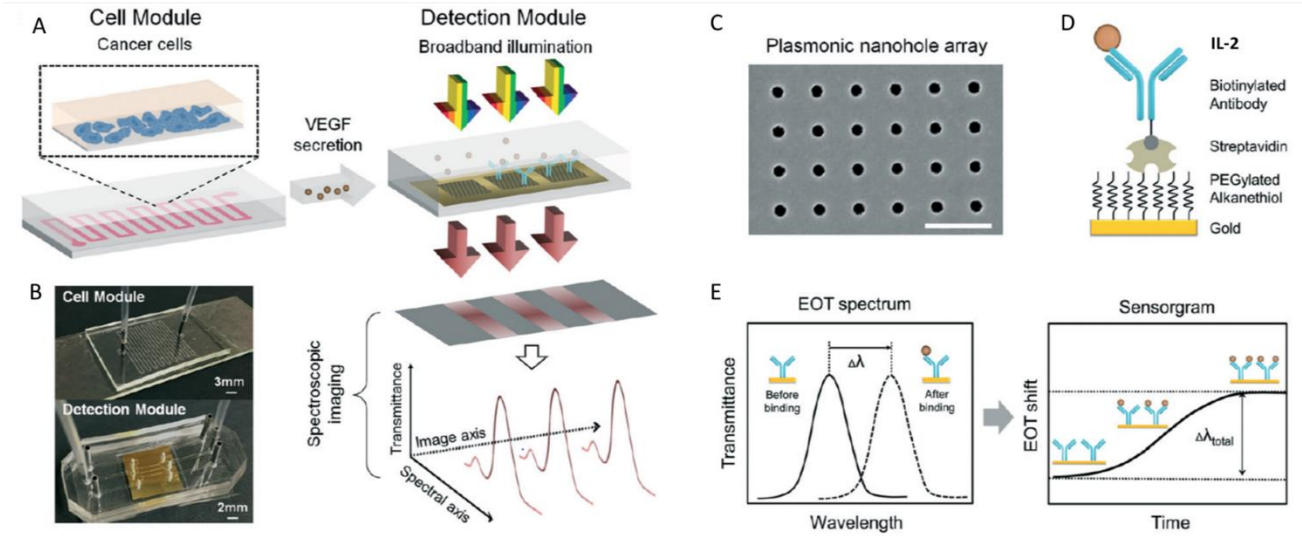

Figure 17: Microfluidic-integrated biosensor design, principal and experimental configuration. A) Representation of the components for the biosensor system consisting of a microfluidic cell module and an optical detection module. CD4 T cell are

immobilized in a zigzag single-channel PDMS unit. Detection modules are directly adjacent to the cells as to capture the secreted cytokines. The module is functionalized with specific anti-cytokine antibodies. A beam of collimated broadband light illuminates the microarrays at normal incidence. The transmitted light is coupled to a spectrometer and dispersed along one dimension to form a spectroscopic image on a CCD camera. This readout system records simultaneously the EOT spectra of all sensors. **B)** Pictures of the cell culture module and the detection module. **C)** SEM image of the nanohole structures with a hole diameter of 200 nm and a periodicity of 600 nm. **D)** This scheme represents the immobilized antibody for the specific detection of IL-2. The biotinylated antibody is bound to a streptavidin in its turn bound the PEGylated alkanethiol molecules sitting on the gold surface. **E)** Sensing principle of the real-time plasmonic detection where the sensorgram (EOT shift vs. time) reveals the real-time binding dynamics of cytokines to antibodies. Adapted from (330).

L.2 Perspectives in epitope prediction and new MHC class II allele targeting

The capacity to predict new target antigens in cancer immunotherapy has always been a challenge since antigens which are exclusively expressed by cancer cells are limited. The identification of novel and appropriate targets which could be used in cancer vaccination therapies is invaluable as there is a need to overcome the peripheral immune tolerance (332). In the second project we thus collaborated with the group of David Gfeller in the development of a new peptide prediction algorithm for MHC class II molecules, MixMHC2pred (MoDec). We are currently using this publicly available tool to identify epitopes derived from tumor-associated antigens and neo-antigens, to be presented by different MHC class II molecules. In particular, we have been focusing on a conserved MHC class II molecules, the HLA-DR52b allele. This HLA allele is of interest for immunotherapy as it less polymorphic than DRB1 alleles, and it is expressed by half of the Caucasian population. The NY-ESO-$1_{119\text{-}143}$ peptide was previously described to bind to the DR52b MHC class II complex and specific responses were observed after vaccination in a significant proportion of patients (333). Using MoDec we have identified several TAA but also shared neo-antigens that contain epitopes predicted to be good binders to this allele. If their immunogenicity is confirmed, they could represent interesting targets for either vaccination in large cohorts of patients or for the generation of TCR banks for ACT.

Further, by combining the use of optimized combinatorial multimer staining and new epitope targeting attempts should be made to identify optimal conditions of tumor-specific CD4 T cell priming, as reported in the CD8 T cell field (334).

L.3 Perspectives for the modulation of CD4 T cell differentiation by miR targeting

In addition to the immunomonitoring approaches described above it would be beneficial in CD4 T cell-based therapies to also select the optimal differentiation stage of the tumor-specific effector CD4 T cells of interest. In fact, T cells become functionally exhausted when being infused in patients (335). Transfer of T_{SCM} and T_{CM} cells would remedy this shortcoming as they offer the capacity to self-renew and are long lived cells. We thus started investigating the possibility to modulate CD4 T cells differentiation into T_{SCM} or T_{CM} cells by acting on the miRNA expression. Unfortunately there is not one single miRNA which modulate such process and often a combination of finely tuned expression of many miRNA gives rise to a particular phenotype as multiple

miRNA can target the same mRNA (336). We thus relied on two sets of data: a miRNA array and a mRNA sequencing of T_N, T_{SCM} and T_{CM} cells from healthy donors. From these data sets we identified miRNA differentially expressed between the various populations and a set of differentially expressed mRNA , that are predicted or validated targets of the miRNA identified. Future experiments will attempt to modulate miRNA expression via the use of miRNA mimics or inhibitors and evaluate their impact on CD4 T cell differentiation. The target mRNA expression will also be measured to identify the mechanistic pathway affected by the miRNA modulation. In parallel, it would also be interesting to monitor the expression of the identified miRNA in a disease context. To that aim, tumor-specific CD4 T cells from melanoma patient samples before and after PD-1 treatment (Pembrolizumab) were sorted to collect the T_N, T_{SCM}, T_{CM} and T_{EM} cells and conserved. Quantification of the candidate miR expression will be performed and compared to the one in T cells of HDs.

Further, the influence of CD4 T helper cell polarization on the level of miR expression in memory and effector subsets should also be considered. In that regard, in an initial evaluation on 4 healthy donors we observed that the frequencies of Th1, Th2, Th17, Th* and Tfh varied among T_N, T_{SCM}, T_{CM} or T_{EM} cell subsets. For example, Th1, Th2, Th17 and Th* frequencies increase in T_{CM} compared to T_{SCM} and a statistically increase in frequency was observed in T_{EM} cells. Tfh cells are mostly found in T_{SCM} and in T_{CM} differentiated cells **(Figure 18)**. These changes in frequency could contribute to the miR phenotype that we have observed and needs further evaluation by directly sorting Thelper subsets based on chemokine receptor expression. Cell sorting would rely on markers for cell differentiation such as CD45RA, CCR7, CD58 and CD95 to discriminate between T_N, T_{SCM}, T_{CM} or T_{EM}. Furthermore, the cell surface markers CXCR3, CRTH2, CCR4, CCR6, CXCR5 would be used to discriminate between a few of the possible polarization of CD4 T cells such as Th1, Th2, Th17, Tfh and Th*.

The road to using miRNA in therapeutic approaches is still long but there are examples of phase 1 or 2 clinical trials with positive results (310,337). The use of Mirvavirsen (miR-122 inhibitor) was shown to reduce levels of hepatitis C virus RNA in patients (338). The TagomiR (miR-16 mimic) was used to target mesothelioma cells of patients with malignant pleural mesothelioma with good safety profile and encouraging signs of activity (339). These results prove the potential of miRNA as a therapeutic agents within the field of cancer and beyond.

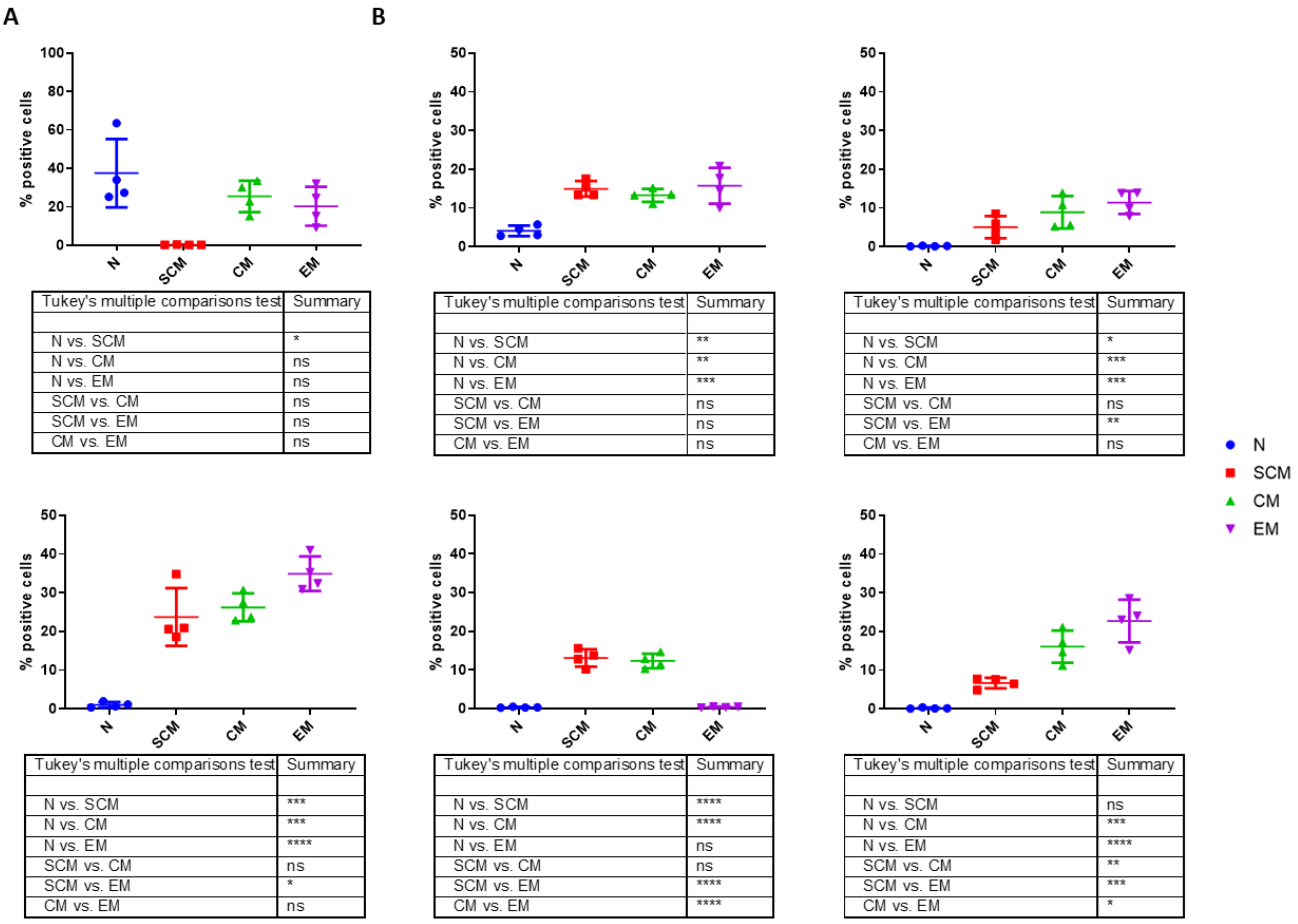

Figure 18: frequency of key Th subsets in differentiated CD4 T cell subsets. From left to right on top is represented **A)** the frequency of differentiated cells within peripheral PBMCs. **B)** Following the first graphic the frequency of Th1 or Th2 among the differentiated cells. On the bottom line similarly represented the Th17, Tfh and Th* frequencies within the four differentiated CD4 T cells subsets.

M References

1. Delves PJ, Roitt IM. The Immune System. New England Journal of Medicine. 2000 Jul 6;343(1):37–49.

2. Gürtler C, Bowie AG. Innate immune detection of microbial nucleic acids. Trends Microbiol. 2013 Aug;21(8):413–20.

3. Mogensen TH. Pathogen Recognition and Inflammatory Signaling in Innate Immune Defenses. Clin Microbiol Rev. 2009 Apr;22(2):240–73.

4. Hoving JC, Wilson GJ, Brown GD. Signalling C-Type lectin receptors, microbial recognition and immunity. Cell Microbiol. 2014 Feb;16(2):185–94.

5. Nakaya Y, Lilue J, Stavrou S, Moran EA, Ross SR. AIM2-Like Receptors Positively and Negatively Regulate the Interferon Response Induced by Cytosolic DNA. mBio [Internet]. 2017 Jul 5 [cited 2019 Oct 10];8(4). Available from: https://www.ncbi.nlm.nih.gov/pmc/articles/PMC5573678/

6. Akira S, Takeda K. Toll-like receptor signalling. Nat Rev Immunol. 2004 Jul;4(7):499–511.

7. O'Neill LAJ, Bowie AG. The family of five: TIR-domain-containing adaptors in Toll-like receptor signalling. Nat Rev Immunol. 2007 May;7(5):353–64.

8. Akira S, Uematsu S, Takeuchi O. Pathogen recognition and innate immunity. Cell. 2006 Feb 24;124(4):783–801.

9. Kawai T, Akira S. Signaling to NF-kappaB by Toll-like receptors. Trends Mol Med. 2007 Nov;13(11):460–9.

10. Iwasaki A, Medzhitov R. Toll-like receptor control of the adaptive immune responses. Nat Immunol. 2004 Oct;5(10):987–95.

11. Zhao E, Xu H, Wang L, Kryczek I, Wu K, Hu Y, et al. Bone marrow and the control of immunity. Cell Mol Immunol. 2012 Jan;9(1):11–9.

12. Geering B, Stoeckle C, Conus S, Simon H-U. Living and dying for inflammation: neutrophils, eosinophils, basophils. Trends Immunol. 2013 Aug;34(8):398–409.

13. Uriarte SM, Powell DW, Luerman GC, Merchant ML, Cummins TD, Jog NR, et al. Comparison of proteins expressed on secretory vesicle membranes and plasma membranes of human neutrophils. J Immunol. 2008 Apr 15;180(8):5575–81.

14. Dibbert B, Weber M, Nikolaizik WH, Vogt P, Schöni MH, Blaser K, et al. Cytokine-mediated Bax deficiency and consequent delayed neutrophil apoptosis: A general mechanism to accumulate effector cells in inflammation. Proc Natl Acad Sci U S A. 1999 Nov 9;96(23):13330–5.

15. Krystel-Whittemore M, Dileepan KN, Wood JG. Mast Cell: A Multi-Functional Master Cell. Front Immunol [Internet]. 2016 Jan 6 [cited 2019 Oct 16];6. Available from: https://www.ncbi.nlm.nih.gov/pmc/articles/PMC4701915/

16. Caligiuri MA. Human natural killer cells. Blood. 2008 Aug 1;112(3):461–9.

17. Vivier E, Artis D, Colonna M, Diefenbach A, Santo JPD, Eberl G, et al. Innate Lymphoid Cells: 10 Years On. Cell. 2018 Aug 23;174(5):1054–66.

18. Varol C, Mildner A, Jung S. Macrophages: Development and Tissue Specialization. Annual Review of Immunology. 2015;33(1):643–75.

19. Atri C, Guerfali FZ, Laouini D. Role of Human Macrophage Polarization in Inflammation during Infectious Diseases. Int J Mol Sci [Internet]. 2018 Jun 19 [cited 2019 Oct 16];19(6). Available from: https://www.ncbi.nlm.nih.gov/pmc/articles/PMC6032107/

20. Patente TA, Pinho MP, Oliveira AA, Evangelista GCM, Bergami-Santos PC, Barbuto JAM. Human Dendritic Cells: Their Heterogeneity and Clinical Application Potential in Cancer Immunotherapy. Front Immunol [Internet]. 2019 [cited 2019 Oct 16];9. Available from: https://www.frontiersin.org/articles/10.3389/fimmu.2018.03176/full

21. O'Keeffe M, Mok WH, Radford KJ. Human dendritic cell subsets and function in health and disease. Cell Mol Life Sci. 2015 Nov;72(22):4309–25.

22. Haniffa M, Shin A, Bigley V, McGovern N, Teo P, See P, et al. Human tissues contain CD141hi cross-presenting dendritic cells with functional homology to mouse CD103+ nonlymphoid dendritic cells. Immunity. 2012 Jul 27;37(1):60–73.

23. Reizis B, Bunin A, Ghosh HS, Lewis KL, Sisirak V. Plasmacytoid dendritic cells: recent progress and open questions. Annu Rev Immunol. 2011;29:163–83.

24. Oliveira C, Silveira I, Veiga F, Ribeiro AJ. Recent advances in characterization of nonviral vectors for delivery of nucleic acids: impact on their biological performance. Expert Opinion on Drug Delivery. 2015 Jan 2;12(1):27–39.

25. Mortensen SA, Sander B, Jensen RK, Pedersen JS, Golas MM, Jensenius JC, et al. Structure and activation of C1, the complex initiating the classical pathway of the complement cascade. Proc Natl Acad Sci USA. 2017 31;114(5):986–91.

26. Charles A Janeway J, Travers P, Walport M, Shlomchik MJ. The complement system and innate immunity. Immunobiology: The Immune System in Health and Disease 5th edition [Internet]. 2001 [cited 2019 Oct 10]; Available from: https://www.ncbi.nlm.nih.gov/books/NBK27100/

27. Godfrey DI, MacDonald HR, Kronenberg M, Smyth MJ, Kaer LV. NKT cells: what's in a name? Nature Reviews Immunology. 2004 Mar;4(3):231–7.

28. Lepore M, Mori L, De Libero G. The Conventional Nature of Non-MHC-Restricted T Cells. Front Immunol [Internet]. 2018 Jun 14 [cited 2020 Jan 13];9. Available from: https://www.ncbi.nlm.nih.gov/pmc/articles/PMC6010553/

29. Kalyan S, Kabelitz D. Defining the nature of human γδ T cells: a biographical sketch of the highly empathetic. Cellular & Molecular Immunology. 2013 Jan;10(1):21–9.

30. Godfrey DI, Koay H-F, McCluskey J, Gherardin NA. The biology and functional importance of MAIT cells. Nature Immunology. 2019 Sep;20(9):1110–28.

31. Bonilla FA, Oettgen HC. Adaptive immunity. J Allergy Clin Immunol. 2010 Feb;125(2 Suppl 2):S33-40.

32. Elhanati Y, Sethna Z, Marcou Q, Callan CG, Mora T, Walczak AM. Inferring processes underlying B-cell repertoire diversity. Philos Trans R Soc Lond B Biol Sci [Internet]. 2015 Sep 5 [cited 2019 Oct 16];370(1676). Available from: https://www.ncbi.nlm.nih.gov/pmc/articles/PMC4528420/

33. Laydon DJ, Bangham CRM, Asquith B. Estimating T-cell repertoire diversity: limitations of classical estimators and a new approach. Philos Trans R Soc Lond B Biol Sci [Internet]. 2015 Aug 19 [cited 2019 Oct 16];370(1675). Available from: https://www.ncbi.nlm.nih.gov/pmc/articles/PMC4528489/

34. Hoffman W, Lakkis FG, Chalasani G. B Cells, Antibodies, and More. Clin J Am Soc Nephrol. 2016 Jan 7;11(1):137–54.

35. Hua Z, Hou B. TLR signaling in B-cell development and activation. Cellular & Molecular Immunology. 2013 Mar;10(2):103–6.

36. Hong S, Zhang Z, Liu H, Tian M, Zhu X, Zhang Z, et al. B Cells Are the Dominant Antigen-Presenting Cells that Activate Naive CD4+ T Cells upon Immunization with a Virus-Derived Nanoparticle Antigen. Immunity. 2018 16;49(4):695-708.e4.

37. Menard LC, Minns LA, Darche S, Mielcarz DW, Foureau DM, Roos D, et al. B cells amplify IFN-gamma production by T cells via a TNF-alpha-mediated mechanism. J Immunol. 2007 Oct 1;179(7):4857–66.

38. Mizoguchi A, Bhan AK. A case for regulatory B cells. J Immunol. 2006 Jan 15;176(2):705–10.

39. Hernandez JB, Newton RH, Walsh CM. Life and death in the thymus--cell death signaling during T cell development. Curr Opin Cell Biol. 2010 Dec;22(6):865–71.

40. Wu LC, Tuot DS, Lyons DS, Garcia KC, Davis MM. Two-step binding mechanism for T-cell receptor recognition of peptide MHC. Nature. 2002 Aug;418(6897):552–6.

41. Yokosuka T, Takase K, Suzuki M, Nakagawa Y, Taki S, Takahashi H, et al. Predominant Role of T Cell Receptor (TCR)-α Chain in Forming Preimmune TCR Repertoire Revealed by Clonal TCR Reconstitution System. Journal of Experimental Medicine. 2002 Apr 15;195(8):991–1001.

42. Schatz DG, Swanson PC. V(D)J Recombination: Mechanisms of Initiation. Annual Review of Genetics. 2011;45(1):167–202.

43. König R. Interactions between MHC molecules and co-receptors of the TCR. Curr Opin Immunol. 2002 Feb;14(1):75–83.

44. Condotta SA, Richer MJ. The immune battlefield: The impact of inflammatory cytokines on CD8+ T-cell immunity. PLOS Pathogens. 2017 Oct 26;13(10):e1006618.

45. Phares TW, Stohlman SA, Hwang M, Min B, Hinton DR, Bergmann CC. CD4 T Cells Promote CD8 T Cell Immunity at the Priming and Effector Site during Viral Encephalitis. Journal of Virology. 2012 Mar 1;86(5):2416–27.

46. Perera J, Zheng Z, Li S, Gudjonson H, Kalinina O, Benichou JIC, et al. Self-antigen-driven thymic B cell class switching promotes T cell central tolerance. Cell Rep. 2016 Oct 4;17(2):387–98.

47. Yu X, Zhang H, Yu L, Liu M, Zuo Z, Han Q, et al. Intestinal Lamina Propria CD4+ T Cells Promote Bactericidal Activity of Macrophages via Galectin-9 and Tim-3 Interaction during Salmonella enterica Serovar Typhimurium Infection. Infection and Immunity. 2018 Aug 1;86(8):e00769.

48. Takeuchi A, Saito T. CD4 CTL, a Cytotoxic Subset of CD4+ T Cells, Their Differentiation and Function. Front Immunol [Internet]. 2017 Feb 23 [cited 2019 Dec 5];8. Available from: https://www.ncbi.nlm.nih.gov/pmc/articles/PMC5321676/

49. Juno JA, van Bockel D, Kent SJ, Kelleher AD, Zaunders JJ, Munier CML. Cytotoxic CD4 T Cells—Friend or Foe during Viral Infection? Front Immunol [Internet]. 2017 [cited 2019 Dec 5];8. Available from: https://www.frontiersin.org/articles/10.3389/fimmu.2017.00019/full

50. Vignali DAA, Collison LW, Workman CJ. How regulatory T cells work. Nat Rev Immunol. 2008 Jul;8(7):523–32.

51. Claman HN, Chaperon EA, Triplett RF. Thymus-marrow cell combinations. Synergism in antibody production. Proc Soc Exp Biol Med. 1966 Sep;122(4):1167–71.

52. Katz DH, Benacerraf B. The regulatory influence of activated T cells on B cell responses to antigen. Adv Immunol. 1972;15:1–94.

53. Tanchot C, Rocha B. CD8 and B cell memory: same strategy, same signals. Nature Immunology. 2003 May;4(5):431–2.

54. Starr TK, Jameson SC, Hogquist KA. Positive and negative selection of T cells. Annu Rev Immunol. 2003;21:139–76.

55. Gounari F, Aifantis I, Khazaie K, Hoeflinger S, Harada N, Taketo MM, et al. Somatic activation of beta-catenin bypasses pre-TCR signaling and TCR selection in thymocyte development. Nat Immunol. 2001 Sep;2(9):863–9.

56. Ioannidis V, Beermann F, Clevers H, Held W. The beta-catenin--TCF-1 pathway ensures CD4(+)CD8(+) thymocyte survival. Nat Immunol. 2001 Aug;2(8):691–7.

57. Sun Z, Unutmaz D, Zou YR, Sunshine MJ, Pierani A, Brenner-Morton S, et al. Requirement for RORgamma in thymocyte survival and lymphoid organ development. Science. 2000 Jun 30;288(5475):2369–73.

58. Saito T, Watanabe N. Positive and negative thymocyte selection. Crit Rev Immunol. 1998;18(4):359–70.

59. Wang L, Bosselut R. CD4-CD8 lineage differentiation: Thpok-ing into the nucleus. J Immunol. 2009 Sep 1;183(5):2903–10.

60. Gascoigne NRJ, Palmer E. Signaling in thymic selection. Curr Opin Immunol. 2011 Apr;23(2):207–12.

61. Snow AL, Pandiyan P, Zheng L, Krummey SM, Lenardo MJ. The Power and the Promise of Restimulation-Induced Cell Death in Human Immune Diseases. Immunol Rev. 2010 Jul;236:68–82.

62. Germain RN. T-cell development and the CD4–CD8 lineage decision. Nat Rev Immunol. 2002 May;2(5):309–22.

63. Charles A Janeway J, Travers P, Walport M, Shlomchik MJ. The major histocompatibility complex and its functions. Immunobiology: The Immune System in Health and Disease 5th edition [Internet]. 2001 [cited 2019 Oct 22]; Available from: https://www.ncbi.nlm.nih.gov/books/NBK27156/

64. Gruen JR, Weissman SM. Human MHC class III and IV genes and disease associations. Front Biosci. 2001 Aug 1;6:D960-972.

65. Wieczorek M, Abualrous ET, Sticht J, Álvaro-Benito M, Stolzenberg S, Noé F, et al. Major Histocompatibility Complex (MHC) Class I and MHC Class II Proteins: Conformational Plasticity in

Antigen Presentation. Front Immunol [Internet]. 2017 Mar 17 [cited 2019 Dec 5];8. Available from: https://www.ncbi.nlm.nih.gov/pmc/articles/PMC5355494/

66. Wright CA, Kozik P, Zacharias M, Springer S. Tapasin and other chaperones: models of the MHC class I loading complex. Biol Chem. 2004 Sep;385(9):763–78.

67. Pos W, Sethi DK, Call MJ, Schulze M-SED, Anders A-K, Pyrdol J, et al. Crystal structure of the HLA-DM-HLA-DR1 complex defines mechanisms for rapid peptide selection. Cell. 2012 Dec 21;151(7):1557–68.

68. Guce AI, Mortimer SE, Yoon T, Painter CA, Jiang W, Mellins ED, et al. HLA-DO acts as a substrate mimic to inhibit HLA-DM by a competitive mechanism. Nat Struct Mol Biol. 2013 Jan;20(1):90–8.

69. Bankovich AJ, Girvin AT, Moesta AK, Garcia KC. Peptide register shifting within the MHC groove: theory becomes reality. Molecular Immunology. 2004 Feb 1;40(14):1033–9.

70. McFarland BJ, Sant AJ, Lybrand TP, Beeson C. Ovalbumin(323-339) peptide binds to the major histocompatibility complex class II I-A(d) protein using two functionally distinct registers. Biochemistry. 1999 Dec 14;38(50):16663–70.

71. Roth DB. V(D)J Recombination: Mechanism, Errors, and Fidelity. Microbiol Spectr [Internet]. 2014 Dec [cited 2019 Oct 22];2(6). Available from: https://www.ncbi.nlm.nih.gov/pmc/articles/PMC5089068/

72. Bassing CH, Swat W, Alt FW. The Mechanism and Regulation of Chromosomal V(D)J Recombination. Cell. 2002 Apr 19;109(2, Supplement 1):S45–55.

73. Lythe G, Callard RE, Hoare RL, Molina-París C. How many TCR clonotypes does a body maintain? Journal of Theoretical Biology. 2016 Jan 21;389:214–24.

74. De Simone M, Rossetti G, Pagani M. Single Cell T Cell Receptor Sequencing: Techniques and Future Challenges. Front Immunol [Internet]. 2018 [cited 2019 Nov 6];9. Available from: https://www.frontiersin.org/articles/10.3389/fimmu.2018.01638/full

75. Bäckström BT, Milia E, Peter A, Jaureguiberry B, Baldari CT, Palmer E. A Motif within the T Cell Receptor α Chain Constant Region Connecting Peptide Domain Controls Antigen Responsiveness. Immunity. 1996 Nov 1;5(5):437–47.

76. Dong D, Zheng L, Lin J, Zhang B, Zhu Y, Li N, et al. Structural basis of assembly of the human T cell receptor–CD3 complex. Nature. 2019 Sep;573(7775):546–52.

77. Wucherpfennig KW, Gagnon E, Call MJ, Huseby ES, Call ME. Structural Biology of the T-cell Receptor: Insights into Receptor Assembly, Ligand Recognition, and Initiation of Signaling. Cold Spring Harb Perspect Biol [Internet]. 2010 Apr [cited 2019 Oct 22];2(4). Available from: https://www.ncbi.nlm.nih.gov/pmc/articles/PMC2845206/

78. Call ME, Wucherpfennig KW. The T cell receptor: critical role of the membrane environment in receptor assembly and function. Annu Rev Immunol. 2005;23:101–25.

79. Love PE, Hayes SM. ITAM-mediated Signaling by the T-Cell Antigen Receptor. Cold Spring Harb Perspect Biol. 2010 Jan 6;2(6):a002485.

80. Courtney AH, Lo W-L, Weiss A. TCR Signaling: Mechanisms of Initiation and Propagation. Trends in Biochemical Sciences. 2018 Feb 1;43(2):108–23.

81. Balagopalan L, Coussens NP, Sherman E, Samelson LE, Sommers CL. The LAT story: a tale of cooperativity, coordination, and choreography. Cold Spring Harb Perspect Biol. 2010 Aug;2(8):a005512.

82. Wange RL. LAT, the linker for activation of T cells: a bridge between T cell-specific and general signaling pathways. Sci STKE. 2000 Dec 19;2000(63):re1.

83. Zhang W, Trible RP, Zhu M, Liu SK, McGlade CJ, Samelson LE. Association of Grb2, Gads, and phospholipase C-gamma 1 with phosphorylated LAT tyrosine residues. Effect of LAT tyrosine mutations on T cell angigen receptor-mediated signaling. J Biol Chem. 2000 Jul 28;275(30):23355–61.

84. Liu SK, Fang N, Koretzky GA, McGlade CJ. The hematopoietic-specific adaptor protein gads functions in T-cell signaling via interactions with the SLP-76 and LAT adaptors. Curr Biol. 1999 Jan 28;9(2):67–75.

85. Yablonski D, Kuhne MR, Kadlecek T, Weiss A. Uncoupling of nonreceptor tyrosine kinases from PLC-gamma1 in an SLP-76-deficient T cell. Science. 1998 Jul 17;281(5375):413–6.

86. Das J, Ho M, Zikherman J, Govern C, Yang M, Weiss A, et al. Digital signaling and hysteresis characterize ras activation in lymphoid cells. Cell. 2009 Jan 23;136(2):337–51.

87. Janknecht R, Ernst WH, Pingoud V, Nordheim A. Activation of ternary complex factor Elk-1 by MAP kinases. EMBO J. 1993 Dec 15;12(13):5097–104.

88. Andreotti AH, Schwartzberg PL, Joseph RE, Berg LJ. T-cell signaling regulated by the Tec family kinase, Itk. Cold Spring Harb Perspect Biol. 2010 Jul;2(7):a002287.

89. Melowic HR, Stahelin RV, Blatner NR, Tian W, Hayashi K, Altman A, et al. Mechanism of diacylglycerol-induced membrane targeting and activation of protein kinase Ctheta. J Biol Chem. 2007 Jul 20;282(29):21467–76.

90. Matsumoto R, Wang D, Blonska M, Li H, Kobayashi M, Pappu B, et al. Phosphorylation of CARMA1 plays a critical role in T Cell receptor-mediated NF-kappaB activation. Immunity. 2005 Dec;23(6):575–85.

91. Narayan P, Holt B, Tosti R, Kane LP. CARMA1 is required for Akt-mediated NF-kappaB activation in T cells. Mol Cell Biol. 2006 Mar;26(6):2327–36.

92. Sun L, Deng L, Ea C-K, Xia Z-P, Chen ZJ. The TRAF6 ubiquitin ligase and TAK1 kinase mediate IKK activation by BCL10 and MALT1 in T lymphocytes. Mol Cell. 2004 May 7;14(3):289–301.

93. Zhou H, Wertz I, O'Rourke K, Ultsch M, Seshagiri S, Eby M, et al. Bcl10 activates the NF-kappaB pathway through ubiquitination of NEMO. Nature. 2004 Jan 8;427(6970):167–71.

94. Hoffmann A, Natoli G, Ghosh G. Transcriptional regulation via the NF-kappaB signaling module. Oncogene. 2006 Oct 30;25(51):6706–16.

95. Hayden MS, West AP, Ghosh S. NF-kappaB and the immune response. Oncogene. 2006 Oct 30;25(51):6758–80.

96. Gorentla BK, Wan C-K, Zhong X-P. Negative regulation of mTOR activation by diacylglycerol kinases. Blood. 2011 Apr 14;117(15):4022–31.

97. Delgoffe GM, Powell JD. mTOR: taking cues from the immune microenvironment. Immunology. 2009 Aug;127(4):459–65.

98. Štefanová I, Hemmer B, Vergelli M, Martin R, Biddison WE, Germain RN. TCR ligand discrimination is enforced by competing ERK positive and SHP-1 negative feedback pathways. Nat Immunol. 2003 Mar;4(3):248–54.

99. Teft WA, Kirchhof MG, Madrenas J. A molecular perspective of CTLA-4 function. Annu Rev Immunol. 2006;24:65–97.

100. Chemnitz JM, Parry RV, Nichols KE, June CH, Riley JL. SHP-1 and SHP-2 associate with immunoreceptor tyrosine-based switch motif of programmed death 1 upon primary human T cell stimulation, but only receptor ligation prevents T cell activation. J Immunol. 2004 Jul 15;173(2):945–54.

101. Gaud G, Lesourne R, Love PE. Regulatory mechanisms in T cell receptor signalling. Nat Rev Immunol. 2018 Aug;18(8):485–97.

102. Dustin ML. Signaling at neuro/immune synapses. J Clin Invest. 2012 Apr;122(4):1149–55.

103. Arden B, Clark SP, Kabelitz D, Mak TW. Human T-cell receptor variable gene segment families. Immunogenetics. 1995;42(6):455–500.

104. Rowen L, Koop BF, Hood L. The complete 685-kilobase DNA sequence of the human beta T cell receptor locus. Science. 1996 Jun 21;272(5269):1755–62.

105. Garcia KC, Degano M, Stanfield RL, Brunmark A, Jackson MR, Peterson PA, et al. An alphabeta T cell receptor structure at 2.5 A and its orientation in the TCR-MHC complex. Science. 1996 Oct 11;274(5285):209–19.

106. Hennecke J, Wiley DC. T Cell Receptor–MHC Interactions up Close. Cell. 2001 Jan 12;104(1):1–4.

107. Bjorkman PJ. MHC Restriction in Three Dimensions: A View of T Cell Receptor/Ligand Interactions. Cell. 1997 Apr 18;89(2):167–70.

108. Cole DK, Pumphrey NJ, Boulter JM, Sami M, Bell JI, Gostick E, et al. Human TCR-Binding Affinity is Governed by MHC Class Restriction. J Immunol. 2007 May 1;178(9):5727–34.

109. Martinez RJ, Andargachew R, Martinez HA, Evavold BD. Low-affinity CD4+ T cells are major responders in the primary immune response. Nat Commun. 2016 Dec 15;7(1):1–10.

110. Li Y, Yin Y, Mariuzza RA. Structural and Biophysical Insights into the Role of CD4 and CD8 in T Cell Activation. Frontiers in Immunology [Internet]. 2013 [cited 2019 Oct 23];4. Available from: https://www.ncbi.nlm.nih.gov/pmc/articles/PMC3717711/

111. Stone JD, Chervin AS, Kranz DM. T-cell receptor binding affinities and kinetics: impact on T-cell activity and specificity. Immunology. 2009 Feb;126(2):165–76.

112. Altman JD, Moss PA, Goulder PJ, Barouch DH, McHeyzer-Williams MG, Bell JI, et al. Phenotypic analysis of antigen-specific T lymphocytes. Science. 1996 Oct 4;274(5284):94–6.

113. Brooks SE, Bonney SA, Lee C, Publicover A, Khan G, Smits EL, et al. Application of the pMHC Array to Characterise Tumour Antigen Specific T Cell Populations in Leukaemia Patients at Disease Diagnosis. PLoS ONE. 2015;10(10):e0140483.

114. Soen Y, Chen DS, Kraft DL, Davis MM, Brown PO. Detection and characterization of cellular immune responses using peptide-MHC microarrays. PLoS Biol. 2003 Dec;1(3):E65.

115. Newell EW, Klein LO, Yu W, Davis MM. Simultaneous detection of many T-cell specificities using combinatorial tetramer staining. Nat Methods. 2009 Jul;6(7):497–9.

116. Hadrup SR, Bakker AH, Shu CJ, Andersen RS, van Veluw J, Hombrink P, et al. Parallel detection of antigen-specific T-cell responses by multidimensional encoding of MHC multimers. Nat Methods. 2009 Jul;6(7):520–6.

117. Bentzen AK, Marquard AM, Lyngaa R, Saini SK, Ramskov S, Donia M, et al. Large-scale detection of antigen-specific T cells using peptide-MHC-I multimers labeled with DNA barcodes. Nat Biotechnol. 2016 Oct;34(10):1037–45.

118. Schmidt J, Guillaume P, Irving M, Baumgaertner P, Speiser D, Luescher IF. Reversible major histocompatibility complex I-peptide multimers containing Ni(2+)-nitrilotriacetic acid peptides and histidine tags improve analysis and sorting of CD8(+) T cells. J Biol Chem. 2011 Dec 2;286(48):41723–35.

119. Kwok WW. Challenges in staining T cells using HLA class II tetramers. Clin Immunol. 2003 Jan;106(1):23–8.

120. Kalandadze A, Galleno M, Foncerrada L, Strominger JL, Wucherpfennig KW. Expression of recombinant HLA-DR2 molecules. Replacement of the hydrophobic transmembrane region by a leucine zipper dimerization motif allows the assembly and secretion of soluble DR alpha beta heterodimers. J Biol Chem. 1996 Aug 16;271(33):20156–62.

121. Schmidt J, Dojcinovic D, Guillaume P, Luescher I. Analysis, Isolation, and Activation of Antigen-Specific CD4(+) and CD8(+) T Cells by Soluble MHC-Peptide Complexes. Front Immunol. 2013;4:218.

122. Grotenbreg GM, Nicholson MJ, Fowler KD, Wilbuer K, Octavio L, Yang M, et al. Empty class II major histocompatibility complex created by peptide photolysis establishes the role of DM in peptide association. J Biol Chem. 2007 Jul 20;282(29):21425–36.

123. Fremont DH, Hendrickson WA, Marrack P, Kappler J. Structures of an MHC class II molecule with covalently bound single peptides. Science. 1996 May 17;272(5264):1001–4.

124. Uchtenhagen H, Rims C, Blahnik G, Chow I-T, Kwok WW, Buckner JH, et al. Efficient ex vivo analysis of CD4+ T-cell responses using combinatorial HLA class II tetramer staining. Nat Commun [Internet]. 2016 Aug 30;7. Available from: http://www.ncbi.nlm.nih.gov/pmc/articles/PMC5013714/

125. Batard P, Peterson DA, Devêvre E, Guillaume P, Cerottini J-C, Rimoldi D, et al. Dextramers: new generation of fluorescent MHC class I/peptide multimers for visualization of antigen-specific CD8+ T cells. J Immunol Methods. 2006 Mar 20;310(1–2):136–48.

126. Dustin ML. The immunological synapse. Cancer Immunol Res. 2014 Nov;2(11):1023–33.

127. Chen L, Flies DB. Molecular mechanisms of T cell co-stimulation and co-inhibition. Nat Rev Immunol. 2013 Apr;13(4):227–42.

128. Curtsinger JM, Mescher MF. Inflammatory Cytokines as a Third Signal for T Cell Activation. Curr Opin Immunol. 2010 Jun;22(3):333–40.

129. Mueller SN, Gebhardt T, Carbone FR, Heath WR. Memory T Cell Subsets, Migration Patterns, and Tissue Residence. Annual Review of Immunology. 2013;31(1):137–61.

130. Sallusto F, Lenig D, Förster R, Lipp M, Lanzavecchia A. Two subsets of memory T lymphocytes with distinct homing potentials and effector functions. Nature. 1999 Oct;401(6754):708–12.

131. Wherry EJ, Teichgräber V, Becker TC, Masopust D, Kaech SM, Antia R, et al. Lineage relationship and protective immunity of memory CD8 T cell subsets. Nat Immunol. 2003 Mar;4(3):225–34.

132. Lugli E, Gattinoni L, Roberto A, Mavilio D, Price DA, Restifo NP, et al. Identification, isolation and in vitro expansion of human and nonhuman primate T stem cell memory cells. Nat Protoc. 2013 Jan;8(1):33–42.

133. Gattinoni L, Lugli E, Ji Y, Pos Z, Paulos CM, Quigley MF, et al. A human memory T cell subset with stem cell-like properties. Nat Med. 2011 Sep 18;17(10):1290–7.

134. Mahnke YD, Brodie TM, Sallusto F, Roederer M, Lugli E. The who's who of T-cell differentiation: Human memory T-cell subsets. European Journal of Immunology. 2013;43(11):2797–809.

135. Lugli E, Goldman CK, Perera LP, Smedley J, Pung R, Yovandich JL, et al. Transient and persistent effects of IL-15 on lymphocyte homeostasis in nonhuman primates. Blood. 2010 Oct 28;116(17):3238–48.

136. Wilk MM, Mills KHG. CD4 TRM Cells Following Infection and Immunization: Implications for More Effective Vaccine Design. Frontiers in Immunology [Internet]. 2018 [cited 2019 Oct 28];9. Available from: https://www.ncbi.nlm.nih.gov/pmc/articles/PMC6095996/

137. Jandus C, Usatorre AM, Viganò S, Zhang L, Romero P. The Vast Universe of T Cell Diversity: Subsets of Memory Cells and Their Differentiation. In: Lugli E, editor. T-Cell Differentiation: Methods and Protocols [Internet]. New York, NY: Springer; 2017 [cited 2019 Dec 10]. p. 1–17. (Methods in Molecular Biology). Available from: https://doi.org/10.1007/978-1-4939-6548-9_1

138. O'Shea JJ, Paul WE. Mechanisms Underlying Lineage Commitment and Plasticity of Helper CD4+ T Cells. Science. 2010 Feb 26;327(5969):1098–102.

139. Fu J, Heinrichs J, Yu X-Z. Helper T-Cell Differentiation in Graft-Versus-Host Disease After Allogeneic Hematopoietic Stem Cell Transplantation. Arch Immunol Ther Exp. 2014 Aug 1;62(4):277–301.

140. Végran F, Apetoh L, Ghiringhelli F. Th9 Cells: A Novel CD4 T-cell Subset in the Immune War against Cancer. Cancer Res [Internet]. 2015 Jan 14 [cited 2019 Oct 28]; Available from: https://cancerres.aacrjournals.org/content/early/2015/01/14/0008-5472.can-14-2748

141. Swain SL, McKinstry KK, Strutt TM. Expanding roles for CD4 + T cells in immunity to viruses. Nat Rev Immunol. 2012 Feb;12(2):136–48.

142. Bailey SR, Nelson MH, Himes RA, Li Z, Mehrotra S, Paulos CM. Th17 Cells in Cancer: The Ultimate Identity Crisis. Front Immunol [Internet]. 2014 [cited 2019 Oct 28];5. Available from: https://www.frontiersin.org/articles/10.3389/fimmu.2014.00276/full

143. Rao A, Avni O. Molecular aspects of T-cell differentiation. Br Med Bull. 2000;56(4):969–84.

144. Fiorentino DF, Bond MW, Mosmann TR. Two types of mouse T helper cell. IV. Th2 clones secrete a factor that inhibits cytokine production by Th1 clones. J Exp Med. 1989 Dec 1;170(6):2081–95.

145. O'Shea JJ, Paul WE. Mechanisms underlying lineage commitment and plasticity of helper CD4+ T cells. Science. 2010 Feb 26;327(5969):1098–102.

146. Huber S, Gagliani N, O'Connor W, Jr, Geginat J, Caprioli F. CD4+ T Helper Cell Plasticity in Infection, Inflammation, and Autoimmunity. Mediators of Inflammation [Internet]. 2017 [cited 2019 Oct 29];2017. Available from: https://www.ncbi.nlm.nih.gov/pmc/articles/PMC5303579/

147. Hirahara K, Poholek A, Vahedi G, Laurence A, Kanno Y, Milner JD, et al. Mechanisms Underlying Helper T cell Plasticity: Implications for Immune-mediated Disease. J Allergy Clin Immunol. 2013 May;131(5):1276–87.

148. Hegazy AN, Peine M, Helmstetter C, Panse I, Fröhlich A, Bergthaler A, et al. Interferons Direct Th2 Cell Reprogramming to Generate a Stable GATA-3+T-bet+ Cell Subset with Combined Th2 and Th1 Cell Functions. Immunity. 2010 Jan 29;32(1):116–28.

149. Monticelli S, Ansel KM, Xiao C, Socci ND, Krichevsky AM, Thai T-H, et al. MicroRNA profiling of the murine hematopoietic system. Genome Biology. 2005 Aug 1;6(8):R71.

150. Denli AM, Tops BBJ, Plasterk RHA, Ketting RF, Hannon GJ. Processing of primary microRNAs by the Microprocessor complex. Nature. 2004 Nov;432(7014):231–5.

151. Yi R, Qin Y, Macara IG, Cullen BR. Exportin-5 mediates the nuclear export of pre-microRNAs and short hairpin RNAs. Genes Dev. 2003 Dec 15;17(24):3011–6.

152. Bartel DP. MicroRNAs: Genomics, Biogenesis, Mechanism, and Function. Cell. 2004 Jan 23;116(2):281–97.

153. Meister G, Tuschl T. Mechanisms of gene silencing by double-stranded RNA. Nature. 2004 Sep;431(7006):343–9.

154. Place RF, Li L-C, Pookot D, Noonan EJ, Dahiya R. MicroRNA-373 induces expression of genes with complementary promoter sequences. Proc Natl Acad Sci U S A. 2008 Feb 5;105(5):1608–13.

155. Kim DH, Saetrom P, Snøve O, Rossi JJ. MicroRNA-directed transcriptional gene silencing in mammalian cells. Proc Natl Acad Sci USA. 2008 Oct 21;105(42):16230–5.

156. Tang R, Li L, Zhu D, Hou D, Cao T, Gu H, et al. Mouse miRNA-709 directly regulates miRNA-15a/16-1 biogenesis at the posttranscriptional level in the nucleus: evidence for a microRNA hierarchy system. Cell Res. 2012 Mar;22(3):504–15.

157. Ameyar-Zazoua M, Rachez C, Souidi M, Robin P, Fritsch L, Young R, et al. Argonaute proteins couple chromatin silencing to alternative splicing. Nat Struct Mol Biol. 2012 Oct;19(10):998–1004.

158. Catalanotto C, Cogoni C, Zardo G. MicroRNA in Control of Gene Expression: An Overview of Nuclear Functions. Int J Mol Sci [Internet]. 2016 Oct 13 [cited 2019 Oct 30];17(10). Available from: https://www.ncbi.nlm.nih.gov/pmc/articles/PMC5085744/

159. Muljo SA, Ansel KM, Kanellopoulou C, Livingston DM, Rao A, Rajewsky K. Aberrant T cell differentiation in the absence of Dicer. Journal of Experimental Medicine. 2005 Jul 18;202(2):261–9.

160. Warth SC, Hoefig KP, Hiekel A, Schallenberg S, Jovanovic K, Klein L, et al. Induced miR-99a expression represses Mtor cooperatively with miR-150 to promote regulatory T-cell differentiation. The EMBO Journal. 2015 May 5;34(9):1195–213.

161. Montoya MM, Maul J, Singh PB, Pua HH, Dahlström F, Wu N, et al. A Distinct Inhibitory Function for miR-18a in Th17 Cell Differentiation. J Immunol. 2017 15;199(2):559–69.

162. Gagnon JD, Kageyama R, Shehata HM, Fassett MS, Mar DJ, Wigton EJ, et al. miR-15/16 Restrain Memory T Cell Differentiation, Cell Cycle, and Survival. Cell Rep. 2019 Aug 20;28(8):2169-2181.e4.

163. Scholz G, Jandus C, Zhang L, Grandclément C, Lopez-Mejia IC, Soneson C, et al. Modulation of mTOR Signalling Triggers the Formation of Stem Cell-like Memory T Cells. EBioMedicine. 2016 Feb;4:50–61.

164. Zhang Y, Joe G, Hexner E, Zhu J, Emerson SG. Host-reactive CD8 + memory stem cells in graft-versus-host disease. Nat Med. 2005 Dec;11(12):1299–305.

165. He L, Hannon GJ. MicroRNAs: small RNAs with a big role in gene regulation. Nature Reviews Genetics. 2004 Jul;5(7):522–31.

166. Zamora AE, Crawford JC, Thomas PG. Hitting the Target: How T Cells Detect and Eliminate Tumors. The Journal of Immunology. 2018 Jan 15;200(2):392–9.

167. Dunn GP, Old LJ, Schreiber RD. The Three Es of Cancer Immunoediting. Annual Review of Immunology. 2004;22(1):329–60.

168. Shankaran V, Ikeda H, Bruce AT, White JM, Swanson PE, Old LJ, et al. IFNγ and lymphocytes prevent primary tumour development and shape tumour immunogenicity. Nature. 2001 Apr;410(6832):1107–11.

169. Diefenbach A, Jensen ER, Jamieson AM, Raulet DH. Rae1 and H60 ligands of the NKG2D receptor stimulate tumour immunity. Nature. 2001 Sep 13;413(6852):165–71.

170. Coca S, Perez-Piqueras J, Martinez D, Colmenarejo A, Saez MA, Vallejo C, et al. The prognostic significance of intratumoral natural killer cells in patients with colorectal carcinoma. Cancer. 1997 Jun 15;79(12):2320–8.

171. Hayakawa Y, Kelly JM, Westwood JA, Darcy PK, Diefenbach A, Raulet D, et al. Cutting edge: tumor rejection mediated by NKG2D receptor-ligand interaction is dependent upon perforin. J Immunol. 2002 Nov 15;169(10):5377–81.

172. Johnsen AC, Haux J, Steinkjer B, Nonstad U, Egeberg K, Sundan A, et al. Regulation of APO-2 ligand/trail expression in NK cells-involvement in NK cell-mediated cytotoxicity. Cytokine. 1999 Sep;11(9):664–72.

173. Guillerey C, Huntington ND, Smyth MJ. Targeting natural killer cells in cancer immunotherapy. Nature Immunology. 2016 Sep;17(9):1025–36.

174. Marcus A, Gowen BG, Thompson TW, Iannello A, Ardolino M, Deng W, et al. Recognition of tumors by the innate immune system and natural killer cells. Adv Immunol. 2014;122:91–128.

175. Braumüller H, Wieder T, Brenner E, Aßmann S, Hahn M, Alkhaled M, et al. T-helper-1-cell cytokines drive cancer into senescence. Nature. 2013 Feb 21;494(7437):361–5.

176. Yuan A, Hsiao Y-J, Chen H-Y, Chen H-W, Ho C-C, Chen Y-Y, et al. Opposite Effects of M1 and M2 Macrophage Subtypes on Lung Cancer Progression. Scientific Reports. 2015 Sep 24;5:14273.

177. Poh AR, Ernst M. Targeting Macrophages in Cancer: From Bench to Bedside. Front Oncol [Internet]. 2018 Mar 12 [cited 2019 Oct 31];8. Available from: https://www.ncbi.nlm.nih.gov/pmc/articles/PMC5858529/

178. Woo S-R, Corrales L, Gajewski TF. Innate Immune Recognition of Cancer. Annual Review of Immunology. 2015;33(1):445–74.

179. Hernandez C, Huebener P, Schwabe RF. Damage-associated molecular patterns in cancer: A double-edged sword. Oncogene. 2016 Nov 17;35(46):5931.

180. Chen DS, Mellman I. Oncology meets immunology: the cancer-immunity cycle. Immunity. 2013 Jul 25;39(1):1–10.

181. Warrington R, Watson W, Kim HL, Antonetti FR. An introduction to immunology and immunopathology. Allergy Asthma Clin Immunol. 2011 Nov 10;7 Suppl 1:S1.

182. Pandya PH, Murray ME, Pollok KE, Renbarger JL. The Immune System in Cancer Pathogenesis: Potential Therapeutic Approaches. Journal of Immunology Research [Internet]. 2016 [cited 2019 Nov 1];2016. Available from: https://www.ncbi.nlm.nih.gov/pmc/articles/PMC5220497/

183. Fridman WH, Pagès F, Sautès-Fridman C, Galon J. The immune contexture in human tumours: impact on clinical outcome. Nat Rev Cancer. 2012 Apr;12(4):298–306.

184. Janssen EM, Lemmens EE, Wolfe T, Christen U, Herrath MG von, Schoenberger SP. CD4 + T cells are required for secondary expansion and memory in CD8 + T lymphocytes. Nature. 2003 Feb;421(6925):852–6.

185. Bevan MJ. Helping the CD8 + T-cell response. Nature Reviews Immunology. 2004 Aug;4(8):595–602.

186. Tran E, Turcotte S, Gros A, Robbins PF, Lu Y-C, Dudley ME, et al. Cancer immunotherapy based on mutation-specific CD4+ T cells in a patient with epithelial cancer. Science. 2014 May 9;344(6184):641–5.

187. Parkhurst MR, Riley JP, Robbins PF, Rosenberg SA. Induction of CD4+ Th1 lymphocytes that recognize known and novel class II MHC restricted epitopes from the melanoma antigen gp100 by stimulation with recombinant protein. J Immunother. 2004 Apr;27(2):79–91.

188. Ott PA, Hu Z, Keskin DB, Shukla SA, Sun J, Bozym DJ, et al. An immunogenic personal neoantigen vaccine for patients with melanoma. Nature. 2017 Jul;547(7662):217–21.

189. Rivera Vargas T, Humblin E, Végran F, Ghiringhelli F, Apetoh L. TH9 cells in anti-tumor immunity. Semin Immunopathol. 2017;39(1):39–46.

190. Singh D, Ganesan AP, Panwar B, Eschweiler S, Hanley CJ, Madrigal A, et al. CD4+ follicular helper-like T cells are key players in anti-tumor immunity. bioRxiv. 2020 Jan 9;2020.01.08.898346.

191. Gallimore A, Godkin A. Regulatory T cells and tumour immunity – observations in mice and men. Immunology. 2008;123(2):157–63.

192. Disis ML. Immune Regulation of Cancer. JCO. 2010 Jun 1;28(29):4531–8.

193. Kurose K, Ohue Y, Wada H, Iida S, Ishida T, Kojima T, et al. Phase Ia Study of FoxP3+ CD4 Treg Depletion by Infusion of a Humanized Anti-CCR4 Antibody, KW-0761, in Cancer Patients. Clin Cancer Res. 2015 Oct 1;21(19):4327–36.

194. Gabrilovich D. Mechanisms and functional significance of tumour-induced dendritic-cell defects. Nat Rev Immunol. 2004 Dec;4(12):941–52.

195. Pistoia V, Morandi F, Bianchi G, Pezzolo A, Prigione I, Raffaghello L. Immunosuppressive microenvironment in neuroblastoma. Front Oncol. 2013;3:167.

196. Vanichapol T, Chutipongtanate S, Anurathapan U, Hongeng S. Immune Escape Mechanisms and Future Prospects for Immunotherapy in Neuroblastoma. Biomed Res Int [Internet]. 2018 Feb 25 [cited 2019 Nov 1];2018. Available from: https://www.ncbi.nlm.nih.gov/pmc/articles/PMC5845499/

197. Noy R, Pollard JW. Tumor-Associated Macrophages: From Mechanisms to Therapy. Immunity. 2014 Jul 17;41(1):49–61.

198. Geiger R, Rieckmann JC, Wolf T, Basso C, Feng Y, Fuhrer T, et al. L-Arginine Modulates T Cell Metabolism and Enhances Survival and Anti-tumor Activity. Cell. 2016 Oct 20;167(3):829-842.e13.

199. Jiang X, Wang J, Deng X, Xiong F, Ge J, Xiang B, et al. Role of the tumor microenvironment in PD-L1/PD-1-mediated tumor immune escape. Molecular Cancer [Internet]. 2019 [cited 2019 Nov 1];18. Available from: https://www.ncbi.nlm.nih.gov/pmc/articles/PMC6332843/

200. Iwai Y, Hamanishi J, Chamoto K, Honjo T. Cancer immunotherapies targeting the PD-1 signaling pathway. J Biomed Sci. 2017 Apr 4;24(1):26.

201. Yu J, Du W, Yan F, Wang Y, Li H, Cao S, et al. Myeloid-Derived Suppressor Cells Suppress Antitumor Immune Responses through IDO Expression and Correlate with Lymph Node Metastasis in Patients with Breast Cancer. The Journal of Immunology. 2013 Apr 1;190(7):3783–97.

202. Motz GT, Santoro SP, Wang L-P, Garrabrant T, Lastra RR, Hagemann IS, et al. Tumor endothelium FasL establishes a selective immune barrier promoting tolerance in tumors. Nature Medicine. 2014 Jun;20(6):607–15.

203. Jovanovic P, Mihajlovic M, Djordjevic-Jocic J, Vlajkovic S, Cekic S, Stefanovic V. Ocular melanoma: an overview of the current status. Int J Clin Exp Pathol. 2013 Jun 15;6(7):1230–44.

204. Gowthami C, Kumar P, Ravikumar A, Joseph LD, Rajendiran S. Malignant Melanoma of the External Auditory Canal. J Clin Diagn Res. 2014 Aug;8(8):FD04–6.

205. Gandini S, Sera F, Cattaruzza MS, Pasquini P, Abeni D, Boyle P, et al. Meta-analysis of risk factors for cutaneous melanoma: I. Common and atypical naevi. Eur J Cancer. 2005 Jan;41(1):28–44.

206. Krebs in der Schweiz: wichtige Zahlen. 2018;12.

207. Rass K, Reichrath J. UV damage and DNA repair in malignant melanoma and nonmelanoma skin cancer. Adv Exp Med Biol. 2008;624:162–78.

208. Gandini S, Sera F, Cattaruzza MS, Pasquini P, Picconi O, Boyle P, et al. Meta-analysis of risk factors for cutaneous melanoma: II. Sun exposure. European Journal of Cancer. 2005 Jan 1;41(1):45–60.

209. Anna B, Blazej Z, Jacqueline G, Andrew CJ, Jeffrey R, Andrzej S. Mechanism of UV-related carcinogenesis and its contribution to nevi/melanoma. Expert Rev Dermatol. 2007;2(4):451–69.

210. Agar NS, Halliday GM, Barnetson RS, Ananthaswamy HN, Wheeler M, Jones AM. The basal layer in human squamous tumors harbors more UVA than UVB fingerprint mutations: a role for UVA in human skin carcinogenesis. Proc Natl Acad Sci USA. 2004 Apr 6;101(14):4954–9.

211. Hussain SP, Harris CC. p53 biological network: at the crossroads of the cellular-stress response pathway and molecular carcinogenesis. J Nippon Med Sch. 2006 Apr;73(2):54–64.

212. Gandini S, Sera F, Cattaruzza MS, Pasquini P, Zanetti R, Masini C, et al. Meta-analysis of risk factors for cutaneous melanoma: III. Family history, actinic damage and phenotypic factors. European Journal of Cancer. 2005 Sep 1;41(14):2040–59.

213. Abbasi NR, Shaw HM, Rigel DS, Friedman RJ, McCarthy WH, Osman I, et al. Early diagnosis of cutaneous melanoma: revisiting the ABCD criteria. JAMA. 2004 Dec 8;292(22):2771–6.

214. Dummer R, Hauschild A, Lindenblatt N, Pentheroudakis G, Keilholz U, ESMO Guidelines Committee. Cutaneous melanoma: ESMO Clinical Practice Guidelines for diagnosis, treatment and follow-up. Ann Oncol. 2015 Sep;26 Suppl 5:v126-132.

215. Liu JC, Zaitz J, Mansson J, Goldenkranz R. Lymph node dissection for a congenital mole? We amputated part of the patient's finger when a nevus became a malignant melanoma [Internet]. Contemporary Surgery. 2007 [cited 2019 Dec 10]. Available from: https://link.galegroup.com/apps/doc/A168390670/HRCA?sid=lms

216. Hodis E, Watson IR, Kryukov GV, Arold ST, Imielinski M, Theurillat J-P, et al. A Landscape of Driver Mutations in Melanoma. Cell. 2012 Jul 20;150(2):251–63.

217. Flaherty KT, Hodi FS, Fisher DE. From genes to drugs: targeted strategies for melanoma. Nat Rev Cancer. 2012 May;12(5):349–61.

218. Alexandrov LB, Nik-Zainal S, Wedge DC, Aparicio SAJR, Behjati S, Biankin AV, et al. Signatures of mutational processes in human cancer. Nature. 2013 Aug;500(7463):415–21.

219. Maleki Vareki S. High and low mutational burden tumors versus immunologically hot and cold tumors and response to immune checkpoint inhibitors. Journal for ImmunoTherapy of Cancer. 2018 Dec 27;6(1):157.

220. Michielin O, van Akkooi A, Ascierto P, Dummer R, Keilholz U. Cutaneous melanoma: ESMO Clinical Practice Guidelines for diagnosis, treatment and follow-up. Ann Oncol [Internet]. [cited 2019 Oct 31]; Available from: https://academic.oup.com/annonc/advance-article/doi/10.1093/annonc/mdz411/5578477

221. Helgadottir H, Rocha Trocoli Drakensjö I, Girnita A. Personalized Medicine in Malignant Melanoma: Towards Patient Tailored Treatment. Front Oncol [Internet]. 2018 Jun 12 [cited 2019 Oct 31];8. Available from: https://www.ncbi.nlm.nih.gov/pmc/articles/PMC6006716/

222. Couzin-Frankel J. Cancer Immunotherapy. Science. 2013 Dec 20;342(6165):1432–3.

223. Smyth MJ, Teng MW. 2018 Nobel Prize in physiology or medicine. Clin Transl Immunology [Internet]. 2018 Oct 24 [cited 2019 Dec 10];7(10). Available from: https://www.ncbi.nlm.nih.gov/pmc/articles/PMC6200707/

224. Vigneron N. Human Tumor Antigens and Cancer Immunotherapy. Biomed Res Int [Internet]. 2015 [cited 2019 Nov 2];2015. Available from: https://www.ncbi.nlm.nih.gov/pmc/articles/PMC4487697/

225. Welters MJP, Kenter GG, Piersma SJ, Vloon APG, Löwik MJG, Berends-van der Meer DMA, et al. Induction of tumor-specific CD4+ and CD8+ T-cell immunity in cervical cancer patients by a human papillomavirus type 16 E6 and E7 long peptides vaccine. Clin Cancer Res. 2008 Jan 1;14(1):178–87.

226. Chomez P, De Backer O, Bertrand M, De Plaen E, Boon T, Lucas S. An overview of the MAGE gene family with the identification of all human members of the family. Cancer Res. 2001 Jul 15;61(14):5544–51.

227. Chen YT, Scanlan MJ, Sahin U, Türeci O, Gure AO, Tsang S, et al. A testicular antigen aberrantly expressed in human cancers detected by autologous antibody screening. Proc Natl Acad Sci USA. 1997 Mar 4;94(5):1914–8.

228. Gure AO, Türeci O, Sahin U, Tsang S, Scanlan MJ, Jäger E, et al. SSX: a multigene family with several members transcribed in normal testis and human cancer. Int J Cancer. 1997 Sep 17;72(6):965–71.

229. Peng M, Mo Y, Wang Y, Wu P, Zhang Y, Xiong F, et al. Neoantigen vaccine: an emerging tumor immunotherapy. Molecular Cancer. 2019 Aug 23;18(1):128.

230. Hilf N, Kuttruff-Coqui S, Frenzel K, Bukur V, Stevanović S, Gouttefangeas C, et al. Actively personalized vaccination trial for newly diagnosed glioblastoma. Nature. 2019;565(7738):240–5.

231. Keskin DB, Anandappa AJ, Sun J, Tirosh I, Mathewson ND, Li S, et al. Neoantigen vaccine generates intratumoral T cell responses in phase Ib glioblastoma trial. Nature. 2019;565(7738):234–9.

232. Brichard V, Van Pel A, Wölfel T, Wölfel C, De Plaen E, Lethé B, et al. The tyrosinase gene codes for an antigen recognized by autologous cytolytic T lymphocytes on HLA-A2 melanomas. J Exp Med. 1993 Aug 1;178(2):489–95.

233. Vigneron N, Ooms A, Morel S, Ma W, Degiovanni G, Van den Eynde BJ. A peptide derived from melanocytic protein gp100 and presented by HLA-B35 is recognized by autologous cytolytic T lymphocytes on melanoma cells. Tissue Antigens. 2005 Feb;65(2):156–62.

234. Coulie PG, Brichard V, Van Pel A, Wölfel T, Schneider J, Traversari C, et al. A new gene coding for a differentiation antigen recognized by autologous cytolytic T lymphocytes on HLA-A2 melanomas. J Exp Med. 1994 Jul 1;180(1):35–42.

235. Hollingsworth RE, Jansen K. Turning the corner on therapeutic cancer vaccines. npj Vaccines. 2019 Feb 8;4(1):1–10.

236. Baumgaertner P, Jandus C, Rivals J-P, Derré L, Lövgren T, Baitsch L, et al. Vaccination-induced functional competence of circulating human tumor-specific CD8 T-cells. Int J Cancer. 2012 Jun 1;130(11):2607–17.

237. Melief CJM, van der Burg SH. Immunotherapy of established (pre)malignant disease by synthetic long peptide vaccines. Nature Reviews Cancer. 2008 May;8(5):351–60.

238. Valmori D, Souleimanian NE, Tosello V, Bhardwaj N, Adams S, O'Neill D, et al. Vaccination with NY-ESO-1 protein and CpG in Montanide induces integrated antibody/Th1 responses and CD8 T cells through cross-priming. PNAS. 2007 May 22;104(21):8947–52.

239. Jiang T, Shi T, Zhang H, Hu J, Song Y, Wei J, et al. Tumor neoantigens: from basic research to clinical applications. Journal of Hematology & Oncology. 2019 Sep 6;12(1):93.

240. Bassani-Sternberg M, Coukos G. Mass spectrometry-based antigen discovery for cancer immunotherapy. Current Opinion in Immunology. 2016 Aug 1;41:9–17.

241. Rosenberg SA, Restifo NP, Yang JC, Morgan RA, Dudley ME. Adoptive cell transfer: a clinical path to effective cancer immunotherapy. Nat Rev Cancer. 2008 Apr;8(4):299–308.

242. Spitzer MH, Carmi Y, Reticker-Flynn NE, Kwek SS, Madhireddy D, Martins MM, et al. Systemic Immunity Is Required for Effective Cancer Immunotherapy. Cell. 2017 26;168(3):487-502.e15.

243. Hunder NN, Wallen H, Cao J, Hendricks DW, Reilly JZ, Rodmyre R, et al. Treatment of Metastatic Melanoma with Autologous CD4+ T Cells against NY-ESO-1. N Engl J Med. 2008 Jun 19;358(25):2698–703.

244. Yao X, Lu Y-C, Parker LL, Li YF, El-Gamil M, Black MA, et al. Isolation and Characterization of an HLA-DPB1*04: 01-restricted MAGE-A3 T-Cell Receptor for Cancer Immunotherapy. J Immunother. 2016;39(5):191–201.

245. Lu Y-C, Parker LL, Lu T, Zheng Z, Toomey MA, White DE, et al. Treatment of Patients With Metastatic Cancer Using a Major Histocompatibility Complex Class II–Restricted T-Cell Receptor Targeting the Cancer Germline Antigen MAGE-A3. J Clin Oncol. 2017 Oct 10;35(29):3322–9.

246. Rosenberg SA, Restifo NP. Adoptive cell transfer as personalized immunotherapy for human cancer. Science. 2015 Apr 3;348(6230):62–8.

247. Guedan S, Calderon H, Posey AD, Maus MV. Engineering and Design of Chimeric Antigen Receptors. Mol Ther Methods Clin Dev. 2018 Dec 31;12:145–56.

248. Brown CE, Mackall CL. CAR T cell therapy: inroads to response and resistance. Nat Rev Immunol. 2019 Feb;19(2):73–4.

249. Scarfò I, Maus MV. Current approaches to increase CAR T cell potency in solid tumors: targeting the tumor microenvironment. Journal for ImmunoTherapy of Cancer. 2017 Mar 21;5(1):28.

250. Shah NN, Fry TJ. Mechanisms of resistance to CAR T cell therapy. Nat Rev Clin Oncol. 2019 Jun;16(6):372–85.

251. Pardoll DM. The blockade of immune checkpoints in cancer immunotherapy. Nat Rev Cancer. 2012 Apr;12(4):252–64.

252. Galluzzi L, Kroemer G, Eggermont A. Novel immune checkpoint blocker approved for the treatment of advanced melanoma. OncoImmunology. 2014 Nov 2;3(11):e967147.

253. Bowyer S, Prithviraj P, Lorigan P, Larkin J, McArthur G, Atkinson V, et al. Efficacy and toxicity of treatment with the anti-CTLA-4 antibody ipilimumab in patients with metastatic melanoma after prior anti-PD-1 therapy. British Journal of Cancer. 2016 May;114(10):1084–9.

254. Attia P, Phan GQ, Maker AV, Robinson MR, Quezado MM, Yang JC, et al. Autoimmunity correlates with tumor regression in patients with metastatic melanoma treated with anti-cytotoxic T-lymphocyte antigen-4. J Clin Oncol. 2005 Sep 1;23(25):6043–53.

255. Phan GQ, Yang JC, Sherry RM, Hwu P, Topalian SL, Schwartzentruber DJ, et al. Cancer regression and autoimmunity induced by cytotoxic T lymphocyte-associated antigen 4 blockade in patients with metastatic melanoma. Proc Natl Acad Sci USA. 2003 Jul 8;100(14):8372–7.

256. Wolchok JD, Kluger H, Callahan MK, Postow MA, Rizvi NA, Lesokhin AM, et al. Nivolumab plus ipilimumab in advanced melanoma. N Engl J Med. 2013 Jul 11;369(2):122–33.

257. Postow MA, Chesney J, Pavlick AC, Robert C, Grossmann K, McDermott D, et al. Nivolumab and Ipilimumab versus Ipilimumab in Untreated Melanoma. New England Journal of Medicine. 2015 May 21;372(21):2006–17.

258. Qin S, Xu L, Yi M, Yu S, Wu K, Luo S. Novel immune checkpoint targets: moving beyond PD-1 and CTLA-4. Mol Cancer [Internet]. 2019 Nov 6 [cited 2019 Dec 12];18. Available from: https://www.ncbi.nlm.nih.gov/pmc/articles/PMC6833286/

259. Dougall WC, Kurtulus S, Smyth MJ, Anderson AC. TIGIT and CD96: new checkpoint receptor targets for cancer immunotherapy. Immunological Reviews. 2017;276(1):112–20.

260. Marin-Acevedo JA, Dholaria B, Soyano AE, Knutson KL, Chumsri S, Lou Y. Next generation of immune checkpoint therapy in cancer: new developments and challenges. Journal of Hematology & Oncology. 2018 Mar 15;11(1):39.

261. Zhang X, Wang Y, Ouyang Q, Levy H. The Current Immunoassays and Emerging Immunogenomic Approaches For Immunomonitoring Cancer and Infectious Diseases. JCGB. 2019 Jan 8;1(3):1.

262. Buuren MM van, Dijkgraaf FE, Linnemann C, Toebes M, Chang CXL, Mok JY, et al. HLA Micropolymorphisms Strongly Affect Peptide–MHC Multimer–Based Monitoring of Antigen-Specific CD8+ T Cell Responses. The Journal of Immunology [Internet]. 2013 Dec 16 [cited 2019 Nov 2]; Available from: https://www.jimmunol.org/content/early/2013/12/15/jimmunol.1301770

263. Jansen DTSL, Ramnoruth N, Loh KL, Rossjohn J, Reid HH, Nel HJ, et al. Flow Cytometric Clinical Immunomonitoring Using Peptide–MHC Class II Tetramers: Optimization of Methods and Protocol Development. Front Immunol [Internet]. 2018 Jan 22 [cited 2019 Nov 2];9. Available from: https://www.ncbi.nlm.nih.gov/pmc/articles/PMC5786526/

264. Lissina A, Ladell K, Skowera A, Clement M, Edwards E, Seggewiss R, et al. Protein kinase inhibitors substantially improve the physical detection of T-cells with peptide-MHC tetramers. J Immunol Methods. 2009 Jan 1;340(1):11–24.

265. Dolton G, Tungatt K, Lloyd A, Bianchi V, Theaker SM, Trimby A, et al. More tricks with tetramers: a practical guide to staining T cells with peptide-MHC multimers. Immunology. 2015 Sep;146(1):11–22.

266. Dolton G, Zervoudi E, Rius C, Wall A, Thomas HL, Fuller A, et al. Optimized Peptide–MHC Multimer Protocols for Detection and Isolation of Autoimmune T-Cells. Front Immunol [Internet]. 2018 [cited 2019 Nov 6];9. Available from: https://www.frontiersin.org/articles/10.3389/fimmu.2018.01378/full

267. Demotte N, Stroobant V, Courtoy PJ, Van Der Smissen P, Colau D, Luescher IF, et al. Restoring the association of the T cell receptor with CD8 reverses anergy in human tumor-infiltrating lymphocytes. Immunity. 2008 Mar;28(3):414–24.

268. Petit A-E, Demotte N, Scheid B, Wildmann C, Bigirimana R, Gordon-Alonso M, et al. A major secretory defect of tumour-infiltrating T lymphocytes due to galectin impairing LFA-1-mediated synapse completion. Nat Commun [Internet]. 2016 Jul 22 [cited 2019 Nov 6];7. Available from: https://www.ncbi.nlm.nih.gov/pmc/articles/PMC4961845/

269. Kao C, Daniels MA, Jameson SC. Loss of CD8 and TCR binding to Class I MHC ligands following T cell activation. Int Immunol. 2005 Dec;17(12):1607–17.

270. Mekala DJ, Geiger TL. Functional segregation of the TCR and antigen-MHC complexes on the surface of CTL. J Immunol. 2003 Oct 15;171(8):4089–95.

271. James EA, LaFond R, Durinovic-Bello I, Kwok W. Visualizing Antigen Specific CD4+ T Cells using MHC Class II Tetramers. J Vis Exp [Internet]. 2009 Mar 6 [cited 2019 Nov 7];(25). Available from: https://www.ncbi.nlm.nih.gov/pmc/articles/PMC2789100/

272. Rius C, Attaf M, Tungatt K, Bianchi V, Legut M, Bovay A, et al. Peptide–MHC Class I Tetramers Can Fail To Detect Relevant Functional T Cell Clonotypes and Underestimate Antigen-Reactive T Cell Populations. J Immunol. 2018 Apr 1;200(7):2263–79.

273. Whelan JA, Dunbar PR, Price DA, Purbhoo MA, Lechner F, Ogg GS, et al. Specificity of CTL Interactions with Peptide-MHC Class I Tetrameric Complexes Is Temperature Dependent. The Journal of Immunology. 1999 Oct 15;163(8):4342–8.

274. Beyranvand Nejad E, Welters MJP, Arens R, van der Burg SH. The importance of correctly timing cancer immunotherapy. Expert Opin Biol Ther. 2017;17(1):87–103.

275. Baumgaertner P, Costa Nunes C, Cachot A, Maby-El Hajjami H, Cagnon L, Braun M, et al. Vaccination of stage III/IV melanoma patients with long NY-ESO-1 peptide and CpG-B elicits robust CD8+ and CD4+ T-cell responses with multiple specificities including a novel DR7-restricted epitope. Oncoimmunology. 2016;5(10):e1216290.

276. Xu X-N, Purbhoo MA, Chen N, Mongkolsapaya J, Cox JH, Meier U-C, et al. A Novel Approach to Antigen-Specific Deletion of CTL with Minimal Cellular Activation Using α3 Domain Mutants of MHC Class I/Peptide Complex. Immunity. 2001 May 5;14(5):591–602.

277. Kelly R, Greiff D. Toxicity of Pneumococcal Neuraminidase. Infect Immun. 1970 Jul;2(1):115–7.

278. Weiss L. Guest Editorial. J Natl Cancer Inst. 1973 Jan 1;50(1):3–19.

279. Melssen M, Slingluff CL. Vaccines Targeting Helper T Cells for Cancer Immunotherapy. Curr Opin Immunol. 2017 Aug;47:85–92.

280. Aarntzen EHJG, Vries IJMD, Lesterhuis WJ, Schuurhuis D, Jacobs JFM, Bol K, et al. Targeting CD4+ T-Helper Cells Improves the Induction of Antitumor Responses in Dendritic Cell–Based Vaccination. Cancer Res. 2013 Jan 1;73(1):19–29.

281. Jensen KK, Andreatta M, Marcatili P, Buus S, Greenbaum JA, Yan Z, et al. Improved methods for predicting peptide binding affinity to MHC class II molecules. Immunology. 2018;154(3):394–406.

282. Nielsen M, Lundegaard C, Blicher T, Lamberth K, Harndahl M, Justesen S, et al. NetMHCpan, a Method for Quantitative Predictions of Peptide Binding to Any HLA-A and -B Locus Protein of Known Sequence. PLOS ONE. 2007 Aug 29;2(8):e796.

283. Karosiene E, Rasmussen M, Blicher T, Lund O, Buus S, Nielsen M. NetMHCIIpan-3.0, a common pan-specific MHC class II prediction method including all three human MHC class II isotypes, HLA-DR, HLA-DP and HLA-DQ. Immunogenetics. 2013 Oct 1;65(10):711–24.

284. Lin HH, Zhang GL, Tongchusak S, Reinherz EL, Brusic V. Evaluation of MHC-II peptide binding prediction servers: applications for vaccine research. BMC Bioinformatics. 2008 Dec 12;9(12):S22.

285. Zhang L, Udaka K, Mamitsuka H, Zhu S. Toward more accurate pan-specific MHC-peptide binding prediction: a review of current methods and tools. Brief Bioinform. 2012 May 1;13(3):350–64.

286. Srivastava PK. Neoepitopes of Cancers: Looking Back, Looking Ahead. Cancer Immunol Res. 2015 Sep 1;3(9):969–77.

287. Nielsen M, Andreatta M. NNAlign: a platform to construct and evaluate artificial neural network models of receptor-ligand interactions. Nucleic Acids Res. 2017 03;45(W1):W344–9.

288. Andreatta M, Alvarez B, Nielsen M. GibbsCluster: unsupervised clustering and alignment of peptide sequences. Nucleic Acids Res. 2017 03;45(W1):W458–63.

289. Lee RC, Feinbaum RL, Ambros V. The C. elegans heterochronic gene lin-4 encodes small RNAs with antisense complementarity to lin-14. Cell. 1993 Dec 3;75(5):843–54.

290. Song L, Tuan RS. MicroRNAs and cell differentiation in mammalian development. Birth Defects Research Part C: Embryo Today: Reviews. 2006;78(2):140–9.

291. Shim J, Nam J-W. The expression and functional roles of microRNAs in stem cell differentiation. BMB Rep. 2016 Jan;49(1):3–10.

292. Felli N, Fontana L, Pelosi E, Botta R, Bonci D, Facchiano F, et al. MicroRNAs 221 and 222 inhibit normal erythropoiesis and erythroleukemic cell growth via kit receptor down-modulation. Proc Natl Acad Sci U S A. 2005 Dec 13;102(50):18081–6.

293. Khalaj M, Woolthuis CM, Hu W, Durham BH, Chu SH, Qamar S, et al. miR-99 regulates normal and malignant hematopoietic stem cell self-renewal. The Journal of Experimental Medicine. 2017 Aug 7;214(8):2453.

294. Kim C, Hu B, Jadhav RR, Jin J, Zhang H, Cavanagh MM, et al. Activation of miR-21-Regulated Pathways in Immune Aging Selects against Signatures Characteristic of Memory T Cells. Cell Reports. 2018 Nov 20;25(8):2148-2162.e5.

295. Ivey KN, Srivastava D. MicroRNAs as Regulators of Differentiation and Cell Fate Decisions. Cell Stem Cell. 2010 Jul 2;7(1):36–41.

296. Gattinoni L, Speiser DE, Lichterfeld M, Bonini C. T memory stem cells in health and disease. Nat Med. 2017 Jan 6;23(1):18–27.

297. Gattinoni L, Zhong X-S, Palmer DC, Ji Y, Hinrichs CS, Yu Z, et al. Wnt signaling arrests effector T cell differentiation and generates CD8 + memory stem cells. Nature Medicine. 2009 Jul;15(7):808–13.

298. Stemberger C, Huster KM, Koffler M, Anderl F, Schiemann M, Wagner H, et al. A Single Naive CD8+ T Cell Precursor Can Develop into Diverse Effector and Memory Subsets. Immunity. 2007 Dec 21;27(6):985–97.

299. Gattinoni L, Klebanoff CA, Palmer DC, Wrzesinski C, Kerstann K, Yu Z, et al. Acquisition of full effector function in vitro paradoxically impairs the in vivo antitumor efficacy of adoptively transferred $CD8^+$ T cells. J Clin Invest. 2005 Jun 1;115(6):1616–26.

300. Tabler CO, Lucera MB, Haqqani AA, McDonald DJ, Migueles SA, Connors M, et al. CD4+ Memory Stem Cells Are Infected by HIV-1 in a Manner Regulated in Part by SAMHD1 Expression. Journal of Virology. 2014 May 1;88(9):4976–86.

301. Buzon MJ, Sun H, Li C, Shaw A, Seiss K, Ouyang Z, et al. HIV-1 persistence in CD4 + T cells with stem cell–like properties. Nature Medicine. 2014 Feb;20(2):139–42.

302. Morgan R, Ankrah R, El-Tanani S, Loadman PM, Pattterson L, Rudland PS, et al. Chapter 20 - Wnt Signaling as a Therapeutic Target in Cancer and Metastasis. In: Ahmad A, editor. Introduction to Cancer Metastasis [Internet]. Academic Press; 2017 [cited 2019 Nov 12]. p. 375–94. Available from: http://www.sciencedirect.com/science/article/pii/B9780128040034000207

303. Tong X, Gui H, Jin F, Heck BW, Lin P, Ma J, et al. Ataxin-1 and Brother of ataxin-1 are components of the Notch signalling pathway. EMBO reports. 2011 May 1;12(5):428–35.

304. Sánchez I, Balagué E, Matilla-Dueñas A. Ataxin-1 regulates the cerebellar bioenergetics proteome through the GSK3β-mTOR pathway which is altered in Spinocerebellar ataxia type 1 (SCA1). Hum Mol Genet. 2016 Sep 15;25(18):4021–40.

305. Karur VG, Lowell CA, Besmer P, Agosti V, Wojchowski DM. Lyn kinase promotes erythroblast expansion and late-stage development. Blood. 2006 Sep 1;108(5):1524.

306. Wang L, Huang D, Jiang Z, Luo Y, Norris C, Zhang M, et al. Akt3 is responsible for the survival and proliferation of embryonic stem cells. Biology Open. 2017 Jun 15;6(6):850.

307. Yin Y, Yin Y, Shen Q, Shen Q, Tao R, Tao R, et al. Wee1 inhibition can suppress tumor proliferation and sensitize p53 mutant colonic cancer cells to the anticancer effect of irinotecan. Molecular Medicine Reports. 2018 Feb 1;17(2):3344–9.

308. Kim H-Y, Cho Y, Kang H, Yim Y-S, Kim S-J, Song J, et al. Targeting the WEE1 kinase as a molecular targeted therapy for gastric cancer. Oncotarget. 2016 Jun 23;7(31):49902–16.

309. Garzon R, Marcucci G, Croce CM. Targeting MicroRNAs in Cancer: Rationale, Strategies and Challenges. Nat Rev Drug Discov. 2010 Oct;9(10):775–89.

310. Lin H-M, Nikolic I, Yang J, Castillo L, Deng N, Chan C-L, et al. MicroRNAs as potential therapeutics to enhance chemosensitivity in advanced prostate cancer. Sci Rep [Internet]. 2018 May 18 [cited 2019 Nov 15];8. Available from: https://www.ncbi.nlm.nih.gov/pmc/articles/PMC5959911/

311. Roitbak T. Silencing a Multifunctional microRNA Is Beneficial for Stroke Recovery. Front Mol Neurosci [Internet]. 2018 [cited 2019 Nov 15];11. Available from: https://www.frontiersin.org/articles/10.3389/fnmol.2018.00058/full

312. Haftmann C, Riedel R, Porstner M, Wittmann J, Chang H-D, Radbruch A, et al. Direct uptake of Antagomirs and efficient knockdown of miRNA in primary B and T lymphocytes. J Immunol Methods. 2015 Nov;426:128–33.

313. Zammit V, Brincat MR, Cassar V, Muscat-Baron Y, Ayers D, Baron B. MiRNA influences in mesenchymal stem cell commitment to neuroblast lineage development. Non-coding RNA Research. 2018 Dec 1;3(4):232–42.

314. Ostroumov D, Fekete-Drimusz N, Saborowski M, Kühnel F, Woller N. CD4 and CD8 T lymphocyte interplay in controlling tumor growth. Cell Mol Life Sci. 2018;75(4):689–713.

315. Marzo AL, Lake RA, Robinson BWS, Scott B. T-Cell Receptor Transgenic Analysis of Tumor-specific CD8 and CD4 Responses in the Eradication of Solid Tumors. Cancer Res. 1999 Mar 1;59(5):1071–9.

316. Church SE, Jensen SM, Antony PA, Restifo NP, Fox BA. Tumor-specific CD4+ T cells maintain effector and memory tumor-specific CD8+ T cells. European Journal of Immunology. 2014;44(1):69–79.

317. Zippelius A, Batard P, Rubio-Godoy V, Bioley G, Liénard D, Lejeune F, et al. Effector Function of Human Tumor-Specific CD8 T Cells in Melanoma Lesions: A State of Local Functional Tolerance. Cancer Res. 2004 Apr 15;64(8):2865–73.

318. Schmid DA, Irving MB, Posevitz V, Hebeisen M, Posevitz-Fejfar A, Sarria J-CF, et al. Evidence for a TCR Affinity Threshold Delimiting Maximal CD8 T Cell Function. The Journal of Immunology. 2010 May 1;184(9):4936–46.

319. Bobisse S, Genolet R, Roberti A, Tanyi JL, Racle J, Stevenson BJ, et al. Sensitive and frequent identification of high avidity neo-epitope specific CD8 + T cells in immunotherapy-naive ovarian cancer. Nat Commun. 2018 Mar 15;9(1):1–10.

320. Saini SK, Tamhane T, Anjanappa R, Saikia A, Ramskov S, Donia M, et al. Empty peptide-receptive MHC class I molecules for efficient detection of antigen-specific T cells. Science Immunology [Internet]. 2019 Jul 19 [cited 2019 Nov 15];4(37). Available from: https://immunology.sciencemag.org/content/4/37/eaau9039

321. Allard M, Couturaud B, Carretero-Iglesia L, Duong MN, Schmidt J, Monnot GC, et al. TCR-ligand dissociation rate is a robust and stable biomarker of CD8+ T cell potency. JCI Insight [Internet]. [cited 2019 Nov 15];2(14). Available from: https://www.ncbi.nlm.nih.gov/pmc/articles/PMC5518551/

322. Soler M, Li X, John-Herpin A, Schmidt J, Coukos G, Altug H. Two-Dimensional Label-Free Affinity Analysis of Tumor-Specific CD8 T Cells with a Biomimetic Plasmonic Sensor. ACS Sens. 2018 Nov 26;3(11):2286–95.

323. Martinez RJ, Evavold BD. Lower Affinity T Cells are Critical Components and Active Participants of the Immune Response. Front Immunol [Internet]. 2015 [cited 2019 Nov 15];6. Available from: https://www.frontiersin.org/articles/10.3389/fimmu.2015.00468/full

324. Czerkinsky C, Andersson G, Ekre H-P, Nilsson L-Å, Klareskog L, Ouchterlony Ö. Reverse ELISPOT assay for clonal analysis of cytokine production I. Enumeration of gamma-interferon-secreting cells. Journal of Immunological Methods. 1988 May 25;110(1):29–36.

325. Elshal MF, McCoy JP. Multiplex bead array assays: performance evaluation and comparison of sensitivity to ELISA. Methods. 2006 Apr;38(4):317–23.

326. Yatsula V, Shelburne C, Ning Q, Krai P, Cheo D, Ranganathan S, et al. Rapid Immunoassay Development using the U-PLEX® Assay Platform. The Journal of Immunology. 2017 May 1;198(1 Supplement):81.18-81.18.

327. Assenmacher M, Schmitz J, Radbruch A. Flow cytometric determination of cytokines in activated murine T helper lymphocytes: Expression of interleukin-10 in interferon-γ and in interleukin-4-expressing cells. European Journal of Immunology. 1994;24(5):1097–101.

328. Torres AJ, Hill AS, Love JC. Nanowell-Based Immunoassays for Measuring Single-Cell Secretion: Characterization of Transport and Surface Binding. Anal Chem. 2014 Dec 2;86(23):11562–9.

329. Bradshaw EM, Kent SC, Tripuraneni V, Orban T, Ploegh HL, Hafler DA, et al. Concurrent detection of secreted products from human lymphocytes by microengraving: Cytokines and antigen-reactive antibodies. Clinical Immunology. 2008 Oct 1;129(1):10–8.

330. Li X, Soler M, Özdemir CI, Belushkin A, Yesilköy F, Altug H. Plasmonic nanohole array biosensor for label-free and real-time analysis of live cell secretion. Lab Chip. 2017 Jun 27;17(13):2208–17.

331. Li X, Soler M, Szydzik C, Khoshmanesh K, Schmidt J, Coukos G, et al. Label-Free Optofluidic Nanobiosensor Enables Real-Time Analysis of Single-Cell Cytokine Secretion. Small. 2018;14(26):1800698.

332. Buonaguro L, Petrizzo A, Tornesello ML, Buonaguro FM. Translating Tumor Antigens into Cancer Vaccines. Clin Vaccine Immunol. 2011 Jan 1;18(1):23–34.

333. Bioley G, Dousset C, Yeh A, Dupont B, Bhardwaj N, Mears G, et al. Vaccination with Recombinant NY-ESO-1 Protein Elicits Immunodominant HLA-DR52b-restricted CD4+ T Cell Responses with a Conserved T Cell Receptor Repertoire. Clin Cancer Res. 2009 Jul 1;15(13):4467–74.

334. Gutjahr A, Papagno L, Nicoli F, Kanuma T, Kuse N, Cabral-Piccin MP, et al. The STING ligand cGAMP potentiates the efficacy of vaccine-induced CD8+ T cells. JCI Insight [Internet]. [cited 2019 Dec 17];4(7). Available from: https://www.ncbi.nlm.nih.gov/pmc/articles/PMC6483644/

335. Kondo T, Imura Y, Chikuma S, Hibino S, Omata-Mise S, Ando M, et al. Generation and application of human induced-stem cell memory T cells for adoptive immunotherapy. Cancer Sci. 2018 Jul;109(7):2130–40.

336. Peter ME. Targeting of mRNAs by multiple miRNAs: the next step. Oncogene. 2010 Apr;29(15):2161–4.

337. Hanna J, Hossain GS, Kocerha J. The Potential for microRNA Therapeutics and Clinical Research. Front Genet [Internet]. 2019 May 16 [cited 2019 Nov 16];10. Available from: https://www.ncbi.nlm.nih.gov/pmc/articles/PMC6532434/

338. Janssen HLA, Reesink HW, Lawitz EJ, Zeuzem S, Rodriguez-Torres M, Patel K, et al. Treatment of HCV infection by targeting microRNA. N Engl J Med. 2013 May 2;368(18):1685–94.

339. van Zandwijk N, Pavlakis N, Kao SC, Linton A, Boyer MJ, Clarke S, et al. Safety and activity of microRNA-loaded minicells in patients with recurrent malignant pleural mesothelioma: a first-in-man, phase 1, open-label, dose-escalation study. Lancet Oncol. 2017;18(10):1386–96.

N CV

Georg Alexander Rockinger

Ave. De la Harpe 49

CH – 1007 Lausanne

Portable: 079 796 22 87

Email: georgalexander.rockinger@unil.ch

Swiss and Italian citizenship.

Personal characteristics: Organized, perseverant, patient, trustworthy, enjoys teamwork.

Education

Class of 2014	University of Lausanne Master of Science in Molecular Biology.
Class of 2011	Università degli studi di Milano Bachelor's degree in Biological Sciences.
Class of 2007	Lycée français Valmont de Lausanne Baccalauréat serie "S" scientific.

Languages

French	Mother tongue
Italian	Mother tongue
English	Fluent (lived 5 years in the U.S.A.), obtained PET, FCE and CAE Cambridge certificates.
German	Basic

Research

From May 2016 PhD student	Department of Fundamental Oncology of the UNIL. **Analysis of tumor antigen-specific CD4+T cell responses.** Use of new technologies for the analysis of the secretome at a single cell level. Optimisation and usage of pMHC II multimer technologies for the detection of tumor- viral- and bacterial-specific CD4 T cells.
February 2014 to March 2016 PhD student	Institute of Immunology and Allergy of the CHUV. **Development of bifunctional antibodies for the targeted depletion of the latent HIV reservoirs of infected cells.** Use of flow cytometry and CyToff platformes for antibody characterization. Testing of the antibodies in viral infection models. ADC and ADCC development.
February 2013 to	University of Lausanne Institute of Microbiology of the CHUV.

January 2014 Master's student	**Expression and purification of *Waddlia chondrophila* membrane proteins to be used for the development of an ELISA.** Bacterial cloning and transformation. Protein production, extraction and purification. ELISA development.
October to December 2012 Master's student	University of Lausanne Institute of Microbiology of the CHUV. **Establishing a new model to study virulence in *Candida albicans* using amoebae.** Culturing of *Candida albicans, Klebsiella aerogenes, Dictyostelium discoideum* and *Acanthamoeba castellanii.* Data analysis.
October 2010 Bachelor student	Università degli studi dell'Insubria-Varese and Como laboratory of Neuropsychopharmacology. **Studies of epigenetic modifications induced by exposure to ∆-9-tetrahydrocannabinol during adolescence.** Pharmacological preparation of animals. Preparation and making of electrophoresis and Western blotting.

Professional experience

27 and 30 August 2013 Participant	ESCMID Postgraduate Technical Workshop, Villars. Intracellular Bacteria From Biology to Clinic. Clinical presentation, diagnostic approaches and treatment. Pathogenesis & biology. Practical Workshop.
2 to 20 August 2010 Intern	Laboratory HFR of Fribourg hospital, Riaz site. Help the deputy director of the laboratory in his preanalitic control tasks, the rendering of test results, quality control, and other tasks aiming at managing the laboratory. Introduced to a few analytic domains such as hematology, clinical chemistry, immunohematology by certified laboratory assistants.
26 to 30 July 2010 Intern	Unilabs analytic medical laboratory. Observation of medical analysis laboratory organization. More specific observation of clinical chemistry, special chemistry, hematology and bacteriology. Introduction to laboratory techniques.

Teaching

2016 – current Teaching of practical work 2nd year medical students and 3rd year biology students at the University of Lausanne, Switzerland

Publications

G.A. Rockinger, P. Guillaume, A. Cachot, M. Saillard, D.E. Speiser, G. Coukos, A. Harari, P. Romero, J. Schmidt and C. Jandus. Optimized combinatorial pMHC class II multimer labelling for precision immune monitoring of tumor-specific CD4 T cells in patients. Submitted to JITC for revision on the 14.12.2019.

Julien Racle, Justine Michaux, **Georg Alexander Rockinger**, Marion Arnaud, Sara Bobisse, Chloe Chong, Philippe Guillaume, George Coukos, Alexandre Harari, Camilla Jandus, Michal Bassani-Sternberg & David

Gfeller. Robust prediction of HLA class II epitopes by deep motif deconvolution of immunopeptidomes. Nature Biotechnology volume 37, pages1283–1286(2019)

Conference participation

Poster presentation

2019 - SSAI annual Congress, Lugano, Switzerland
Poster tittle: Optimized pMHC class II staining procedure for the detection of tumor-, viral- and bacterial-specific CD4+T cells
2018 - SSAI annual Congress, Interlaken, Switzerland.
Poster tittle: Analysis of miRNA involvement in CD4+T cell differentiation
2018 - European Congress of Immunology, Amsterdam, Nederlands.
Poster tittle: Analysis of miRNA involvement in CD4+T cell differentiation
2018 - D Day 2018, CHUV, Lausanne, Switzerland.
Poster tittle: Development of novel methods for high-throughput analyses of human tumor antigen-specific CD4+T cell responses
2018 - XXX Meeting of the Swiss Immunology PhD students, Seepark Thun, Switzerland.
Poster tittle: Development of novel methods for high-throughput analyses of human tumor antigen-specific CD4+T cell responses

Oral presentation

2019 - XXXI Wolfsberg Meeting of the Swiss Immunology PhD students, Seepark Thun, Switzerland.
Presentation tittle: Optimized pMHC class II staining procedure for the detection of tumor, viral and bacterial specific CD4+T cells
2018 - 4th Summer Joint Scientific Retreat, Prémanon, Jura, France.
Presentation tittle: Analysis of miRNA involvement in CD4+T cell differentiation
2017 - 7th PhD Retreat EPFL-UNIL, Les Diablerets, Switzerland.
Presentation tittle: Analysis of tumor antigen-specific CD4 T cell responses
2016 - 6th EPFL-UNIL PhD retreat, Les Diablerets, Switzerland.
Presentation tittle: The targeted depletion of the latent HIV reservoirs

Membership

Swiss Society for Allergology and Immunology (SSAI)

Other

23 april 2005	10 kms of Lausanne.
First responder	Secure a specific area of the 10 km race making patrols. Helped an injured person by administering first aid.
March 2005	Swiss federation of Samaritans. First responder certificate.

Hobbies

Fitness and all kinds of sports, cinema, music, cooking, dog agility training and beer brewing